Defining Mechanisms of NOD2 Receptor Function in Myeloid Cells





Thomas Patrick Errington Chapman

St Catherine's College

University of Oxford

A thesis submitted to the University of Oxford for the degree of

Doctor of Philosophy in Biomedical and Clinical Sciences

Trinity Term 2017

This dissertation is my own work and contains nothing which is the outcome of work done in collaboration with others, except where specifically indicated in the text.

No part of this thesis has been, or is currently being submitted by the author for any other degree, diploma or qualification.

This work does not exceed 50,000 words, exclusive of appendices, bibliography, diagrams, figures, tables and their legends.

Acknowledgements

I would like to thank Professor Alison Simmons for her supervision and encouragement throughout this work. I am also grateful to my co-supervisor, Professor Katja Simon for her invaluable insights. Thanks to all members of the Oxford Translational Gastroenterology Unit, and WIMM Human Immunology Unit for providing a supportive and stimulating environment.

I am hugely grateful to all members of the Simmons laboratory, but would particularly like to thank Seiji Shiraishi who provided great assistance with interrogating the deubiquitinating function of ataxin-3. I would also like to thank Anna Aulicino for her help with the bacterial infection experiments, and Daniele Corridoni and Hannah Chen for their wise counsel on many aspects of this thesis.

I am grateful to members of the Kessler laboratory, in particular Roman Fischer and Marie-Laetitia Thezenas, for their help with the multiple proteomic experiments in this work. I would also like to thank Simon Wigfield in the Harris laboratory for his assistance with the human cell line Seahorse experiments, and Sumeet Pandey in the Uhlig laboratory for his assistance with FACS experiments and the murine cell Seahorse experiments.

I am grateful to members of the Paulson laboratory, in particular Carmo Pereira da Costa, for the provision of bone marrow from ataxin-3 knockout mice.

I am also indebted to my funding bodies, the Wellcome Trust and the NIHR Oxford Biomedical Research Centre, without whom this work would not have been possible.

I would lastly like to thank my family for their unwavering support and encouragement throughout this journey. To my wife Saara, thank you for your understanding, strength and optimism. Together we faced both the challenges of this work and of Finlay's early arrival and have emerged stronger the other side.

This thesis is dedicated to my two children Isla and Finlay – remember that nothing in this world can take the place of persistence.

Abbreviations

A	Alanine
A20	Tumour necrosis factor, alpha-induced protein
aa	Amino acid
AD	Acidic domain
ADP	Adenosine diphosphate
Ag	Antigen
AIEC	Adherent invasive *Escherichia coli*
AIM2	Absent in melanoma 2
ALS	Amyotrophic lateral sclerosis
AMPK	AMP-activated protein kinase
ANOVA	Analysis of variance
APC	Antigen presenting cell
ATG	Autophagy related gene
ATP	Adenosine triphosphate
ATXN3	Ataxin-3
BCL2	B-cell lymphoma 2
BIR	Baculovirus inhibitor of apoptosis protein repeat
BSA	Bovine serum albumin
BTAF1	B-TFIID TATA-BOX binding protein associated factor 1
CAD	Carbamoyl-phosphate synthetase 2, aspartase transcarbamylase and dihydroorotase
CARD	Caspase recruitment domain
CARKL	Carbohydrate kinase-like protein
CBP	CREB-binding protein
CCD	Coiled-coil domain
CCL	Chemokine (C-C motif) ligand
CD	Crohn's disease
CD4	Cluster of differentiation 4
CD8	Cluster of differentiation 8
cDC	Classical dendritic cell
CHAPS	(3-((3-cholamidopropyl)dimethylammonio)-1-propanesulfonate)
CHIP	C terminus of HSC70-interacting protein
cIAP	Cellular inhibitor of apoptosis protein
CK	Casein kinase
CLR	C-type lectin receptor
CMA	Chaperone mediated autophagy
CNS	Central nervous system
CT	Cycle threshold
CXCL	Chemokine (C-X-C motif) ligand
CYLD	Cylindromatosis (turban tumour syndrome)
DAMP	Danger associated molecular pattern
DAPI	4',6-diamidino-2-pheylindole
DNA	Deoxyribonucleic acid
DRP1	Dynamin related protein 1
DSS	Dextran sulphate sodium

DUB	Deubiquitinase
DYNLT3	Dynein light chain Tctex-type 3
ECSIT	Evolutionary conserved signalling intermediate in Toll pathways
EDTA	Ethylenediaminetetraacetic acid
ELISA	Enzyme linked immunosorbent assay
ELOV1	Elongation of very long chain fatty acids protein 1
ER	Endoplasmic reticulum
ERAD	Endoplasmic reticulum-associated protein degradation
ERK	Extracellular signal-regulated kinase
ERRα	Oestrogen-related receptor-α
ETC	Electron transport chain
FACS	Fluorescence activated cell sorting
FAO	Fatty acid oxidation
FAR2	Fatty acyl-CoA reductase 2
FASN	Fatty acid synthase
FCS	Foetal calf serum
FDR	False discovery rate
FS	Frame shift
FTD	Frontotemporal dementia
GABARAP	GATE-16/γ-aminobutyric acid receptor-associated family
GAPDH	Glyceraldehyde-3-phosphate dehydrogenase
GRIM-19	Gene associated with retinoic and IFN-induced mortality 19 protein
GSK3β	Glycogen synthase kinase 3β
GTP	Guanosine triphosphate
HBS	Hanks buffered saline
HD	Helical domain
HDAC6	Histone deacetylase 6
HEK293	Human embryonic kidney cells
HIF	Hypoxia inducible factor
HMGB1	High mobility group box protein 1
HRE	Hypoxia responsive element
HSP	Heat shock protein
IEC	Intestinal epithelial cell
iE-DAP	d-glutamyl-meso-diaminopimelic acid
IKK	Inhibitor of nuclear factor kappa-B kinase
IκB	Inhibitor of nuclear factor kappa-B alpha
IL	Interleukin
IFN	Interferon
iNOS	inducible nitric oxide synthase
IP	Immunoprecipitation
IRAK	IL1-R-associated kinase
IRE1α	Inositol requiring protein 1 alpha
IRF	Interferon regulatory factor
JNK	c-Jun N-terminal kinase
JOSD	Josephin domain-containing
K	Lysine
kDa	Kilodalton

KO	Knockout
LAMP1	Lysosomal-associated membrane protein 1
LAMTOR1	Late endosomal/lysosomal adaptor, MAPK and MTOR activator 1
LAP	LC3-mediated phagocytosis
LB	Lysogeny broth
LC3	Microtubule-associated protein 1A/1B-light chain 3
LC-MS/MS	Liquid chromatography tandem mass spectrometry
LDS	Lithium dodecyl sulphate
LIR	LC3 interacting region
LPS	Lipopolysaccharide
LRBA	LPS-responsive vesicle trafficking, beach and anchor containing gene
LRR	Leucine rich repeat
LRSAM1	Leucine rich repeat and sterile alpha motif containing 1
LUBAC	Linear ubiquitin chain assembly complex
LVP	Lentiviral particle
MΦ	Macrophage
MAPK	Mitogen activated protein kinase
MAVS	Mitochondrial antiviral signalling protein
MDP	Muramyl dipeptide
MHC	Major histocompatibility complex
MICOS	Mitochondrial contact site and cristae organising structure
MJD	Machado Josephin domain
MMP	Matrix metalloproteinase
moDC	Monocyte derived dendritic cell
mROS	Mitochondrial reactive oxygen species
MS	Mass spectrometry
mtDNA	Mitochondrial DNA
mtND	NADH-ubiquinone oxidoreductase
MTORC1	Mammalian target of rapamycin complex 1
MyD88	Myeloid differentiation primary response 88
NADP	Nicotinamide adenine dinucleotide phosphate
NADPH	Dihydronicotinamide adenine dinucleotide phosphate
NBR1	Neighbour of BRCA1 gene
NDP52	Nuclear dot protein 52
NFκB	Nuclear factor κ B
NLR	Nod-like receptor
NLRC	NLR family, CARD domain containing
NLRP	NLR family, Pyrin domain containing
NLS	Nuclear localisation signal
NO	Nitric oxide
NOD	Nucleotide binding oligomerisation domain
NOX	NADPH oxidase
OCR	Oxygen consumption rate
OPTN	Optineurin
ORMLD3	ORM1-like protein 3
OTU	Ovarian tumour protease
OXPHOS	Oxidative phosphorylation

PAMP	Pathogen-associated molecular pattern
PAGE	Polyacrylamide gel electrophoresis
PBMC	Peripheral blood mononuclear cells
PBS	Phosphate buffered saline
PCA	Principal component analysis
PCAF	p300/CBP-associated factor
pDC	Plasmacytoid dendritic cell
PGC-1	PPARγ-coactivator-1
PGE_2	Prostaglandin E2
PI4P	Phosphatidylinositol-4-phosphate
PINK1	PTEN-induced putative kinase 1
PKA	Protein kinase A
PKM	Pyruvate kinase muscle isozyme
PLD3	Phospholipase D3
PMA	Phorbol 12-myristate 13-acetate
PMN	Polymorphonuclear neutrophils
POLRMT	Mitochondrial RNA polymerase
PPP	Pentose phosphate pathway
PRR	Pattern recognition receptor
PTEN	Phosphatase and tensin homologue
PTM	Post translational modification
PVDF	Polyvinylidene fluoride
PYD	Pyrin domain containing
qRT-PCR	Semi-quantitative reverse transcription polymerase chain reaction
RAC1	Ras-related C3 botulinum toxin substrate 1
RIPK	Receptor interacting serine/threonine protein kinase
RIG-I	Retinoic acid inducible gene 1
RLR	Rig-I-like receptor
RNA	Ribonucleic acid
ROS	Reactive oxygen species
RPLP0	Ribosomal protein, large, P0
RPMI	Roswell Park Memorial Institute-1640
RSV	Respiratory syncytial virus
S	Serine
SAM	Sorting and assembly machinery
SCA	Spinocerebellar ataxia
SDH	Succinate dehydrogenase
SEM	Standard error of mean
SERCA-ATPase	Sarco/endoplasmic reticulum Ca(2+)-ATPase
shRNA	Short hairpin RNA
siRNA	Short interfering RNA
SNARE	Soluble N-ethylmaleimide-sensitive factor attachment protein receptors
SNP	Single nucleotide polymorphism
SRC	Spare respiratory capacity
ssRNA	Single stranded RNA
STAT	Signal transducer and activator of transcription-6

STUB1	STIP1 homology and U-Box containing protein 1
TAK	Transforming growth factor β-activated kinase 1
TANK	TRAF family member associated NFκB activator
TBK	TANK-binding kinase-1
TBST	Tris-buffered saline with Tween-20
TCA cycle	Tricarboxylic acid cycle
TFAM	Mitochondrial transcription factor A
Th1	Type 1 T helper
Th2	Type 2 T helper
Th17	Type 17 T helper
TIR	Toll/interleukin-1 receptor domain
TLR	Toll-like receptor
TNF	Tumour necrosis factor
TOM	Translocase of the outer membrane
TRAF	TNF receptor associated factor
TRAPS	Tumour necrosis factor receptor-associated periodic syndrome
TREG	Regulatory T cell
tRNA	Transfer RNA
TUBE	Tandem ubiquitin binding entity
Ub	Ubiquitin
UBA	Ubiquitin binding domain
UCH	Ubiquitin C-terminal hydrolase
UCP2	Mitochondrial uncoupling protein 2
UIM	Ubiquitin interacting motif
ULD	Ubiquitin like domain
ULK1	Unc-5 like autophagy activating kinase-1
UPR	Unfolded protein response
USP	Ubiquitin specific protease
V-ATPase	Vacuolar-type H+-ATPase
VCP/p97	Valosin containing protein
VEGF	Vascular endothelial growth factor
WH	Winged helix domain
WT	Wild type
XBP1	X-box binding protein 1
XIAP	X-linked inhibitor of apoptosis protein

Table of Contents

Abstract **1**

1 Introduction **2**
1.1 Innate immunity **2**
1.1.1 Overview of the innate immune system 2
1.1.2 Pattern recognition receptors 2
1.1.3 Toll-like receptors 3
1.1.4 Toll-like receptor 2 4
1.1.5 Nod-like receptors 5
1.2 The NOD2 receptor **7**
1.2.1 Overview of NOD1 and NOD2 7
1.2.2 NOD2 receptor expression 7
1.2.3 NOD2 receptor structure, ligand binding and activation 8
1.2.4 NOD2 signalling pathways 9
1.2.5 Consequences of NOD2 activation 12
1.2.6 The role of NOD2 in autophagy 13
1.2.7 The interrelationship of NOD2 and Toll-like receptors 17
1.3 NOD2 in disease **19**
1.3.1 Mutations in NOD2 are associated with Crohn's disease 19
1.3.2 Mechanisms of NOD2 associated Crohn's disease pathogenesis 20
1.3.3 NOD2 in other diseases 24
1.4 Immunometabolism and the inflammatory microenvironment **26**
1.4.1 The concept of immunometabolism 26
1.4.2 The inflammatory microenvironment 26
1.5 Hypoxia-inducible Factor **29**
1.5.1 Hypoxia-inducible Factor structure and regulation 29
1.5.2 The role of HIF1α in immunity 31
1.6 Metabolic reprogramming **34**
1.6.1 Metabolic reprogramming in macrophages 34
1.6.2 Metabolic reprogramming in dendritic cells 38
1.7 The role of mitochondria in immunity **40**
1.7.1 The origin and structure of mitochondria 40
1.7.2 Mitochondrial dynamics 40
1.7.3 Mitochondrial reactive oxygen species 41
1.7.4 Mitochondria provide a structural hub for immune signalling 43
1.7.5 Activation of the immune response following mitochondrial damage 43
1.7.6 Mitochondria and Crohn's disease 44
1.8 Ataxin-3 ..... **46**
1.8.1 Mutations in ataxin-3 cause neurodegenerative disease 46
1.7.2 Ataxin-3 cellular location 46
1.8.3 Ataxin-3 structure and post-translational modification 47
1.8.4 The deubiquitinating function of ataxin-3 49
1.8.5 Additional roles of ataxin-3 in DNA repair and transcriptional regulation 52
1.8.6 Ataxin-3 and autophagy 53
1.9 Aims and objectives of this thesis **55**

2 Materials and Methods 57
2.1 Cell culture 57
2.1.1 Cell culture media 57
2.1.2 Cell culture conditions 58
2.1.3 Isolation of human peripheral blood mononuclear cells and generation of monocyte derived dendritic cells 58
2.1.4 Isolation of murine bone marrow derived mononuclear cells and generation of bone marrow derived macrophages 59
2.1.5 Culture of cell lines 60
2.1.6 Freezing, storage and thawing of primary cells and cell lines 61
2.2 Protein biology techniques 61
2.2.1 Cell lysis 61
2.2.2 Protein quantification by the Bicinchoninic acid assay 62
2.2.3 Protein quantification by the Bradford assay 62
2.2.4 Polyacrylamide gel electrophoresis 63
2.2.5 Immunoblotting 63
2.2.6 Silver staining 64
2.2.7 *In vitro* kinase assay (non-radioactive) 65
2.2.8 Enzyme-linked immunosorbent assay 65
2.2.9 Subcellular fractionation 66
2.2.10 Phosphoprotein purification 66
2.2.11 Immunoprecipitation 67
2.2.12 Immunoprecipitation – Protein G agarose beads protocol 68
2.2.13 Tandem ubiquitin binding entities (TUBEs) ubiquitin immunoprecipitation 70
2.2.14 Sample preparation for liquid chromatography tandem mass spectrometry 71
2.2.15 Liquid chromatography tandem mass spectrometry sample analysis 72
2.2.16 Analysis of mass spectrometry data 74
2.3 Nucleic acid techniques 75
2.3.1 DNA isolation 75
2.3.2 Mitochondrial DNA copy number quantification 75
2.3.3 RNA isolation 76
2.3.4 Reverse transcription 77
2.3.5 Quantitative real time polymerase chain reaction 77
2.3.6 DNA transformation and amplification 78
2.3.7 DNA maxiprep 79
2.3.8 Site directed mutagenesis 79
2.3.9 Adherent cell transfection 81
2.3.10 Electroporation of human monocyte derived dendritic cells 81
2.3.11 Lentivirus particle production 82
2.3.12 Lentiviral transduction and stable cell-line selection 83
2.4 Cellular techniques 84
2.4.1 Flow cytometry 84
2.4.2 Confocal immunofluorescence microscopy 85
2.4.3 Seahorse mitochondrial stress assay 86
2.4.4 Bacterial killing assay 88
2.5 Phosphatidic acid quantification 90
2.6 Statistical analysis 91

2.7 Materials Appendix 92

3 Interrogation of NOD2/TLR2 signalling through quantitative phosphoproteomics

3.1 Introduction 96

3.1.1 Protein phosphorylation is an important post-translational modification 96

3.1.2 Quantitative phosphoproteomics allows the dissection of signalling pathways.. 98

3.2 Aims 99

3.3 Results 99

3.3.1 NOD2 signalling is enhanced in hypoxia and interacts with HIF1α 99

3.3.2 Quantitative phosphoproteomics screen of NOD2/TLR2 signalling in hypoxia.. 105

3.3.3 Selection and validation of candidate proteins 111

3.3.4 Preliminary investigation of the functional relevance of validated proteins 116

3.4 Discussion 123

4 Defining the NOD2/TLR2 driven ataxin-3 signalling axis and interactome

4.1 Introduction 131

4.2 Aims 132

4.3 Results 132

4.3.1 Ataxin-3 is phosphorylated by NOD2 and TLR2 both in isolation and synergistically, and by other PRRs 132

4.3.2 RIPK2 and TBK1 are required for NOD2 induced ataxin-3 phosphorylation 134

4.3.3 Ataxin-3 phosphorylation by NOD2/TLR2 does not lead to nuclear migration. 138

4.3.4 NOD2/TLR2 stimulation leads to phosphorylation of ataxin-3 at S265 138

4.3.5 Identification of novel ataxin-3 binding partners 146

4.4 Discussion 151

5 Exploration of the roles of ataxin-3 in NOD2/TLR2 mediated immunity

5.1 Introduction 156

5.1.1 Ubiquitin signalling is critical to the immune response 156

5.1.2 The ataxin-3 knockout mouse 158

5.2 Aims 160

5.3 Results 160

5.3.1 Ataxin-3 is required for mitochondrial respiration and mROS generation 160

5.3.2 Ataxin-3 may be important for NOD2 driven autophagy 171

5.3.3 The deubiquitinating role of ataxin-3 is important in monocytes following NOD2/TLR2 stimulation 176

5.3.4 Investigation of the functional importance of ataxin-3 in a KO mouse model... 188

5.4 Discussion 191

6 Concluding discussion

6.1 Introduction 196

6.2 Dissection of NOD2 signalling in hypoxia 197

6.3 Defining the signalling cascade and phosphorylation site of ataxin-3 198

6.4 The interacting partners of ataxin-3 200

6.5 The immune function of ataxin-3 201

6.6 Wider implications – the links to neurodegeneration 203

6.7 Closing remarks and future experiments 206

7 Bibliography 209

8 Appendix 252

Abstract

Pattern recognition receptors (PRRs) recognise foreign antigen to direct innate and adaptive immune responses against invading pathogens. Polymorphisms in the PRR NOD2 represent the strongest genetic risk factor for the inflammatory bowel disease Crohn's, and thus this bacterial sensor is the focus of particular research interest. By recapitulating the hypoxic conditions encountered at sites of inflammation, this study utilised quantitative phosphoproteomics to identify novel downstream signalling hubs of NOD2 and its synergistic partner Toll-like receptor 2 (TLR2). The deubiquitinase ataxin-3 was identified as being phosphorylated on serine 265, and this was mediated by RIPK2 and TBK1. Ataxin-3 was found to associate with the mitochondrial inner membrane protein MIC60, with ataxin-3 depletion leading to dysregulation of mitochondrial DNA transcript expression and impaired oxidative phosphorylation, demonstrating a novel mitochondrial role. Interrogation of the ataxin-3 regulated ubiquitome in response to NOD2/TLR2 triggering revealed a broader immunometabolic function for ataxin-3, with the metabolism related proteins HIF1a, phospholipase D3 and LAMTOR1 identified as novel DUB targets. Ataxin-3 depleted cells show defects in PRR triggered autophagic flux, mitochondrial ROS generation and bacterial killing, suggesting the importance of this protein in the innate immune response.

Chapter 1: Introduction

1.1 Innate immunity

1.1.1 Overview of the innate immune system

Host responses to invading pathogens are essential physiological reactions of all living organisms. The innate immune system represents the first line of defence against pathogens, providing an immediate response to infection, and is conserved throughout evolution.[1, 2] In vertebrates, the innate immune system also serves to prime the adaptive immune system, generating long lasting immunological memory. The critical importance of the innate immune system is underlined by the observation that defects are almost always lethal to the host.[1]

The innate immune system faces two key challenges. Firstly, it is faced with a near constant barrage of microorganisms. Secondly, it must accurately and rapidly discriminate between non-infectious self and infectious pathogen. To achieve this, it relies upon a relatively small number of pattern recognition receptors (PRRs) that recognise features common to many pathogens, known as pathogen-associated molecular patterns (PAMPs).[1] PAMPs are typically critical for survival of the pathogen and thus cannot be mutated by the pathogen to avoid detection; consequently they are often invariant across entire classes of pathogens.[3]

1.1.2 Pattern Recognition Receptors

PRRs are germline encoded receptors that are expressed on the cell surface, in intracellular compartments such as the cytosol or endosomes, or secreted into serum or tissue fluid.[4] Pattern recognition receptors are classified according to their function, localisation and ligand specificity. Two main classes of PRRs have been described in mammalian cells,

namely membrane bound receptors including Toll-like receptors (TLRs) and C-type lectin receptors (CLRs), and cytoplasmic receptors including NOD-like receptors (NLRs) and RIG-I-like receptors (RLRs). The varied location of PRRs provides the ability to detect pathogens invading a range of cellular compartments. Multiple PRRs are capable of recognising a single microorganism which may present a broad array of antigenic ligands, ensuring a robust immune response even if a specific PRR or its signalling pathway is targeted by the organism. Further, and as discussed in more detail later, PRRs often act in synergy allowing rapid amplification of the initial immune response, or may regulate each other's actions.

1.1.3 Toll-like receptors

The best characterised PRRs are the TLRs[5]. First identified in *Drosophila*,[6] to date 11 separate receptors have been identified in humans, classified as TLR1 - 10, with human TLR11 believed to be a pseudogene.[7] A further two TLRs, TLR12 and TLR13 have been described in mice, but are not found in humans.[8]

Receptor	Location	Ligand(s)	Ligand origin
TLR1	Cell membrane	Triacyl lipopeptides	Bacteria
TLR2	Cell membrane	Diacyl lipopeptides Lipoteichoic acid Peptidoglycan Zymosan Glycolipids Glycoprotein	Bacteria Bacteria Bacteria Fungi Protozoa Viruses
TLR3	Endosome	Double stranded RNA	Viruses
TLR4	Cell membrane	Lipopolysaccharide	Bacteria
TLR5	Cell membrane	Flagellin Profilin	Bacteria *Toxoplasmosis gondii*
TLR6	Cell membrane	Diacyl lipopeptides	Bacteria Fungi
TLR7	Endosome	Single stranded RNA	Viruses
TLR8	Endosome	Single stranded RNA	Viruses
TLR9	Endosome	CpG DNA	Bacteria Viruses
TLR10	Endosome	Unknown	Unknown

Table 1. Human TLRs, their location, ligands and ligand origin.

In addition to the pathogen derived ligands described in Table 1, it is important to note that PRRs also recognise host derived endogenous ligands known as danger-associated molecular patterns (DAMPs). These endogenous danger response signals, such are uric acid and HMGB1, are released by stressed cells upon necrosis to promote an innate immune response through activation of PRRs.[9, 10]

1.1.4 Toll-like receptor 2

Given the particular importance of TLR2 to the work contained in this thesis, the structure and signalling of TLR2 is now covered in more detail. TLR2 is a membrane bound receptor that acts at the cell surface to recognise a wide variety of PAMPs including the acylated amino terminus of bacterial lipoproteins, mimicked by its synthetic ligand PAM_3CSK_4[11]. It is expressed widely and found in all major cells of the immune system, epithelial cells including the intestinal epithelium, and microglia and other cells of the brain[11]. The basic structure of TLR2 is shared with other TLRs, comprising a leucine rich repeat (LRR) extracellular domain and the cytoplasmic Toll/interleukin-1 receptor (TIR) domain. TLRs can exist as dimers[12]. In the case of TLR2, it heterodimerises with TLR1 to recognise triacylated lipopeptides[13], or with TLR6 to recognise diacylated lipopeptides[14], both of which arise from bacteria. Following dimerisation, the activation of TLR2 results from the TIR domain associating with a TIR domain containing adapter, MyD88. MyD88 recruits IRAK-4, with phosphorylation of IRAK-1 and activation of TAK1 through TRAF6[15]. TAK1 then activates the IKK-complex-NFκB and MAPK pathways resulting in NFκB, ERK1/2, p38 and JNK signalling[11]. TLR2 can also signal through a MyD88/RIPK2 axis[16, 17].

1.1.5 NOD-like receptors

The NLR family of proteins are cytosolic pattern recognition receptors that sense a diverse range of microbial structures such as peptidoglycan and flagellin, and also endogenous danger signals, to trigger innate immune activation.[18, 19] NLRs are highly conserved throughout evolution, with NLR orthologues present in plant R genes.[20] To date at least 23 human and 34 murine NLR genes have been identified, although the precise function of many is not yet understood.[21]

NLRs consist of three domains – an N-terminal protein interaction domain, a central nucleotide-binding domain (NOD) and a C terminal leucine rich repeat (LRR). The NLRs are divided into four subfamilies on the basis of their N-terminal effector domains: NLRA, acidic domain containing (AD); NLRB, Baculovirus inhibitor of apoptosis protein repeat (BIR) domain containing; NLRC, Caspase recruitment domain (CARD) domain containing; NLRP, pyrin domain containing (PYD). NLRX represents other NLR genes with no significant homology to the N-terminal domain of the other NLR subfamilies.[21]

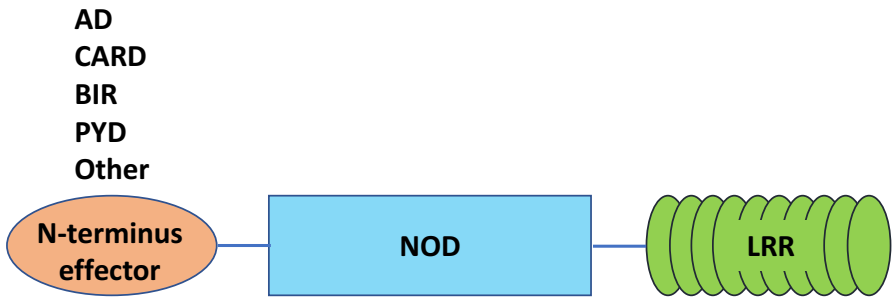


Figure 1.1 Basic structure of the NLRs. The simplified tripartite modular structure of human NLRs is shown.

Functionally, the NLR family can be divided into further subgroups related to inflammasome assembly, autophagy, antigen presentation, signalling transduction and transcription activation[22]. The N-terminus effector domain that mediates protein-protein interactions is important in determining function, for example the pyrin domain of the NLRP subfamily allows binding and activation of the caspase-1 inflammasome, while the CARD domain of the NLRC subfamily binds and activates the serine-threonine kinase RIPK2, activating downstream NFκB and MAPK signalling pathways[23, 24]. The LRR domain is required for binding and detection of ligands, and consists of leucine-rich amino acid strands forming a peptide loop.

The NOD domain, which has ATPase activity, is required for self-oligomerisation of NLRs following binding of ligand to the LRR domain, likely facilitating binding and activation of downstream effector molecules via the N-terminus effector domain[25]. The structural diversity of the LRR and N-terminus effector domains allows NLRs to interact with a wide array of ligands and binding partners, activating a broad range of signalling pathways. This breadth of role is reflected in the wide variety of human diseases that result from mutations in NLR encoding genes[26].

1.2 The NOD2 receptor

1.2.1 Overview of NOD1 and NOD2

Two related members of the NLR family, NOD1 and NOD2, are critical for the innate immune response to many bacterial infections. Both NOD1 and NOD2 respond to distinct structural motifs derived from intracellular peptidoglycan, a fragment of bacterial cell walls. NOD1 recognises the dipeptide d-glutamyl-meso-diaminopimelic acid (iE-DAP), present in all Gram-negative, and a limited number of Gram-positive bacteria such as *Listeria* spp. and *Bacillus* spp[27, 28]. In contrast, NOD2 recognises muramyl dipeptide (MDP), the largest fraction of peptidoglycan consisting of one carbohydrate and two amino acids, present in all Gram-negative and Gram-positive bacteria[29]. In 2001, NOD2 was the first gene found to be associated with the inflammatory bowel disease Crohn's, and it remains one of the strongest genetic risk factors[30, 31]. Consequently, it is one of the most well studied NLRs.

1.2.2 NOD2 receptor expression

NOD2 is expressed in cells of the gastrointestinal tract, specifically Paneth cells[32], intestinal epithelial cells[33], stem cells[34] and stromal cells[35]. It is also expressed in the haematopoietic compartment in monocytes derived cells including dendritic cells and macrophages[36], and T lymphocytes[37]. Importantly, given the later described links in this thesis to neurodegenerative disease, functional expression of NOD2 has also been described in resident central nervous system cells including microglia[38] and astrocytes[39].

NOD2 predominantly resides in the cytosol, and lacks a transmembrane domain. However, it is clear that NOD2 can also function at the plasma membrane, with the C-terminal end of the protein responsible for membrane targeting[40, 41]. Indeed, in intestinal epithelial cells,

membrane targeting of NOD2 is required for NFκB activation by MDP[40]. NOD2 also recruits the autophagy protein ATG16L1 to the plasma membrane at the site of bacterial entry to drive autophagy[342]. It remains unclear where NOD2 engages ligand in other cellular locations, such as ligand from endosome resident bacteria including *Salmonella enterica* serovar Typhimurium[43].

1.2.3 NOD2 receptor structure, ligand binding and activation

NOD2 consists of an LRR domain, a central NOD domain and an N-terminal effector domain that contains two CARDs in tandem. Extrapolation of the recently solved crystal structure of NLRC4 predicts that the NOD domain is followed by a proximal helical domain (HD1), a winged-helix domain (WH) and a distal helical domain (HD2)[44]. The ADP-mediated interaction between the NOD domain and WH help stabilise a closed, autoinhibited conformation, with the LRR occluding these two domains and maintaining a monomeric state[44, 45].

The precise mechanisms by which MDP enters cells and activates NOD2 remains uncertain, but a number of entry routes have been described: 1) phagocytosis of bacteria and degradation into fragments including MDP, 2) shedding of peptidoglycan by invasive bacteria[46] 2) uptake of peptidoglycan fragments from bacteria derived extracellular outer membrane vesicles[47], 3) endocytosis[48], 4) transport across host membranes through bacterial secretion systems or channels[45, 49]. The relative importance of these varied mechanisms is likely to differ depending on the host cell type. Taken together, these mechanisms suggest that NOD2 may be able to sense extracellular bacteria, significantly expanding upon its classically described role as a sensor of invading cytosolic bacteria[43].

The ability of soluble MDP to stimulate NOD2 *in vitro* further supports the presence of routes of direct entry for the ligand[45].

Although it was initially uncertain whether MDP binds directly to NOD2 once it has reached the cytosol, recent reports support a direct interaction but do not exclude the requirement for accessory molecules[50, 51]. It is generally believed that recognition is mediated by the LRR domain, although a potential role for the NOD domain has also been suggested[51]. A mechanism has been proposed whereby ATP binding to NOD2 leads to homo-oligomerisation and enhances MDP binding and subsequent signal transduction[51]. It is likely that HD2 is required to mediate NOD2 conformational change to an open activated structure upon ligand binding[44]. However, further structural data is required to confirm the mechanism of NOD2 activation.

1.2.4 NOD2 signalling pathways

Following MDP binding and conformational change of NOD2 to an open structure and homo-oligomerisation, NOD2 recruits receptor interacting serine/threonine protein kinase 2 (RIPK2) via interaction between their CARD domains[16, 45]. The NOD2-RIPK2 signalling axis has been extensively studied and mapped for two reasons. Firstly, RIPK2 is essential for NOD2 signalling, as evidenced by the failure of RIPK2-deficient murine macrophages to respond to MDP[52]. Secondly, engagement of RIPK2 distinguishes NOD2 signalling from related TLR mediated signalling pathways.[43]

Post-translational modification of RIPK2 is critical for its activation. RIPK2 is polyubiquitylated with lysine-63-linked polyubiquitin chains by E3 ubiquitin ligases cIAP1

and cIAP2[53]. It was initially suggested that TRAF6 was also required[54], but subsequent work has cast doubt on its importance[53]. A third E3 ubiquitin ligase XIAP is however definitively involved[55, 56], and recruits the linear-chain ubiquitin assembly complex LUBAC to the NOD2-RIPK2 complex[57]. It is noteworthy that mutations in XIAP are independently associated with Crohn's disease in males[58]. Activated RIPK2 also undergoes autophosphorylation on S176 and Y474, enhancing downstream signalling[59].

The stable ubiquitination of RIPK2 leads to the recruitment and activation of the kinase TAK1[45]. This activated TAK1 complex interacts with the simultaneously bound IKK complex, ubiquitinating and degrading IKKγ, which allows IKKα and IKKβ to phosphorylate IκKBα (NFκB inhibitor IκB)[49]. Phosphorylated IκKBα is degraded, allowing the translocation of NFκB to the nucleus and inflammatory gene transcription[45, 60]. In addition to NFκB pathways, NOD2 activation via RIPK2/TAK1 also activates the MAPK regulated extracellular ERK1/2, JNK and p38[16]. NOD2 can also activate p38 and JNK via CARD9[61]. The NOD2 signalling cascade is presented in simplified form in Figure 1.2.

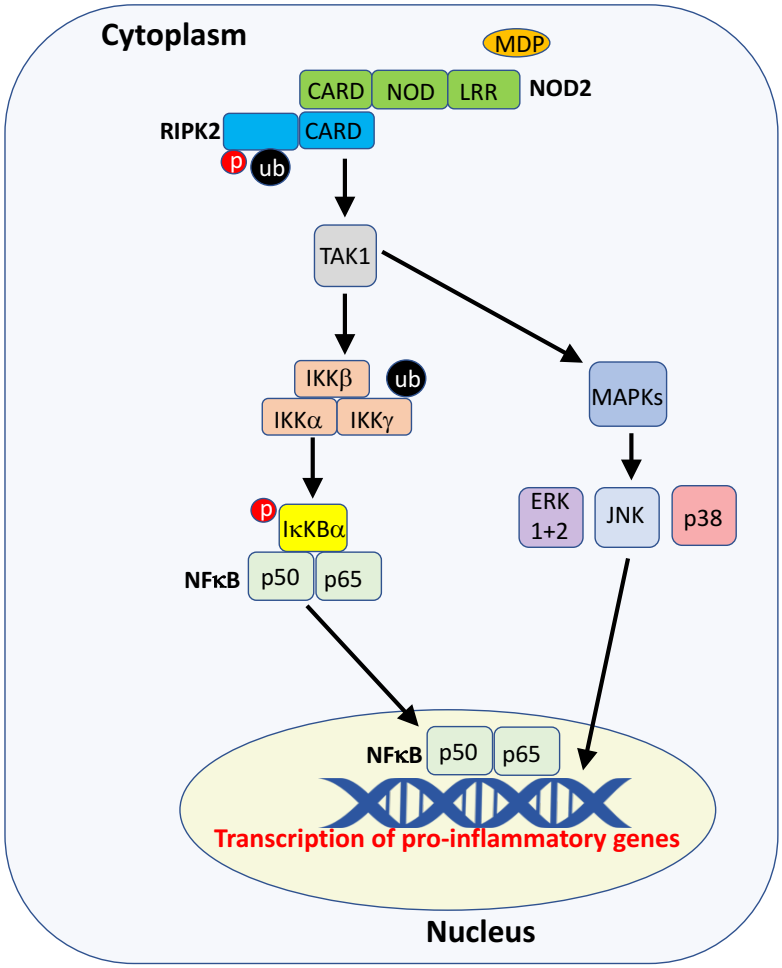


Figure 1.2 The NOD2 signalling cascade. MDP triggers a NOD2/RIPK2 interaction, leading to TAK1 recruitment and activation of the IKK complex and MAPK pathway. The IKK complex allows nuclear translocation of NFκB, while MAPKs activate ERK, JNK and p38 dependent pathways, leading to the transcription of pro-inflammatory genes.

More recently, it has been shown that NOD2 is able to respond to PAMPs other than MDP, most notably viral ssRNA[62]. This results in a quite separate RIPK2 independent signalling pathway, mediated by the mitochondrial anti-virus signalling protein (MAVS). Engagement of MAVS at the mitochondria leads to a signalling cascade involving interferon regulatory factor 3 (IRF3) that produces interferon-β[62]. It was shown *in vitro* that NOD2 drives type 1 IFN production in response to a range of viruses containing an ssRNA genome including respiratory syncytial virus (RSV) and influenza virus[62]. This was confirmed *in vivo,* with

NOD2 knockout mice demonstrating an increased susceptibility to infection with RSV or influenza, although this has not yet been shown in humans with NOD2 patients[62].

Much remains to be understood about how NOD2 signalling pathways are regulated, but it is clear that a complex system of protein-protein interactions underlies this. In addition to the actions of the E3 ligases described above, roles for TRAF 2, 4 and 5 have been described[60, 63]. NOD2 signalling can also be fine-tuned by the removal of ubiquitin. An important example is the action of ovarian tumour (OTU) deubiquitinase A20, which inhibits NOD2 signalling by regulating the MDP induced ubiquitination of RIPK2[64].

Additional negative regulators include erbin, that directly binds to NOD2 and inhibits MDP signalling[65], rac1 GTPase[66] and RIG-I[67]. In contrast, GRIM-19[33], a cell death protein, and CARD9[61] positively regulate NOD2 signalling. It appears that the cytoskeleton plays a key role in modulating NOD2 activity; in addition to cytoskeletal related proteins erbin and rac1 GTPase, the intermediate protein filament vimentin is also important[68]. Intriguingly, three RHO GTPases, including Rac1 GTPase, that play important roles in cytoskeletal modelling, are apparently able to activate NOD2 in the absence of MDP, raising the possibility of NO2 stimulation in the absence of a bacterial pathogen[43, 69].

1.2.5 Consequences of NOD2 activation

Activation of NFκB and MAPK signalling pathways by NOD2 results in an array of innate immune responses. Production of the pro-inflammatory cytokines IL-6, IL8 and TNFα, and the chemokines CXCL1, CXCL2 and CCL5 are stimulated, driving the recruitment and priming of innate immune cells[43, 70]. NOD2 activation also plays a key role in NLRP1 inflammasome

activation and induces IL1-β secretion[71]. In the gut, NOD2 activation leads to the production of antimicrobial compounds, including defensins that are secreted primarily by Paneth cells[72].

The importance of NOD2 in the immune response extends to adaptive immunity. MDP triggering of NOD2 leads to an antigen specific immune response with a Th2-type polarisation profile[73]. NOD2 modulates Th17 responses[74, 75] and is important for induction of both Th1 and Th2 responses following co-stimulation with TLR agonists[73]. *In vivo* murine infection experiments have confirmed the importance of NOD2 in adaptive immunity[76, 77, 78], and demonstrated a T-cell intrinsic role[77].

1.2.6 The role of NOD2 in autophagy

An additional and distinct role for NOD2 is the induction of a form of autophagy, macroautophagy[42, 79], a highly conserved mechanism for the bulk degradation of cellular contents. Macroautophagy is distinguished from the two other primary types of autophagy in mammalian cells, microautophagy and chaperone-mediated autophagy, by the formation of a double membrane bound phagophore and autophagosome[80]. In its most basic form, autophagy represents a cellular adaptation to starvation, and allows the non-specific breakdown of a cell's own constituents to recycle nutrients and balance biosynthetic pathways[81, 82]. This form of autophagy, known as non-selective autophagy, is also induced by cellular stress. However, autophagy can also be utilised by cells in a more precisely targeted process (selective autophagy) for a variety of indications, and indeed is not restricted to "self constituents" as it can target invading pathogens[83]. This important host defence against pathogens, termed xenophagy, can target a range of invasive bacteria

including *Salmonella enterica* serovar Typhimurium, *Listeria monocytogenes, Shigella flexneri* and *Mycobacterium tuberculosis,* as well as bacteria internalised by phagocytosis[84]. Both NOD2 and TLRs can mediate xenophagy. NOD2 specifically directs autophagy by recruiting the autophagy protein ATG16L1, another Crohn's susceptibility gene, to the plasma membrane at the site of bacterial entry, facilitating bacterial trafficking to the autophagosome, through a signalling pathway independent of RIPK2[42]. NOD2 signalling via RIPK2 also upregulates autophagosome formation and increases autophagic flux, further potentiating autophagy[42, 43, 79].

An important event that triggers antibacterial xenophagy and other forms of selective autophagy is ubiquitination[84]. This is driven by E1 (ubiquitin-activating enzyme), E2 (ubiquitin-conjugating enzyme) and E3 (ubiquitin ligase)[84]. To date two E3 ubiquitin ligases have been linked to bacterial ubiquitination – parkin[85] and LRSAM1[86], although it is likely that other E3s are also important. It remains uncertain whether bacteria are ubiquitinated directly or whether the bacteria-containing endosomal vacuole is ubiquitinated following rupture[84]. A further xenophagy trigger is the cytosolic lectin, galectin-8, which monitors endo-lysosomal integrity and clusters on damaged bacteria-containing vacuoles.[87]

Following induction of autophagy, the core pathway of macroautophagy begins with the nucleation of a double membrane phagophore. The origin of the phagophore is a source of considerable debate, with a role proposed for numerous membrane compartments including the endoplasmic reticulum (ER) and the mitochondria[88, 89]. This step, and the subsequent extension of the phagophore into an autophagosome that engulfs the targeted cytoplasmic components requires the autophagy ubiquitin-like protein LC3 (the mammalian

homologue of ATG8)[90]. To date over 40 proteins have been identified as important for macroautophagy, primarily the autophagy-related genes (ATGs) first mapped in yeast[91] with mammalian homologues subsequently described. Broadly, they can be grouped according the stage of autophagy at which they function – 1) Induction 2) Nucleation and expansion 3) Fusion 4) Degradation and efflux[90]. A number of these proteins are involved in the processing of LC3, underlining its importance. The ATG4 protease first cleaves the inactive pro-form of LC3 at its C-terminus to generate the cytosolic LC3-I. LC3-I is then conjugated to phosphatidylethanolamine (PE) in the phagophore membrane by ATG3 and 7, producing the lipidated LC3-II, which initiates the formation and maturation of the autophagosome. A critical role of LC3 is to recruit other autophagy proteins to the autophagosome, including the ULK1 kinase[90, 92] and ATG13[90]. This typically requires an LC3-interacting region (LIR), characterised by a WXXI/L sequence, with tryptophan (W) beginning the sequence, any two amino acids (XX) following, and either isoleucine (I) or leucine(L) two residues downstream[93]. A number of LIR containing autophagy proteins also contain a ubiquitin-binding domain (UBA), allowing recruitment of the aforementioned ubiquitinated targets to the autophagosome. Important examples in xenophagy are p62 (SQSTM1)[94], NDP52[95], NBR1[96] and optineurin (OPTN)[97]. Additionally, and vital to the concept of xenophagy, an LC3-decorated single membrane phagosome may also become sequestered within an autophagosome[98]. This type of xenophagy is restricted to phagocytic cells (macrophages, dendritic cells and neutrophils).

During the process of autophagosome maturation, LC3-II is deconjugated by ATG4 and thus released from the outer membrane. In contrast, the GATE-16/γ-aminobutyric acid receptor-associated family (GABARAPs) appear important for the maturation of the

autophagosome[99]. Following closure and maturation, the autophagosome progresses towards fusion with the lysosome. The autophagosome may fuse with a late endosome forming an amphisome[100], which subsequently fuses with a lysosome to generate an autolysosome. Alternatively, an autophagosome may fuse directly with a lysosome, and this should also be termed an autolysosome[101]. In contrast, when a phagosome is incorporated into an autophagosome and fuses with a lysosome, this should be distinguished as an autophagolysosome[101]. The term autophagolysosome also describes the fusion of an LC-decorated phagosome with a lysosome[102], a process independent of autophagy termed LC3-mediated phagocytosis (LAP), but which shares a number of overlapping features with autophagy.

Three protein families are key to the process of autophagosome-lysosome fusion. Rab GTPases localise to the membranes of both structures, recruiting membrane-tethering complexes that bridge the autophagosome to the lysosome. Soluble N-ethylmaleimide-sensitive factor attachment protein receptors (SNAREs) then drive the fusion of the opposing lipid bilayer membranes[103]. In addition, GABARAPs also regulate modulate autophagosome-lysosome fusion by regulating the generation of phosphatidylinositol-4-phosphate (PI4P)[104]. Once fused, lysosomal hydrolases digest the contents of the autophagolysosome.

In addition to direct killing of microbial pathogens, NOD2 mediated autophagy fulfils other important immune roles. Autophagy regulates the NLR inflammasome mediated production of IL-1β and IL18. Following viral infection, the NOD2-RIPK2 axis suppresses activation of the NLRP3 inflammasome, by limiting the accumulation of damaged

mitochondria through ULK1 via another selective form of autophagy, mitophagy[105]. In adaptive immunity, it Is required for the generation of major histocompatibility complex (MHC) class II antigen-specific CD4+ T cell responses, through the processing of antigen via autophagic degradation.[79, 106] Intriguingly, the interaction between NOD2 and ATG16L1 is also able to regulate inflammatory responses independently of autophagy. ATG16L1 can suppress inflammatory cytokine release induced by NOD2 by interfering with the recruitment of RIPK2[107].

1.2.7 The interrelationship of NOD2 and Toll-like receptors

A complex interplay between PRRs provides cross-regulation of innate immune receptor signalling, and can both amplify or suppress the immune response[108]. The intricacy of this interrelationship results from the varied array of PRR ligands, many of which may arise from the same pathogen, and the divergent signalling pathways they may simultaneously induce[108]. Synergistic signalling results from NOD2 acting together with a number of PRR-mediated pathways including NOD1, TLR2, TLR3, TLR4 and TLR9 to boost production of a range of both pro and anti-inflammatory cytokines (Il-6, IL-8, TNF, IL-1β and IL-10) in antigen presenting cells[25, 109, 110, 111]. The cross-talk between NOD2 and TLR2 is perhaps the most important, and certainly the best described. Their close relationship is not surprising given that both respond to ligands derived from the same bacterial component, peptidoglycan. Although the precise mechanisms of cross-regulation are not well understood, both NOD2 and TLR2 activate separate upstream signalling cascades to recruit the same MAPK and NFκB pathways which play a central role in cytokine production[108]. NOD2 and TLR2 also collaborate in adaptive immune roles, and they have been shown to cooperatively regulate the functional maturation of DCs[112].

As the synergistic crosstalk between NOD2 and PRRs including TLR2 risks overactivation of the immune system with potentially deleterious consequences, it is unsurprising that suppressive mechanisms have also evolved[108]. NOD2 signalling inhibits TLR2 activation of the NFκB c-Rel, suppressing Th1 driven responses[113]. Importantly, and potentially of direct relevance to the pathogenesis of Crohn's disease, loss of NOD2 inhibition of TLR2 mediated pathways increased susceptibility to antigen-specific colitis in a murine model[114]. A further study suggested that very high doses of MDP downregulate cytokine responses of TLR2 primed monocytes, providing a further safety mechanism for high bacterial burdens, which may be lost in NOD2 mutation Crohn's patients.[115].

1.3 NOD2 in disease

1.3.1 Mutations in NOD2 are associated with Crohn's disease

While over 70 CD susceptibility genes have been mapped, NOD2 remains the strongest association by far in genetic studies[30, 31, 116, 117]. CD is a lifelong, debilitating inflammatory bowel disease that represents a global health problem, but in the UK alone it affects approximately 100,000 patients[118]. It causes significant morbidity with an associated heavy socioeconomic burden. Although treatment with current pharmacological agents can control disease, relapse is common and most patients will eventually require surgery[119, 120].

Three variants, which either occur in or adjacent to the LRR region critical for MDP sensing, account for more than 80% of the identified NOD2 variants[121, 122]. These are the single nucleotide polymorphisms (SNPS) R702W [SNP8], G908R [SNP12] and the frameshift polymorphism 1007fs [SNP13], with the 1007frameshift resulting in a truncated NOD2 protein and causing the most significant impairment to MDP sensing. A further important variant, P268S [SNP5] lies in the region between the NOD and CARD domains[122]. The location of these mutations within the protein structure of NOD2 are displayed in Figure 1.3. Use of deep sequencing in larger cohorts has recently identified other rarer NOD2 variants associated with CD[123]. Individuals who carry just one variant show only a small increase in risk of CD, but homozygotes or compound heterozygotes show a 20 to 40 fold increased risk[124]. The relative risk conferred by specific NOD2 variants differs between populations[125]. Importantly, the penetrance of these risk phenotypes is low, supporting the concept that a cumulative burden of additional gene mutations, environmental factors and the gut microbiota are required for development of NOD2 associated CD[45, 124]. However, the importance of NOD2 in Crohn's is not limited to aetiology, as research suggests that NOD2

variants also predict clinical course, with the presence of 2 NOD2 mutations providing a 98% specificity for complicated disease[116].

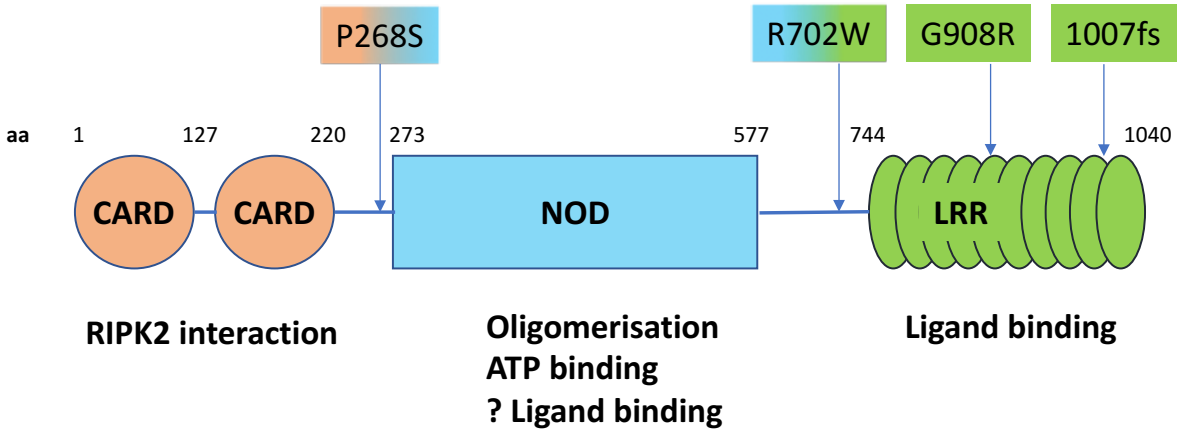


Figure 1.3 Structure of NOD2 and position of the most common mutations in Crohn's disease. The amino acid (aa) positions of each domain are also indicated.

1.3.2 Mechanisms of NOD2 associated Crohn's disease pathogenesis

The precise mechanisms through which NOD2 variants contribute to Crohn's disease are still uncertain, and indeed there remains debate over whether CD associated variants confer a gain or loss-of-function. Initial evidence for a gain-of-function came from experiments on knock-in mice homozygous for the equivalent of the human 1007fs variant. Mutant macrophages showed elevated NFκB response to MDP and enhanced processing and secretion of IL-1β, with parallel *in vivo* experiments demonstrating more severe colonic inflammation in the mutant mice on dextran sulphate sodium (DSS) challenge[126]. However, these mice were subsequently found to have an additional duplication of the 3' end of the NOD2 locus which was targeted by the mutation, casting some doubt on the proposed gain-of-function[127]. Indeed a separate mouse model, which also examined an equivalent of the human 1007fs variant, demonstrated a loss-of-function with impaired IL-6 and TNFα

production[128]. This loss-of-function phenotype is consistently described in monocytes from patients homozygous for CD associated NOD2 variants, which show impaired pro-inflammatory cytokine release on MDP triggering[129, 130, 131]. Patients with the 1007fs show the most significant impairment in MDP driven cytokine production, with those carrying the R702W or G908R demonstrating a more modest impairment, supporting a varying MDP sensitivity depending on the mutation[132]. One loss-of-function hypothesis suggests that NOD2 mutations result in ineffective sensing and clearance of bacterial pathogens, perpetuating inflammation through NOD-2 independent pathways[45]. Further, NOD2 may regulate the important anti-inflammatory cytokine IL-10, with impaired MDP driven IL-10 transcription reported in DCs from patients with NOD2 associated CD[133]. Reduced IL-10 levels may further exacerbate the inflammation seen in CD.

Various models have been proposed to explain how loss-of-function might translate into intestinal inflammation. As monocytes and neutrophils are recruited to the intestine, impairment of their NOD2 mediated immune roles is likely to be important when bacteria are encountered. Further, a number of cell types resident in the gastrointestinal tract, and essential for maintaining intestinal homeostasis, express NOD2. Paneth cells, located in crypts of the small intestine and the primary producers of the antimicrobial peptide α-defensin, are one example. It has been proposed that patients with NOD2 associated CD demonstrate impaired α-defensins production[134]. The importance of Paneth cells to the aetiopathogenesis of Crohn's is suggested by their restricted expression to the ileum, which corresponds to the primary site of inflammation in NOD2 associated CD[32]. However, it has also been suggested that reduction in α-defensins are independent of NOD2 status and result from loss of surface epithelium due to the generalised inflammation seen in CD[135]. It

has been proposed that loss of antimicrobial peptides and goblet cell alterations in intestinal crypts might both impair intestinal barrier function and alter the resident gut microbiota, resulting in an accumulation of pathogenic bacteria that trigger CD[70, 136]. However other work has found no consistent reduction in antimicrobial peptide expression in NOD2-deficient mice[137], or evidence of a resultant dysbiosis[138]. It is possible that NOD2 associated CD only results in reduced antimicrobial peptide production on bacterial challenge, rather than causing a constitutive defect, but more work is needed to clarify[43, 78].

A further hypothesis arising from murine models suggests that NOD2 restrains TLR signalling, and that loss of this function exacerbates inflammation[45]. Most research has focussed on TLR2, with NOD2 deficient mice demonstrating a dysregulated TLR2 response to peptidoglycan, with enhanced IL-12 production from APCs increasing susceptibility to colitis[114]. This could potentiate CD4+ Th1 mediated inflammatory responses, which is a key signature of CD[139]. However, associations between TLR2 polymorphisms and CD remain controversial[140], and the majority of studies in humans have failed to show that NOD2 variant APCs have enhanced cytokine production following TLR2 stimulation[45, 141, 142]. As discussed earlier, NOD2 signalling typically acts in synergy with TLR2, so in contrast it would be expected that NOD2 variants would lack MDP induced enhancement of TLR2 signalling, and indeed this is reported in human studies[129, 141, 142].

A final loss-of-function hypothesis centres around NOD2 mediated autophagy. The potential importance of autophagy in CD is illustrated by the discovery that multiple autophagy related genes confer susceptibility to the disease, including ATG16L1 and IRGM[143]. It has been shown in cell lines homozygous for the NOD2 1007fs variant that

mutant NOD2 fails to recruit ATG16L1 to the plasma membrane and induction of autophagy in response to bacterial invasion is impaired[42]. Further, DCs from patients with CD-associated NOD2 or ATG16L1 variants are defective in autophagy induction, bacterial killing and antigen presentation[79].

Autophagy is also closely linked to the unfolded protein response (UPR) and endoplasmic reticulum (ER) stress. The accumulation of unfolded proteins in the ER, which is responsible for the production and folding of secretory and transmembrane proteins and plays a critical role in sensing and responding to protein abnormalities, results in ER stress[144]. This triggers the UPR that acts to restore homeostasis through a transcriptional/translational response[144]. Unresolved ER stress in intestinal epithelial cells leads to intestinal inflammation[145], and the UPR genes XBP1 and ORMDL3 are associated with CD susceptibility[145, 146]. In intestinal epithelial cells (IECs), impairment of autophagy function through deletion of ATG16L1 or ATG7, or impairment of the UPR through deletion of XBP1 results in the compensatory engagement of the other, while compromise of both mechanisms leads to spontaneous Crohn's like ileitis in mice[147]. It appears autophagy is essential to restrain the pro-inflammatory effects of ER stress, with Paneth cells central to this intersection. Defective ATG16L1 mediated autophagy in IECs also impairs clearance of aggregates of the ER stress sensor IRE1a that accumulate during ER stress, again driving a Crohn's like ileitis in older mice[148]. It is plausible that NOD2 mediated autophagy fulfils a similar role, and this regulation could be lost in patients with NOD2-associated CD. Further, NOD2 has recently been shown to transduce ER stress signals to elicit pro-inflammatory responses[149]. Intriguingly, NOD2 could be activated without its exogenous ligand MDP, suggesting that it can participate in ligand independent inflammatory responses[149, 150]. It

has also been proposed that a sphingolipid, sulfatide, may act as an endogenous NOD2 ligand driving autophagy[151]. Sulfatide is a widely expressed component of the plasma membrane, and is particularly abundant in myelin in the brain and peripheral nervous system[152]. Sulfatide has been linked to diverse immune roles, and it has been suggested that abnormal release in areas of demyelination might act as an endogenous trigger in brain resident immune cells, exacerbating neuroinflammatory conditions[153]. However, a potential interaction with NOD2 has not been further elucidated.

1.3.3 NOD2 in other diseases

While the majority of research has focussed on the role of NOD2 in intestinal disease, NOD2 polymorphisms are associated with a range of other conditions, summarised in Table 2. The key polymorphisms for many of these immune related conditions are typically shared with Crohn's. It is intriguing to note that Blau syndrome and Early Onset Sarcoidosis mirror the extraintestinal manifestations of Crohn's disease, yet do not themselves lead to intestinal disease. As expected, NOD2 mutations are also associated with increased susceptibility to a number of infections, including development of spontaneous bacterial peritonitis[154], and *Mycobacterium leprae* causing leprosy[155]. A potential association with bacterial meningitis further underlines its potential importance in the immune response of the central nervous system[156, 157].

Disease	Comments
Blau syndrome	Familial disease with autosomal dominant inheritance pattern. Mutations lie predominantly within the NOD domain, which may favour oligomerisation and auto-activation[43]. Defined as a triad of granulomatous dermatitis, arthritis and uveitis that likely results from constitutive NF-κB activation[158].
Early Onset Sarcoidosis (EOS)	Considered by some to be the sporadic phenotype of the same granulomatous disease as Blau syndrome[159].
Graft-versus-host disease (GVHD)	A major complication after allogeneic haematopoietic stem cell transplantation caused by alloreactive donor T cells and characterised by tissue damage in the gut, skin and liver. NOD2 may regulate GVHD through an inhibitory effect on host APC function, potentially impairing regulatory T cell induction[43, 160].
Experimental autoimmune encephomyelitis (EAE)	NOD2 sensing of peptidoglycan activates central nervous system infiltrating dendritic cells, exacerbating a murine model of multiple sclerosis.[161]
Asthma	NOD2 sensing of MDP leads to Th2 driven allergic inflammation in a murine model[162]. Association between polymorphisms in NOD2 and allergy described in two German populations[163].
Arthritis	NOD2 is important in models of peptidoglycan and antigen induced arthritis by driving pro-inflammatory cytokine release[164, 165], but no NOD2 variants have been associated with rheumatoid arthritis[43].
Colonic cancer	NOD2 deficiency increases risk of colitis associated colonic cancer in murine cancer model, through disruption of the gut microbial balance and induction of an IL-6 driven inflammatory response[166].
H. pylori associated gastric cancer	Links between NOD2 polymorphisms and two forms of gastric cancer associated with *H. pylori* infection, noncardia gastric carcinoma[167] and gastric lymphoma[168]. The underlying mechanism is unclear but it may result from impaired clearance of *H. pylori*[43].

Table 2 The role of NOD2 in other diseases.

1.4 Immunometabolism and the inflammatory microenvironment

1.4.1 The concept of immunometabolism

In recent years there has been an explosion of interest in the field of immunometabolism, the concept that metabolism regulates immune function across a broad range of immune cells including macrophages, dendritic cells and T cells, and that immune signals in these cells will also alter their intrinsic metabolism. It has become clear that this crosstalk between metabolic and immune pathways is central to the regulation of host defence[169].

1.4.2 The inflammatory microenvironment

A key determinant of immune cell metabolism is the availability of oxygen and nutrients. Immune cells face particular challenges in this regard. Firstly, their metabolic requirements change dramatically as they switch from a relatively quiescent steady state to an activated state in response to immune triggering. Secondly, they must migrate through a range of microenvironments as they patrol the tissues of the body or are recruited to the site of an immune response. Healthy uninflamed tissue with an intact vascular system is typically nutrient and oxygen replete[170]. It is notable however that even in the uninflamed intestinal mucosa an oxygen gradient exists, transitioning from the well vascularised and oxygenated submucosa, through the lamina propria to the more hypoxic intestinal epithelium which sits in contact with the almost anoxic lumen. The metabolic microenvironment of the intestinal mucosa is further modulated by a variety of factors including the microbiome, and is subject to significant fluctuations even under physiological conditions[171]. As an exemplar, mucosal perfusion and subsequent oxygen and nutrient availability changes markedly at times of food digestion[171, 172].

During inflammation, oxygen levels may fall markedly in all affected tissues, with hypoxia a characteristic feature of inflamed tissue[173, 174, 175, 176]. Indeed, oxygen levels may fall to below 1% in the inflammatory gut lesions seen in CD[171, 177]. This is paralleled by nutrient depletion of glucose, amino acids and lipids, and the development of lactic acidosis. A number of mechanisms underlie this metabolic shift (outlined in Figure 1.3). The vascular supply may be compromised through surrounding inflammation leading to direct damage including stenosis and microthrombosis[178]. Further, the oxygen and nutrient demands of activated resident or infiltrating inflammatory cells are substantial[179]. The majority of myeloid immune cells including DCs, macrophages and polymorphonuclear neutrophils (PMN) migrate to the inflamed tissue, a complex process which requires large quantities of ATP[179, 180]. Once there, these cells rapidly consume both oxygen and nutrients to mount an immune response. Indeed, PMNs increase their oxygen demands close to fifty-fold through an oxidative burst to generate reactive oxygen species (ROS) during phagocytosis[175]. Importantly, PMNs predominantly utilise glycolysis, with few energetically functional mitochondria and consequently minimal oxidative phosphorylation, allowing them to maintain their oxidative burst even in hypoxic conditions[181, 182]. The oxygen and nutrient consuming production of ROS is also a critical antimicrobial component of macrophages and DCs. In addition, adaptive immune responses are characterised by high rates of B and T lymphocyte proliferation, a metabolically demanding process powered by a switch from oxidative phosphorylation to glycolysis (the Warburg effect), leading to a dramatic increase in glucose utilisation and lactate production[179]. Invading pathogens that breach the epithelial barrier also have significant energy requirements, competing with the host and further depleting both infected host cells and the local tissue environment[170, 183]. Pathogens may also deliberately limit availability of metabolic substrates to the host to evade the

immune response, with *Salmonella Typhimurium* recently shown to produce an asparaginase that depletes asparagine, an important amino acid for T cell responses[184].

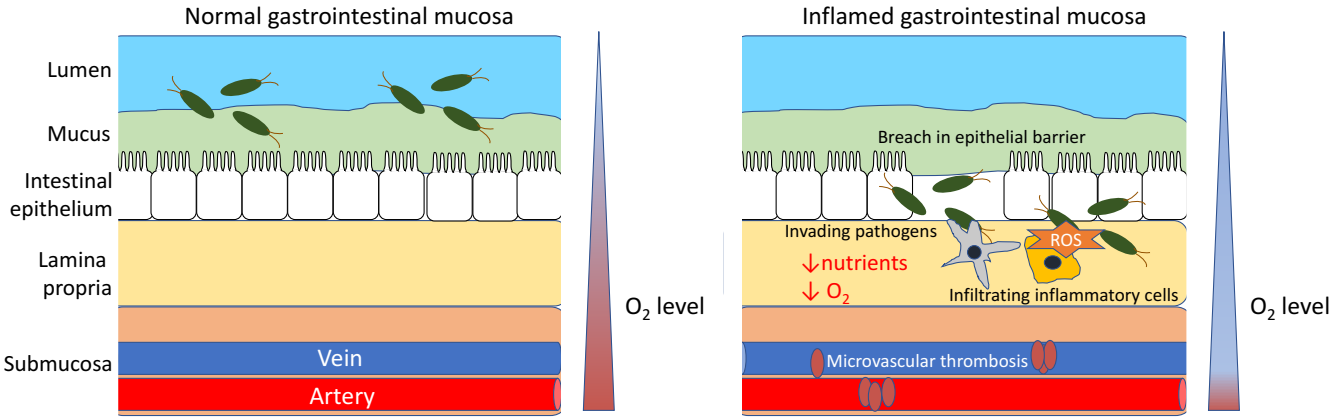


Figure 1.4 The inflammatory microenvironment of the gastrointestinal mucosa. Infiltrating inflammatory cells and invading pathogens rapidly consume available oxygen and nutrients, which are further limited by microvascular compromise.

1.5 Hypoxia-inducible factor

1.5.1 Hypoxia-inducible factor structure and regulation

Hypoxia-inducible factor (HIF) transcription factors are central to the cellular adaptation to hypoxia[185]. Unsurprisingly, given its role as the master hypoxia regulator, HIF is ubiquitously expressed, with HIF1 found in almost all innate and adaptive immune cells including DCs[186] and macrophages[185, 187]. HIF2, a paralog of HIF1, is less widely expressed, and considerably less studied in immune cells[185].

HIF is a basic helix-loop-helix heterodimer[188], composed of HIF-1β and one of two isoforms, HIF-1α or HIF-2α. HiF-1β is constitutively expressed, and its stability is independent of oxygen levels. In contrast, although the HIF-α subunits are also constitutively expressed, their stability is tightly regulated by oxygen availability[189]. In normoxia, they are hydroxylated by the iron-dependent enzymes prolylhydroxylases (PHDs) at conserved proline residues. Hydroxylation leads to their recognition and ubiquitination by the von Hippel-Lindau tumour suppressor protein (VHL) E3 ubiquitin ligase, which marks them for proteasomal degradation[190]. Consequently the half life of HIF1α is less than 5 minutes in normoxia. When oxygen is limited, the PHDs are inactive as they require oxygen as a cofactor, resulting in an accumulation of HIF-α. The HIF-α subunits translocate from the cytoplasm to the nucleus, where they dimerise with HIF-1β, leading to a transcriptionally active HIF1 or HIF2 complex. A further regulatory mechanism for HIF-1α is provided by the transcriptional coactivators CBP and p300, which form a DNA binding complex with HIF1 or HIF2. Factor inhibiting HIF (FIH) hydroxylates a key asparagine residue within the transactivation domain of the HIFα subunits during normoxia, preventing the binding of CBP and p300[185]. If allowed to form, the HIF transcriptional complex binds to hypoxia-

responsive elements (HRE) to control target gene expression. HIF1 and HIF2 are thought to have distinct targets, although there is a degree of overlap[191, 192]. The metabolic reprogramming that results from HIF1 activation, with upregulation of glycolysis, appears of particular importance in determining the fate and function of immune cells – this concept is discussed in more detail later.

Intriguingly, NOD2 was recently identified as a HIF1 target gene[151]. There are two canonical HREs (G/ACGTG) in the NOD2 promoter region, and in HeLa cells, hypoxia led to an increase in HIF1 binding in this region, increasing NOD2 messenger ribonucleotide (mRNA) expression. NOD2 gene expression was also found to increase on hypoxia in DCs[151]. However, no other research to date has investigated NOD2 signalling in hypoxic conditions.

In recent years it has emerged that HIF1α can be stabilised independently of hypoxia by a variety of pathological stressors including infection and inflammation[185]. Early work demonstrated that the TLR4 ligand LPS increased transcription of HIF-1α in macrophages, leading to protein expression comparable to induction by hypoxia, and a functional HIF1 complex[193]. It was subsequently shown HIF1α expression was increased following exposure to an array of Gram-positive (*Streptococcus and Staphylococcus*) and Gram-negative (*Salmonella and Pseudomonas*) bacteria[194]. NF-κB, which as described earlier plays a central role in the innate immune response, acts as a critical transcriptional activator of HIF-1α[195]. In macrophages, it acts to increase HIF1α transcription on TLR engagement. Importantly, and further underlining the crosstalk between hypoxic and immune responses, hypoxia can separately induce NFkB though both HIF dependent[196] and HIF independent mechanisms[197]. TNFα has also been reported to induce HIF in macrophages[198]; it seems

likely that a broad range of inflammatory signals including ROS may also enhance HIF expression in innate immune cells, although further investigation is required[185]. In T cells, separate regulatory mechanisms appear important. For example it has been shown that T cell receptor activation induces HIF1α through STAT3[199]. Both IL6 and TGFβ, which are required for Th17 CD4+ differentiation, increase HIF1 transcription[199].

Recent data shows that HIF1α can also be degraded in a proteasome independent manner, via chaperone mediated autophagy (CMA)[200, 201]. CMA is a selective targeting of cytosolic protein for direct lysosomal degradation[202]. HIF1a is targeted for CMA through K63 linked ubiquitination by the E3 ubiquitin ligase STUB1, also known as CHIP[203]. The relevance of this degradative mechanism in immune cells is unknown, but the link to autophagy is intriguing.

1.5.2 The role of HIF1α in immunity

HIF1α is essential for both the survival and function of cells of the innate immune system. Seminal work in a conditional HIF1α knockout mouse, targeting the myeloid lineage, demonstrated the critical requirement of HIF1α for inflammatory responses[204]. This correlated with defects in glycolysis and metabolic activation, which is tightly regulated by HIF1α. Isolated peritoneal macrophages showed impairment of the energy demanding processes of motility, invasiveness and aggregation. Further, intracellular killing of Group B *Streptococcus* was inhibited, although phagocytosis was unimpaired. *In vivo* experiments demonstrated impaired myeloid cell infiltration, oedema formation and tissue destruction. Later work demonstrated the importance of HIF-1α mediated inducible nitric oxide synthase (iNOS) expression and hence NO production for macrophage bacterial killing[194]. HIF-1α regulated NO production was also a significant contributor to macrophage TNF-α response

to bacterial infection[194]. The same group subsequently found that HIF-1α promotes the production of the inflammatory cytokines TNF-α, IL1, IL6 and IL12 in a mouse model of LPS-induced sepsis, and HIF1α deletion in macrophages protects against LPS induced mortality[205]. In granulocytes, HIF-1α prolongs cell survival[196], enhancing neutrophil mediated inflammation in a Zebrafish model[196, 206]. Knockdown or conditional deletion of HIF1α in murine DCs has shown HIF1α promotes differentiation, activation, migration and antigen presentation in both low oxygen environments and in response to LPS[186, 207]. Conditional deletion of HIF1α in DCs results in more severe intestinal inflammation in a murine DSS-colitis model[208]. A key driver appears to be the impairment in induction of regulatory T cells (Tregs)[208]. In intestinal epithelial cells, HIF1α is required to maintain autophagic flux, promoting the clearance of adherent and invasive *Escherichia coli* (AIEC)[209].

The role of HIF1α in adaptive immunity is a topic of much current research interest[185]. HIF1α is highly expressed in Th17 cells and acts as a metabolic checkpoint driving CD+ Th17 cell differentiation[199]. This control of Th17/Treg balance has *in vivo* relevance, as mice with a T cell conditional knockout of HIF1α were resistant to experimental autoimmune encephalitis[199]. HIF1α also regulates the migration and effector responses of CD8+ T cells[210, 211]. In B cells, HIF1α deficiency has been associated with abnormal maturation[212].

Recent work has focused on pharmacological strategies to stabilise HIF as a means of regulating the inflammatory response. PHD inhibitors, which prevent the PHD mediated degradation of HIF, have received most attention. Strikingly, PHD inhibitors are protective in murine models of colitis[213, 214]. The protective effects of PHD inhibitors in colitis relate to the stabilisation of HIF in both immune cells and importantly in IECs where HIF regulates

apoptosis and barrier function[215]. Work is ongoing to optimise PHD inhibitors, with the aim of specifically targeting HIF1α in the disease relevant tissue compartment, minimising potential systemic side effects. PHD inhibitors with specific HIF1α activity may be particularly relevant in IBD, as chronic activation of HIF2α in IECS leads to spontaneous intestinal inflammation in a dose dependent manner[216].

1.6 Metabolic reprogramming

Immune cells undertake significant metabolic reprogramming during an immune response, both as a result of changes in the metabolic microenvironment, but also in response to immune triggering[217]. Prototypical examples of immune cells which undergo this reprogramming are macrophages and DCs, which are here explored in more detail given their direct relevance to this thesis.

1.6.1 Metabolic reprogramming in macrophages

The Warburg effect is a concept central to our understanding of the metabolic changes that occur in immune cells on activation[218]. In the 1920s Otto Warburg observed that cancer cells favour glycolysis over oxidative phosphorylation to metabolise glucose, even in the presence of adequate oxygen[218]. Almost 100 years later it was shown that PRR stimulation of macrophages and DCs leads to a similar switch from a state of relative metabolic quiescence utilising oxidative phosphorylation to a metabolically active state utilising glycolysis[219, 220]. TLR agonists promote the classical (M1) activation of macrophages, which depend upon glycolysis for ATP production even in an oxygen-replete context, in comparison to unpolarised (M0) macrophages which exhibit greater oxygen consumption through mitochondrial oxphos. Conversely the cytokines IL-4 and IL-13 promote alternative (M2) activation which exhibit enhanced mitochondrial oxphos. Although this basic classification is thought by some to be too simplistic[221], broadly M1 “killer” macrophages are considered to be pro-inflammatory, producing IL-12, IL-23 and TNFα, nitric oxide (NO) and ROS. They are important for pathogen killing and activation of adaptive immunity through antigen presentation[220]. In contrast M2 “repair” macrophages are considered to modulate inflammation through production of anti-inflammatory cytokines such as IL-10, regulate

adaptive immune responses and participate in tissue repair and metabolic homeostasis[220]. They are also important for clearance of the Helminth parasite[220, 222].

M1 macrophages rely on the less energy efficient glycolysis for a number of reasons. Importantly it can be activated more quickly than oxphos allowing a rapid upregulation of ATP production which may help to meet the swift bursts of energy needed at sites of inflammation or infection[217, 223]. Glucose metabolism by glycolysis also feeds into the pentose phosphate pathway (PPP), which is central to M1 macrophage function. PPP flux is limited by the enzyme carbohydrate kinase-like protein (CARKL) which is downregulated by LPS to direct macrophage polarisation[224]. Activity of the PPP is increased in M1 macrophages, generating NADPH for NADPH oxidase (NOX) catalysed ROS generation. NADPH is also important in redox homeostasis, helping to dampen excessive tissue damage through the production of antioxidants. Enhanced PPP activity increases purine and pyrimidine synthesis, although it is uncertain why nucleotide production is boosted in macrophages which have low proliferative capacity[169].

Further, oxidative phosphorylation is impaired in M1 macrophages, necessitating an alternative energy source. The tricarboxylic acid (TCA) cycle that takes place in mitochondria and is coupled to oxphos is broken in two places, resulting in the accumulation of citrate and succinate[225, 226]. These two metabolites serve important pro-inflammatory purposes. Citrate is metabolised to oxaloacetate via an intermediary acetyl Co-A. This can be used to generate NADPH which serves as a substrate in both iNOS catalysed NO production and NOX catalysed ROS generation[227]. Notably, in M1 macrophages iNOS metabolises arginine to produce NO, with differences in arginine

metabolism key to the separate functions of M1 and M2 macrophages[228]. NO directly inhibits oxphos by acting directly on the electron transport chain, and this is important for the metabolic switch to glycolysis[229, 230]. Citrate can also generate immunoregulatory prostaglandins[231] and itaconic acid which has bactericidal effects[232]. Meanwhile, the accumulation of succinate acts as an inflammatory signal that enhances IL-1β production through stabilisation of HIF1α[225]. Further, mitochondrial oxidation of succinate via succinate dehydrogenase (SDH) drives mitochondrial ROS (mROS) production, while the switch to glycolysis also allows macrophages to repurpose mitochondrial respiration to further increase mROS[233].

The contrasting metabolic phenotype of M2 macrophages, which rely on oxphos, is driven by IL4. This key regulatory cytokine activates signal transducer and activator of transcription-6 (STAT6) which increases the expression of metabolic transcriptional coregulator PPARγ-coactivator-1β (PGC-1β)[234]. STAT6 both directly regulates genes required for β-oxidation of fatty acids, and enhances PGC1β expression which increases fatty acid oxidation (FAO) and mitochondrial biogenesis. This results in increased oxphos, which is essential for M2 polarisation[234]. Lysosomal lipolysis of triacylglycerols by lysosomal acid lipase, which is upregulated in M2 macrophages, is an important source of fatty acids for oxidation[235]. IL-4 also increases CARKL expression, limiting PPP activity[224]. In contrast to M1 macrophages, the TCA cycle is intact, allowing unhindered oxphos[226]. M2 but not M1 macrophages express Arginase-1 (Arg-1) which hydrolyses arginine, preventing its conversion into the inflammatory NO. The arginase pathway may also be important in wound healing[236]. An additional important amino acid in M2 macrophages is glutamine. It fulfils two roles, both required for M2 polarisation. Firstly, it fuels the TCA cycle and

supports oxphos. Secondly it acts as a substrate for the hexosamine pathway. The downstream product, UDP-GlcNAc, provides substrate for N-glycosylation which is necessary for M2 polarisation[226]. Conversely, other pathways that drive the glycolytic switch in M1 macrophages are downregulated in M2 macrophages[237].

Beyond a critical role in differentiation, the reasons why M2 macrophages are skewed towards fatty acid oxidation and oxphos remain to be elucidated. It is possible that FAO favours the more sustained immune response required to deal with helminth infections, an important role for M2 macrophages[217]. However, while FAO supports longevity of T cells, it is uncertain whether this is also important for M2 macrophages[238]. This metabolic phenotype may also relate to the capacity of M2 macrophages to proliferate, although the simultaneous inhibition of PPP activity which limits nucleotide production would contradict this[220].

Although fatty acid oxidation was historically thought to be less important in M1 macrophages, with fatty acid synthesis predominating[239], an essential role for FAO has recently been linked to c13orf31 (FAMIN)[240]. Importantly, SNPs in FAMIN are associated with increased risk of systemic juvenile idiopathic arthritis[241], leprosy[242] and CD[117, 243]. FAMIN was found to associate with fatty acid synthase (FASN) at peroxisomes, controlling acyl-coA synthesis to drive both FAO and glycolysis, thereby increasing ATP production. FAMIN regulated inflammasome activation, mROS and NOX catalysed ROS production and macrophage bacterial killing capability[240]. An in vivo murine LPS sepsis challenge model demonstrated that FAMIN protects against potentially lethal overactivation of IL1-β.

1.6.2 Metabolic reprogramming in dendritic cells

Dendritic cells are heterogeneous and comprise a number of subsets, determined in part by their lineage. DCs can broadly be considered as classical (cDCs), plasmacytoid (pDCs), Langerhans cells and monocyte derived DCs (moDCs)[244]. Dendritic cells are considered professional antigen presenting cells, and are potent orchestrators of the adaptive immune response[245]. As with macrophages, TLR engagement results in a switch to glycolysis. In inflammatory DC subsets expressing NO, a delayed glycolytic switch supports longevity after inhibition of oxphos[219, 229]. However, across a broader range of DC subsets, a more rapid glycolytic switch supports the anabolic demands of activation[246], although It should be noted that the metabolism of Langerhans cells and pDCs has not been interrogated. Again, an important sequela of glycolysis in this setting is an increase in citrate. This drives fatty acid synthesis, which is also upregulated through the pentose phosphate pathway. As in macrophages, the fatty acids are used for the pro-inflammatory prostaglandin PGE_2[231], but are also required for membrane biogenesis in the ER and Golgi apparatus. The expansion of these two organelles allows for the increased synthesis and export of proteins essential both for DC activation and their ability to activate T cells[246]. Conversely, there is increasing evidence that fatty acid oxidation and enhanced oxphos are important in the development of tolerogenic DCs[217, 247]. When considering the varied cells of the immune system, it broadly appears that anabolic pathways favour inflammatory activation, while catabolic pathways favour anti-inflammatory phenotypes. This may also be the case for DCs, with catabolic pathways favouring a tolerogenic phenotype[248].

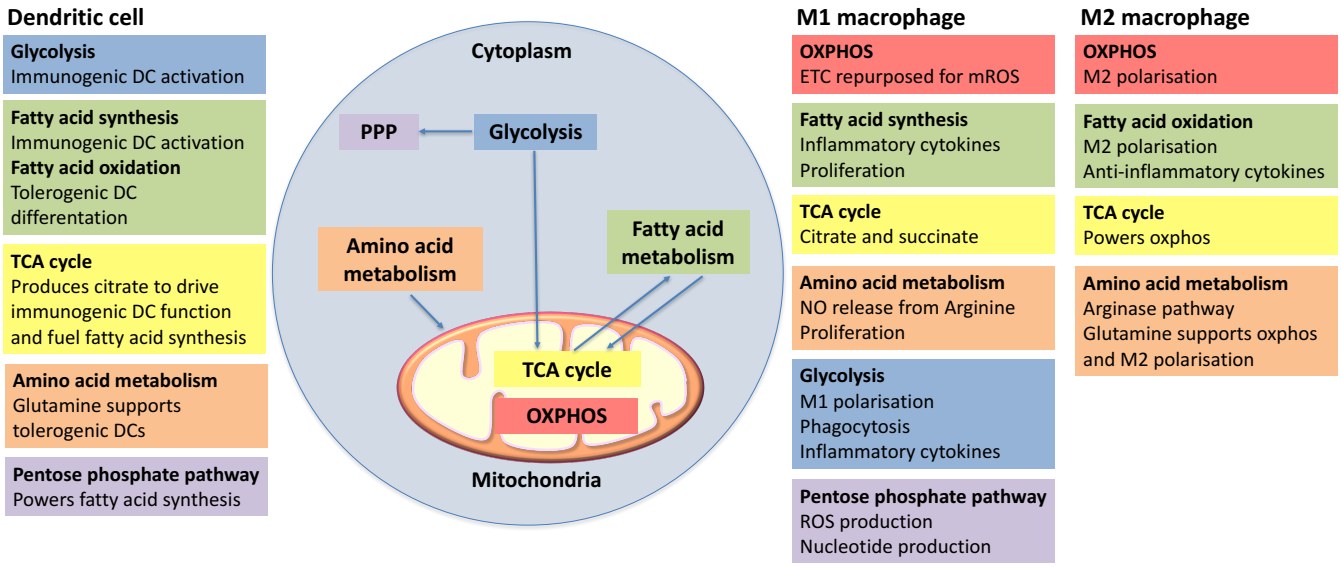


Figure 1.5 Important metabolic pathways in DCs, M1 and M2 macrophages.

1.7 The role of mitochondria in immunity

1.7.1 The origin and structure of mitochondria

Although historically considered mere bioenergetic and biosynthetic organelles, mitochondria have emerged as a key hub of immune signalling. Mitochondria are thought to have originated through endosymbiosis from α-proteobacterium, which were phagocytosed by the ancestor of the eukaryotic cell[249]. They possess their own genome in the form of circular mitochondrial DNA (mtDNA), but this contains just 37 genes which encode 13 proteins required for oxidative phosphorylation, 22 transfer RNAs and 2 ribosomal RNAs. Consequently the vast majority of mitochondrial proteins are encoded by nuclear DNA and transported to the mitochondria, crossing the mitochondrial membranes via a complex system of protein translocases[250, 251]. Mitochondria are double-membrane bound structures with the inner membrane forming invaginations in the mitochondrial matrix called cristae, where the electron transport chain (ETC) is carried out. The outer membrane fulfils an essential structural role, but also acts as a platform for regulatory proteins with a number linked to immunity.

1.7.2 Mitochondrial dynamics

Mitochondria are highly active organelles that continuously undergo fission, fusion, biogenesis, mitophagy and movement. These processes are termed mitochondrial dynamics and control mitochondrial morphology, quality, abundance and location which are critical to the immune role of mitochondria[252]. There is still much to understand about how the innate immune system regulates mitochondrial dynamics, but a recent study provides an interesting insight. Following recognition of bacteria by TLRs, macrophages were found to adapt their ETC architecture by destabilising complex I in a NLRP3 and ROS dependent

manner[253]. This resulted in enhanced mitochondrial respiration from complex I and II and increased mROS, and may regulate IL1β and IL10 production. Ongoing work in our own laboratory has linked NOD2 to mitochondrial dynamics and mitophagy through phosphorylation and activation of the mitochondrial fission protein dynamin-related protein 1 (DRP1) (unpublished data).

In contrast, mitochondrial dynamics are better characterised in T cells, with mitochondrial remodeling regulating T cell metabolic programming and differentation[252, 254]. Enforced fusion leads to a catabolic T memory cell phenotype with enhanced oxphos and FAO, while enforced fission results in an anabolic T effector cell phenotype[254]. Mitochondrial dynamics are clearly also important in regulating oxphos in cells of the innate immune system, which as discussed earlier is an important determinant of phenotype in macrophages and DCs[252].

1.7.3 Mitochondrial reactive oxygen species

In addition to the essential bioenergetic role of mitochondria, the electron transport chain generates mROS which is required for optimal pathogen responses. mROS helps to control bacterial infection by enhancing phagocyte bacterial killing and pro-inflammatory cytokine release[250]. In macrophages, bacterial engagement of TLR1, 2 and 4 promotes mitochondrial recruitment of TNF receptor-associated factor 6 (TRAF6) where it engages evolutionary conserved signalling intermediate in Toll pathways (ECSIT)[255]. ECSIT is ubiquitinated by TRAF6 and acts to increase mROS and cellular ROS production, augmenting bacterial killing by phagocytosis[255]. The precise mechanism by which ECSIT increases mROS has not been clarified, although it is known to function in the assembly of Complex I part of the oxidative phosphorylation machinery[256]. Additional immune pathways that regulate mROS

production have been described. Mitochondrial uncoupling protein 2 (UCP2) is localised to the mitochondrial inner membrane, and can induce uncoupling of the ETC, which reduces electron leak and inhibits mROS production[250]. LPS stimulation decreases expression of UCP2 in macrophages, leading to an increase in mROS[257]. UCP2 knockout mice show enhanced killing of a range of bacteria including *Salmonella enterica* serovar Typhimurium through increased ROS production[258]. The augmentation of mROS in the absence of UCP2 also appears to enhance LPS triggered inflammatory cytokine production via activation of MAPK and NFκB pathways[257, 259]. In a separate pathway, IFN-γ has been shown to act via oestrogen-related receptor-α (ERRα) and the transcriptional co-activators PGC1α and PGC1β to increase transcription of mitochondrial respiration encoding genes[260]. This promotes mitochondrial respiration and mROS production, and is required for IFN-γ mediated clearance of *Listeria monocytogenes*[260].

NLRs also require mROS for their signalling pathways. An important example is the role of mROS in the optimal activation of the NLRP3 inflammasome, which serves as a platform for activation of caspase-1 and maturation of the pro-inflammatory cytokine IL1β[261]. Impairment of lysosomal acidity by NLRP3 mediated mROS production appears important for inflammasome activation[262]. The importance of the mitochondrial metabolites succinate and citrate in both the generation of mROS and other immune roles have been discussed earlier, and are a further example of the varied mechanisms through which mitochondria regulate the immune response. The direct relevance of mROS to human disease is illustrated by the autoimmune tumour necrosis factor receptor-associated periodic syndrome (TRAPS), where elevated mROS leads to enhanced responsiveness to LPS[263].

1.7.4 Mitochondria provide a structural hub for immune signalling

Mitochondria act as a platform for innate immune signaling, with immunoregulatory proteins assembling on the outer mitochondrial membrane[252, 264]. One of the first proteins discovered was mitochondrial antiviral-signaling protein (MAVS), a key adapter protein for the RIG-I-like receptor (RLR) signalling pathway that responds to viral infections[265]. On viral infection and RLR triggering, MAVS is targeted to the outer membrane by a C-terminal transmembrane domain. Although it remains unclear precisely why MAVS must be recruited to the mitochondria, localisation here is essential to mediate downstream signalling via NF-κB and IRF3 to regulate type-1 interferon production[264, 265]. As described earlier, NOD2 can also engage MAVS in response to viral ssRNA triggering a similar interferon cascade[62]. MAVS activation is additionally regulated by mitochondrial dynamics[266] and mROS[267]. A further illustration of the intersecting nature of mitochondrial signalling pathways is the recent discovery of the regulation of the NLRP3 inflammasome by MAVS[268]. Another mitochondrial membrane protein, cardiolipin, also controls NLRP3 inflammasome activation in an mROS independent manner[269].

1.7.5 Activation of the immune response following mitochondrial damage

Given the ancient bacterial roots of mitochondria, it is unsurprising that mitochondrial injury releases compounds carrying bacterial molecular motifs, sensed as DAMPs, to trigger an immune response[270]. Mitochondrial DNA which shares hypomethylated CpG motifs with bacterial DNA, is one such DAMP which can be sensed by the innate immune receptor for CpG DNA, TLR9[270]. TLR9 activation leads to NF-kB and MAPK inflammatory cascades, and can also signal through IRF7 to enhance type 1 IFN responses[271]. mtDNA is also an important endogenous agonist for NLRP3 inflammasome[272], and in macrophages has been

shown to activate the NLRC4[273] and AIM2 (absent in melanoma 2) inflammasomes[272]. Finally, mtDNA can also trigger pro-inflammatory cytokine responses via the cyclic GMP-AMP synthase (cGAS) PRR[274, 275]. Mitochondrial DNA-dependent inflammatory pathology has been described in a diverse range of diseases including heart failure, atherosclerosis, rheumatoid arthritis and liver disease, and following bacterial infection[271].

It is essential that cells are able to efficiently eliminate damaged mitochondria and their DAMPs to prevent aberrant inflammation, and here autophagy plays a vital role. Mitophagy inhibits NLRP3 inflammasome activation by clearing damaged mitochondria and limiting the release of both mROS and mtDNA[272, 276]. Mice deficient in the autophagy protein LC3B showed enhanced caspase-1 dependent cytokines in sepsis models[272]. As described earlier, following viral infection the NOD2-RIPK2 axis also acts to increase mitophagy and limit inflammasome activation. These studies underline the importance of mitophagy in responding to the mitochondrial damage that occurs during an immune response, thereby preventing hyperactivation of the immune system.

1.7.6 Mitochondria and Crohn's disease

While it is clear that mitochondria are of central importance in immunity, their role in Crohn's disease is not well understood. A number of studies suggest the presence of mitochondrial dysfunction in inflammatory bowel disease. Enterocytes isolated from patients with IBD have abnormal mitochondrial morphology[277], and murine models of colitis result in similar mitochondrial changes in IECs[278]. There is evidence of elevated ROS, although the source was not clarified, and impaired mitochondrial membrane potential in patients with active Crohn's, which was found to improve on disease remission[279]. In

paediatric CD patients, proteomic analysis of mucosal biopsies suggested a marked downregulation of mitochondrial proteins, including components of the mitochondrial respiratory chain[280]. It has been suggested that inflammatory bowel disease is a state of energy deficiency, with impaired mitochondrial β-oxidation of fatty acids implicated[281]. This theory is supported by the finding that mutations in SLC22A5 (OCTN2) which encodes a carnitine transporter are associated with CD[146], with carnitine essential for fatty acid oxidation. Mice lacking OCTN2 develop spontaneous intestinal inflammation and atrophy[282]. Conversely, mice carrying mutations that increase mitochondrial oxphos activity and ATP generation are protected from chemical models of colitis[283]. It is clear that more research is needed to elucidate the contribution of mitochondrial dysfunction to CD, but the potential intersection with processes such as autophagy and inflammasome activation is intriguing.

1.8 Ataxin-3

1.8.1 Mutations in ataxin-3 cause neurodegenerative disease

Ataxin-3 was identified in this thesis to be downstream of NOD2 signalling and is thus explored in more detail here. Ataxin-3 is a small 42 kilodalton protein that is ubiquitously expressed[284]. It is encoded by the gene ATXN3 on the long (q) arm of chromosome 14 at position 32.12[285]. Ataxin-3 first attracted research interest in the neurology community after unstable CAG repeat expansions in the ATXN3 gene were identified as the cause of the neurodegenerative condition spinocerebellar ataxia Type 3 (SCA3), also known as Machado-Joseph Disease, the most common autosomal dominant ataxia[285]. Importantly, the expanded polyglutamine stretch results in more complex sequelae than a simple loss of protein function, and likely leads to a toxic gain of function through altered binding properties, aggregation and subcellular localisation[286]. Indeed, an ataxin-3 knockout mouse model does not reproduce the histopathological findings and neurological phenotype of SCA3[287], in contrast to a humanised polyglutamine knock-in mouse model which shows similarities to the human disease[288].

1.8.2 Ataxin-3 cellular location

The cellular location of ataxin-3 is still incompletely understood. First described as a predominantly cytoplasmic protein, it was subsequently found to translocate to and from the nucleus[289], although the functional relevance of this is unclear. Sequences within the Josephin domain, specifically the first 27 amino acids (aa)[290] and two nuclear export signals (aa 77-99 and aa 141-158) appear important in regulating nuclear localisation[291]. Conversely, while ataxin-3 is also predicted to contain a nuclear localisation signal (NLS) close to the polyglutamine domain, mutating it does not affect cellular location[292]. Post-

translational modification can also affect nuclear localisation with casein kinase (CK2) phosphorylation of serines 236, 340 and 352, and CK2 and glycogen synthase kinase 3β (GSK3β) phosphorylation of serine 29 directing ataxin-3 to the nucleus[292, 293]. Two studies have suggested that ataxin-3 may localise to the mitochondria[290, 294]. In the latter study, subcellular fractionation demonstrated ataxin-3 associated with both the mitochondrial membrane and the mitochondrial matrix under basal conditions. The mitochondrial membrane localisation was lost in a truncated form of the protein lacking aa 291-end, but nothing else is known about how ataxin-3 might be targeted to the mitochondria, or its role once there. Finally, ataxin-3 may also associate with the ER membrane[295].

1.8.3 Ataxin-3 structure and post-translational modification

Biochemically, the ATXN3 gene encodes a 364 amino acid protein which comprises multiple functional domains (Figure 1.6). At the N-terminus is the catalytic Josephin domain, which is shared with two other members of the Josephin family, josephin-1 and josephin-2. Ataxin-3-like protein (encoded by ATXN3L), which shares close sequence homology with Ataxin-3, is considered the fourth member of this family. However, it has also been suggested that the intronless gene ATXN3L is actually a pseudogene. The Josephin domain acts as a cysteine protease that hydrolyses ubiquitin linkages and allows ataxin-3 to function as a deubiquitinating enzyme (DUB). A triad of amino acids: cysteine 14, histidine 119 and asparagine 134 within the Josephin domain of ataxin-3 are essential for its protease activity, and are highly conserved between other ubiquitin C-terminal hydrolases and ubiquitin-specific proteases[286, 296]. Mutating the C14 amino acid alone leads to a marked accumulation of ubiquitinated proteins *in vitro,* underlining the functional necessity of this

residue[297]. Two separate ubiquitin binding sites are also contained within the Josephin domain [298].

A flexible C-terminal tail contains either two or three ubiquitin-interacting motifs (UIMs), depending on the isoform. The UIMs mediate selective binding to ubiquitin chains, determining the type of chain that can be cleaved by the Josephin domain[299]. Ataxin-3 shows a preference for cleavage of K63-Ub chains, although it is able to bind both K63 and K48 chains. Indeed, it shows particularly high activity for K63 linkages in K63/K48 mixed chains with four or more ubiquitins[300]. It appears to shorten rather than entirely disassemble ubiquitin chains[300]. Unusually for a DUB, ubiquitination of ataxin-3 enhances its catalytic activity and ability to cleave ubiquitin chains, with the preference for K63 linkages maintained[301]. The primary ubiquitination site was identified as lysine 117, which is close to the catalytic triad[302]. The polyglutamine domain is also contained within the tail, downstream of the first two UIMs.

Phosphorylation also modifies the location, stability and function of ataxin-3. CK2 mediated phosphorylation within the 2nd UIM at s236 and 3rd UIM at s340 and s352 is important for both basal and thermal stress induced nuclear translocation, and appears to stabilise the protein[292]. Glycogen synthase kinase 3β (GSK3β) phosphorylates s256 in the 2nd UIM. This regulates aggregation of the polyglutamine mutant form of the protein, but the functional relevance in wild type ataxin-3 is uncertain[303]. Two studies have found that mutating s256 either alone or in combination with s260/261 may restrict binding to ubiquitin chains greater than 4 moieties in length, suggesting a potential role in determining specificity of DUB target[292, 304]. Phosphorylation within the 2nd and 3rd UIMs may also regulate the

transcriptional regulatory function of ataxin-3, with phosphomimetic mutatations of the serine residues within these domains enhancing the transcriptional repression of a known target, matrix metalloproteinase 2 (MMP2)[292].

Phosphorylation within the Josephin domain at s12 and s29[293] has also been demonstrated, with *in vitro* DUB assays suggesting s12 phosphorylation may inhibit deubiquitinating activity[305]. Further exploration of the role of s12 phosphorylation in the polyglutamine mutant found that a phosphometic form protected against neuronal defects in a rat model of SCA3[305], but again the relevance for wild type ataxin-3 remains to be shown.

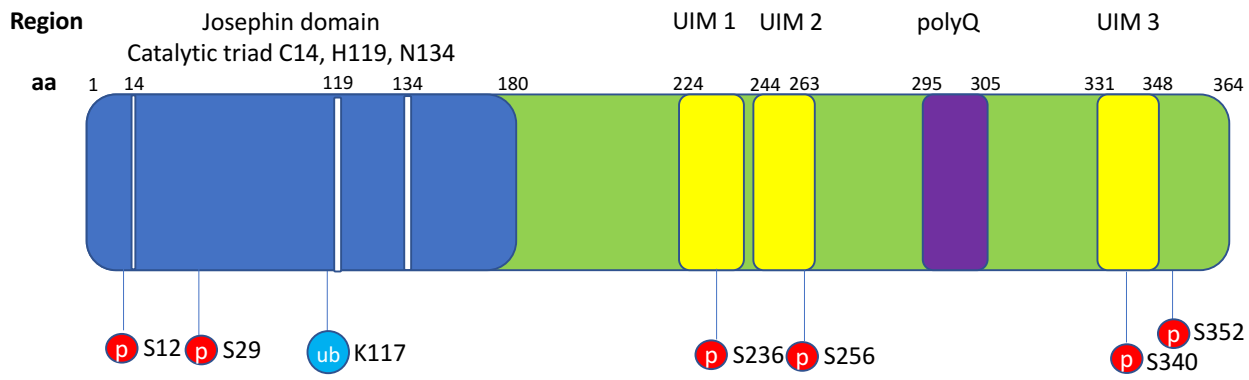


Figure 1.6 The structure of Ataxin-3. The key domains and post-translational modification sites are indicated.

1.8.4 The deubiquitinating function of ataxin-3

The initial discovery that ataxin-3 can both bind to and deubiquitinate Ub-conjugated proteins led to a hunt for potential substrates. Early work showed that transient knockdown of ataxin-3 in human HeLa cells and subsequent immunoblot of the lysate with an anti-ubiquitin antibody led to a marked increase in ubiquitinated proteins across a broad range of molecular weights[300]. An ataxin-3 mouse knockout model generated similar

results, and provided the first *in vivo* evidence of DUB activity[287]. Taken together, these results suggest that ataxin-3 may regulate the ubiquitination state of a large number of proteins[300].

Two of the first described binding partners were hHR23 and valosin-containing protein (VCP/p97), two ubiquitin and proteasome binding proteins involved in substrate delivery to the proteasome[306]. Together with the finding in yeast that ataxin-3 can itself bind to the proteasome[306], this suggested a role for ataxin-3 in the ubiquitin-proteasome degradation pathway[307]. Later work demonstrated that ataxin-3 binding to VCP/p97 modulates the flow of proteins through the endoplasmic reticulum-associated protein degradation (ERAD) pathway, which serves to target misfolded ER proteins for ubiquitination and proteasomal degradation[308]. A separate group found that overexpression of an ataxin-3 mutant defective in deubiquitination resulted in the accumulation of misfolded ER proteins triggering ER stress, suggesting the importance of the DUB activity of ataxin-3 for this role[295].

DUBs frequently deubiquitinate and regulate the activity of E3 ubiquitin ligases, and this is seen with ataxin-3. The first E3 ligase found to interact with ataxin-3 was C terminus of heat shock protein (HSP) 70-interacting protein (CHIP), also known as STUB1[300]. Interestingly, ataxin-3 deubiquitinates both CHIP and ubiquitinated CHIP substrates in the same complex, acting to regulate and terminate the ubiquitination activity of CHIP[309]. It has been suggested that this may be of particular importance in ubiquitin-dependent protein quality control, complementing its VCP/p97 role[309]. Further support for this theory was provided by the finding that CHIP-mediated ubiquitination of IRE1a regulates UPR activity in response

to ER stress[310]. The complex interrelationships in this system are further demonstrated by the cross regulation of ataxin-3 by VCP/p97 and CHIP. VCP/p97 binding enhances the DUB activity of ataxin-3[311], while CHIP mono-ubiquitinates ataxin-3 at lysine 117 to increase its protease activity[302]. Finally, it is intriguing that CHIP has recently been linked to other diverse roles which ataxin-3 could plausibly help to regulate. In both macrophages and DCs, CHIP facilitates TLR4 and TLR9 driven pro-inflammatory cytokine release, type 1 IFN production and maturation of antigen presenting cells, by recruiting, ubiquitinating and hence activating two kinases Src and PKCζ in the TLR complex[312]. CHIP is also required for HIF1α degradation by chaperone-mediated autophagy[201], and appears to regulate the Warburg effect in cancer by targeting the glycolytic enzyme PKM2 in ovarian cancer cells[313].

Ataxin-3 deubiquitinates parkin, a second E3 ligase. Mutations in the parkin gene (PARK2) result in another neurodegenerative disease, Parkinson's[314], and have also been linked to increased susceptibility to intracellular bacterial pathogens in humans[315, 316]. Ataxin-3 prevents the self-ubiquitination of parkin through an atypical deubiquitination process. This does not regulate the stability of parkin, raising the possibility that it instead regulates its activity[317]. Parkin self-ubiquitination, mitochondrial recruitment and subsequent ubiquitination of mitochondrial associated proteins are known to be critical for the process of parkin mediated mitophagy[318, 319]. However, ataxin-3 does not appear to regulate this pathway[320]. Indeed the functional importance of the wild type ataxin-3/parkin interaction remains to be determined, but once again, it is tempting to speculate. Of particular interest is the requirement for parkin in ubiquitin mediated autophagy of bacteria including *M. tuberculosis*[85].

A separate role for ataxin-3 in protein quality control has been suggested through regulation of aggresome formation[321]. Aggresomes are aggregates of misfolded proteins that accumulate when classical protein degradation pathways are overwhelmed[322]. Ataxin-3 has been shown to colocalise with aggresomes and associate with two proteins critical for aggresome formation and transport, histone deacetylase 6 and dynein[321]. The DUB activity of Ataxin-3 was required in an *in vitro* cell model of aggresome formation. The DUB function of ataxin-3 was later shown to promote aggresome formation of mutant SOD1; mutations in SOD1 are associated with the neurodegenerative disease amyotrophic lateral sclerosis (ALS)[323].

1.8.5 Additional roles of ataxin-3 in DNA repair and transcriptional regulation

Ataxin-3 is also important in DNA repair. This was first suggested by the association between ataxin-3 and the protein hHR23 which also functions in DNA repair, but this specific role was not demonstrated[306]. Two complementary papers then demonstrated an interaction with polynucleotide kinase 3'-phosphatase (PNKP), a DNA phosphatase involved in repair of single and double stranded breaks[324, 325]. Ataxin-3 binding promotes PNKP DNA repair activity through an unknown mechanism, with the relevance of the DUB function of ataxin-3 not demonstrated here[324]. A subsequent paper found that ataxin-3 regulates the stability of checkpoint kinase 1 (CHK1) through deubiqutination, and hence regulates the CHK1 mediated DNA repair damage response[326].

A final recently described DUB target of ataxin-3 is p53. In this case, ataxin-3 regulates the stability of p53, thereby inhibiting its role as a transcription factor and limiting apoptosis[327].

Ataxin-3 can also act as a transcriptional regulator - broadly it appears to repress transcription. In addition to transcription regulation of MMP2, other postulated gene targets include p300, CBP, p300/CBP-associated factor (PCAF)[328] and HDAC3 and 6[321, 329]. The mechanism of transcriptional regulation remains to be clarified, although it has been reported that ataxin-3 can bind directly to DNA through a leucine zipper motif located between aa 223 to 270[329].

1.8.6 Ataxin-3 and autophagy

During the course of this thesis, a separate laboratory determined that ataxin-3 can regulate beclin-1 dependent autophagy[330]. Beclin-1 serves as a platform for the assembly and activation of the phosphatidylinositol 3 kinase VPS34 complex, which leads to the recruitment of other autophagy proteins involved in nucleation of the autophagosome[331]. Intriguingly, the polyglutamine domain of ataxin-3 was found to be important for binding to beclin-1. This domain is not well conserved among other species, which has historically led some authors to speculate that it may not have a function. It was however not the only binding domain, and thus other regions of ataxin-3 may compensate in other species. Once bound, ataxin-3 deubiquitinates beclin-1. Although ataxin-3 typically shows a preference for K63 linkages, it was found to cleave K48 chains from beclin-1 at lysine 402 which resides within an evolutionary conserved domain, protecting it from proteasome-mediated degradation. Beclin-1 plays a key role in starvation induced autophagy, and thus this condition was further studied. Ataxin-3 knockdown in primary mouse neurons *in vitro* and in mouse liver cells *in vivo* led to a reduction in beclin-1 levels during starvation. There was a corresponding decrease in autophagosome biogenesis, as evidenced by a reduction in LC3-II both *in vitro* and *in vivo*. The autophagy defect was confirmed to be in the formation of

autophagosomes, using the mTag-RFP-mWasabi-LC3 reporter system in human HeLa cells. The authors went on to demonstrate that a range of disease-associated polyglutamine expanded proteins compete with the wild type polyglutamine tract of ataxin-3 for binding to beclin-1, impairing beclin-1 mediated starvation induced autophagy. The potential role of ataxin-3 in other forms of autophagy was not explored.

1.9 Aims and objectives of this thesis

Although mutations in NOD2 represent the strongest genetic risk factor for Crohn's disease, there is still much to understand about NOD2 signalling in both health and disease. Indeed, while it is clear that sites of tissue inflammation, including the gastrointestinal lesions seen in Crohn's disease, are subject to profound reductions in oxygen availability, the impact of this hypoxic inflammatory milieu on NOD2 signalling has never been mapped. This is of potential importance given the emerging evidence that the hypoxic inflammatory microenvironment is a key determinant of immune cell signalling and function, with metabolic reprogramming central to this modulation.

It is hypothesised that oxygen availability modulates NOD2 signalling and function, and that detailed study of this receptor in hypoxia will reveal novel NOD2 mediated pathways and interaction partners. Further, study of NOD2 in this physiologically relevant context may aid interrogation of the intersection of NOD2 signalling with metabolic pathways, which is of particular relevance given the increasing links between metabolic dysfunction and immune related diseases including Crohn's disease.

Aims (1): Definition of NOD2 signalling in hypoxia

This first part of this thesis therefore seeks to define NOD2 signalling, together with the synergistic PRR TLR2, in hypoxia and compare this with normoxia. Cells of the myeloid lineage, specifically monocytes, moDCs and macrophages which are prototypical innate immune cells which express high levels of NOD2, have been chosen for study. Initial work will focus on a preliminary characterisation of NOD2/TLR2 signalling in hypoxia, establishing core experimental conditions. Large scale quantitative phosphoproteomics will then be

utilised to map the downstream signalling cascade in both normoxia and hypoxia. Potential novel interacting partners will be validated and promising targets selected for further study.

Aims (2): Interrogation of the NOD2 mediated recruitment of ataxin-3, with definition of the signalling cascade, interacting partners and functional relevance in the immune response

The deubiquitinase ataxin-3 was identified through this phosphoproteomic approach as a novel NOD2 interacting protein. Subsequent work in this thesis seeks to dissect the precise signalling pathway from NOD2 to ataxin-3, including identification of the phosphorylation site of ataxin-3 following NOD2 stimulation. Immunoprecipitation will be undertaken to identify additional interacting partners. This work will aid understanding of the potential functional relevance of ataxin-3 in NOD2 mediated immune responses, which will be interrogated through the use of ataxin-3 depleted human cells and a KO mouse model. The deubiquitinating function of ataxin-3 will also be specifically assessed following NOD2 triggering, given the central importance of this enzymatic activity to the known roles of ataxin-3.

The overarching aim of this thesis is to shed further light on how NOD2 exerts its immune effects, with particular focus on a potential immunometabolic role, with the hope of better understanding how dysregulation of NOD2 function might lead to human pathology including Crohn's disease.

Chapter 2: Materials and Methods

2.1 Cell culture

2.1.1 Cell culture media

R10

Roswell Park Memorial Institute medium (RPMI-1640) (Sigma) supplemented with 10% (v/v) heat-inactivated foetal calf serum (FCS) (Sigma), 2mM (1% v/v) L-glutamine, and 1U/ml penicillin and 50µg/ml streptomycin (1% v/v penicillin/streptomycin).

R10 without antibiotics

As for R10, but without penicillin/streptomycin

R10 with HEPES buffer

RPMI-1640 (Sigma) supplemented with 10% (v/v) FCS (Sigma), 2mM L-glutamine, 1U/ml penicillin and 50µg/ml streptomycin (Sigma) and 10mM HEPES buffer solution.

R10 with HEPES buffer without antibiotics

As for R10 with HEPES buffer, but without penicillin/streptomycin

D10

Dulbecco's modified Eagle high glucose medium (DMEM) (Sigma) supplemented with 10% (v/v) FCS (Sigma), 2mM L-glutamine, and 1U/ml penicillin and 50 µg/ml streptomycin.

D10 without antibiotics

As for D10, but without penicillin/streptomycin

2.1.2 Cell culture conditions

Cells were cultured in humidified incubators (Binder) with 21% O_2, 5% CO_2 at 37°C, with continuous monitoring of CO_2 levels unless otherwise stated (standard normoxic conditions). Hypoxic conditions were achieved by culturing cells in a hypoxic workstation (InVivo) with 1%O_2, 5% CO_2 and 94% N_2 at 37°C, with continuous monitoring of O_2 and CO_2 levels. Depending on the duration of hypoxia, moDCs were transferred on day 3, day 4 or day 5 following isolation. Cells were harvested in the hypoxic incubator, and subsequently processed rapidly on ice to avoid reoxygenation.

2.1.3 Isolation of human peripheral blood mononuclear cells (PBMCs) and generation of monocyte derived dendritic cells (moDCs)

Leucocyte cones from healthy anonymised donors were supplied by the UK National Blood Centre with consent obtained via local ethical guidelines granted by Milton Keynes Research Ethics Committee Ref.07/H063/43. PBMCs were separated using the density gradient medium Lymphoprep (StemCell Technologies). First leucocyte cones were diluted six-fold with room temperature RPMI-1640. Then the leucocyte cone/RPMI mix was layered over Lymphoprep (AXIS-SHIELD), with centrifugation for 25 minutes, 2000 rpm without deceleration. The mononuclear cell layer was then harvested, before resuspension in cold RPMI-1640. Following three washes with cold RPMI-1640 with centrifugation for 10 minutes at decreasing speeds (2000 rpm, 1800rpm, 1500rpm), the PBMCs were used for generation of monocyte derived dendritic cells. PBMCs were resuspended in 3ml ice cold MACS buffer (Phosphate buffered saline (PBS) (Sigma) with 1% (v/v) BSA (Sigma) and 2mM EDTA), followed by addition of 250ul anti-CD14 MicroBeads (Miltenyl Biotech) and incubation for 20 minutes on ice. The cell/bead suspension was then washed in 35ml ice

cold MACS buffer before centrifugation (1500rpm for 8 minutes) and then resuspended in 4ml ice cold MACS buffer. An LS column (Miltenyl Biotech) was placed in the magnetic field of a MACS separator (Miltenyl Biotech) and washed with 3ml ice cold MACS. The cell/bead suspension was added to the column and the unlabelled cells allowed to pass completely through before washing the column three times with 3ml ice cold MACS. CD14 positive cells were then collected by removing the LS column from the magnetic field and flushing with 5ml ice cold MACS. The cell suspension was washed in 50ml cold RPMI followed by centrifugation (1500rpm for 8 minutes). The cells were then resuspended in R10 media containing 40ng/ml recombinant IL-4 (Peprotech) and 40ng/ml recombinant GM-CSF (Peprotech) at a concentration of $1x10^6$ cells/ml. On day 3, fresh IL-4 and GM-CSF were added to the culture plates at 40ng/ml. Monocyte derived dendritic cells (moDCs) were harvested on day 4 or day 5 depending on the downstream application. Flow cytometry was used periodically to check purity and maturity.

2.1.4 Isolation of murine bone marrow derived mononuclear cells (BMMCs) and generation of bone marrow derived macrophages (BMDMs)

Dissected legs were sterilised in 70% ethanol for one minute, and then washed in sterile PBS. The tibia and femur were carefully separated, and the proximal and distal epiphyses removed. A 26-gauge needle attached to a 20ml syringe containing PBS was used to flush the bone marrow from both the tibia and femur into a sterile collection tube. Marrow from both tibias and femurs from a single mouse was combined into a single tube. The suspension was then gently homogenised using a 70uM cell strainer and the plunger from a sterile 5ml syringe. The strainer was then washed with PBS. Following centrifugation at 1500rpm 5 minutes and resuspension in PBS, cell number was counted. After a further

centrifugation at 1500rpm 5 minutes, the pellet was resuspended in sterile freezing media (90% FCS, 10% DMSO) at $1x10^7$ cells/ml, and 1ml aliquots were transferred to cryovials for freezing. Seven days before the planned experiment, the cells were thawed and cultured in R10 with HEPES buffer containing 10ng/ml GM-CSF (Peprotech) at $1x10^6$ cells/ml. 50% of the media was replaced with fresh R10 with HEPES buffer containing 10ng/ul GM-CSF on day 3 and day 5. Differentiated macrophages were harvested on day 6 using Versene (Invitrogen) to detach. For M0 macrophages, no further cytokines were used in the media and cells were plated for experiments in fresh R10 with or without antibiotics. Alternatively, M0 macrophages were further differentiated for 16 hours in R10 media with ultra-pure LPS 20ng/ml (Invitrogen) and IFN-γ 50ng/ml (Peprotech) for M1 macrophages or 20ng/ml IL4 (Peprotech) for M2 macrophages. Experiments were performed on day 7 of culture.

2.1.5 Culture of cell lines

Human THP-1 cell line

The human THP-1 cell line was purchased from ATCC and cultured in R10. The cells were split to a density of $0.5x10^6$ cells/ml twice weekly, to a maximum of 20 passages.

Murine RAW264.7 cell line

The murine RAW264.7 cell line was purchased from ATCC and cultured in D10. The cells were split 1:6 twice weekly, to a maximum of 20 passages.

Human HEK293T cell line

The human HEK293T cell line were kindly provided by Prof. Jan Rehwinkel's group, WIMM, University of Oxford and cultured in D10. The cells were split 1:6 twice weekly, to a maximum of 20 passages.

Human HEK293/NOD2 cell line

The human HEK293/NOD2 cell line was purchased from InvivoGen. The line was produced by stable transfection of HEK293 cells with the pUNO-hNOD2 plasmid which expresses the human NOD2 gene with blasticidin resistance. Cells were cultured in D10 containing 10μg/ml Blasticidin (InvivoGen) and split 1:6 twice weekly, to a maximum of 20 passages.

2.1.6 Freezing, storage and thawing of primary cells and cell lines

Aliquots of 5-10^6 cells were resuspended in 1ml freezing media (10% (v/v) DMSO (Sigma) and 90% (v/v) FCS (Sigma)) and transferred to 2ml cryovials (Sigma) in a Mr Frosty freezing container (Thermo Fisher) filled with Isopropanol. This was placed in a -80°C freezer, producing a sample cooling rate of 1°C per minute. After 24 hours the cryovials were transferred to the liquid nitrogen storage facility for long term storage.

When required, frozen cells were thawed rapidly by placing the cryovial in a 37°C waterbath. The thawed cell suspension was washed in pre-warmed media, and then resuspended in the appropriate growth media and transferred to the incubator for culture.

2.2 Protein biology techniques

2.2.1 Cell lysis

Cells were harvested and washed in ice cold PBS. Cell pellets were resuspended in lysis buffer (Cell Signaling Lysis Buffer 20mM Tris-HCL pH7.5, 1mM Na2EDTA, 1mM EGTA, 1% Triton, 2.5mM sodium pyrophosphate, 1mM beta-glycerophosphate, 1mM Na_3O_4, 1μg/ml leupeptin supplemented with 1% (v/v) HALT protease inhibitor cocktail (Thermo Fisher) and 1% (v/v) Phosphatase inhibitor cocktail 3 (Sigma) and 1mM PMSF (Cell Signaling)). Samples were then incubated on ice for 15 minutes, with vortexing every 3 minutes. Cell debris was

removed by centrifugation of the lysate at 12000rpm for 20 minutes at 4°C. The clarified lysate was then transferred to fresh pre-cooled Eppendorfs. Lysates were processed for SDS-PAGE with NuPage LDS Sample buffer (Life Technologies) and 100mM dithriothreitol (Sigma), followed by heating at 70oC for 5 minutes. Samples were then either used immediately for immunoblotting or frozen at -80°C until immunoblotting was performed.

2.2.2 Protein quantification by the Bicinchoninic acid assay

The protein concentration of each cell lysate was calculated using the Bicinchoninic acid assay (BCA). A bovine serum albumin (BSA) standard was produced by plating decreasing volumes of 1mg/ml BSA in triplicate, made up to 20ul total volume with PBS to provide a range of BSA concentrations from 1mg/ml to 0.025mg/ml in a flat bottom 96 well plate, 20μl of lysis buffer was plated in triplicate as the blank. 2μl cell lysate was added to 18ul PBS in triplicate to produce 10 fold dilutions of the cell lysates. Pierce BCA Reagent A was added to Pierce BCA Reagent B (Thermo Fisher) at a ratio of 50:1. 150μl of BCA Reagent mix was added to each well, and the plate incubated at 37°C for 30 minutes. Absorbance was read at 570nm. A standard curve was then constructed to allow calculation of protein concentration.

2.2.3 Protein quantification by the Bradford assay

Alternatively, protein concentration of cell lysate was determined using the Bradford assay. In brief, 5μl of cell lysate or BSA standard (BioRad) in the range 2mg/ml to 0.125mg/ml was plated in triplicate in a 96 well flat bottom plate and mixed with 250μl Bradford reagent (BioRad). Absorbance was read immediately on a BioRad iMark Microplate reader at 595nm

subtracting the value at 450nm, a standard curve constructed and protein concentration calculated.

2.2.4 Polyacrylamide gel electrophoresis (PAGE)

If frozen, lysates with LDS sample buffer/DTT previously added were thawed by heating at 70^{o}C for 1 minute. Equal concentrations of protein (typically 30-50μg) were loaded into lanes of NuPage pre-cast polyacrylamide gels (Invitrogen). Amersham ECL rainbow marker (GE Healthcare) pre-stained protein ladder was also loaded. Electrophoresis of the gel was performed in Invitrogen mini or midi tanks depending on gel size at 120V in NuPage MES SDS (Life Technologies) or NuPage MOPS SDS (Life Technologies) running buffer diluted in dd$H_2$0. Electrophoresis was continued until adequate separation of the molecular marker was achieved.

2.2.5 Immunoblotting

Following electrophoresis, transfer of the proteins on the gel to PVDF membrane (GE Healthcare) was performed using a wet transfer method, in NuPage (Life Technologies) transfer buffer containing 10% (v/v) methanol in a NuPage (Life Technologies) transfer tank at 30V for 90 minutes on ice. An alternative transfer method, using the iBlot2 dry blotting system (Invitrogen) with PVDF membrane stacks (Invitrogen) for 7 minutes at 20V was used for larger gels. When the iBlot 2 system was used, the gels were washed in 20% ethanol before transfer.

Membranes were blocked with 5% (v/v) bovine serum albumin (Sigma) or 5% (v/v) skimmed milk powder (Sigma) in Tris-buffered saline with tween (TBST) (10mM Tris-HCL pH8, 150mM

NaCl in double distilled H_20) with 0.075% (v/v) Tween 20 (Sigma) for one hour at room temperature on a roller-mixer. Primary antibodies were then added at the manufacturer's recommended dilution in the recommended buffer and incubated overnight at 4°C on a roller-mixer. The following day, the membranes were washed 6 times in TBST. Then species specific HRP-conjugated secondary antibodies were added to 5% skimmed milk powder in TBST at the manufacturer's recommended dilution, with incubation for one hour at room temperature on a roller-mixer. When a β-actin HRP conjugate was used, incubation in 5% skimmed milk powder in TBST for one hour at room temperature in 5 was sufficient. Membranes were then washed 6 times in TBST before addition of Amersham enhanced chemiluminescence (ECL) solution (GE Healthcare) or Amersham ECL prime (GE Healthcare). Membranes were then developed using Amersham Hyperfilm (GE Healthcare) and a radiograph developing system (Xograph Healthcare).

2.2.6 Silver staining

This was performed using a silver staining kit (Pierce). Proteins were separated by electrophoresis, and the gels washed twice in ddH_20. The gels were then fixed by incubating twice for 15 minutes each time with fixing solution (30% (v/v) ethanol, 10% (v/v) acetic acid). They were washed twice in 10% (v/v) ethanol for 5 minutes each and once in ddH_20 for 5 minutes. Gels were then incubated in 0.2% (v/v) silver stain sensitizer diluted in ddH_20 for 1 minute, and washed in ddH_20 twice for 1 minute each. They were then incubated in 2% (v/v) silver stain enhancer in silver stain solution for 30 minutes, followed by two washes with ddH_20 for 20 seconds each. The gels were developed in developer solution, with the reaction terminated with 5% (v/v) acetic acid stop solution, which was briefly added, washed off, then added again for 10 minutes.

2.2.7 *In vitro* kinase assay (non-radioactive)

200ng of the recombinant kinase protein GST-TBK1 (Sigma) was mixed with 1x kinase buffer (25mM Tris-HCL (pH7.5), 5mM β-glycerophosphate, 2mM DTT, 0.1mM Na_3VO_4, 10mM $MgCl_2$) (Cell Signaling) with or without 0.2mM ATP (Cell Signaling). Next 200ng of the recombinant substrate proteins GST-IRF3 (Abnova) or His-Ataxin-3 (R&D Systems) were added, and finally the samples were made up to a total volume of 25μl. In samples lacking kinase, substrate or ATP, the equivalent volume of ddH_20 was added. The samples were then incubated at 30°C for 1 hour. The reaction was terminated with the addition of LDS sample buffer (Invitrogen) and 100mM DTT, and the samples were heated at 70°C for 10 minutes.

2.2.8 Enzyme-linked immunosorbent assay

Supernatant was harvested from cells at the indicated time point after the relevant treatment and frozen at -80°C. Sandwich ELISA kits for human and mouse IL-1β (R&D Systems) were used according to manufacturer's protocol. Nunc Immuno ELISA plates (Thermo Fisher) were used. Briefly, plates were coated with capture antibody diluted to the recommended working concentration and incubated overnight at room temperature. Following three washes with PBS containing 0.05% (v/v) Tween, the plate was blocked with Reagent Diluent for one hour at room temperature. Following three further washes, diluted samples and standard were added to the plate and incubated at room temperature for 2 hours. Samples were diluted in Reagent Diluent (R&D Systems) following optimization against the sensitivity of the assay and analysed in duplicate or triplicate. A 2 fold serially diluted standard was plated in duplicate or triplicate with blank wells containing Reagent Diluent only. The plate was washed a further three times, and detection antibody diluted to

the recommended working concentration was added for two hours at room temperature. After three washes, Streptavidin-HRP was added at the recommended working dilution to each well for 20 minutes at room temperature. After three further washes, Substrate Solution was added and the plate incubated for 20 minutes in the dark at room temperature. The reaction was terminated with Stop Solution. Absorbances were read using a BMG Labtech Fluostar Optima plate reader - readings at 570nm absorbance were subtracted from readings at 450nm. A seven point 2x serially diluted standard curve was constructed and cytokine concentrations in each sample calculated.

2.2.9 Subcellular fractionation

Cells were fractionated using a NE-PER nuclear and cytoplasmic extraction kit (Thermo Fisher) according to the manufacturer's instructions, using stepwise cell lysis and centrifugal isolation of nuclear and cytoplasmic fractions. Typically 5-10x10^6 cells were used per condition. Heat shock treatment, as a positive control for Ataxin-3 recruitment to the nucleus, was performed by incubating live cells in a water bath at 42^{o}C for 1 hour. Following fractionation, the protein concentration of each fraction was determined by BCA, and equal amounts of protein loaded for immunoblotting.

2.2.10 Phosphoprotein purification

After the appropriate treatment, cells were harvested on ice and washed once with ice cold modified Hanks Buffered Saline (HBS) (20mM HEPES pH 7.4, 150mM NaCl in dd$H_2$0). The Qiagen phosphoenrichment kit (Qiagen) was then used, following the manufacturer's protocol. Cell pellets were lysed in Qiagen "Phosphoprotein lysis buffer" containing 0.25% (v/v) CHAPS with 1% (v/v) phosphatase inhibitor cocktail 3 (Sigma), protease inhibitor tablet

(Qiagen) and the nuclease 0.0002% (v/v) Benzonase (Qiagen) at 4°C for 40 minutes, with vortexing every 10 minutes. Cell debris was removed by centrifugation of the lysate at 13300rpm for 30 minutes at 4°C. The clarified supernatant was then transferred to fresh pre-cooled tubes and protein concentration determined by BCA assay. The samples were then diluted in Qiagen "wash buffer" containing 0.25% (v/v) CHAPS to a concentration of 0.1mg/ml. Aliquots of whole cell lysate and diluted whole cell lysate were kept for subsequent immunoblot. The phosphoenrichment columns were washed with 6ml "wash buffer", before the diluted samples were loaded onto the columns. Following two further washes of the columns with 6ml "wash buffer", the phosphoenriched fraction was eluted from the columns using Qiagen "elution buffer" containing 0.25% (v/v) CHAPS. Following concentration of the eluted fraction to a volume of 200-300µl using 9k molecular weight cut-off concentrator columns (Thermo Fisher) with centrifugation 13000 rpm 30 minutes, protein concentration was measured by BCA. For mass spectrometry (MS) experiments, phosphoenriched lysates were stored at -80°C. Otherwise, whole cell lysate, diluted whole cell lysate and phosphoenriched lysates were processed for SDS-PAGE with NuPage LDS Sample buffer (Life Technologies) and 100mM dithriothreitol (Sigma), followed by heating at 70oC for 5 minutes. Samples were then frozen at -80°C until immunoblotting and silver staining was performed.

2.2.11 Immunoprecipitation

Typically $1x10^7$ cells per condition were used per condition. Cells were washed in ice cold PBS and then lysed in 500µl lysis buffer (Cell Signaling Lysis Buffer 20mM Tris-HCL pH7.5, 1mM Na_2EDTA, 1mM EGTA, 1% Triton, 2.5mM sodium pyrophosphate, 1mM beta-glycerophosphate, 1mM Na_3O_4, 1µg/ml leupeptin supplemented with 1% (v/v) HALT

protease inhibitor cocktail (Thermo Fisher) and 1% (v/v) Phosphatase inhibitor cocktail 3 (Sigma) and 1mM PMSF (Cell Signaling)). Lysates were incubated on ice for 10 minutes, vortexing for 10 seconds every 3 minutes. Lysates were then clarified by centrifugation at 14000g for 10 minutes at 4°C and the supernatant transferred to fresh Eppendorfs. Protein concentrations were quantified by BCA. Protein concentrations were adjusted to 1mg/ml and 400-500μg of protein taken forward for IP. 50μl of input fraction was heated with LDS/DTT and stored for later immunoblot.

Protein G Agarose Beads protocol

Pre-clearance of the cell lysates was performed by adding Protein G Agarose beads (Cell Signaling) (40μl beads) to the lysates, followed by incubation with gentle end over end mixing at 4°C for 1 hour. The beads were pelleted by centrifugation at 6000rpm for 5 minutes at 4°C, and the pre-cleared supernatant transferred to fresh Eppendorfs. The primary antibody was added at a pre-optimised concentration. A matched isotype control was used at the same concentration. Samples were incubated with the antibody with gentle end over end mixing at 4°C overnight.

The following morning, Protein G Agarose beads (Cell Signaling) (10μl of beads per 1μg antibody) were added to the lysates, followed by incubation with gentle end over end mixing at 4°C for 3 hours. The samples were centrifuged at 6000rpm for 5 minutes at 4°C, and the supernatant removed. 50μl of supernatant was heated with LDS/DTT and saved for later immunoblot and silver stain. The bead pellets were washed four times with 500μl of lysis buffer containing all protease and phosphatase inhibitors. Finally, immune complexes were eluted from the bead pellet by adding 80μl 1xLDS/DTT buffer (diluted in ddH_20) and

boiling at 95°C for five minutes. Samples were stored at -80°C until downstream analysis by immunoblot and silver stain or processing for MS.

Protein G Dynabeads protocol for identification of ataxin-3 phosphorylation site

$2.5x10^8$ THP-1 cells were used for both the unstimulated and stimulated conditions. Each condition was divided into 5 identical samples for ease of handling. At the end of the 60 minute stimulation, samples were washed twice in ice cold HBS. Samples were lysed in 1000µl lysis buffer for 30 minutes at 4°C with end over end mixing (Cell Signaling Lysis Buffer 20mM Tris-HCL pH7.5, 1mM Na_2EDTA, 1mM EGTA, 1% Triton, 2.5mM sodium pyrophosphate, 1mM beta-glycerophosphate, 1mM Na_3O_4, 1µg/ml leupeptin supplemented with 1% (v/v) HALT protease inhibitor cocktail (Thermo Fisher) and 1% (v/v) Phosphatase inhibitor cocktail 2 and 3 (Sigma) and 1mM PMSF (Cell Signaling)). Lysates were clarified by centrifugation at 14000g for 15 minutes at 4°C, and the supernatant transferred to fresh Eppendorfs. Protein concentrations were calculated by BCA. 50µl of input lysate was heated with LDS/DTT and stored at -80°C for later immunoblot. Next, concentrations were adjusted to 1mg/ml and 7.5mg of protein was taken forward for IP for each condition. The Ataxin-3 primary antibody (BioLegend mouse monoclonal) was added at a 1:50 dilution to each sample (final concentration 10µg/ml) and samples were incubated with gentle end over end mixing at 4°C overnight.

The next morning, Protein G Dynabeads (Thermo Fisher) were washed once in lysis buffer, using a DynaMag2 magnet (Invitrogen) to separate the beads from solution, and 5µl of beads per 1µg of antibody was added to each sample. Samples were incubated with the beads with gentle end over end mixing for 2 hours at 4°C. Following this, the supernatant

was removed using a magnet to separate the beads, with 50μl of the supernatant heated with LDS/DTT and stored at -80°C later immunoblot. The beads were washed 4 times in total with lysis buffer containing all protease and phosphatase inhibitors, with gentle end over end mixing for 5 minutes at 4°C for each wash. Elution of the beads was then performed by incubating the beads with pH 2.8 elution buffer (Pierce) with gentle end over end mixing for 30 minutes at 4°C. The eluate was collected and neutralised immediately with 1/10 volume of 1M Tris-HCL pH 9. Elution and neutralisation was performed a further two times to ensure complete elution. 50μl of the eluate was heated with LDS/DTT and stored for later immunoblot. The remaining eluate (2ml) was stored at -80°C until processing for MS analysis. To confirm elution efficiency, the beads were also heated in 1x LDS/DTT and this was stored for later immunoblot. All other samples were stored at -80°C until immunoblot and silver stain.

2.2.13 Tandem Ubiquitin Binding Entities (TUBEs) Ubiquitin Immunoprecipitation

Typically $2.5x10^7$ THP-1 cells were used per condition. 30 minutes before the end of the experimental conditions, samples were incubated with 10μM MG132 (Sigma) for 30 minutes at 37°C before harvesting, washing once in ice cold PBS and lysing in 1ml Ub-IP lysis buffer (50mM Tris-HCL (pH 8.0), 150mM NaCl, 5mM EDTA, 1% NP-40, 0.5% Deoxycholate, 0.1% SDS, protease inhibitor cocktail (Roche), 1% (v/v) phosphatase inhibitor cocktail 3 (Sigma), 20μM MG132, 50μM PR619 and 100mM N-ethylmaleimide (Sigma). Cells were lysed for 30 minutes at 4°C with gentle end over end mixing. The lysate was clarified by centrifugation at 13000rpm for 20 minutes at 4°C, and the supernatant transferred to fresh Eppendorfs. Protein concentration was calculated by the Bradford assay and protein concentrations normalized to 2mg/ml. Typically 2mg of protein was taken forward for

TUBEs IP. 50ul of input fraction was heated with LDS/DTT and stored at -80°C for later immunoblot. Samples were incubated with 40µl TUBE1 agarose beads (LifeSensors), or control agarose beads (LifeSensors) for 4 hours at 4°C with gentle end over end mixing. The beads were then centrifuged at 3000g for 3 minutes and washed with lysis buffer containing all inhibitors three times (each wash was performed for 5 minutes at 4°C with gentle end over end mixing), followed by two final washes with lysis buffer without SDS and Deoxycholate. Elution was then performed with 50ul of pH 2.8 elution buffer (Pierce) for 30 minutes with gentle end over end mixing at 4°C, followed by immediate neutralisation with 1/10 volume 1M Tris-HCL pH 9. Elution and neutralisation was performed three times in total. Samples prepared for later MS analysis were frozen at -80°C until further processing (100µl of 150µl total eluate). The remaining 50µl, and all eluate from other experiments were heated with 2xLDS/DTT at 70°C for 10 minutes and stored at -80°C until immunoblot and silver staining.

2.2.14 Sample preparation for liquid chromatography tandem mass spectrometry (LC-MS/MS)

For the phosphoproteomics experiment, 25µg from each phosphoprotein enriched sample was adjusted to 175µl with ddH_2O. For the lysates provided for the initial ataxin-3 IP experiment, the identification of the ataxin-3 phosphorylation site experiment, and the TUBEs experiment, 100µl of sample was adjusted to 175µl with ddH_20. All samples were then successively reduced and alkylated for 30 minutes with 5mM dithiothreitol and 20mM iodoacetamide, respectively. The proteins were then precipitated using chloroform-methanol precipitation and the pellet were solubilized in 6M urea, 0.1M Tris pH 7.8. The sample were diluted to 1M Urea. The digestion was performed overnight at 37°C by adding

500ng of trypsin. The peptides were desalted using a C18 cartridge (Waters). Briefly, the samples were conditioned with buffer A (1% (v/v) acetonitrile, 0.1% (v/v) trifluoroacetic acid (TFA) in water) prior to equilibration with buffer B (65% (v/v) acetonitrile, 0.1% (v/v) TFA in water). The acidified peptides were loaded onto the column, washed with buffer A and eluted with buffer B. The solution containing the peptides was dried with a speedvac and solubilised in 1% (v/v) acetonitrile, 0.1% (v/v) TFA in water for mass spectrometry analysis.

The silver stained proteins provided for the initial ataxin-3 IP experiment were fixed with 50% (v/v) methanol, 5% (v/v) acetic acid overnight. The samples were dried with acetonitrile and successively reduced with 10mM DTT and alkylated with 50mM iodoacetamide for 30 min at room temperature. The gels were washed with 100mM ammonium bicarbonate for 10 minutes and dried with acetonitrile prior to digestion. The gels were incubated with 400ng elastase in 25mM ammonium bicarbonate overnight at 37°C. The next day the peptides were extracted using 3 consecutive incubations of 10 minutes with a 25mM ammonium bicarbonate buffer followed by 50% (v/v) acetonitrile, 5% (v/v) formic acid in ddH_20 buffer and finally 85% (v/v) acetonitrile, 5% (v/v) formic acid in ddH_2O buffer. The samples were dried with a speedvac and resuspended in 1% (v/v) acetonitrile, 0.1% (v/v) TFA in ddH_20 for mass spectrometry analysis.

2.2.15 Liquid chromatography tandem mass spectrometry sample analysis

Phosphoproteomic analysis

Peptides were analysed by liquid chromatography tandem mass spectrometry (LC-MS/MS) using a Q Exactive-HF mass spectrometer (Thermo Scientific) coupled to an ultra-high performance liquid chromatography system (Dionex Ultimate 3000 UHPLC, Thermo). The

samples were loaded in a PepMap RSLC column (C18, 2μm, 100A, 75μm x 50 cm) and analysed using a 1 hour linear gradient at a 250 nl/minute flow rate. The gradient used to elute the peptides started at 3 minutes with 2% buffer B (0.1% (v/v) TFA and 5% (v/v) DMSO in acetonitrile) increasing to 5% by 6 minutes followed by an increase up to 35% by 63 minutes. The total length of the analysis was 100 minutes to allow column re-equilibration. The data were acquired with a resolution of 60,000 full-width at half maximum ion intensity with a mass/charge ratio of 400 and a lockmass enabled at 445.120025 m/z. Top 15 precursor ion selection, dynamic exclusion of 27 seconds and fragmentation were performed in higher-energy C-trap dissociation (HCD) mode with a normalised collision energy of 28.

All other samples

Peptides were analysed with nano ultra-high performance liquid chromatography tandem mass spectrometry (nano-UPLC-MS/MS) using a Dionex Ultimate 3000 nanoUPLC, coupled to an Orbitrap Fusion Lumos mass spectrometer (Thermo Scientific) using the same gradient and flow rate. The data were acquired with a resolution of 120,000 full-width half maximum at mass/charge 200 with EASY-IC using the reagent ion source (202 m/z) for internal calibration enabled, Top speed precursor ion selection, Dynamic Exclusion of 60 seconds and fragmentation performed in Collision Induced dissociation (CID) mode with Collision Energy of 35.

2.2.16 Analysis of mass spectrometry data

Label-free quantitative analysis

The raw MS data were analysed using Progenesis QI (Waters) and searched using Mascot 2.5 (Matrix Science). The search settings were as follows: trypsin with 1 miscleavage allowed, oxidation (M) and Deamidation (N, Q) were set as variable modifications and carbamidomethylation (C) as fixed modification. The data was searched against human protein sequences using the UPR_homoSapiens_20141015 (85,889 sequences; 33,866,397 residues) allowing a peptide mass tolerance of 10 ppm and a fragment mass tolerance of 0.05 Da.

Peaks search for phosphorylation

The raw data was analysed in PEAKS Studio 7.5 (Bioinformatics Solutions Inc). The settings were the following: The database used was the swissprot human database was used for the proteins identification. The enzyme used for the search was trypsin allowing a maximum of 2 miscleavages. Fixed modifications: Carbamidomethyl (C); Variable modifications: Deamidated (N), Deamidated (Q), Oxidation (M), Phospho (STY). 10 ppm mass tolerance were allowed for the precursor ions and 0.05 Da was allowed for the fragment ions.

Mascot search for phosphorylation

The raw data was searched using Mascot with following settings. Enzyme: Trypsin; Fixed modifications: Carbamidomethyl (C); Variable modifications: Deamidated (N), Deamidated (Q), Oxidation (M), Phospho (ST), Phospho (Y); Peptide mass tolerance: ± 10 ppm (# 13C = 1); Fragment mass tolerance: ± 0.5 Da; Max missed cleavages: 1.

2.3 Nucleic acid techniques

Nuclease free pipette filter tips (Starlab) were used for nucleic acid isolation and analysis.

2.3.1 DNA isolation

Typically $1x10^7$ cells per condition were harvested and washed once with cold PBS. A DNA buffer set (Qiagen) and Genomic 20/G tips (Qiagen) were used for DNA extraction according to the manufacturer's protocol. The DNA was precipitated by transferring 1ml aliquots of the eluted sample to two 1.5ml Eppendorfs, and adding 0.7ml isopropanolol (Sigma) to each, followed by inversion of the tubes 25 times. The samples were then frozen at -80^{o}C overnight.

The following day, the samples were thawed on ice. Next, they were centrifuged at 12000rpm for 1 hour at 4^{o}C. The pellet was reuspended in 1ml 70% ethanol, followed by a further centrifugation 12000rpm for 1 hour at 4^{o}C. Following removal of the supernatant, the samples were air dried before resuspension in 100ul TE buffer (10mM Tris-HCL pH 8.0, 0.1mM EDTA) (Thermo Fisher). DNA concentrations and purity were then obtained using a Nanodrop 1000 spectrophotometer (Thermo Fisher) and samples were stored at -20^{o}C until further analysis.

2.3.2 Mitochondrial DNA copy number quantification

DNA samples were diluted to 3ng/μl in 0.1 x TE buffer (10% v/v TE buffer (Thermo Fisher) in nuclease free water (Ambion).

The primers used for mitochondrial DNA content were directed against a 107-bp mitochondrial fragment of tRNA-Leu(UUR) (Sigma):

forward 5'-CAC CCA AGA ACA GGG TTT GT-3'

reverse 5'-TGG CCA TGG GTA TGT TGT TA-3'

The primers used for nuclear DNA content were directed against an 86-bp nuclear fragment of β2-microglobulin (Sigma):

forward 5'-TGC TGT CTC CAT GTT TGA TGT ATC T-3'

reverse 5'-TCT CTG CTC CCC ACC TCT AAG T-3'

A polymerase chain reaction (PCR) mix was prepared with 12.5μl Power SYBR Green Master Mix (Thermo Fisher), 8.5μl nuclease free water (Ambion), 1μl of 10μM forward primer and 1μl of 10μM reverse primer per well. The PCR mix (total 23μl) and 2μl (6ng) of DNA were added to wells of a white 0.2ml 96 well PCR microplate (Starlab). Quantitative PCR (qPCR) of each DNA sample was performed in triplicate. The plate was covered with polyolefin optical film (Starlab), centrifuged 400G for 1 minute, then gently vortexed and centrifuged again at 400G for 1 minute. qPCR was then performed using the Bio-Rad C1000 Thermal cycler CFX Realtime system (Bio-Rad) using a custom program: 50°C 2 minutes, 95°C 10 minutes, then 40 cycles of 95°C 15 seconds, 62°C 1 minute. Mean cycle threshold (Ct) number was calculated from the triplicate values. Relative mitochondrial DNA content (copy number) was calculated using a comparative Ct method, normalising to nuclear DNA content.[332] First, ΔCt was calculated by subtracting the mean mtDNA Ct from the mean nucDNA Ct for each sample. Relative mitochondrial DNA content was then calculated using $2 \times 2^{\Delta Ct}$.

2.3.3 RNA isolation

Typically 2-5 x 10^6 cells per condition were harvested and washed once with cold PBS. Pellets were resuspended in 350μl RLT buffer (Qiagen) containing 1% (v/v) Mercapto-ethanol (Sigma) and stored at -80°C. Samples were thawed on ice and homogenized by adding to Qiashredder columns (Qiagen) and centrifuged 2 minutes 13000rpm. RNA

isolation was then peformed using RNeasy kits (Qiagen) according to manufacturer's instructions. The isolated RNA was eluted by added 25μl nuclease free water (Ambion) to the RNeasy column membrane for 5 minutes, followed by centrifugation into fresh Eppendorfs 8000g 1 minute. RNA concentration and purity were obtained using a Nanodrop 1000 spectrophotometer (Thermo Fisher) and samples were stored at -20°C until further analysis.

2.3.4 Reverse Transcription

RNA was reverse transcribed using a high capacity RNA to cDNA kit (Applied Biosystems). 500ng to 2μg of RNA was normalized to the same concentration for each sample using nuclease free water (Ambion) in polypropylene PCR tubes (Starlab). Then an RT mix containing 2μl 10x RT buffer, 0.8μl 25x dNTP mix, 2μl RT random primers, 1μl multiscribe RT, 1μl RNase inhibitor (Applied Biosystems) and 3.2μl nuclease free water was added to each PCR tube (10μl total RT mix) (Starlab) for a total volume of RNA sample and RT mix of 20μl. This was reverse transcribed using a Thermo Cycler (Applied Biosystems) with the program: 25°C 10 minutes, 37°C 120 minutes, 85°C 5 minutes. The cDNA was stored at -20°C.

2.3.5 Quantitative real time polymerase chain reaction (qPCR)

qPCR was performed using TaqMan chemistry (Applied Biosystems). cDNA was diluted 10 fold with nuclease free water. 4.5μl of diluted cDNA was added in triplicate for each sample to wells of a white 0.2ml 96 well PCR microplate (Starlab). 0.5μl of TaqMan FAM-MGB labelled primer (Applied Biosystems) and 5μl TaqMan Universal PCR Mastermix (Applied Biosystems) was added to each well, resulting in a 10μl total reaction mix. The plate was

covered with a polyolefin optical film (Starlab) and centrifuged at 400g for 1 minute. qPCR was then performed using the Bio-Rad C1000 Thermal cycler CFX Realtime system (Bio-Rad) using the manufacturer's recommended program: 50°C 2 minutes, 95°C 10 minutes, then 40 cycles of 95°C 15 seconds, 60°C 1 minute. Mean cycle threshold (Ct) number was calculated from the triplicate values. Relative gene expression was calculated in comparison to the housekeeping RPLP0 control. The difference in gene expression between conditions was calculated using the $2^{-\Delta\Delta Ct}$. This is derived from:

ΔCT=CT(target gene)-CT(control gene)

$\Delta\Delta$CT=ΔCT(target condition)-CT(control condition)

2.3.6 DNA transformation and amplification

Plasmid DNA was transformed using STBL3 chemically competent E. coli (Invitrogen). 100ng of plasmid DNA was added to a vial containing 50µl STBL3 and incubated on ice for 20 minutes, followed by heat shock transformation at 42°C for 45 seconds. Bacteria were recovered with 200µl SOC media (Invitrogen) for 1 hour at 37°C with shaking at 225rpm. 50µl of the transformation mixture was plated on LB/agar plates with ampicillin (100µg/ml) (Sigma), with incubation overnight at 37°C. Single colonies were then selected for further culture in LB broth containing ampicillin (100µg/ml).

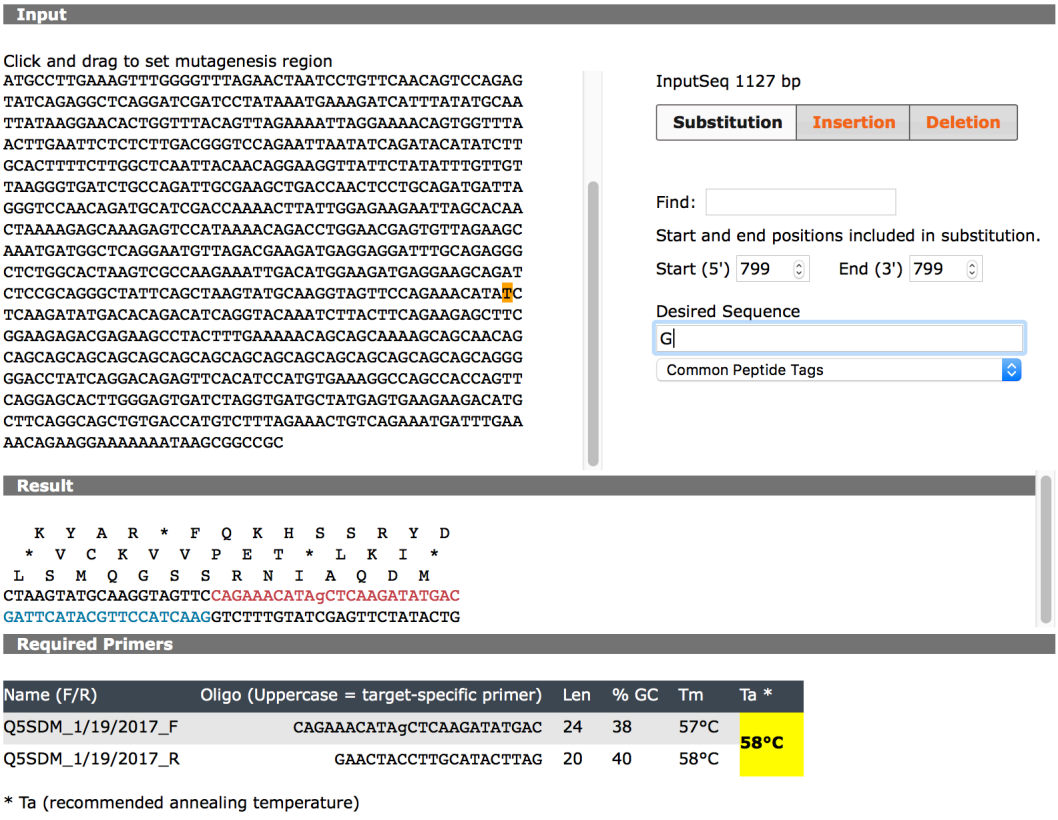
2.3.7 DNA Maxiprep

200ml of bacterial culture was centrifuged 6000g 15 minutes 4°C and the supernatant discarded. Plasmid DNA was extracted using the EndoFree Plasmid Maxi Kit (Qiagen) according to manufacturer's instructions. In brief, bacteria were lysed and then cleared by filtration. Plasmid DNA was purified on gravity-flow Qiagen-tips containing anion-exchange

resin. The DNA was precipitated with 10.5ml isopropanol with centrifugation at 3300g 30 minutes 4°C. The pellet was washed with 5ml 70% ethanol and centrifuged at 3300g 10 minutes 4°C. The supernatant was discarded and the pellet air dried, followed by resuspension in 500ul TE buffer (Invitrogen). DNA concentration and purity was obtained using a Nanodrop 1000 spectrophotometer (Thermo Fisher) and samples were stored at -20°C until use.

2.3.8 Site directed mutagenesis

Primers were designed using the NEBaseChanger software (New England Biolabs) to produce a single substitution of base 799 of the 1127bp Ataxin-3 GFP Plasmid (Dundee MRC PPU) from thymidine to guanine, resulting in a mutation of serine-265 (TCT) to alanine (GCT).



Primers were ordered from Sigma.

Forward primer 5'-CAG AAA CAT AGC TCA AGA TAT GAC-3'

Reverse primer 5'-GAA CTA CCT TGC ATA CTT AG-3'

The NEB Q5 SDM kit (New England Biolabs) was used for site directed mutagenesis. 12.5ul of Hot Start High-Fidelity 2x master mix, 2.5ul of 5uM forward primer and 2.5ul of 5uM reverse primer (final concentration 0.5uM), 1ul of 25ng/μl template DNA (25ng) and 6.5μl nuclease free water were added to a PCR tube (Starlab). PCR was performed in a Thermo Cycler (Applied Biosystems) with the program: 98°C 30 seconds, then 25 cycles of 98°C 10 seconds, 58°C 30 seconds, 72°C 3 minutes 30 seconds, with a final extension 72°C 2 minutes. Kinase, ligase and DpnI treatment was then performed with 1μl PCR product, 5μl 2x KLD reaction buffer, 1ul 10x KLD enzyme mix and 3μl nuclease free water for a total volume of 10μl in a PCR tube (Starlab). The mixture was incubated at room temperature for 5 minutes to complete the reaction.

Bacterial transformation was then performed, and single colonies selected from overnight cultures on LB/Agar plates containing 100μg/ml ampicillin. Following further culture of the colonies, DNA extraction was performed using the Qiagen Miniprep kit (Qiagen) as per the manufacturer's instructions and the plasmids sent for sequencing at the Sanger, Weatherall Institute of Molecular Medicine to confirm successful site directed mutagenesis. For sequencing, the following primers were designed using the NCBI Primer-BLAST tool and made by Sigma.

Primer 1 5'-GAG CAA AGA CCC CAA CGA GA-3'

Primer 2 5'-GGG CAA ACA ACA GAT GGC TG-3'

Primer 3 5'-TCG CAC GTT TTT ACA GCA GC-3'

Primer 4 5'-TTA GCT GAA TAG CCC TGC GG-3'

All five colonies sequenced contained the correct mutagenised plasmid. The mutagenised plasmid originating from a single colony was then amplified following bacterial transformation and the DNA extracted using the Qiagen Maxiprep kit, as above.

2.3.9 Adherent cell transfection

Human HEK293/NOD2 Cells were seeded 24 hours prior to transfection in D10 media without antibiotics. The next day, the media was replaced with fresh media without antibiotics. Transfection mixes were made, comprising Fugene (Promega) at a ratio of 3:1 to amount of DNA plasmid to be transfected, in the appropriate volume of Opti-MEM (Gibco, Thermo Fisher) (10% of volume of media in wells to be transfected). The transfection mixes were incubated at room temperature for 20 minutes and then added dropwise to the wells to be transfected. Cells were either cultured for a further 24 or 48 hours before being used for downstream applications.

2.3.10 Electroporation of human monocyte derived dendritic cells

moDCs were electroporated using the Neon system (Invitrogen). In brief, moDCs were harvested at day 3 post isolation and resuspended at $5x10^7$/ml in Buffer R (Invitrogen). The relevant siRNA (GE Dharmacon) was added at a concentration pre-optimised to achieve maximal protein knockdown at the lowest concentration possible. Final siRNA concentration in the culture media ranged from 4 to 20nM depending on the target. On-Targetplus siRNA SMARTpool (GE Dharmacon), a mix of 4 individual siRNAs against each target, was selected to minimise off-target effects. The control siRNA (On-Taregtplus Non-targeting control pool, GE Dharmacon) used at the same concentration as the target siRNA.

Cells were electroporated in 100ul Neon pipette tips by delivering two pulses with width 20ms at 1475V and 20 ohms. Following electroporation, cells were transferred to pre-warmed R10 media containing IL-4 and GM-CSF at a density of $1x10^6$ cells/ml. Cells were harvested for downstream applications 48 hours later. Protein knockdown efficiency was assessed for every experiment by immunoblot.

2.3.11 Lentivirus particle production

$1x10^6$ HEK293T cells were seeded in 2ml of D10 media without antibiotics in a six well plate. The following day when cells were approximately 75% confluent, the media was replaced with 2ml of fresh D10 without antibiotics. Transfection mixes for each well, containing 8ul Fugene-6 transfection reagent (Promega), 1.6μg shRNA plasmid DNA (SHC016 scrambled control or gene specific shRNA (Mission shRNA, Sigma)), 0.4μg pMD2.G VSV-G encoding plasmid (a gift from Didier Trono, Addgene #12259)[333] and 1μg PAX2 packaging plasmid (a gift from Malin Parmar, Addgene #35002)[334] made up to 200μl with Opti-MEM (Gibco, Thermo Fisher). Transfection mixes were incubated for 20 minutes at room temperature and then added dropwise to the HEK293T cells. Media was replaced with 3ml fresh D10 without antibiotics after 24 hours.

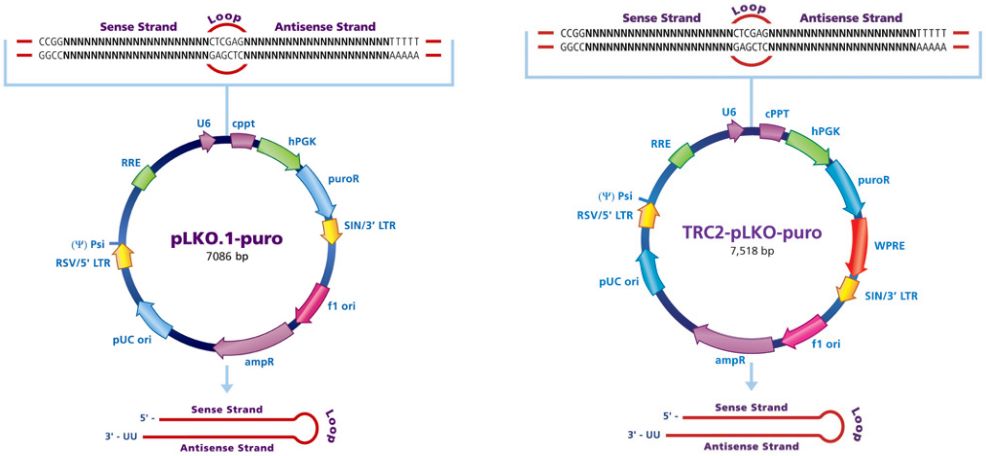


Figure 2.2 Vector maps of lentiviral shRNA plasmids.

Vector maps of TRC1.5 (left) and TRC2 (right) backbone plasmids, encoding scrambled shRNA that targets no known genes or genes of interest.

Vector map images from Sigma, retrieved from:

http://www.sigmaaldrich.com/life-science/functional-genomics-and-rnai/shrna/library-information/vector-map.html#pLKO

2.3.12 Lentiviral transduction and stable cell-line selection

48 hours following transfection, the supernatant containing lentiviral particles (LVP) was harvested passed through a 0.45μm filter (Sartorius), and then added directly to the cells to be transfected. 2ml of LVP containing supernatant was added to 2ml of THP-1 cells in R10 media without antibiotics in individual wells of a six well plate, together with 8μg/ml Polybrene (Sigma) to improve transfection efficiency. Following incubation for 3 hours at 37^{o}C, the cells were harvested, washed, and resuspended at 1x10^{6} cells/ml in R10 media with antibiotics.

After 72 hours, the cells were harvested and resuspended in R10 media with antibiotics and the selection antibiotic puromycin (Sigma) at a pre-optimised concentration of 1μg/ml. After 10 days of continuous selection pressure with puromycin, knockdown efficiency was assessed by immunoblot. For ongoing culture, puromycin selection at 1μg/ml was maintained for alternate passages.

2.4 Cellular techniques

2.4.1 Flow cytometry

Typically $0.5x10^6$ THP-1 cells per condition were plated in 1ml of media in 12 well plates and differentiated for 16 hours with 25ng/ml PMA (Sigma). Following differentiation, the indicated treatments were applied. Cells were then harvested with gentle scraping and transferred to a FACS tube. The following staining protocols were then followed. Cytofluorometric evaluation was by the LSRII flow cytometer (BD Biosciences) with analysis of the data by FLOWJo.

LAMP1 staining

The cells were pelleted by centrifugation (all centrifugation steps for FACS were 1700 rpm for 3 minutes at 4°C), and resuspended in ice cold FACS staining buffer (PBS with 1% (v/v) BSA). Following further centrifugation, the cells were resuspended in 100µl of Cytofix/Cytoperm buffer (BD Biosciences) and incubated for 20 minutes on ice. 300µl of Perm/Wash buffer (BD Biosciences) was added, and the tube centrifuged. The cells were resuspended in 100ul Perm/Wash buffer containing Brilliant Violet 421 LAMP1 antibody (BD Biosciences), and incubated on ice for 30 minutes. The tube was then centrifuged and the cells resuspended in 250ul FACS staining buffer before undertaking cytofluorometric evaluation.

MitoSOX Red staining

The cells were pelleted by centrigugation and resuspended in room temperature HBSS (Thermo Fisher) to wash, then centrifuged. The cells were resuspended in 200µl MitoSOX red solution (final concentration 5µM MitoSOX red (Invitrogen) in HBSS) and incubated for

15 minutes in the 37°C cell culture incubator. 200μl of HBSS was added, and the tube centrifuged. The cells were resuspended in 250μl HBSS and cytofluorometric evaluation performed.

LysoTracker staining

The cells were pelleted by centrifugation and resuspended in room temperature HBSS (Thermo Fisher) to wash, then centrifuged. The cells were resuspended in 200μl LysoTracker Deep Red solution (final concentration 100nM LysoTracker Deep Red (Invitrogen) in HBSS) and incubated for 10 minutes in the 37°C cell culture incubator. 200μl of HBSS was added, and the tube centrifuged. The cells were resuspended in 250μl HBSS and cytofluorometric evaluation performed.

Dihydrorhodamine 123 (DHR) staining

The cells were pelleted by centrifugation and resuspended in room temperature PBS to wash, then centrifuged. The cells were resuspended in 50μl DHR solution (final concentration 2.5μg/ml DHR 123 (Invitrogen) in PBS) and incubated for 30 minutes at 37°C in a water bath. As a positive control, 50μl of PMA (final concentration 100ng/ml (Sigma) in PBS) was added to control samples for the final 15 minutes. The cells were centrifuged and then washed once with PBS, before resuspension in 200μl FACS staining buffer. Cells were fixed with the addition of 200μl 1% PFA and cytofluorometric evaluation performed.

2.4.2 Confocal immunofluorescence microscopy

Cells were plated in 8-well detachable tissue culture chambers on a PCA slide (Sarstedt) coated with 0.01% poly-l-lysine (Sigma) – cells were at a density of 1-2x10^5 cell per well in

250ul of appropriate media. At the end of the experiment, cells were washed twice with PBS, fixed with 4% paraformaldehyde (Sigma) for 15 minutes and permeabilised with 0.5% (v/v) Triton X-100 (Sigma) for one minute twice. Cells were blocked overnight at 4°C with 150µl blocking solution per well (5% (v/v) human serum (Sigma), 5% (v/v) goat serum (Sigma), 5% (v/v) FCS (Sigma).

The following day, cells were incubated with primary antibody diluted in 140µl blocking solution at a pre-optimised or manufacturer recommended concentration for 1 hour at room temperature. Following three washes with PBS (250µl per well, 5 minutes gentle shaking), cells were incubated with the species appropriate fluorescently labelled secondary antibody for 1 hour at room temperature. Cells were washed three further times with PBS, and the detached slide was then mounted with Vectashield mounting media containing DAPI (Vector Laboratories). Alternatively, cells were incubated with 200µl PBS containing 1:100 DAPI (Thermo Fisher) for 15 minutes at room temperature and the detached slide was mounted with Vectashield mounting media without DAPI (Vector Laboratories). A cover slip was attached, and the edges sealed with nail varnish. Slides were stored in the dark at 4°C until imaging. A Zeiss LSM 780 inverted confocal microscope or a Leica SP8 STED system was used for imaging. ImageJ was used for image processing and analysis.

2.4.3 Seahorse mitochondrial stress assay

The Seahorse XFe96 Extracellular Flux Analyser was used to measure mitochondrial respiration and glycolysis (Seahorse Bioscience). As THP-1 cells are non-adherent until stimulation, the Seahorse 96 well assay plates (Seahorse Bioscience) were coated with Cell-Tak suspension (Corning). A cell titration assay was run to determine the correct cell

seeding density for THP-1 cells – this was determined to be $1.5x10^5$ cells/well. Next, the optimal working concentrations of the compounds used for the mitochondrial stress test (oligomycin, FCCP and antimycin/rotenone) and the glycolysis stress test (oligomycin and 2-DG) were determined for THP-1 cells. The aim was to maximise the response to each compound with the lowest concentration possible.

The cell seeding density and working concentrations of compounds for murine BMDMs was derived from published literature.[240]

An XFe96 sensor cartridge (Seahorse) was hydrated overnight prior to Seahorse assays by adding 200μl of XF calibrant solution to each well and incubating in a CO2 free incubator at 37°C. The sensor cartridge (Seahorse) was loaded with the test drug compounds immediately prior to the assay and loaded on the Seahorse Analyser.

For experiments involving THP-1 cells, 24 hours before the assay was run, cells were harvested, counted and resuspended at $1.88x10^6$ cells/ml. 2ml of cell suspension was plated in 6 well plates for each condition, with or without the appropriate ligand stimulation for the required duration. On the day of the assay, 1ml of cell suspension from each condition was harvested into 1.5ml Eppendorf tubes. For the mito stress test, cells were resuspended in mito stress test media with or without ligand(s) (XF base media (Seahorse Bioscience) supplemented with 1mM sodium pyruvate (Sigma), 5mM glucose (Life Technologies) and 2% FCS (Sigma) adjusted to pH 7.4 at 37°C and sterile filtered). 80μl of cell suspension ($1.5x10^5$ cells) was then seeded in quadruplicate for each condition and the plate was centrifuged at 200g for 1 minute. Following 30 minutes in a CO_2 free incubator at

37°C, 95ul of fresh mito stress test media was added to each well, and after a further 15 minutes in a CO_2 free incubator the assay was run.

For experiments involving murine BMDMs, cells were harvested on day 6, counted and resuspended in R10 media with HEPES and antibiotics at $0.75x10^6$ cells/ml. 100μl of cell suspension ($0.75x10^5$ cells) were plated in quintuplicate in a Seahorse 96 well assay plate. Cells were then differentiated into M1 or M2 macrophages for 16 hours by adding 50μl of R10 media with HEPES and antibiotics with LPS (final concentration 20ng/ml) and IFN-γ (50ng/ml) for M1 or IL4 (20ng/ml) for M2. The following day, the media was removed, and 180μl of mito stress test media with or without ligands (XF base media (Seahorse Bioscience) supplemented with 1mM sodium pyruvate (Sigma), 2mM glutamine (Sigma), 10mM glucose (Life Technologies) and 1% FCS (Sigma) adjusted to pH 7.4 at 37°C and sterile filtered). Following incubation for 1 hour in a CO_2 free incubator at 37°C, the Seahorse assay was run.

For the THP-1 cells for the mito stress test, final concentrations of injected drugs were 1μM oligomycin, 1μM FCCP, 0.3μM rotenone and 0.3μM antimycin.

For the murine BMDMs for the mito stress test, the final concentrations of injected drugs were 1μM oligomycin, 1.5μM FCCP, 0.5μM rotenone and 0.5μM antimycin.

2.4.4 Bacterial killing assay

For experiments with THP-1 cells, $1x10^6$ cells were seeded per condition in 1ml R10 media without antibiotics in a 24 well plate, and differentiated overnight with 25ng/ml PMA. After

16 hours, the media was changed for 500μl fresh R10 media without antibiotics. Two hours later, *Salmonella Typhimurium* LT2 was added at a multiplicity of infection (MOI) of 20:1. Thirty minutes post infection, wells were washed twice with PBS and 500μl fresh R10 supplemented with Gentamicin 100μg/ml was added. After a further thirty minutes, wells were washed once with PBS and 500μl fresh R10 supplemented with Gentamicin 30μg/ml was added. At the end of the designated post infection period, the medium was removed (and stored at -80°C until later analysis by ELISA) and 500μl of PBS with 1% (v/v) saponin was added to the wells, followed by incubation for 5 minutes at 37°C. 500μl of PBS was added and serial dilutions plated on LB/agar plates. LB/agar plates were prepared in advance by mixing 35g LB/agar powder (Sigma) in 1L ddH_20, and autoclaving for 15 minutes at 121°C to sterilize. The broth was then poured into petri dishes and allowed to solidify, with plates stored at 4°C until the day of use. Once the supernatants were plated on the LB/agar plates, they were incubated overnight at 37°C, and colonies then counted. Alternatively, when cell viability post infection was assessed, cells were detached by incubating with 500μl of trypsin per well for 5 minutes at 37°C, then viability assessed by trypan blue staining (Invitrogen) and counting of live/dead cells.

For experiments with murine BMDMs, cells were harvested and counted on day 6 of differentiation. $3.5x10^5$ cells were seeded per condition in 500μl R10 media with HEPES without antibiotics in a 48 well plates. Cells were either left as M0 macrophages, or differentiated into M1 or M2 macrophages with LPS and IFN-γ or IL4 respectively for 16 hours. The following morning, pre-stimulation of the macrophages was performed with MDP and PAM_3CSK_4 if specified. After two hours, the media was changed for 500ul fresh R10 media with HEPES without antibiotics. *Salmonella Typhimurium* LT2 was added at an

MOI of 10. One hour post infection wells were washed twice with PBS and 500μl fresh R10 with HEPES supplemented with Gentamicin 100μg/ml was added. After a further thirty minutes, wells were washed once with PBS and 500μl fresh R10 with HEPES supplemented with Gentamicin 30μg/ml was added. The remainder of the post infection protocol was as for the THP-1 cell infections.

For confocal microscopy experiments, $2x10^5$ THP-1 cells per well in 250ul R10 without antibiotics were seeded in 8-well detachable tissue culture chambers on a PCA slide (Sarstedt) coated with 0.01% poly-l-lysine (Sigma). They were differentiated with 25ng/ml PMA for 16 hours. The following day, the medium was replaced with 300μl R10 without antibiotics, and then *Salmonella Typhimurium* LT2 added at MOI 20:1. Thirty minutes post infection, cells were washed twice with PBS and the medium replaced with 300ul R10 with supplemented with Gentamicin 100μg/ml was added. After a further thirty minutes, wells were washed once with PBS and 300μl fresh R10 supplemented with Gentamicin 30μg/ml was added. When Lysotracker Deep Red (Invitrogen) was used, it was added one hour before the end of the designated post infection period at a final concentration of 200nM. At the end of the designated post infection period, cells were washed with ice cold PBS and the standard confocal microscopy preparation protocol followed. A single change was made – goat serum was removed from the blocking buffer as the Salmonella antibody used for staining bacteria was raised in goat.

2.5 Phosphatidic acid quantification

$1x10^7$ THP-1 cells were used per condition. The Total Phosphatidic Acid Assay kit (Cell Biolabs) was used as per the manufacturer's instructions. In brief, cells were washed once

in ice cold PBS and resuspended in 1ml cold PBS, transferring to 1.5ml Eppendorfs. Samples were sonicated (32% power, three cycles of 4s with 9s gap between). 1.5ml methanol, 2.25ml 1M NaCl and 2.5ml chloroform were added to the samples and mixed by vortexing. The pahases were separated by centrifuging 1500g for 10 minutes at 4°C. The upper aqueous phase was discarded and the lower chloroform phase washed twice with 2ml of PEU (pre-equilibrated upper phase produced by mixing 50ml chloroform, 50ml methanol and 45ml 1M NaCl and allowing to separate, with the upper phase used). Each time the phases were separated by centrifuging 1500g for 10 minutes at 4°C, with the upper phase discarded each time. After the final wash, the lower phase was split into 1.5ml Eppendorfs and dried in a speedvac. The dried sample was resuspended in 50μl 1x assay buffer (diluted in ddH_20). The samples were stored at -80°C until analysis.

For analysis, Phosphatidic Acid standard was prepared by making two fold serial dilutions of the standard to achieve a range from 250μM to 3.9μM. 10μl of standard and samples was plated in duplicate in a 96 well fluorescence black microtiter plate (Greiner, Sigma). 40μl of lipase solution was added to each well, and the plate incubated at 37°C for 30 minutes. The fluorometric probe was diluted 1:100 in Enzyme Mixture, and 50μl added to each well. The plate was incubated in the dark for 10 minutes at room temperature, and then the fluorescence read with excitation at 560nM and emission at 595nM on a BMG Labtech Fluostar Optima plate reader. A standard curve was constructed and the total phosphatidic acid levels calculated.

2.6 Statistical analysis

Prism (GraphPad) was used to determine the statistical significance in the means of experimental groups. When making multiple comparisons on a data set, analysis was by

one-way ANOVA with post-hoc Bonferroni analysis. For experiments with two sample groups (one condition, one control) and a single comparison, analysis was by paired, two-tailed Student's t-test. Error bars represent Standard Error of the Mean (SEM).

2.7 Materials Appendix

Primary antibodies				
Protein	**Identifier/clone**	**Supplier**	**Species**	**Dilution**
Ataxin-3	65042 1H9-2	BioLegend	Mouse monoclonal	IB 1:1000
Ataxin-3	ab96316	Abcam	Rabbit polyclonal	IB 1:500
Ataxin-3	GTX115032	Genetex	Rabbit polyclonal	IB 1:1000
MIC60	ab110329	Abcam	Mouse monoclonal	IP 1:100
MIC60	ab137057	Abcam	Rabbit monoclonal	IB 1:1000, IF 1:250
LC3B	#3868 D11	Cell Signaling	Rabbit monoclonal	IB 1:1000
LC3	PM036	MBL International	Rabbit polyclonal	IF 1:600
p62	#8025	Cell Signaling	Rabbit monoclonal	IB 1:1000
p62	Clone 3 610832	BD BioSciences	Mouse monoclonal	IF1:200, IB 1:500
LAMP1	328602 H4A3	BioLegend	Mouse monoclonal	IF 1:200
DYNLT3	HPA003938	Sigma	Rabbit polyclonal	IB 1:1000
TBK1	#3504 D1B4	Cell Signaling	Rabbit monoclonal	IB 1:1000
RIPK2	#4142 D10B11	Cell Signaling	Rabbit monoclonal	IB 1:1000
pp38	#4511 D3F9	Cell Signaling	Rabbit monoclonal	IB 1:1000
p38	#9212	Cell Signaling	Rabbit monoclonal	IB 1:1000
IRF3	#11904 D6I4C	Cell Signaling	Rabbit monoclonal	IB 1:1000
pIRF3	#29047 D6O1M	Cell Signaling	Rabbit monoclonal	IB 1:1000
PINK	#6946 D8G3	Cell Signaling	Rabbit monoclonal	IB 1:1000
DRP1	#5391 D8H5	Cell Signaling	Rabbit monoclonal	IB 1:1000, IF 1:100
p-DRP1 ser616	#4494 D9A1	Cell Signaling	Rabbit monoclonal	IB 1:1000
pS6 ser235/6	#4858 D57.2.2E	Cell Signaling	Rabbit monoclonal	IB 1:1000
LAMTOR1	#8975 D11H6	Cell Signaling	Rabbit monoclonal	IB 1:1000, IF 1:100
PLD3	HPA012800	Sigma	Rabbit polyclonal	IB 1:1000
HA	#3724 C29F4	Cell Signaling	Rabbit monoclonal	IB 1:1000

FLAG DYKDDDDK	#14793 D6W5B	Cell Signaling	Rabbit monoclonal	IB 1:1000
TOM20	sc-17764	Santa Cruz	Mouse monoclonal	IF 1:50
HDAC6	#7558 D2E5	Cell Signaling	Rabbit monoclonal	IB 1:1000
Aprataxin	PA5-28952	Thermo Fisher	Rabbit polyclonal	IB 1:500
BTAF1	#2637	Cell Signaling	Rabbit polyclonal	IB 1:1000
Spartin	#13520	Cell Signaling	Rabbit polyclonal	IB 1:1000
MDH2	#11908	Cell Signaling	Rabbit monoclonal	IB 1:1000
LRBA	HPA019366	Sigma	Rabbit polyclonal	IB 1:500
Secondary antibodies				
Rabbit HRP conjugate	#7074	Cell Signaling		IB 1:3000
Mouse HRP conjugate	#7076	Cell Signaling		IB 1:3000
Alexa fluor 488	A-11034	Invitrogen	Goat anti-rabbit	IF 1:200
Alexa fluor 488	A-11029	Invitrogen	Goat anti-mouse	IF 1:200
Alexa fluor 568	A-11036	Invitrogen	Goat anti-rabbit	IF 1:200
Alexa fluor 568	A-11004	Invitrogen	Goat anti-mouse	IF 1:200
Alexa fluor 647	A-21245	Invitrogen	Goat anti-rabbit	IF 1:200
Alexa fluor 647	A-21235	Invitrogen	Goat anti-mouse	IF 1:200
Conjugated antibodies				
Beta actin HRP conjugate	#5125 13E5	Cell Signaling	Rabbit monoclonal	IB 1:100000
Salmonella CSA-1 FITC conjugate	5330-0059	KPL	Goat polyclonal	IF 1:100
Brilliant Violet 421 LAMP1	328626 H4A3	BioLegend	Mouse monoclonal	FACS 1:200

Table 2.1 Antibodies used.

PRR	Catalogue number	Supplier	Dilution
Mitosox Red	M36008	Invitrogen	FACS 5uM
Lysotracker red	L12492	Invitrogen	FACS 100nM
DHR 123	D23806	Invitrogen	FACS 2.5μg/ml

Table 2.2 Additional intracellular stains.

siRNA Target	Catalogue Number
ATXN3	L-012013-00-0005
APTX	L-013368-00-0005
DYNLT3	L-019957--00005
BTAF1	L-01268-00-0005
HDAC6	L-003499-00-0005
Control siRNA	D-001810-10-05

Table 2.3 siRNA Targets (On-Targetplus SMARTpool GE Dharmacon).

Target	Sequence	Clone
Atxn3	CCGGCGTCGGTTGTAGGACTAAATACTC GAGTATTTAGTCCTACAACCGACGTTTTT	TRCN0000007405
Atxn3	CCGGGCAGGGCTATTCAGCTAAGTACTC GAGTACTTAGCTGAATAGCCCTGCTTTTT	TRCN0000007407
Atxn3	CCGGACAGCAGCCTTCTGGAAATATCTCG AGATATTTCCAGAAGGCTGCTGTTTTTTG	TRCN0000435828
Atxn3	CCGGATGTCTAAAGTTAGGGCATTTCTCG AGAAATGCCCTAACTTTAGACATTTTTTG	TRCN000043180
Atxn3	CCGGCGAGTGTTAGAAGCAAATGATCTC GAGATCATTTGCTTCTAACACTCGTTTTT	TRCN0000007406
TBK1	CCGGGCGGCAGAGTTAGGTGAAATTCTCG AGAATTTCACCTAACTCTGCCGCTTTTTG	TRCN0000314840
Scrambled	CCGGGCGCGATAGCGCTAATAATTTCTC GAGAAATTATTAGCGCTATCGCGCTTTTT	SHC016 SHC216

Table 2.4 shRNA plasmids (Mission shRNA Sigma).

PRR	Agonist	Concentration	Supplier
NOD2	MDP	10μg/ml	Invivogen
TLR2	PAM_3CSK_4	1μg/ml	Invivogen
TLR4	LPS	100ng/ml	Invivogen
TLR7/8	R848	1μg/ml	Invivogen

Table 2.5 Pattern recognition receptor agonists.

Compound	Target	Concentration	Supplier
BX795	TBK1	10mM	Invivogen
Ponatinib	RIPK2	50nM	Selleckchem

Table 2.6 Small molecule inhibitors.

Human TaqMan primer	Assay ID
IL6	Hs00985639_m1
IL8	Hs00174103_m1
Il1β	Hs01555410_m1
IL12B	Hs01011518_m1
IL23A	Hs00372324_m1
TNF	Hs00174128_m1
RPLP0	Hs99999902_m1
β-actin	Hs99999903_m1
GAPDH	Hs02758991_g1
ATXN3	Hs00245259_m1
ATXN3L	Hs03300664_s1
JOSD1	Hs00208420_m1
JOSD2	Hs00370615_g1
BTAF1	Hs00287727_m1
HDAC6	Hs00195869_m1
LRBA	Hs01032231_m1
CA9	Hs00154208_m1
VEGFA	Hs0090055_m1
APTX	Hs00214452_m1
PTEN	Hs02621230_s1
HSPD1	Hs010036753_g1
HSPE1	Hs01654720_g1
LRBA	Hs01032231_m1

Table 2.7 Taqman Primers.

Chapter 3: Interrogation of NOD2/TLR signalling through quantitative phosphoproteomics

3.1 Introduction

Hypoxia is a characteristic finding in inflamed tissue including the gastrointestinal lesions seen in Crohn's disease, and it exerts a profound effect upon the immune response. Although hypoxia is known to influence PRR signalling, no studies to date have attempted to map these effects on a systems level. Further, the impact of hypoxia on NOD2 signalling is essentially unknown, despite recent intriguing evidence that the NOD2 gene contains a hypoxia responsive element. Work in this chapter seeks to define novel NOD2/TLR2 signalling pathways by recapitulating the physiologically relevant hypoxic conditions found in inflamed tissue. Quantitative phosphoproteomics is undertaken to provide a proteome-wide analysis of NOD2/TLR2 signalling in both normoxia and hypoxia.

3.1.1 Protein phosphorylation is an important post-translational modification

Protein phosphorylation is a fundamental post-translational modification that regulates signal transduction pathways across almost all known cellular pathways. Indeed, it is estimated that in humans up to 30% of all proteins may be modified by phosphorylation[335]. Changes in the phosphorylation state of a protein are tightly coordinated by the complementary actions of protein kinases which add phosphate groups, and phosphatases which remove phosphate groups, following stimuli[336]. Classically, the terms "phosphoprotein" and "protein phosphorylation" describe the addition of a phosphate group to a serine (S), threonine (T) or tyrosine residue (Y)[337]. Phosphorylation of serine residues is the most common, with the relative abundance ratio of pS:pT:pY estimated at 1800:200:1[338]. Histidine, arginine, lysine, aspartate, glutamate and cysteine may also be

phosphorylated, but in practice these phosphobonds are acid labile and hence undetected in conventional studies of protein phosphorylation. It is however notable that phosphohistidine may account for up to 6% of total protein phosphorylation[339].

Changes in phosphorylation state can modify a protein's activity, localisation, stability and interacting partners. Specifically, it can induce conformational changes within a protein, which are highly dependent on the pre-existing structure, modifying the protein's behaviour. Alternatively, it can directly alter the protein surface for protein-ligand interactions[340]. The ability of phosphorylated proteins to recruit other proteins underlies their role in signalling pathways.

The simplicity, rapidity and reversibility of phosphorylation as a means of regulating protein activity allows the more cumbersome requirement for *de novo* protein synthesis to be bypassed. Further, phosphorylating kinases can target many proteins, including multiple additional kinases, in response to a single stimulus allowing the rapid amplification of a signal. Consequently, this post translational modification is ideally suited to mediate the rapid and wide ranging cellular responses required following an immune challenge. Indeed phosphorylation is central to critical innate immune signalling cascades including the NF-κB and MAPK pathways. The intricate regulation of protein function that can be provided by phosphorylation is exemplified by NF-κB signalling. Activation of NF-κB depends upon the phosphorylation induced proteasomal degradation of the inhibitor of NF-κB proteins (IKBs)[341]. Further, phosphorylation of NF-kB subunits may enhance or downregulate the transcription of specific NF-κB target genes[342]. These examples serve to illustrate that

changes in phosphorylation status can either activate or inhibit cellular pathways, while also providing a level of control more subtle than a simple “on-off switch”.

3.1.2 Quantitative phosphoproteomics allows the dissection of signalling pathways

Given the central importance of phosphorylation in cellular pathways, there has been great interest in the development of analytical strategies for the proteome-wide identification of phosphorylated proteins, and the characterisation of phosphorylation changes under biologically relevant conditions[343]. However, phosphoproteomic analysis faces particular challenges. The first relates to the complexity of the phosphoproteome, with the PhosphoSitePlus database suggesting there are over 200,000 non-redundant phosphorylation sites on approximately 20,000 human proteins;[344] over 95% of these sites have been mapped in mass spectrometry experiments. This strikingly large dynamic range leads to the second challenge of identifying and analysing low abundant proteins that may still play vital functional roles. Thirdly, the rapid temporal changes in phosphorylation state provide a further analytical challenge.

The emergence of highly sensitive mass spectrometry (MS) technology, coupled with advances in the power of computational biology have underpinned recent dramatic advances in the field of phosphoproteomics. Quantitative phosphoproteomics now provides a sensitive, high throughput method of profiling protein phosphorylation, allowing the dissection of diverse cellular pathways. Consequently, it serves as a powerful tool to interrogate immune signalling pathways and has been used by both our laboratory and others to study innate immune cell responses to PRR stimulation[345, 346].

3.2 Aims

This chapter aims to:

1. Undertake preliminary characterisation of NOD2/TLR2 signalling in innate immune cells in hypoxia.

2. Identify changes in phosphorylation state of proteins in signalling pathways downstream of NOD2/TLR2 in both normoxic and hypoxic conditions through quantitative phosphoproteomics.

3. Validate selected candidate proteins identified in the phosphoproteomics screen as differentially regulated by NOD2/TLR2 signalling and hypoxia.

4. Perform preliminary screen of functional significance of validated proteins.

3.3 Results

3.3.1 NOD2 signalling is enhanced in hypoxia and interacts with HIF1α

Two key questions when examining the role of hypoxia in PRR signalling using *in vitro* models relate to the percentage of oxygen used and the duration of hypoxia. For this work, a consistent 1% oxygen was chosen, which recapitulates the oxygen levels described in inflamed tissue and is classically used in the published immunology research to date[186, 207]. To determine the optimal duration of hypoxia, a range of time points were examined between 6 and 24 hours. Human monocyte derived dendritic cells (moDCs) were chosen for study, as they are prototypical innate immune cells which express high levels of NOD2[75].

For initial experiments exploring NOD2 and TLR2 signalling in hypoxia, the protein expression of the master hypoxia regulator HIF1α was examined. CD14+ monocytes were isolated from the peripheral blood of healthy human donors and differentiated into moDCs

with IL-4 and GMCSF in a standard cell culture incubator (normoxic conditions). Following maturation, moDCs were harvested and either returned to standard normoxic conditions or transferred to a 1% oxygen (hypoxic) incubator on day 4 or day 5 post-isolation, depending on the duration of hypoxia. As expected, HIF1α was undetectable in normoxia but was rapidly stabilised in hypoxia and could be detected by immunoblot following 2hr of hypoxia (Figure 3.1 A). Interestingly, more prolonged hypoxia led to downregulation of the protein expression of HIF1α. This phenomenon has been described in other primary cells[347]. Having established a working model system for the induction of hypoxia, the effect of NOD2/TLR2 triggering on HIF1α was examined. Dual stimulation with the NOD2 ligand MDP and TLR2 ligand PAM_3CSK_4 for 24 hours was assessed in moDCs incubated in either normoxia or 24 hours of hypoxia (Figure 3.1 B). NOD2/TLR2 stimulation alone was sufficient to upregulate HIF1α, although this strength of this effect varied between donors. There was further enhancement of NOD2/TLR2 induced upregulation of HIF1α in hypoxia.

To further explore NOD2 and TLR2 signalling in hypoxia, cytokine response was studied. As earlier discussed, cytokine release represents a central response to NOD2 stimulation. Further, hypoxia is known to enhance pro-inflammatory cytokine release triggered by a range of other TLRs, including TLR2, in moDCs[186, 348]. Quantitative real time PCR (qRT-PCR) was undertaken to assess mRNA levels of key cytokines. Ribosomal protein large subunit P0 (RPLP0) was selected as the reference or "housekeeping" gene to normalise gene expression changes, following separate evaluation of GAPDH, β–actin and RPLP0. In line with published literature, both GAPDH and β–actin expression was found to change significantly in hypoxia whereas RPLP0 was unaffected (data not shown)[349].

The mRNA levels of the pro-inflammatory cytokines IL6, IL8 and IL1β were assessed following dual ligand stimulation across 6hr, 16hr and 24hr of hypoxia (Figure 3.2 A-C). Although there was no significant effect of hypoxia on IL6 expression, hypoxia significantly enhanced NOD2/TLR2 stimulated IL8 and IL1β expression, with the most striking difference seen at 16hr of hypoxia. The crosstalk between NOD2/TLR2 and hypoxia was further examined through assessment of a critical downstream target of HIF1α, vascular endothelial growth factor (VEGF) which is a master regulator of angiogenesis in response to hypoxia[350]. As expected, hypoxia alone induced VEGF mRNA expression. However, NOD2/TLR2 stimulation alone led to a significant ten-fold induction in VEGF that was further enhanced in hypoxia (Figure 3.2 D).

Having established that 16hr of hypoxia led to the most striking enhancements of NOD2/TLR2 stimulated cytokine release, the effect of NOD2 and TLR2 stimulation in isolation was examined. While individual ligand stimulation of NOD2 or TLR2 in hypoxia did not enhance IL8 or IL1β mRNA expression, there was significant enhancement of synergistic NOD2/TLR2 triggering (Figure 3.3 A+B). When examining VEGF, there was a trend to enhanced expression with individual ligands in hypoxia, but this only reached significance with synergistic NOD2/TLR2 triggering (Figure 3.3 C).

Together, this data suggests that the synergistic NOD2 and TLR2 induction of the pro-inflammatory cytokines IL8 and IL1β is enhanced in hypoxia in human moDCs. It also suggests a significant crosstalk with HIF1α in both normoxia and hypoxia, as evidenced by the enhanced expression of HIF1α protein and the HIF1α target gene, VEGF. However,

knockdown experiments would be required to confirm the definitive requirement for HIF1α in this VEGF signalling pathway.

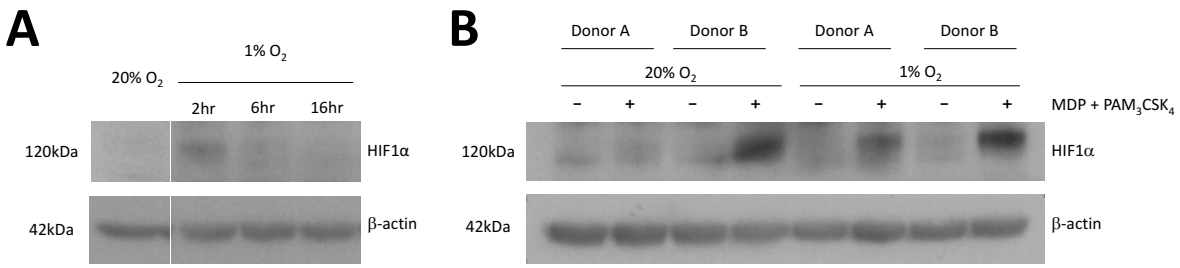


Figure 3.1 NOD2 and TLR2 stimulation increases HIF1α protein expression, and this is enhanced in hypoxia. Immunoblot analysis of moDCs **(A)** incubated for 2-16hr in hypoxia or normoxia and **(B)** incubated for 24hr in hypoxia or normoxia and either unstimulated or stimulated for 24hr with MDP + PAM_3CSK_4. Representative of two independent donors **(A)** or results of two independent donors displayed **(B)**.

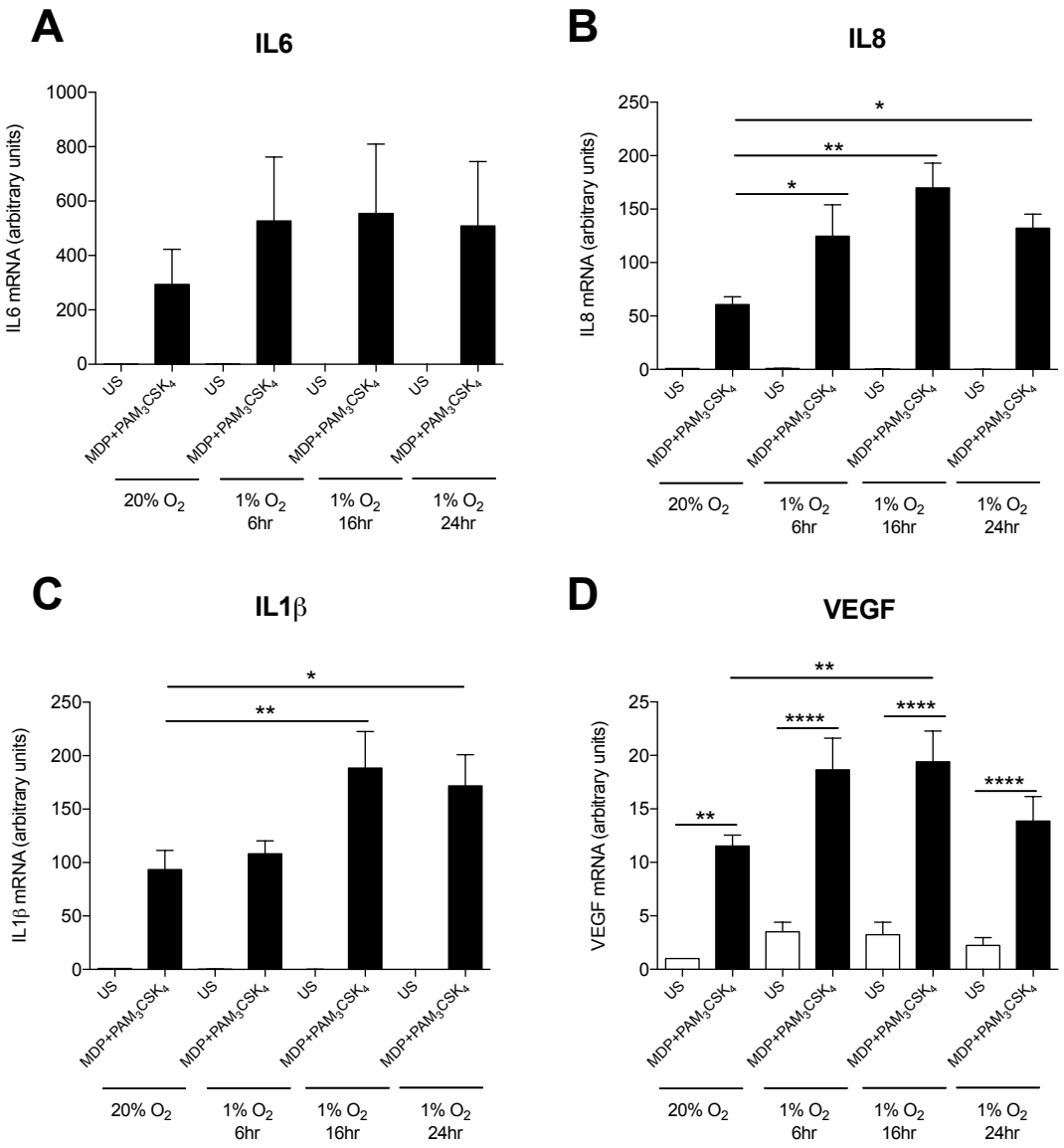


Figure 3.2 NOD2 and TLR2 stimulated production of the cytokines IL6, IL8 and IL1β, and a downstream target of HIF1α, VEGF in different durations of hypoxia. moDCs were assessed by qRT-PCR for mRNA levels of **(A)** IL6, (**B**) IL8, **(C)** IL1β or **(D)** VEGF following 6-24hr of hypoxia or normoxia and 6hr stimulation with MDP + PAM_3CSK_4. n=4, one way ANOVA *p<0.05 **p<0.01, ****p<0.0001

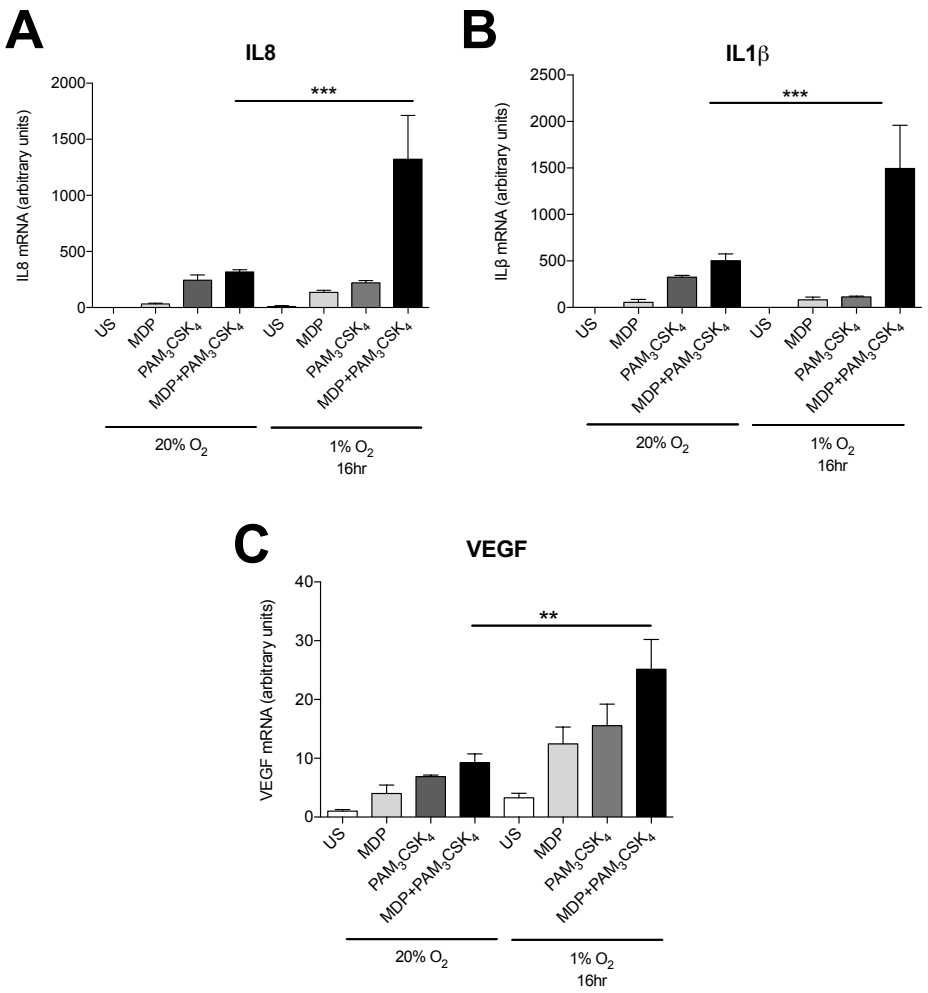


Figure 3.3 NOD2 and TLR2 act synergistically to stimulate production of the cytokines IL8 and IL1β, and a downstream target of HIF1α, VEGF, in hypoxia. moDCs were assessed by qRT-PCR for mRNA levels of **(A)** IL8 **(B)** IL1β and **(C)** VEGF following 16hr of hypoxia or normoxia and 6hr stimulation with MDP or PAM_3CSK_4 or MDP + PAM_3CSK_4. n=3, one way ANOVA **p<0.01 ***p<0.001.

3.3.2 Quantitative phosphoproteomics screen of NOD2/TLR2 signalling in hypoxia

Following these promising exploratory experiments, a quantitative phosphoproteomics screen of NOD2/TLR2 signalling in both normoxia and hypoxia was undertaken. Human moDCs from three healthy donors were used. A 16hr duration of hypoxia was chosen, as this produced the maximal effect on NOD2/TLR signalling in the initial experiments described above. It was decided that the effect of synergistic NOD2/TLR stimulation would be assessed for a number of reasons. Firstly, the exploratory experiments suggested that hypoxia produced the most significant effects on synergistic stimulation. Secondly, use of synergistic stimulation typically produces more striking phosphorylation changes across the proteome than stimulating either NOD2 or TLR2 separately, thus improving the sensitivity of the screen. Thirdly, both these PRRs recognise adjacent components of peptidoglycan, and as such are unlikely to be triggered in isolation in physiological circumstances. Finally, logistical reasons were also taken into account. A minimum of $3x10^7$ cells are required per treatment condition for quantitative phosphoproteomics analysis, and consequently single donors provided insufficient cells to assess stimulation of NOD2 and TLR2 separately. The duration of stimulation was chosen to be 30 minutes, drawing on work from a previous screen in our laboratory demonstrating that this is optimal to assess the effect of NOD2/TLR2 stimulation on the phosphoproteome (unpublished work). This relatively short duration of stimulation emphasises the rapidity of phosphorylation as a post-translational modification.

Figure 3.4 provides an overview of the experimental approach. A label-free approach was undertaken. moDCs were harvested on day 4 for the experiments and subjected to either 16hr of hypoxia or incubated in standard normoxic conditions. For the final thirty minutes

of the treatment, cells were either left unstimulated or stimulated with MDP + PAM_3CSK_4. Following cell lysis, phosphoenrichment was performed using QIAGEN phosphoenrichment columns, which bind phosphorylated proteins through affinity chromatography. Confirmation of successful phosphoenrichment was performed by immunoblot of aliquots of the whole cell lysates and phosphoenriched lysates (Figure 3.5 A). A further quality control check was provided through a silver stain of the phosphoenriched lysates for all conditions (Figure 3.5 B). Phosphoenriched lysates were then prepared for analysis by sequential reduction, alkylation, precipitation, trypsin digestion and desalting. Samples were subjected to liquid chromatography tandem-mass spectrometry (LC-MS/MS) using a Q Exactive-HF mass spectrometer (Thermo Scientific) coupled to an ultra-high performance liquid chromatography system (Dionex Ultimate 3000 UHPLC, Thermo).

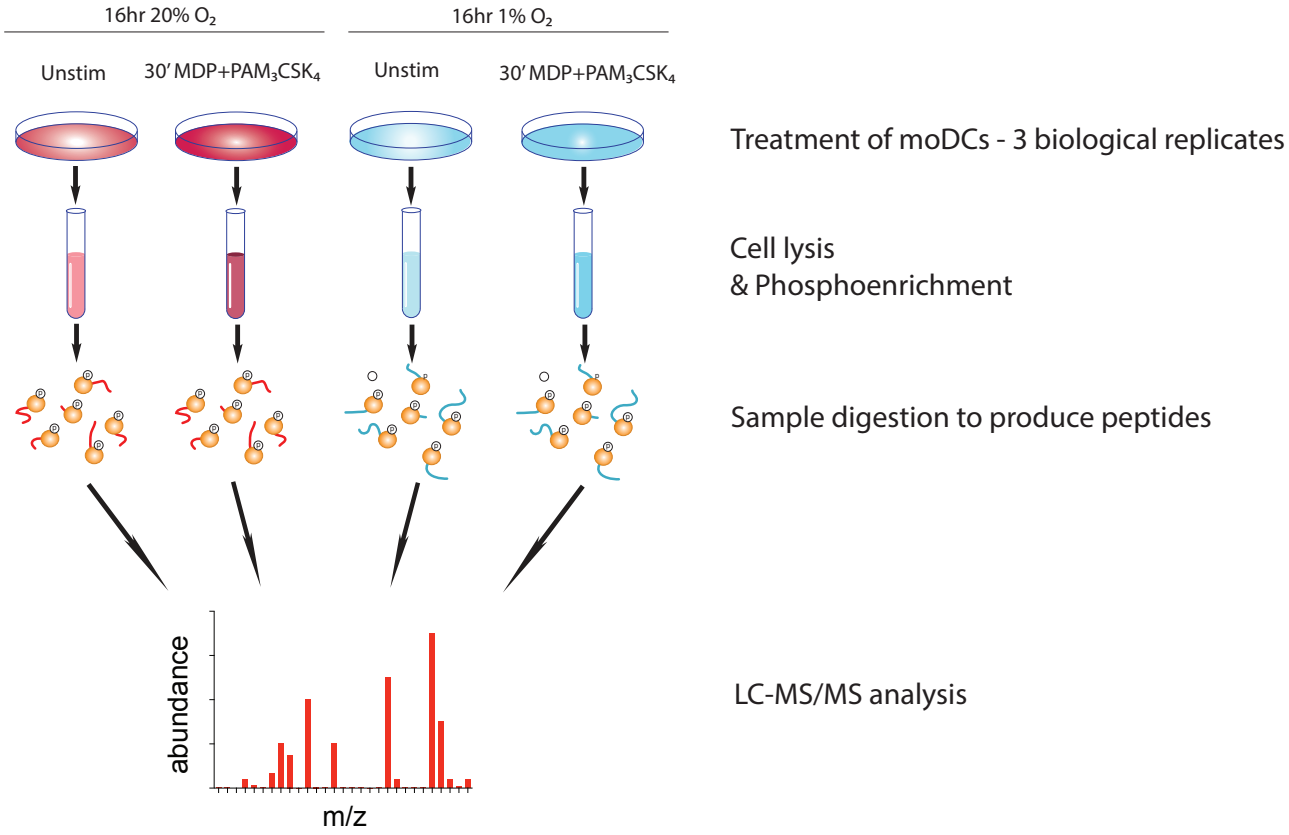


Figure 3.4 Overview of phosphoproteomic experimental approach

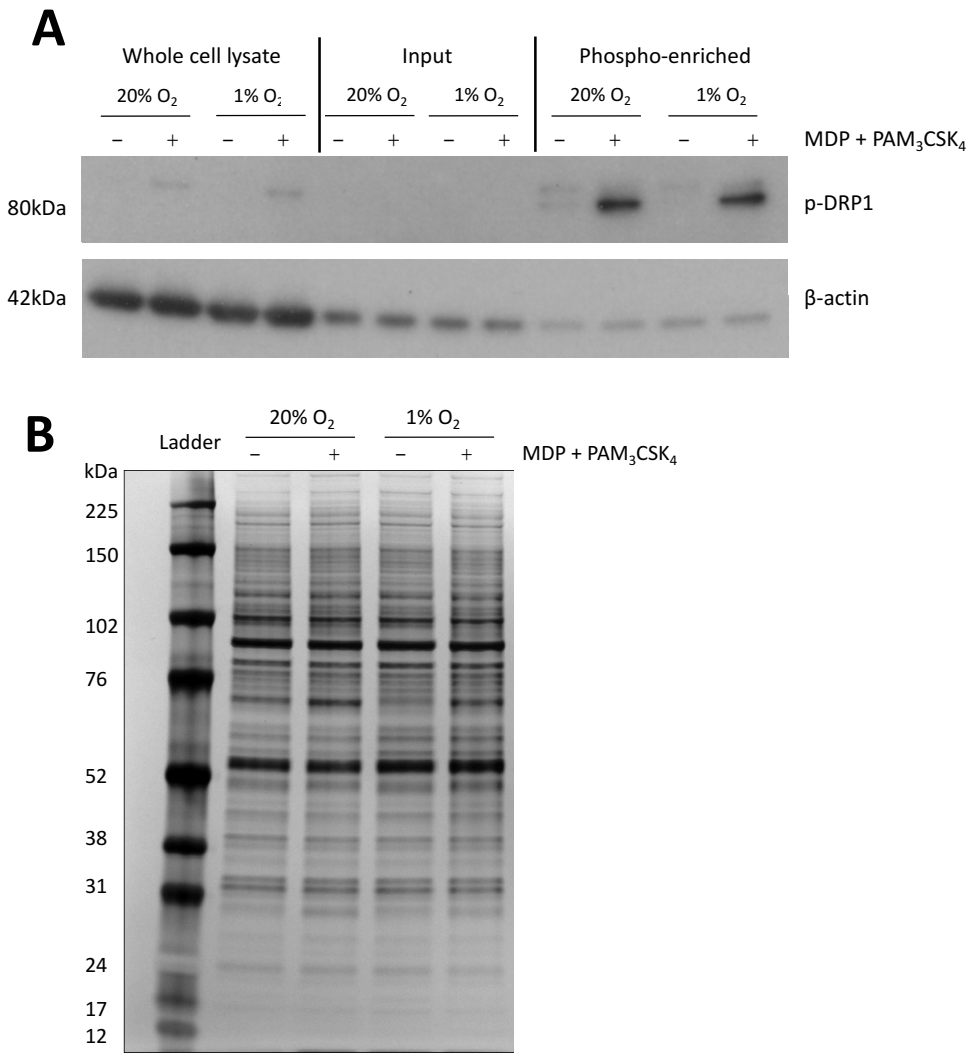


Figure 3.5 Validation of successful phosphoprotein enrichment and silver staining of phosphoenriched proteins. **(A)** Immunoblot using antibodies against p-DRP1 (a known phosphorylation target of NOD2/TLR2 signalling used as a positive control) and β-actin in the whole cell lysates, the normalised diluted lysates loaded onto the phospho-enrichment columns (input) and the phosphoprotein enriched fraction, from one of the three biological replicates. A marked increase in p-DRP1 signal was seen following NOD2/TLR2 stimulation in the phosphoprotein enriched fraction. Reduction in density of β-actin was used both to confirm successful phosphoprotein enrichment, and as an indirect loading control to confirm that equal concentrations of protein were loaded onto the phosphoenrichment columns. **(B)** Silver staining of the phospho-enriched lysates from one of the three biological replicates.

The resultant raw spectral data was analysed using Progenesis QI (Waters Corporation) to identify and quantitate abundance changes in peptides, with proteins then identified by searching the Swiss-Prot proteomics database with Mascot 2.5 (Matrix Science). Comparison of the relative abundance of phosphoproteins in each treatment condition was performed, and averaged across the three biological replicates. This produced a comprehensive dataset of proteins that were phosphoregulated by hypoxia and/or activation of the NOD2 and TLR2 receptors. The LC-MS/MS experiment and analysis was performed in collaboration with the Kessler Laboratory, Target Discovery Institute, University of Oxford.

With an Ions score cut off of 20 and False Discovery Rate (FDR) of 1%, 2880 proteins were identified in all conditions. For each protein in each biological replicate, the relative change in protein abundance induced by any of the four conditions (unstimulated normoxia, unstimulated hypoxia, MDP+PAM_3CSK_4 stimulation in normoxia, MDP+PAM_3CSK_4 stimulation in hypoxia), corresponding to a change in phosphorylation status, was determined as a fold change over its counterpart in a separate condition. 540 proteins were thus identified as changing significantly (ANOVA $p<0.05$) between any condition when averaged across the three biological replicates. Figure 3.6 summarises the process.

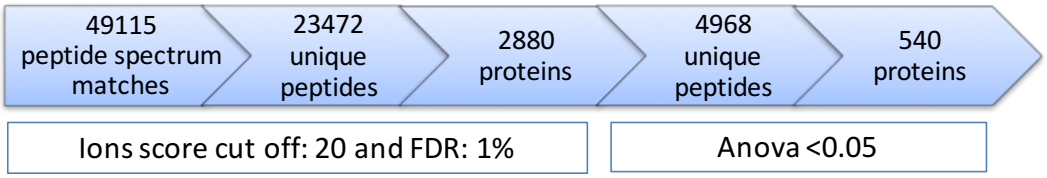


Figure 3.6 Flow chart to demonstrate identification of differentially phosphorylated proteins

Next, principal component analysis (PCA) was performed to explore relationships among the sample replicates for the 540 proteins that met the initial ANOVA criteria. Tight clustering of the biological replicates was seen for all 4 conditions (Figure 3.7). This provides reassurance that there were no significant outliers and acts as a quality control check that differences between the experimental conditions are genuine. The relative impact of the different experimental conditions can also be appreciated.

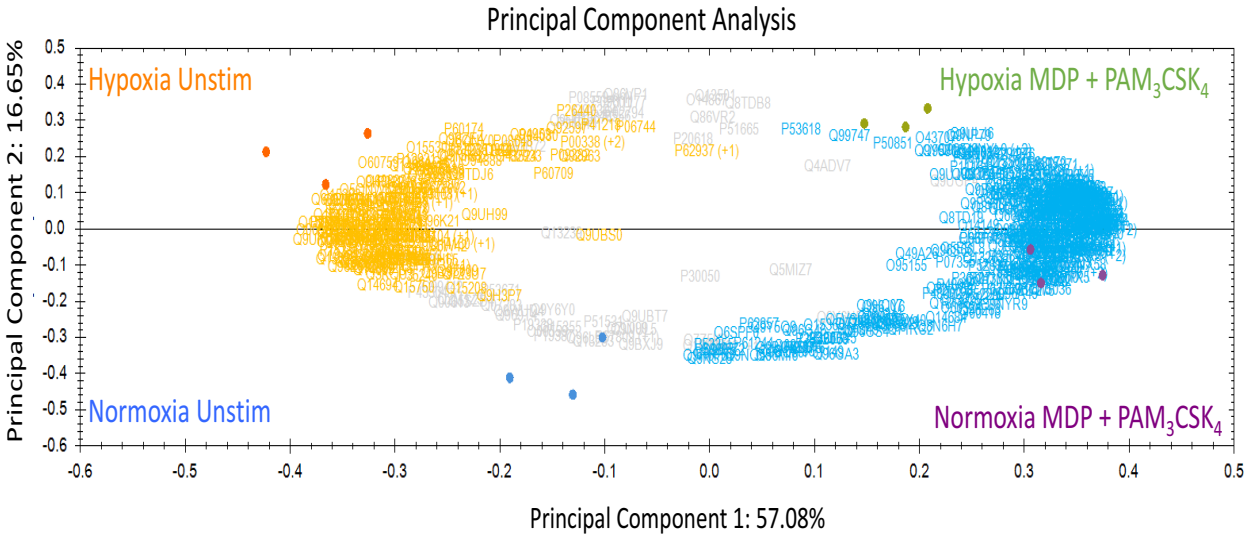


Figure 3.7 Principal Component Analysis of the 540 proteins identified as significant by ANOVA. Each dot represents a biological replicate, with the four separate dot colours representing the different experimental conditions.

The data was further refined by stratifying these proteins according to the mean level of differential phosphorylation. A threshold of a 1.5 fold change between conditions, equivalent to either a 1.5 factor (50%) increase in abundance (phosphorylation) or a 0.67 factor (0.33%) reduction in abundance (dephosphorylation), was selected. The choice of threshold is important – raising it potentially improves the specificity of the screen at the cost of sensitivity, while in contrast lowering it improves sensitivity but reduces specificity. Previous research and quantitative phosphoproteomics screens in our own laboratory

(unpublished data) have determined that this threshold serves as a reasonable proxy for the likelihood of genuine phosphorylation change[351].

When considering the effect of hypoxia alone, 98 proteins were found to be differentially phosphorylated. These proteins were manually cross-referenced with a comprehensive database of approximately 3500 known hypoxia regulated proteins compiled from 1500 publications, HypoxiaDB[352]. 28 of the 98 proteins (28.6%) were listed in the database. A marginal increase in the threshold of the screen, from a fold change of 1.5 to 1.6 (fold change = (mean abundance phosphorylated protein normoxia/mean abundance phosphorylated protein hypoxia) or the converse (mean hypoxia/mean normoxia)), reduced the number of proteins considered to be differentially phosphorylated to 78, but the proportion listed in the database increased to 26/78 (33.3%). This approach of cross-referencing the experimental data with Hypoxia DB provides both a validation of the experimental approach, and suggests the discovery of a number of new hypoxia regulated proteins.

Next, the effect of NOD2/TLR2 stimulation in both normoxic and hypoxic conditions was examined. The phosphorylation status of 259 proteins was found to change significantly upon NOD2/TLR2 triggering in either or both of these two conditions. 96 proteins were found to be differentially phosphorylated on NOD2/TLR2 triggering in hypoxia, in comparison to 37 proteins in normoxia, supporting the hypothesis that hypoxia exerts an additive effect on NOD2/TLR signalling. This data is represented in a VENN diagram (Figure 3.8). As expected, a significant number of proteins known to be involved in the

NOD2/TLR2 signalling cascade were identified including many of the MAPK family, validating the experimental approach.

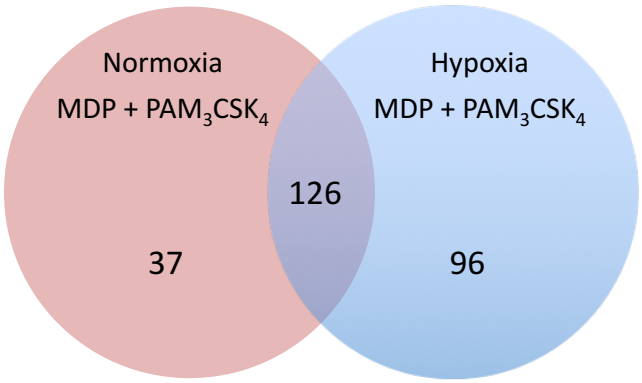


Figure 3.8 Venn diagram demonstrating the distribution of the 259 proteins which were differentially phosphorylated (fold change >1.5 or <0.67) on NOD2/TLR2 stimulation in either normoxia or hypoxia.

3.3.3 Selection and validation of candidate proteins from the phosphoproteomics screen

In order to further refine the list of proteins for validation, a limited literature review was performed of proteins found to be differentially phosphorylated by NOD2/TLR2 stimulation in hypoxia. Intriguingly, a cluster of proteins linked to neurodegenerative diseases were noted including ataxin-3, aprataxin, histone deacetylase 6 (HDAC6), dynein light chain Tctex-type 3 (DYNLT3), spartin and B-TATA binding protein-associated factor 1 (BTAF1) (summarised in Table 3.1). Lipopolysaccharide-responsive and beige-like anchor protein (LRBA) was also of interest, given that LRBA deficiency has been linked to defects in autophagy and CD-like pathology[353, 354]. Mitochondrial malate dehydrogenase (MDH2), an important mitochondrial enzyme in the TCA cycle, was also selected for validation due to a previously described role in the regulation of HIF1α[355]. Table 3.2 lists the proteins selected for secondary validation.

Protein	Neurodegenerative disease	Comments
ataxin-3	SCA3 (Machado-Joseph syndrome)	Hereditary polyglutamine expansion leads to spinocerebellar ataxia
aprataxin	Ataxia oculomotor apraxia-1 (AOA1)[356]	Autosomal recessive cerebellar ataxia caused by mutations in aprataxin gene
DYNLT3	Parkinson's disease[357]	Identified as potential candidate gene in Parkinson's disease and reduced protein expression found in brains of patients with advanced disease
HDAC6	Alzheimer's disease Parkinson's disease Huntington's disease[358]	Linked to neurodegenerative diseases that result from an accumulation of misfolded proteins
spartin	Troyer syndrome[359]	Hereditary mutation in SPARTIN gene causes truncated spartin protein. Complex spastic paraplegia with developmental delay and dysarthria.
BTAF1	Spinocerebellar ataxia Type 17[360]	Indirect link. Acts to remove TATA binding protein from DNA, with polyglutamine expansions in this transcription factor linked to SCA 17

Table 3.1 The link to neurodegeneration.

Protein	Mean fold change in phosphorylation	Confidence score (MASCOT)
ataxin-3	5.09	67.99
aprataxin	2.94	76.78
LRBA	2.71	93.17
DYNLT3	2.51	80.37
HDAC6	2.32	713.48
BTAF1	2.04	81.05
spartin	2.01	36.43
MDH2	0.49	82.75

Table 3.2 Proteins selected for validation. The mean fold change in phosphorylation following NOD2/TLR2 stimulation in hypoxia is provided, together with the MASCOT, which is a scoring index for the validity of protein identification by mass spectrometry, and takes into account the number of unique peptides identified for each protein. A value over 35 is considered significant[361].

A significant advantage of phosphoprotein enrichment is that the lysates can be probed with antibodies raised against the unmodified proteins, with no requirement for phosphospecific antibodies. Indeed a commercially available phosphospecific antibody was only available for one protein selected for validation, HDAC6, but even this may not target

the relevant phosphorylation site. Validation of the 8 proteins was therefore undertaken by immunoblotting phosphoprotein enriched lysates with individual antibodies designed to detect unmodified proteins. Phosphorylation status in moDCs following 30 minutes of NOD2/TLR2 stimulation in both normoxia and hypoxia was studied (Figure 3.9 A). Considering each protein in turn, DYNLT3 showed a consistent reduction in baseline phosphorylation in hypoxia, but NOD2/TLR2 stimulation led to a marked increase in phosphorylation in both hypoxia and normoxia. HDAC6 showed a more subtle increase in phosphorylation on NOD2/TLR2 stimulation in both normoxia and hypoxia, with no differences related to oxygen level. Ataxin-3 was strongly phosphorylated by NOD2/TLR2 stimulation, but this effect was consistently less in hypoxia. Two isoforms of aprataxin were detected, a long and a short form. The long form was phosphorylated by NOD2/TLR2 stimulation in both normoxia and hypoxia. In contrast, appeared to be dephosphorylated by NOD2/TLR2 stimulation in hypoxia only. Notably, the abundance of the short form was markedly increased in the phosphoenriched lysates in comparison to the whole cell lysates, suggesting the importance of phosphorylation as a post-translational modification. BTAF1 showed a subtle increase in phosphorylation on NOD2/TLR2 stimulation in both normoxia and hypoxia.

While the antibodies for MDH2 and spartin detected single bands at the predicted molecular weights when testing the antibodies on moDC whole cell lysates, no bands were detected in the phosphoprotein enriched lysates, even when high sensitivity detection reagent was used. There are a number of possible explanations for this. It may illustrate the exceptionally high sensitivity of LC-MS/MS to detect phosphorylation changes in proteins, which are consequently difficult to validate by the less sensitive method of immunoblotting.

Alternatively these two phosphoproteomic results may simply represent false positives. In the case of LRBA, the antibody tested produced multiple bands at molecular weights ranging from 330kDa to 50kDa in both the whole cell lysates and the phosphoprotein enriched lysates, and thus could not be confidently used for validation. Consequently, qRT-PCR was used to investigate changes in LRBA mRNA levels in hypoxia and following NOD2/TLR2 stimulation (Figure 3.9 B). Interestingly, mRNA levels of LRBA were found to decrease significantly upon NOD2/TLR2 stimulation in normoxia, but this was enhanced in hypoxia. Baseline levels of LRBA were also reduced in hypoxia. The effect of separately stimulating NOD2 or TLR2 was also investigated, and it was shown that stimulation of either PRR also led to a significant reduction in LRBA mRNA level, an effect that was again enhanced in hypoxia.

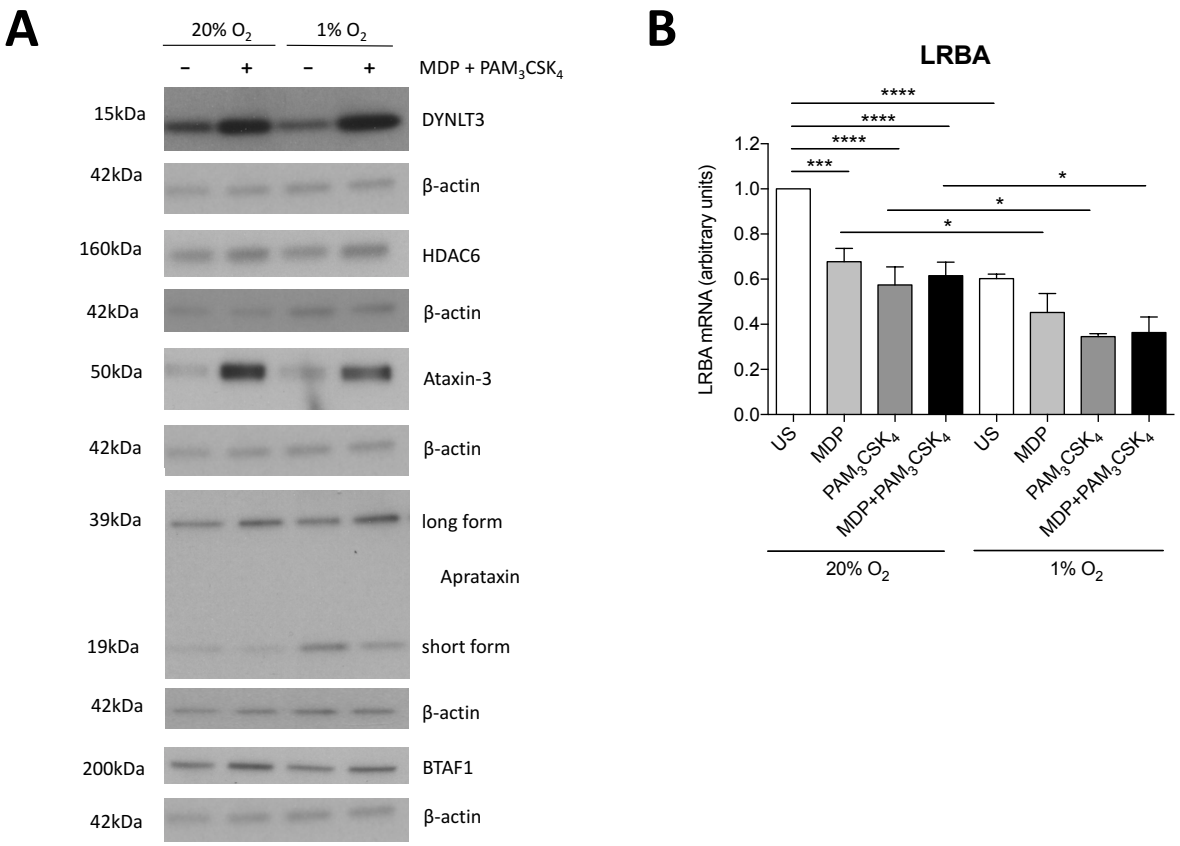


Figure 3.9 Validation of quantitative phosphoproteomics screen. **(A)** Immunoblot of phosphoprotein enriched lysates from moDCs incubated for 16hr in normoxia or hypoxia and then stimulated with 30min MDP+PAM_3CSK_4 or left unstimulated. Representative immunoblots of 2-4 biological replicates. **(B)** qRT-PCR for mRNA levels of LRBA in moDCs incubated for 16hr in normoxia or hypoxia and then stimulated for 6hr with MDP or PAM_3CSK_4. Normalised to RPLP0. n=4, one way ANOVA *p<0.05, ***p<0.001, ****p<0.0001

3.3.4 Preliminary investigation of the functional relevance of validated proteins

Next, a targeted secondary screen to investigate the possible functional relevance of the five proteins validated as differentially phosphorylated (DYNLT3, ataxin-3, HDAC6, aprataxin and BTAF1) was undertaken. First, experiments were undertaken to optimise knockdown of the proteins individually in moDCs using short interfering RNA (siRNA). An important source of error in siRNA experiments are off-target effects. It is known that these effects are largely mediated by antisense seed-region interactions, and consequently a specific siRNA strategy was chosen[362]. On-Targetplus siRNA SMARTpool, a mixture of 4 siRNA sequences, was purchased from GE Dharmacon. During production, the antisense strand seed region has been modified to destabilise off-target activity while the sense strand has also been modified to prevent interaction with the RNA-induced silencing complex (RISC). Further, the simultaneous use of multiple sequences further reduces the chance of off-target effects while also increasing knockdown efficiency[363, 364]. A further source of error relates to the risk of stimulating an immune response. siRNAs can be sensed by PRRs including TLR3, TLR7 and TLR8 to trigger IRF, NF-kB and MAPK pathways, releasing both IFN and inflammatory cytokines[365]. Consequently, the use of a control siRNA with a scrambled sequence is essential to ensure that any observed phenotypic differences following siRNA transfection are not related to the non-specific immunostimulatory effects of siRNA sequences. Finally, use of the lowest possible concentration of siRNA required to produce an effective knockdown of the protein further reduces the chance of off-target effects, and thus different concentrations of siRNA were tested for each protein during the optimisation process. 48hr after transfection with control or target siRNA using an electroporation system, the cells were harvested and processed for immunoblot to assess efficacy of protein knockdown. A dose dependent knockdown effect was seen for each protein (data not

shown), with a final concentration of 10nM typically achieving greater than a 75% knockdown. Consequently, 10nM was selected as the concentration of siRNA for the functional experiments. One protein, HDAC6, could not be efficiently knocked down (< 50% reduction in protein) and thus it was not further assessed. LRBA was also excluded as protein knockdown could not be confidently assessed with the commercial antibody trialled.

For this preliminary screen, NOD2/TLR2 mediated cytokine response was assessed by RT-qPCR. This both focussed on a core NOD2/TLR2 response known to be altered in hypoxia, and allowed the rapid assessment of multiple cytokines (Il8, IL12a, IL23b, TNF, IL1β). The effects of individually knocking down ataxin-3 and aprataxin were assessed in both normoxia and hypoxia. As the NOD2/TLR2 induced phosphorylation of DYNLT3 and BTAF1 appeared unchanged in hypoxia, the effect of knockdown was assessed in normoxia only for these two proteins. moDCs were transfected with the control siRNA or target siRNA on day 3 post isolation, then 36hr later subjected to either 16hr hypoxia or normoxia. In the final 6hr they were either left unstimulated or stimulated with 6hr MDP + PAM_3CSK_4. Cells were then harvested and processed for qRT-PCR.

For all cytokines assessed, there was a marked enhancement of NOD2/TLR2 induced cytokine release in hypoxia. Figure 3.10 shows the complete results for ataxin-3. An excellent protein knockdown was achieved (Figure 3.10 A). Although no significant differences were seen on NOD2/TLR2 stimulation between the control and ataxin-3 knockdown cells in either normoxia or hypoxia, there was a trend to reduced cytokine expression in the ataxin-3 knock down cells, most notably for IL1β. A further 2 donors were assessed in a subsequent experiment in normoxia only (data not shown), with the combined

normoxia data for 5 donors just failing to show a statistically significant reduction in IL1β mRNA levels on NOD2/TLR2 stimulation (p=0.0712). Figure 3.11 shows the results for aprataxin. Protein knockdown was more variable, although consistently greater than 50% reduction in the long isoform was achieved (Figure 3.11 A). Knockdown of the short isoform was however inconsistent, with the relatively low abundance in the whole cell lysates in normoxia also evident. No significant differences in NOD2/TLR2 stimulation of cytokines was evident. While excellent protein knockdown of DYNLT3 and BTAF1 was achieved, no significant differences in cytokine expression were evident (Figures 3.12 and 3.13).

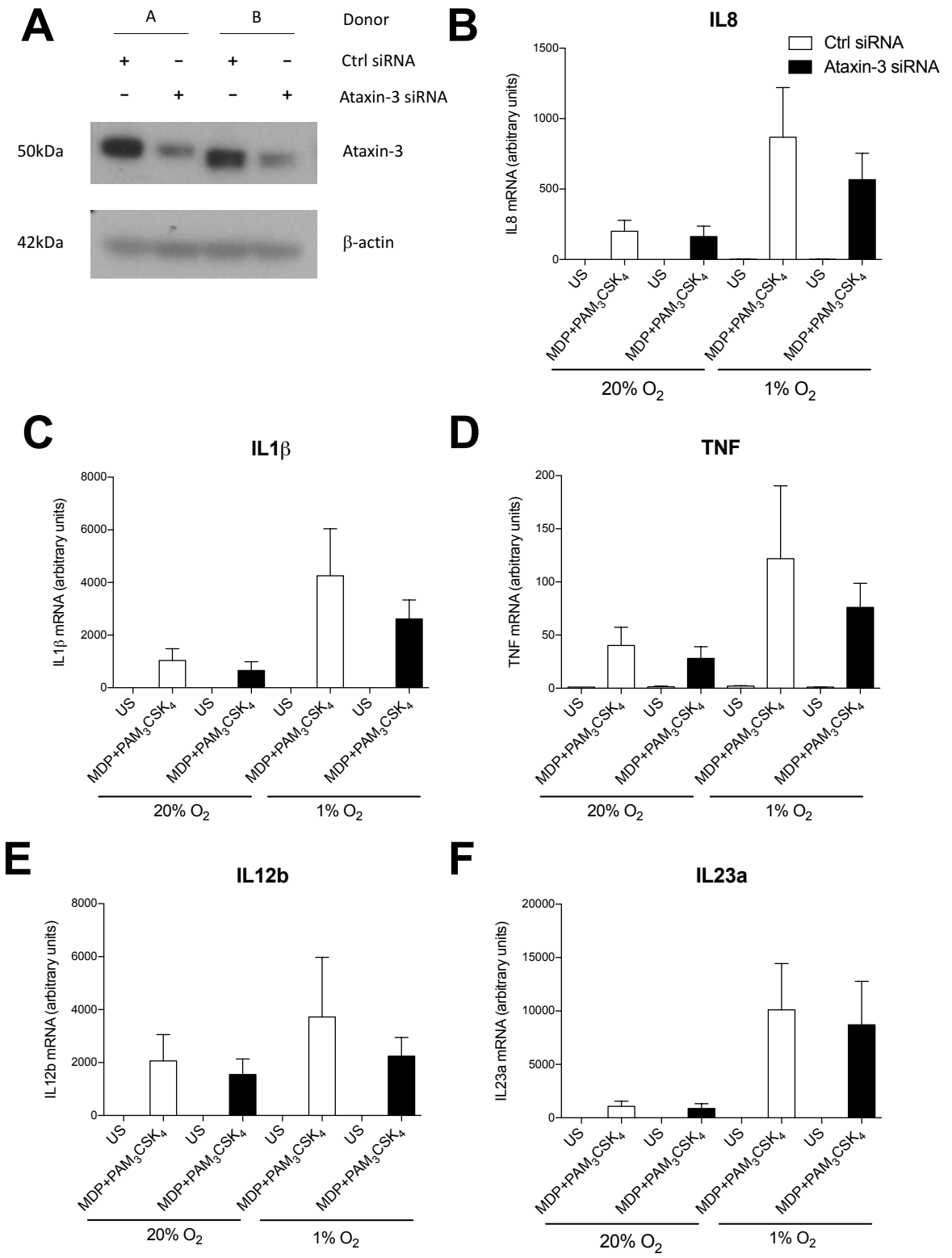


Figure 3.10 NOD2/TLR2 induction of cytokine mRNA expression following ataxin-3 knockdown. **(A)** Immunoblot of ataxin-3 protein levels 48hr after transfection of moDCs with control or ataxin-3 siRNA – 2 representative donors shown. **(B-F)** qRT-PCR analysis of mRNA levels of IL8, IL1β, TNF, IL12a and IL23b in moDCs transfected with either control or Ataxin-3 siRNA for 36hr and then incubated for 16hr in either normoxia or hypoxia and stimulated for the final 6hr with MDP + PAM_3CSK4 or left unstimulated. n=3 biological replicates.

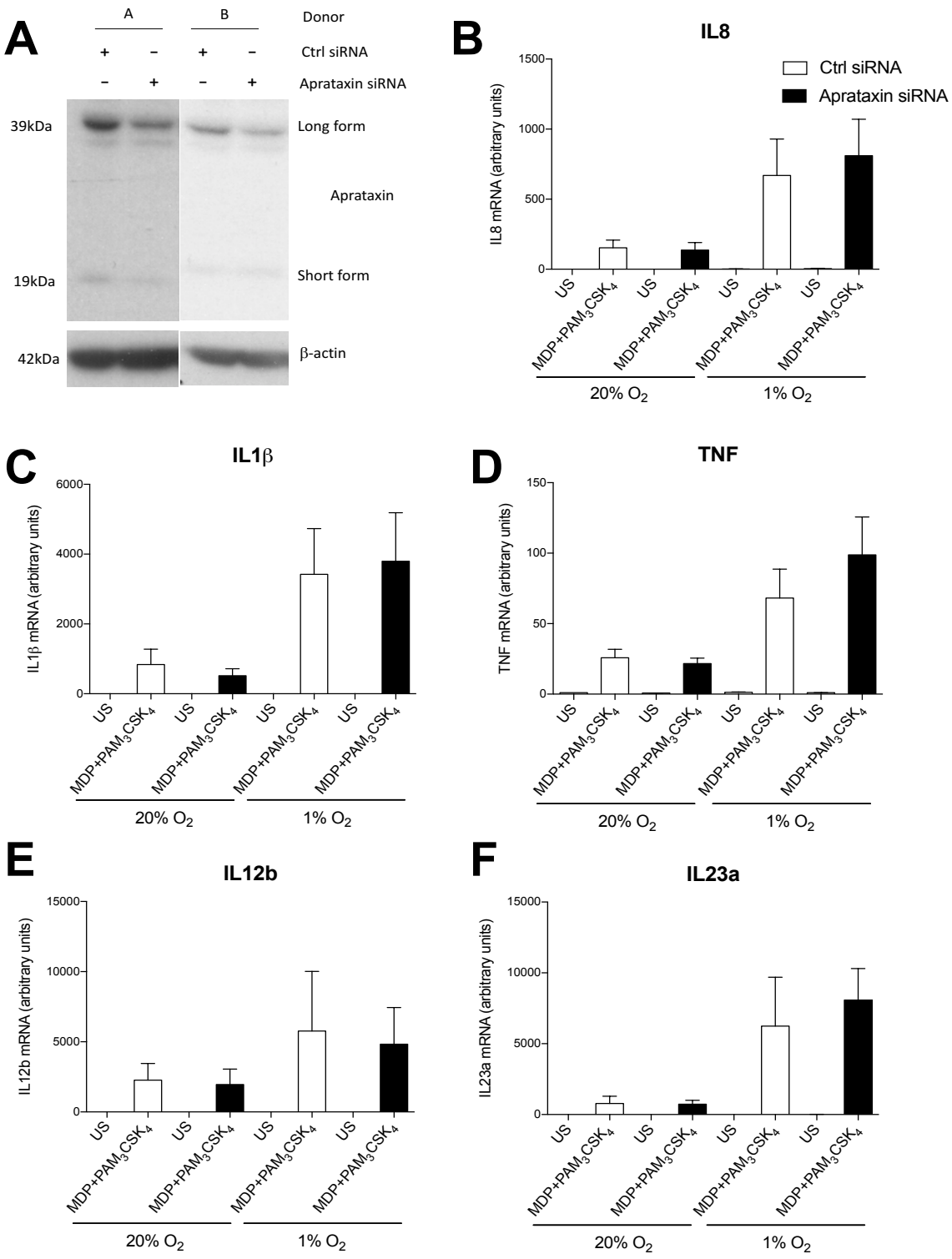


Figure 3.11 NOD2/TLR2 induction of cytokine mRNA expression following apratoxin knockdown. **(A)** Immunoblot of apratoxin protein levels 48hr after transfection of moDCs with control or ataxin-3 siRNA – 2 representative donors shown. **(B-F)** qRT-PCR analysis of mRNA levels of IL8, IL1β, TNF, IL12a and IL23b in moDCs transfected with either control or apratoxin siRNA for 36hr and then incubated for 16hr in either normoxia or hypoxia and stimulated for the final 6hr with MDP + PAM_3CSK4 or left unstimulated. n=3 biological replicates.

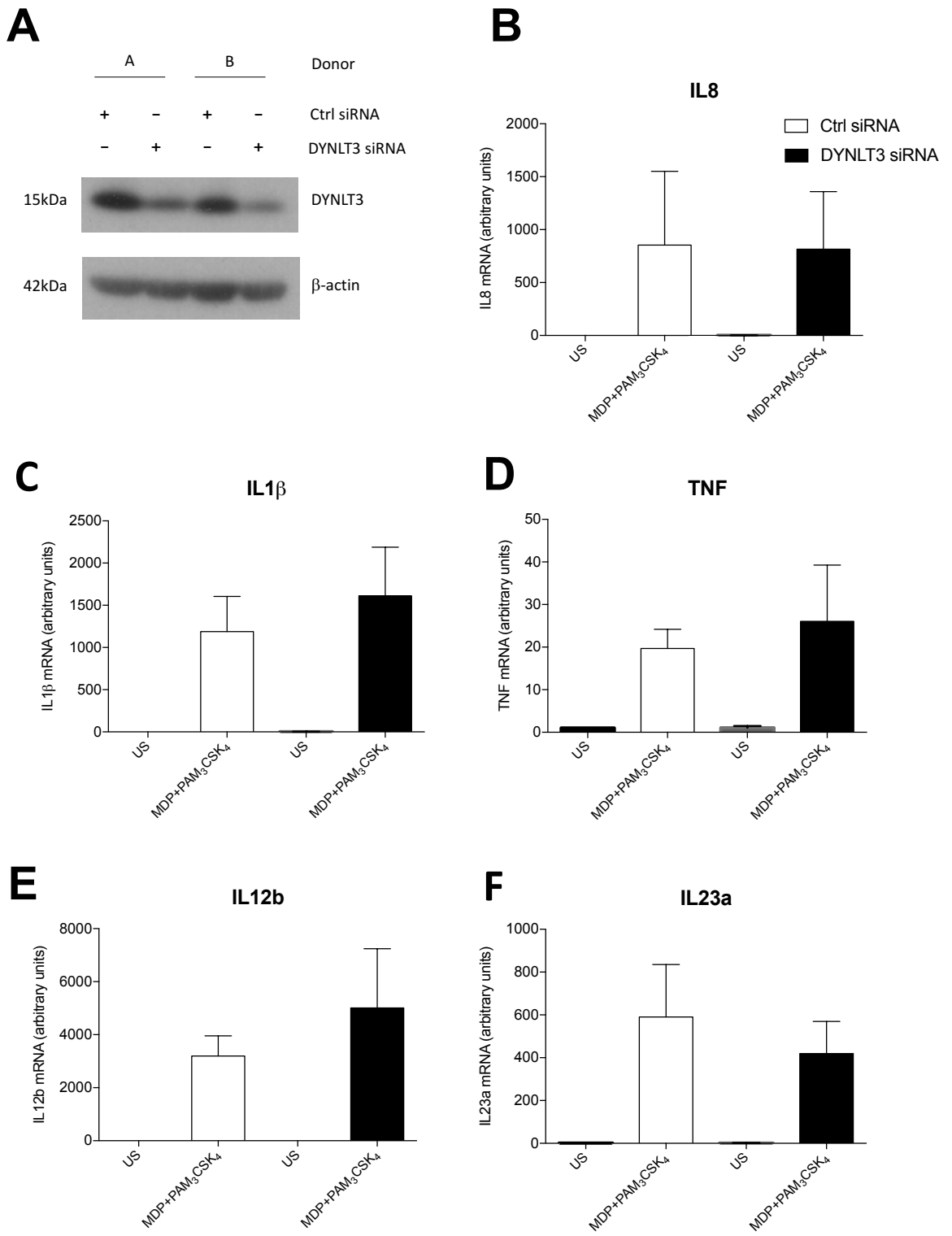


Figure 3.12 NOD2/TLR2 induction of cytokine mRNA expression following DYNLT3 knockdown. (A) Immunoblot of DYNLT3 protein levels 48hr after transfection of moDCs with control or ataxin-3 siRNA – 2 representative donors shown. **(B-F)** qRT-PCR analysis of mRNA levels of IL8, IL1β, TNF, IL12a and IL23b in moDCs transfected with either control or DYNLT3 siRNA for 36hr and then incubated for 16hr in normoxia and stimulated for the final 6hr with MDP + PAM_3CSK4 or left unstimulated. n=3 biological replicates.

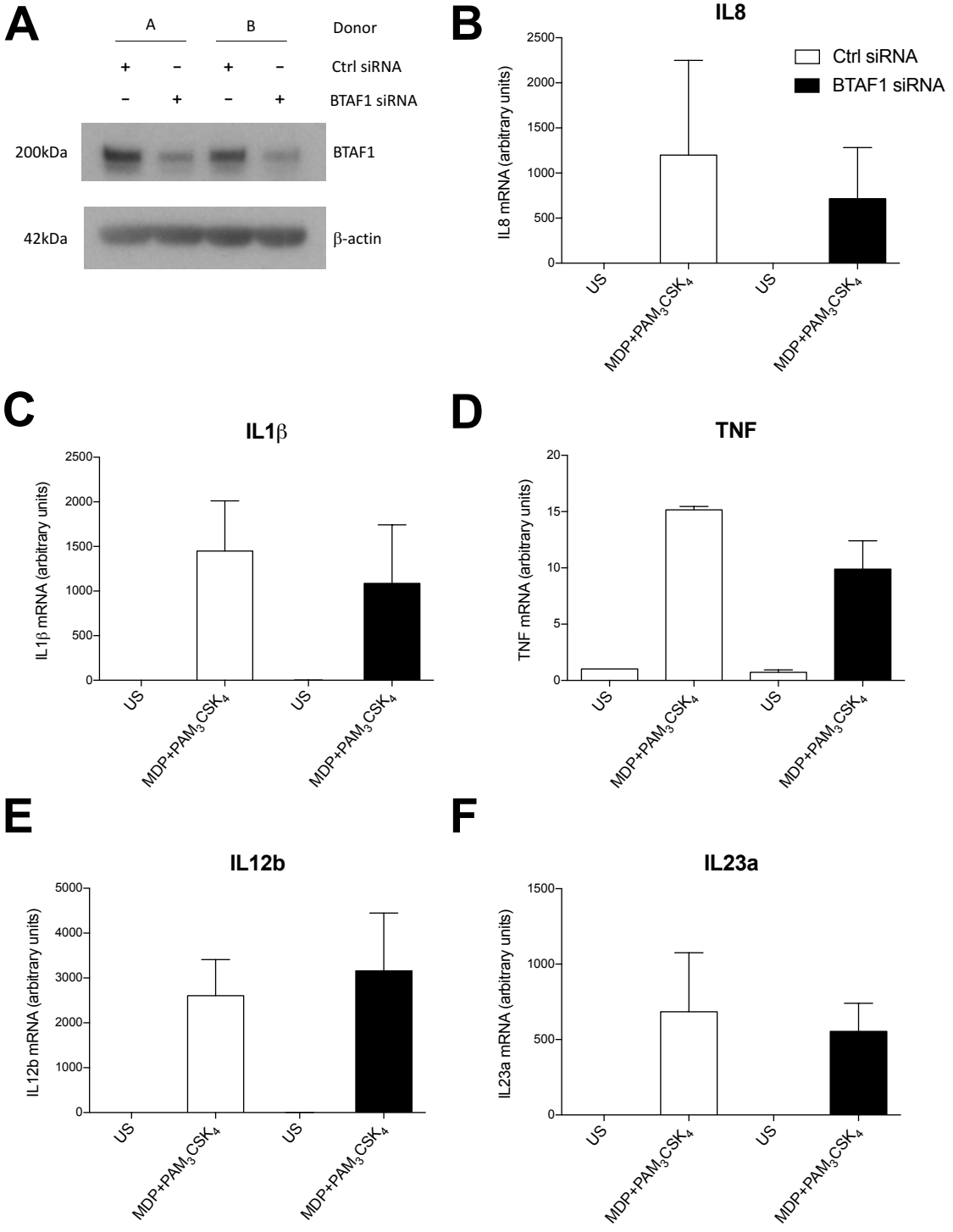


Figure 3.13 NOD2/TLR2 induction of cytokine mRNA expression following BTAF1knockdown. (A) Immunoblot of BTAF1 protein levels 48hr after transfection of moDCs with control or ataxin-3 siRNA – 2 representative donors shown. **(B-F)** qRT-PCR analysis of mRNA levels of IL8, IL1β, TNF, IL12a and IL23b in moDCs transfected with either control or BTAF1 siRNA for 36hr and then incubated for 16hr in normoxia and stimulated for the final 6hr with MDP + PAM_3CSK4 or left unstimulated. n=2 biological replicates.

3.4 Discussion

In the first part of the chapter, it is demonstrated for the first time that NOD2 signalling is altered in the physiologically relevant setting of hypoxia. Specifically, synergistic NOD2/TLR2 mediated cytokine mRNA expression is enhanced in hypoxia. While close correlation has classically been described between mRNA and protein expression of cytokines[366], and previous studies have demonstrated that TLR4 induced cytokine synthesis at a protein level is enhanced in hypoxia in DCs[186], it would be important to confirm that cytokine protein synthesis is also enhanced in this specific experimental context. Further exploration also revealed that NOD2/TLR2 triggering acts synergistically to upregulate HIF1α at a protein level, and a key downstream target VEGF at an mRNA level, and that these pathways are enhanced in hypoxia.

Next, NOD2/TLR2 signalling was examined in both normoxia and hypoxia for the first time on a systems level, in primary moDCs by quantitative phosphoproteomics. Hypoxia was found to induce wide ranging changes in the phosphorylation of proteins, with subsequent cross comparison with HypoxiaDB suggesting the discovery of a number of novel hypoxia regulated targets. As expected, NOD2/TLR2 signalling through the phosphoproteome was significantly altered in hypoxia, supporting the rationale for this approach. Notably a number of proteins linked to neurodegenerative diseases were found to be differentially phosphorylated.

A preliminary screen assessing NOD2/TLR2 stimulated cytokine mRNA expression following knockdown of validated proteins was undertaken. The enhanced effects of NOD2/TLR2 stimulation in hypoxia extended to all pro-inflammatory cytokines assessed. Although no

significant changes were found in cytokine expression following protein knockdown, there was substantial donor variation which is an unavoidable consequence of primary cells. A greater number of donors would be required to exclude a more subtle modulation of cytokine expression. Further, although the protein knockdown typically exceeded 75%, for highly abundant proteins such as DYNLT3 this may not be sufficient to reveal functional consequences.

Clearly NOD2 mediates a wide variety of immune responses far beyond cytokine release, but there was insufficient time to undertake a more extensive functional screen for all proteins. The validated proteins are now discussed in more detail, with particular reference to potential immune roles which could be explored in further work.

Aprataxin

Aprataxin is a member of the histidine triad (HIT) superfamily of nucleotide hydrolases and transferases[367]. It acts to repair adenylated RNA-DNA junction as part of the RNA-DNA damage response[368]. Recently, a number of studies have also suggested a specific mitochondrial role. Initial work found that aprataxin localises to the mitochondria where it participates in mitochondrial DNA repair[369, 370]. However, it was later shown that aprataxin also acts independently of mtDNA repair to maintain mitochondrial function[371]. Aprataxin was required for the transcriptional regulation of mitochondrial function, with bioenergetics deficits seen in both a human cell line depleted of aprataxin, and in fibroblasts from patients with aprataxin mutations[371]. As stated earlier, mutations in the aprataxin gene lead to the inherited neurodegenerative condition, Ataxia oculomotor aprataxia type 1, with defects in both nuclear and mitochondrial genome repair and mitochondrial function hypothesised to

contribute to the disease. Seven phosphorylation sites in humans, including a cluster of three serine residues at s132, s135 and s137, have been described by mass spectrometry but none have been further characterised[344].

Of particular relevance to this work, it is unclear whether the long and short isoforms of the protein have differing functions, although the short isoform lacks the first 188 amino acids which includes a postulated mitochondrial targeting sequence[369]. Further, co-immunoprecipitation experiments suggest that the long form, but not the short form, interacts with the DNA repair protein x-ray repair cross-complementing group 1 (XRCC1)[372]. It is certainly intriguing that only the short isoform of aprataxin is differentially regulated by hypoxia, whereas both isoforms are differentially phosphorylated by NOD2/TLR2, albeit in opposing directions. Of note, there are no previous reports of hypoxia regulating aprataxin.

It is plausible that NOD2/TLR2 signalling to aprataxin mediates a mitochondrial repair role, perhaps dampening an exacerbation of the immune response that results from concurrent mitochondrial damage. Alternatively, the DNA damage response can itself trigger immune signalling, and it is conceivable that NOD2/TLR2 activate this pathway through aprataxin[373]. A role in NOD2 mediated pathogen control is suggested by the recent discovery that an SNP linked to the development of visceral leishmaniasis (VL) lies just outside the aprataxin gene[374]. The NOD2-RIP2 pathway is known to be important in directing the adaptive immune response to VL[375].

HDAC6

HDAC6 is a member of the histone deacetylase family, but unusually also acts to deacetylate a wide variety of non-histone proteins[376]. Many substrates are related to the cytoskeleton, suggesting an important role in the regulation of cytoskeletal dynamics[376]. Indeed, this function may underpin the emerging importance of HDAC6 in immunity. HDAC6 mediated microtubule acetylation has been linked to LPS stimulated macrophage activation[377], and the secretion of the anti-inflammatory cytokine IL10[378]. HDAC6 is also a key player in the cellular management of protein aggregates, and it is thought that this underpins links to neurodegenerative diseases such as Alzheimer's. HDAC6 utilises a ubiquitin binding domain to facilitate the transport of ubiquitinated misfolded proteins in aggresomes through the microtubule network for eventual degradation[379]. HDAC6 also acts to control autophagosome maturation, but notably no role in PRR mediated autophagy has yet been found[380]. A number of phosphorylation sites have been characterised which all appear to regulate deacetylase activity, although PRR triggered phosphorylation has not previously been described. The importance of the specific residue is illustrated by the fact that phosphorylation of Y570 reduces deacetylase activity[381], while phosphorylation at s458 increases deacetylase activity[382]. Taken together, these studies suggest that NOD2/TLR2 induced phosphorylation might act to regulate the deacetylase activity of HDAC6. Although the substrate in this context is uncertain, it might result in modulation of autophagy or immune cell maturation and cytokine response.

DYNLT3

DYNLT3 forms part of the six subunit complex of dynein 1, the cytoskeletal motor protein that transports a variety of cellular cargos including vesicles and organelles along

microtubules[383]. The dynein 1 complex is also required for transport of aggresomes, a shared function with HDAC6. Specifically, DYNLT3 is part of the light chain component that serves as an adaptor for cargo recognition and binding to the dynein complex[384]. A dynein independent role has also been demonstrated for DYNLT3, whereby it is recruited to the nucleus by special AT-rich sequence-binding protein 1 (SATB1) and participates in transcriptional regulation of B-cell lymphoma 2 (BCL2)[385]. Although relatively little is known about this protein, reductions in axonal transport motor proteins including DYNLT3 have been described in the brains of patients with late stage Parkinson's disease[357]. It has also been proposed as a candidate susceptibility gene based on its position in a known risk locus and expression in dopaminergic neurons which are damaged in Parkinson's[386]. A single link to immunity has been reported, with deletions and duplications of DYNLT3 found in association with mutations in the X-linked CYBB gene, also known as NADPH oxidase 2, that results in chronic granulomatous disease (CGD)[387]. CGD results in impairment of phagocyte NADPH oxidase activity, leading to life threatening bacterial and fungal infections, and granuloma formation that can mimic Crohn's in the intestine[388]. Two phosphorylation sites for DYNLT3 have been described by mass spectrometry only, at T93 and T95. The apparent reduction in DYNLT3 phosphorylation in hypoxia represents a further novel finding, as there are no reports of hypoxia regulating DYNLT3 at either mRNA or protein level.

BTAF1

BTAF1 acts to regulate transcription with TATA binding protein (TBP). It inhibits transcription by removing TBP from the TATA box (a conserved promoter sequence found in around one quarter of human genes) in an ATP dependent manner[389]. A possible link to neurodegeneration is suggested by the association of polyglutamine expansions in TBP with

Spinocerebellar ataxia 17 (SCA17). Mutant TBP shows impaired DNA binding leading to transcriptional dysregulation, which appears to contribute to the disease pathogenesis[390]. It is known that BTAF1 can rescue a wide variety of DNA-binding defective TBP1 mutants, although the effect on the polyglutamine mutant has not been established[391].

BTAF1 has not previously been linked to immunity. However, a BTAF1 homologue in Drosphilia, Helicase89B, was found to positively regulate antimicrobial genes activated by Toll pathways, and acts downstream of two NF-κB related transcription factors[392]. It was therefore plausible that NOD2/TLR2 phosphorylation of BTAF1 might regulate NF-κB mediated cytokine release, but no evidence for this was found in the preliminary screen performed in this chapter. Over 25 potential phosphorylation sites for this sizeable (1849 aa) protein have been described by mass spectrometry, but none have been further characterised[344].

LRBA

LRBA has domains homologous to vesicle trafficking proteins and localises to endosomal vesicles, lysosomes and the trans-Golgi, but its function remains unclear[393]. First described as an LPS responsive gene in macrophages and B cells, it is highly expressed in both innate and adaptive immune cells. Biallelic loss of function mutations in LRBA lead to a syndrome of immune deficiency and autoimmunity, with defects in autophagy and apoptosis described[354]. A number of patients also develop inflammatory bowel disease[353, 354]. Neurological involvement, which is thought to result independently of autoimmunity, occurs in around one fifth of patients[394]. A number of patients have shown a dramatic clinical response to abatacept, a cytotoxic T lymphocyte antigen-4 (CTLA4) immunoglobulin fusion

drug, leading to the discovery that LRBA colocalises with CTLA4 in endosomes and regulate its turnover[395].

Interestingly, despite 90% sequence homology in mice, a knockout mouse model shows only subtle changes in adaptive immune function[396]. While in this chapter, technical difficulties with an LRBA antibody prevented validation of the phosphorylation change, there was clear evidence of both hypoxic and NOD2 dependent regulation of LRBA gene expression. Neither NOD2 nor hypoxia have previously been shown to regulate LRBA, but the overlap with known defects in autophagy and inflammatory bowel disease make such an association intriguing.

Ataxin-3

Despite extensive research interest in ataxin-3, the discovery here that NOD2/TLR2 phosphorylates this protein is novel, and indicates a hitherto undescribed immune role. The downregulation of NOD2/TLR2 stimulated phosphorylation in hypoxia is also of interest. A single previous screen, assessing hypoxia modulated gene expression in primary human pulmonary microvascular endothelial cells, found ataxin-3 to be significantly downregulated by hypoxia[397] Overall, it suggests that hypoxia might somehow inhibit the activity of ataxin-3.

While work in this chapter has revealed a number of new targets of NOD2/TLR2, all of which represent intriguing new avenues of inquiry, ataxin-3 is particularly attractive for a number of reasons. Firstly, it was one of the most differentially regulated proteins in both the initial quantitative phosphoproteomics analysis and in the subsequent validation. Secondly,

ataxin-3's known role as a DUB is enticing, given the importance of deubiquitination for the orchestration of the immune response[398]. Thirdly, the association with the human disease Spinocerebellar Ataxia Type 3 ensures that ataxin-3 is of significant interest to the wider research community, and provides an avenue of further investigation for the observation that NOD2/TLR2 signalling pathways may overlap with pathways implicated in neurodegenerative pathways. Finally, an ataxin-3 knockout mouse has already been created, facilitating *in vivo* experiments. Consequently ataxin-3 was selected for further study, and the subsequent chapters in this thesis seek to define a potential immune role for this protein.

Chapter 4: Defining the NOD2/TLR2 driven ataxin-3 signalling axis and interactome

4.1 Introduction

Ataxin-3 mRNA is highly expressed in both innate and adaptive immune cells, but is most abundant in monocytes, macrophages and B cells[399, 400]. Notably the key innate immune effector cells of the central nervous system, microglia and astrocytes, also cluster in the top 10% of cells for expression of ataxin-3[401]. While inflammatory processes have been implicated in the development of Spinocerebellar Ataxia Type 3, with dysregulated cytokine expression and increased numbers of activated microglia and astrocytes found in the brains of patients[402, 403], it has been suggested that this may simply represent a response to the toxic protein aggregates of mutant ataxin-3[404]. Arguing against this, increased expression of IL6, IL1β and IL1-receptor has also been found in neurons lacking these intranuclear aggregates[403], but this observation has not been further explored.

The suggestion that wild type ataxin-3 may itself modulate the immune response opens up an exciting new line of investigation for this protein. Important questions to be answered include the range of PRRs able to engage ataxin-3, the downstream signalling cascade that leads to phosphorylation, and the phosphorylation site. While in quite separate physiological contexts, phosphorylation of ataxin-3 affects nuclear localisation and deubiquitinating activity, what is the consequence of immune triggering? Much previous work has focussed on identifying potential interaction partners of ataxin-3, but this has never been attempted in an immune cell and could shed new light on the functions of this enigmatic protein.

4.2 Aims

This chapter aims to:

1. Interrogate the innate signalling cascade to ataxin-3.

2. Define the phosphophorylation site of ataxin-3 following NOD2/TLR stimulation.

3. Identify novel interaction partners in immune cells to elucidate the function of ataxin-3.

4.3 Results

4.3.1 Ataxin-3 is phosphorylated by NOD2 and TLR2 both in isolation and synergistically, and by other PRRs

As a first step in defining the innate immune signalling pathway to ataxin-3, it was important to examine the independent contributions of NOD2 and TLR2 triggering to ataxin-3 phosphorylation. Both NOD2 and TLR2 stimulation alone led to robust phosphorylation; this effect was enhanced on dual stimulation supporting a synergistic action. The effect of triggering alternative PRRs was also investigated by stimulating TLR4 with its ligand LPS, and TLR7 and 8 with their ligand R848 (Resiquimod). R848 is a potent synthetic TLR7/8 agonist that belongs to the class of imidazoquinolones[405]. Stimulation with LPS or R848 led to phosphorylation of ataxin-3, but to a lesser extent than NOD2 or TLR2 stimulation (Figure 4.1 A). The ability of TLR4 to trigger ataxin-3 phosphorylation is unsurprising, given that like TLR2 it is located in the cell membrane and senses components of the bacterial cell wall. However, the involvement of TLR7/8 is less expected, as they have a quite separate endosomal location and classically respond to viral ssRNA. Most notable is the finding that NOD2 and TLR2 triggering leads to a much greater phosphorylation of ataxin-3 than TLR4 or TLR7/8, potentially suggesting the importance of this specific signalling pathway to ataxin-3.

Next, the effect of NOD2 stimulation was examined in more detail in moDCs by conducting a time course experiment. Ataxin-3 phosphorylation was undetectable after 15 minutes of MDP stimulation, but was markedly induced by 30 minutes before declining again at 60 minutes (Figure 4.1 B).

Finally, while NOD2 is the only known receptor for MDP, the absolute requirement for NOD2 in the MDP stimulated phosphorylation of ataxin-3 was examined. The human monocyte THP-1 cell line stably expressing either control or NOD2 short hairpin RNA was utilised (a kind gift from Daniele Corridoni), having first established that MDP induces ataxin-3 phosphorylation in THP-1 cells. When assessing ataxin-3 phosphorylation in THP-1 cells, a 60 minute stimulation time point for MDP or PAM_3CSK_4 or both was selected after initial experiments determined this produced maximal phosphorylation (data not shown). While NOD2 knock down at an mRNA level was confirmed by RT-qPCR (Figure 4.1 C), the absence of a satisfactory antibody for detecting endogenous NOD2 protein meant that the protein knock down could not be assessed. However, following stimulation, the whole cell and phosphoprotein enriched lysates were additionally probed for p38 to demonstrate the functional consequences of NOD2 knock down (Figure 4.1 C). The requirement for NOD2 was confirmed by the absence of ataxin-3 phosphorylation following MDP stimulation, and the marked reduction in phosphorylation following synergistic MDP and PAM_3CSK_4 stimulation in the NOD2 shRNA cell line (Figure 4.1 C).

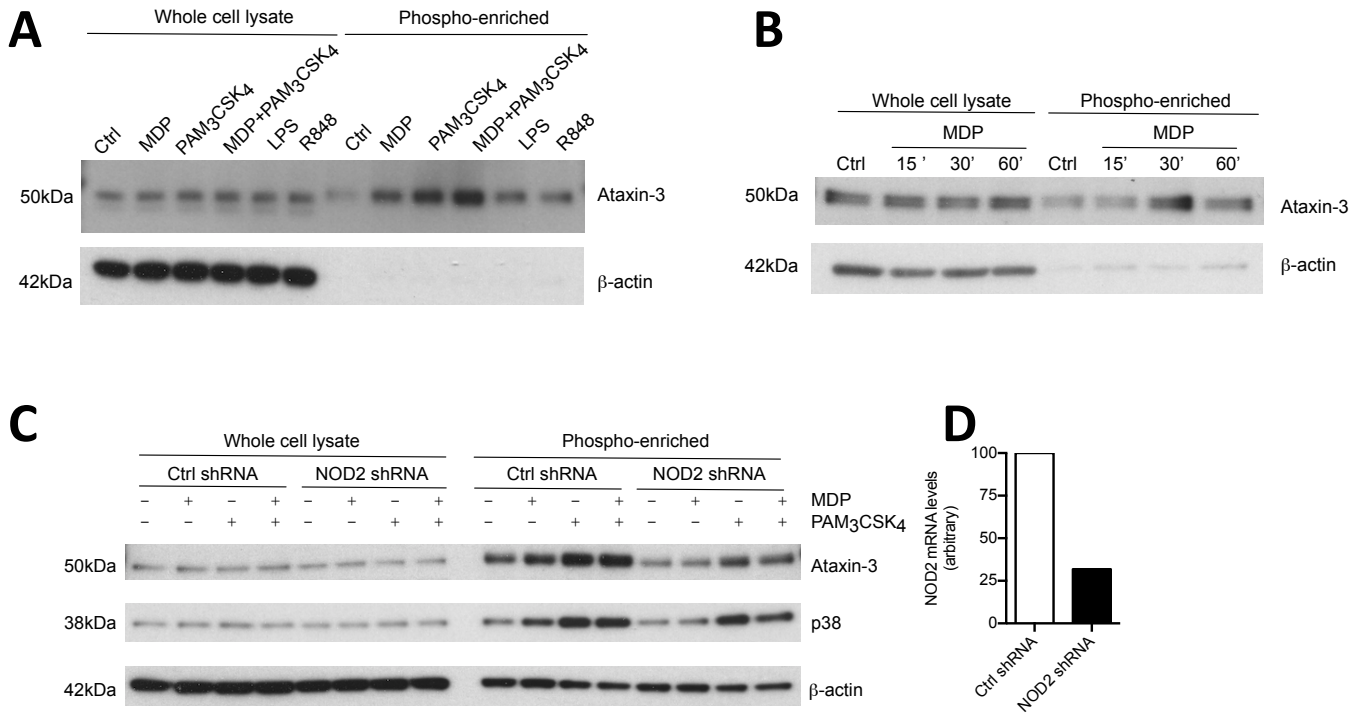


Figure 4.1 Ataxin-3 is phosphorylated by NOD2 and TLR2 both independently and synergistically, and to a lesser extent by TLR4 and TLR7/8. Immunoblot using antibodies against ataxin-3 and β-actin of whole cell and phosphoprotein enriched lysates from moDCs either **(A)** unstimulated or stimulated with the NOD2 ligand MDP 10μg/ml, or the TLR2 ligand PAM_3CSK_4 1μg/ml, or both, or the TLR4 ligand LPS 100ng/ml or the TLR7/8 ligand R848 (Resiquimod) 1μg/ml for 30 minutes or **(B)** unstimulated or stimulated with the NOD2 ligand MDP for 15, 30 or 60 minutes. **(C)** Immunoblot using antibodies against ataxin-3, p38 and β-actin of whole cell and phosphoprotein enriched lysates from THP-1 cells expressing control or NOD2 shRNA and either unstimulated or stimulated with the NOD2 ligand MDP or the TLR ligand PAM_3CSK_4, or both, for 60 minutes. **(D)** The efficacy of the NOD2 knock down is demonstrated by RT-qPCR of NOD2 mRNA levels in the NOD2 shRNA and control shRNA cell lines. All immunoblots are representative of two independent experiments.

4.3.2 RIPK2 and TBK1 are required for NOD2 induced ataxin-3 phosphorylation

Next, the signalling cascade downstream from NOD2 was examined. Given the central importance of RIPK2, the requirement of this protein kinase for the phosphorylation of ataxin-3 by NOD2 was investigated. NOD2-RIPK2 inflammatory signalling can be potently and selectively inhibited by the clinically relevant kinase inhibitor ponatinib, that functions by blocking RIPK2 autophosphorylation and ubiquitination[406]. Both moDCs and THP1 cells were treated with 50nM ponatinib for 60 minutes prior to stimulation with MDP or

PAM_3CSK_4 or both. Phosphorylation of p38 was used as a positive control for the inhibitor. As expected, inhibition of RIPK2 blocked NOD2 induced phosphorylation of p38, but had no effect on induction by TLR2, which signals to p38 via a MyD88 pathway which is independent of RIPK2. Strikingly, inhibition of RIPK2 led to complete inhibition of NOD2 induced phosphorylation of ataxin-3, and significant abrogation of the synergistic NOD2/TLR2 signal in both cell types (Figure 4). This confirms the importance of RIPK2 in the signalling axis.

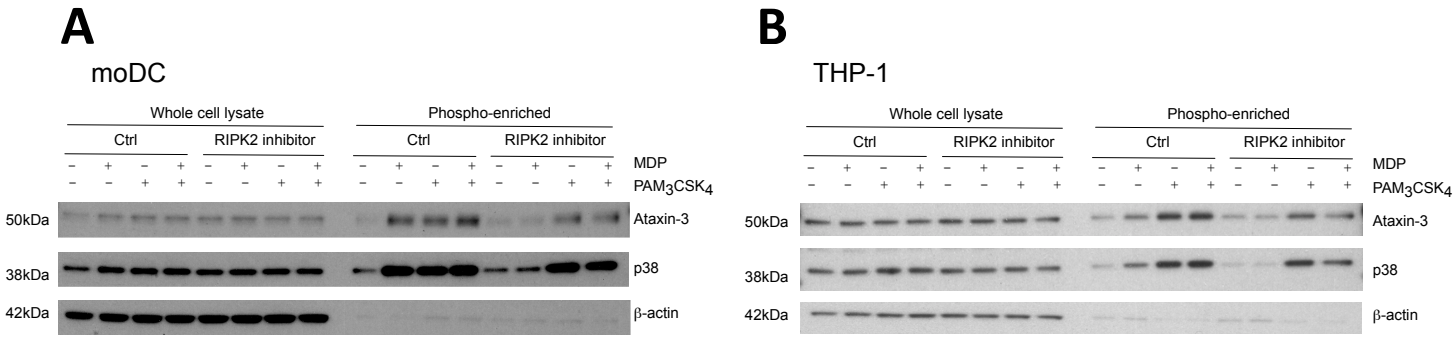


Figure 4.2 RIPK2 is required for the NOD2 induced phosphorylation of ataxin-3. Immunoblot using antibodies against ataxin-3, p38 and β-actin of whole cell and phosphoprotein enriched lysates from **(A)** moDCs or **(B)** THP1 cells which were pre-treated with the RIPK2 inhibitor ponatinib 50nM for 60 minutes and then left unstimulated or stimulated with the NOD2 ligand MDP or the TLR2 ligand PAM_3CSK_4 or both. **(A)** is 3 independent donors combined.

Recent evidence suggests that tank binding kinase 1 (TBK1) may represent a novel but important kinase in the NOD2/RIPK2 signalling cascade[407, 408]. MDP stimulation of the NOD2 receptor has been shown to induce TBK1 phosphorylation at S172[407]. NOD1 activation leads to formation of a protein complex containing RIPK2 and tumour-necrosis-factor-receptor-associated factor 3 (TRAF3), an E3 ubiquitin ligase that mediates K63-linked ubiquitination through a TBK1 dependent mechanism. Although not yet proven for NOD2, it is likely that

TBK1 serves a similar role[409]. Consequently, the requirement for TBK1 in NOD2/RIPK2 dependent phosphorylation of ataxin-3 was examined.

First, the TBK1 inhibitor BX795, which acts through an ATP competitive mechanism to block TBK1 kinase activity[410], was used to inhibit TBK1 in moDCs. Cells were pre-treated for 60 minutes with BX795 at a concentration of 10mM, and then left unstimulated or stimulated with MDP or PAM_3CSK_4 or both for 30 minutes. Phosphorylation of IRF3, a known target of TBK1, was used as a positive control[410]. As expected, TBK1 inhibition reduced the phosphorylation of IRF3 in response to NOD2/TLR2 stimulation. Strikingly, TBK1 inhibition entirely blocked the phosphorylation of ataxin-3 by NOD2, and reduced the phosphorylation by combined NOD2/TLR2 triggering. However, TLR2 induced phosphorylation was unaffected (Figure 4.3 A). Although BX795 is a highly potent and widely used inhibitor of TBK1, it is not entirely specific[410], and consequently the effect of TBK1 knock down by shRNA was also examined in the THP-1 cell line (a kind gift from Daniel Gaughan). This confirmed the results of the TBK1 inhibitor, with NOD2 induced phosphorylation of ataxin-3 downregulated in the TBK1 knock down cell line (Figure 4.3 B). Finally, the possibility that TBK1 might directly phosphorylate ataxin-3, as has been described for a number of other proteins including optineurin[97] and p62[411], was explored using an *in vitro* kinase assay. In this cell free system, purified TBK1 protein was incubated with purified ataxin-3 protein, in a kinase reaction buffer containing magnesium, with or without ATP, for 60 minutes at 30^{o}C. The reaction was then terminated by adding LDS sample buffer and DTT, and immunoblot performed. The expected autophosphorylation of TBK1 is demonstrated by a marginally higher molecular weight of the TBK1 band in samples containing both TBK1 and ATP. Importantly, a significant proportion of the ataxin-3 band was noted at a higher molecular

weight in samples containing ataxin-3, TBK1 and ATP, consistent with ataxin-3 phosphorylation. Notably, no change in migration of the ataxin-3 band was seen in samples containing ataxin-3 and TBK1 but not ATP, confirming the ATP dependency of this shift, which again is entirely consistent with phosphorylation (Figure 4.3 C). Taken together, this data shows that TBK1 is required for the phosphorylation of ataxin-3 by NOD2, and that TBK1 acts to directly phosphorylate ataxin-3.

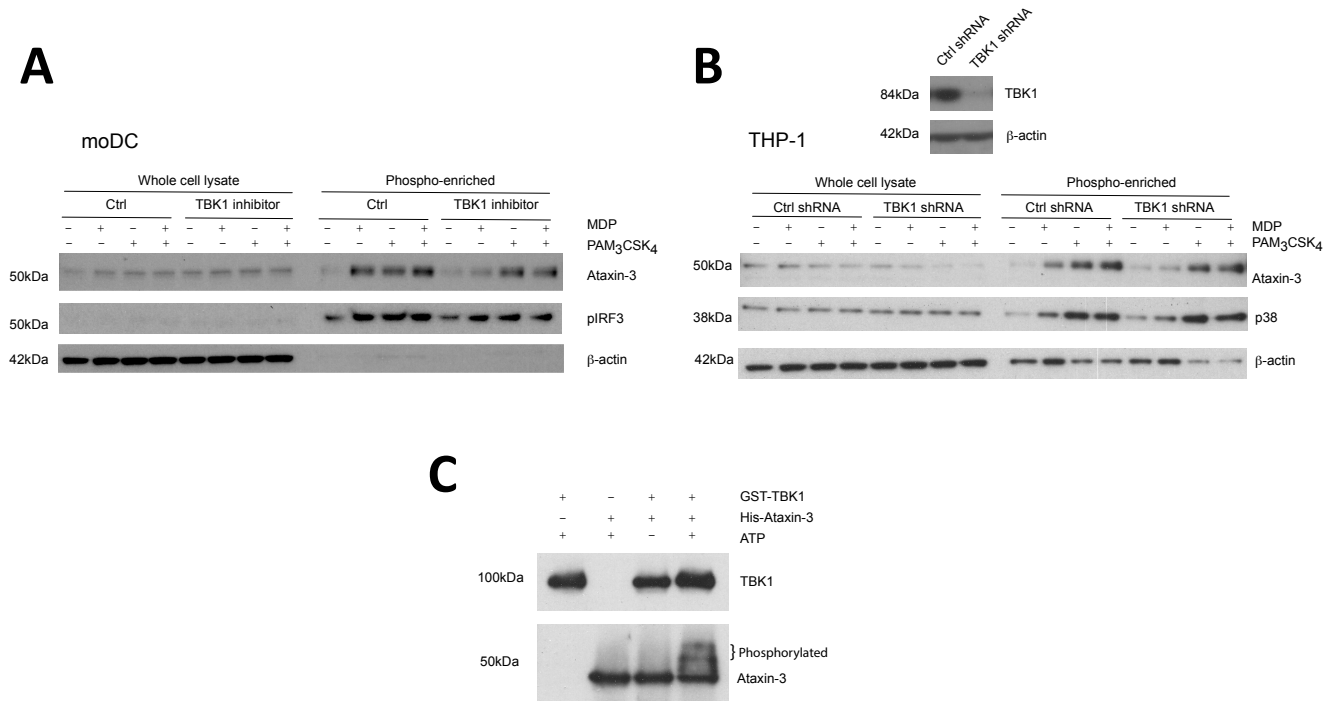


Figure 4.3 TBK1 is the phosphorylating kinase of ataxin-3 following NOD2 stimulation.
(A) Immunoblot using antibodies against ataxin-3, pIRF3 and β-actin of whole cell and phosphoprotein enriched lysates from moDCs which were pre-treated with the TBK1 inhibitor BX795 10mM for 60 minutes and then left unstimulated or stimulated with the NOD2 ligand MDP or the TLR2 ligand PAM_3CSK_4 or both for 30 minutes. **(B)** Immunoblot using antibodies against ataxin-3, p38 and β-actin of whole cell and phosphoprotein enriched lysates from THP-1 cells expressing control or TBK1 shRNA left unstimulated or stimulated with the NOD2 ligand MDP or the TLR2 ligand PAM_3CSK_4 or both for 60 minutes. **(C)** Immunoblot of *in vitro* kinase assay of GST-TBK1 protein or His-ataxin-3 protein with ATP, or both GST-TBK1 and His-ataxin-3 with or without ATP which were incubated for 60 minutes at 30°C. For the immunoblot, antibodies against TBK1 and ataxin-3 were used. **(A)** is 3 independent donors combined.

4.3.3 Ataxin-3 phosphorylation by NOD2/TLR2 does not lead to nuclear migration

Next, the importance of NOD2/TLR2 mediated phosphorylation on the intracellular location of ataxin-3 was examined. Phosphorylation at serine residues 29, 236, 340 and 352 is known to lead to nuclear localisation[292, 293]. Consequently, nuclear/cytoplasmic fractionation was undertaken in the THP-1 cell line following NOD2/TLR2 stimulation, and immunoblot of the cellular fractions performed. Heat shock was used as a positive control for ataxin-3 translocation to the nucleus[412]. Ataxin-3 was significantly more abundant in the cytoplasmic fraction at baseline, but a robust increase in the nuclear fraction was seen following heat shock, with a corresponding decrease in the cytoplasmic fraction (Figure 4.3). However, no change in the nuclear abundance of ataxin-3 was seen on stimulation with MDP + PAM_3CSK_4 over a variety of time points. This suggests that NOD2/TLR2 mediated phosphorylation of ataxin-3 does not lead to nuclear localisation.

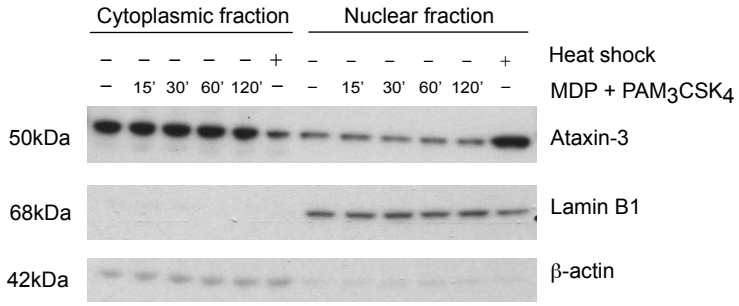


Figure 4.4 NOD2/TLR mediated phosphorylation of ataxin-3 does not affect nuclear localisation. Immunoblot using antibodies against ataxin-3, the nuclear marker lamin B1 and β-actin in cytoplasmic and nuclear fractions of THP-1 cells either left unstimulated or stimulated for 15-120 minutes with MDP+PAM_3CSK_4 or heated at 42°C for 60 minutes (heat shock). Representative of 3 independent experiments.

4.3.4 NOD2/TLR2 stimulation leads to phosphorylation of ataxin-3 at S265

Next, the phosphorylation site of ataxin-3 was sought. This can provide important clues about function, either by mapping a residue which has an already well characterised role, or by considering the location of the novel residue in relation to functional domains of the

protein. Identification of the phosphorylated residue also provides direct evidence of the post-translational modification, in comparison to phosphoprotein enrichment experiments which show a less specific change in abundance of the phosphorylated protein. Further, in phosphoprotein enrichment there is a small possibility that the protein of interest is not differentially phosphorylated in the given experimental context, but is instead enriched due to binding to quite separate proteins that are directly phosphorylated. While phosphorylation sites can be identified in large scale phosphoproteomic experiments, sequence coverage of individual proteins is minimal, and thus accurate mapping of specific proteins is very limited[413].

A simple mapping experiment involves digestion of the purified protein of interest, with the peptides then subjected to LC-MS/MS to identify changes in peptide mass/charge ratio consistent with phosphorylation at a specific residue. One method of protein purification is immunoprecipitation (IP), and initial optimisation experiments demonstrated that endogenous ataxin-3 could be immunoprecipitated from both primary human moDCs and the THP-1 cell line, using a mouse monoclonal antibody. An isotype control antibody was used (the same company, species and isotype) to ensure the specificity of pull down. Ataxin-3 was identified on immunoblotting (Figure 4.5 A shows IP in THP-1 cells) and by the appearance of a band at the expected molecular weight on silver stain (data not shown). As discussed, accurate phosphorylation site mapping requires extensive protein sequence coverage and this can typically be improved by increasing the amount of purified protein provided. Consequently the experiment was performed in the THP-1 cell line, where cell number is not a limiting factor. This allowed a 15 fold upscaling of the IP from 500μg input protein to 7.5mg protein with corresponding increases in amount of antibody and beads.

THP-1 cells were either left unstimulated or stimulated for 60 minutes with MDP + PAM_3CSK_4. Response to stimulation was confirmed by immunoblot of the whole cell lysate for phosphorylated p38, which was upregulated in the stimulated sample (Figure 4.5 B). Following immunoprecipitation, samples were eluted using a low pH buffer to preserve the phosphorylated residue. Efficient elution was confirmed by subsequently boiling the beads in LDS/DTT, with no residual protein found in this fraction. A final quality check was performed by immunoblotting the supernatant following the removal of the bead-antibody-protein complex, confirming a significant depletion of ataxin-3 in this sample compared to the input. Figure 4.5 C shows the input, IP fraction, LDS/DTT repeat elution and supernatant post bead-antibody-protein complex removal, confirming the efficient IP and elution of ataxin-3.

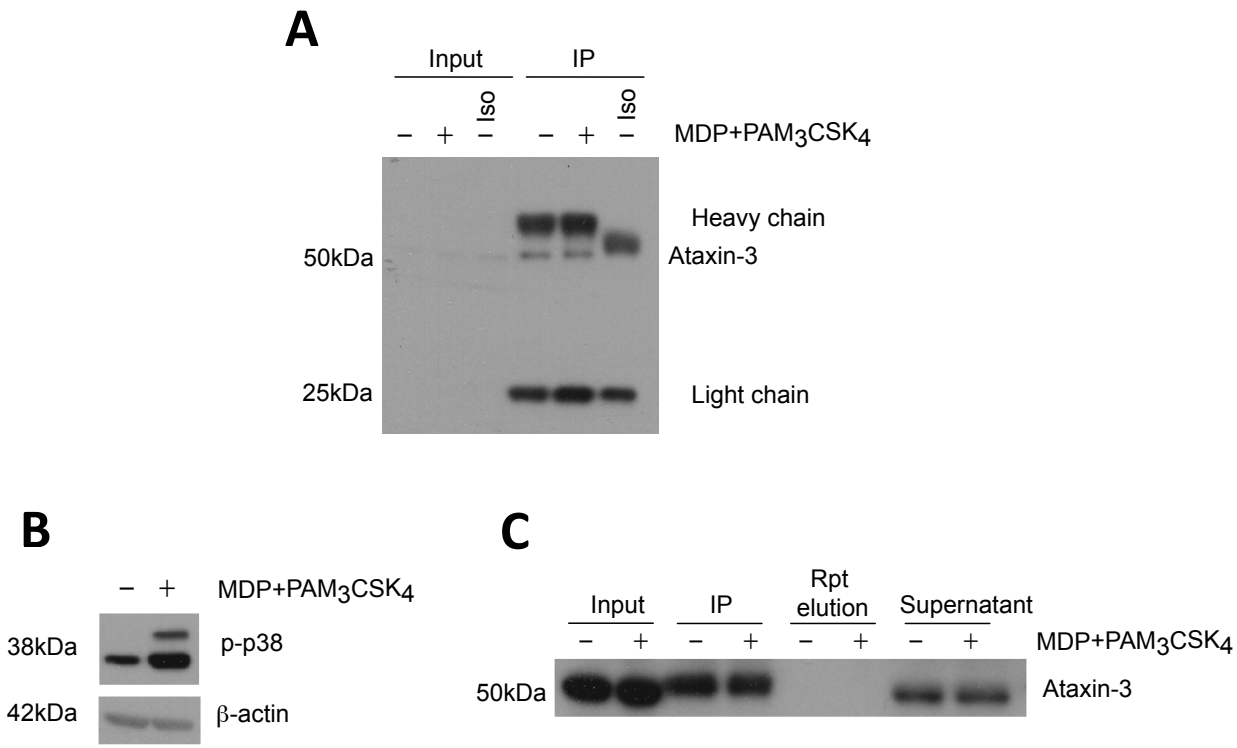


Figure 4.5 Ataxin-3 can be efficiently purified by immunoprecipitation. (A) Immunoblot using an antibody against ataxin-3 of THP-1 cells left unstimulated or stimulated for 60 minutes with MDP+PAM_3CSK_4 and then subjected to immunoprecipitation with either an antibody to ataxin-3 or an isotype control. **(B)** Immunoblot using antibodies against p-p38 and β-actin of THP-1 cells left unstimulated or stimulated for 60 minutes with MDP+PAM_3CSK_4, with stimulation response confirmed in the whole cell lysate. **(C)** Immunoblot using antibody against ataxin-3 of samples from the same experiment, showing ataxin-3 expression in the input and IP fractions, and also in the repeat elution and supernatant following removal of the bead-antibody-protein complex. These samples were subsequently used for LC-MS/MS identification of the phosphorylation site.

The immunoprecipitated samples were digested and the peptides subjected to LC-MS/MS analysis in collaboration with the Kessler Laboratory, Target Discovery Institute, University of Oxford. Good protein coverage was achieved, with 57% of the protein mapped in the stimulated sample and 37% in the unstimulated sample (Figure 4.6 A). The minor difference in displayed peptide sequences at the C terminus between the unstimulated and stimulated samples merely represents subtle ataxin-3 isoform variations. The computer modelling has identified two separate isoforms due to varying extents of sequence coverage between the samples. There is however no evidence that abundance of the different isoforms varies according to NOD2/TLR2 stimulation. The majority of the known functionally important

phosphorylation sites, including S12, S29 and S256 were mapped, and showed no change in phosphorylation on NOD2/TLR2 stimulation. It is important to note that failure to observe that a site is phosphorylated is insufficient to conclude that the site is not phosphorylated, and thus phosphorylation here cannot be entirely excluded. Relatively poor sequence coverage of the C terminus was achieved, and thus phosphorylation of residues within the 3rd UIM could not be assessed. It is most likely that poor sequence coverage of this region resulted from a lack of cleavage sites during digestion. Despite these technical limitations, a shift in mass/charge ratio was found in one peptide in the stimulated sample only, corresponding to phosphorylation of S265 (Figure 4.6 B).

A

Unstimulated (Ctrl) sample

Protein sequence coverage: 37%

Matched peptides shown in ***bold red***.

```
  1 MESIFHEKQE GSLCAQHCLN NLLQGEYFSP VELSSIAHQL DEEERMRMAE
 51 GGVTSEDYRT FLQQPSGNMD DSGFFSIQVI SNALKVWGLE LILFNSPEYQ
101 RLRIDPINER SFICNYKEHW FTVRKLGKQW FNLNSLLTGP ELISDTYLAL
151 FLAQLQQEGY SIFVVKGDLP DCEADQLLQM IRVQQMHRPK LIGEELAQLK
201 EQRVHKTDLE RVLEANDGSG MLDEDEEDLQ RALALSRQEI DMEDEEADLR
251 RAIQLSMQGS SRNISQDMTQ TSGTNLTSEE LRKRREAYFE KVRLRLQKYI
301 QQQKQQQQQQ QQQQGDLSGQ SSHPCERPAT SSGALGSDLG DAMSEEDMLQ
351 AAVTMSLETV RNDLKTEGKK
```

Stimulated MDP+PAM$_3$CSK$_4$ sample

Protein sequence coverage: 57%

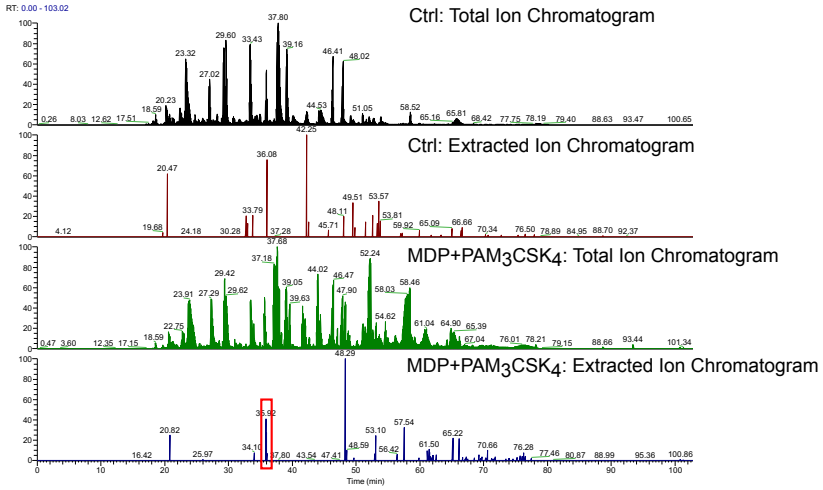
Matched peptides shown in ***bold red***.

```
  1 MESIFHEKQE GSLCAQHCLN NLLQGEYFSP VELSSIAHQL DEEERMRMAE
 51 GGVTSEDYRT FLQQPSGNMD DSGFFSIQVI SNALKVWGLE LILFNSPEYQ
101 RLRIDPINER SFICNYKEHW FTVRKLGKQW FNLNSLLTGP ELISDTYLAL
151 FLAQLQQEGY SIFVVKGDLP DCEADQLLQM IRVQQMHRPK LIGEELAQLK
201 EQRVHKTDLE RVLEANDGSG MLDEDEEDLQ RALALSRQEI DMEDEEADLR
251 RAIQLSMQGS SRNISQDMTQ TSGTNLTSEE LRKRREAYFE KQQQKQQQQQ
301 QQQQQGDLSG QSSHPCERPA TSSGALGSDL GDAMSEEDML QAAVTMSLET
351 VRNDLKTEGK K
```

B

pS265 ataxin-3

peptide sequence: NIpSQDMTQTSGTNLTSEELRK



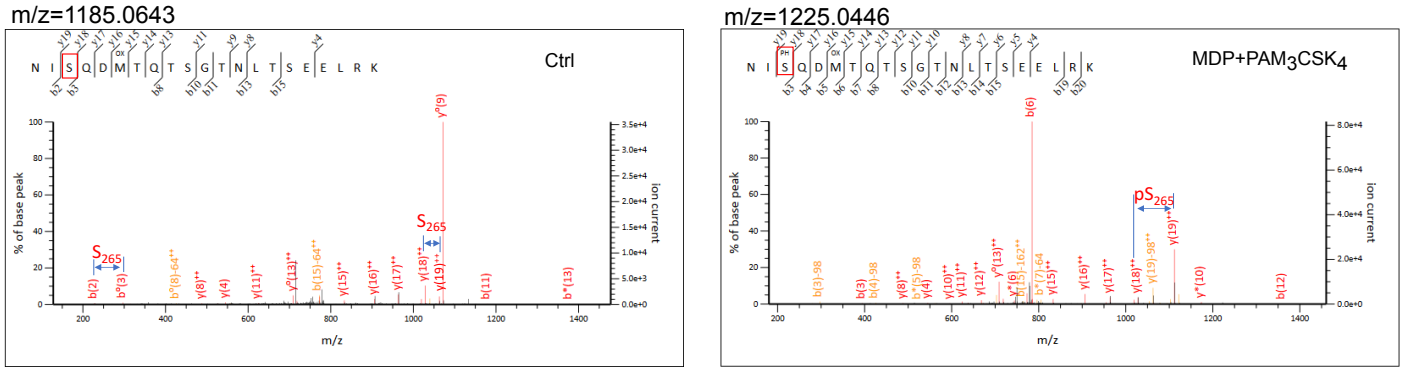


Figure 4.6 Ataxin-3 is phosphorylated at S265 following NOD2/TLR2 stimulation. (A) The sequence coverage of ataxin-3 in the unstimulated and stimulated samples is shown. Residues with a green box represent previously described functionally important phosphorylation sites. The phosphorylated peptide sequence is marked with a blue box. **(B)** Identification of the phosphorylates serine residue (S265) with a characteristic increase in mass/charge ratio in the stimulated sample.

This residue has been described as a phosphorylation site in 12 separate large scale MS screens of human primary cells and cell lines[344], but nothing is known about its functional relevance. The importance of the sequence is suggested by the fact it is highly conserved among placental bearing mammals ranging from the African elephant to the naked mole-rat (Figure 4.7 A)[414]. Interestingly, while the sequence is conserved in members of the Rodentia order including the Chinese hamster, it is lost in both mice and rats. However, they have an additional serine residue at 268 which has been shown to be phosphorylated in 8 separate MS screens[344], including one examining the phosphoproteome of TLR activated murine macrophages[346]. Further, phosphoprotein enrichment of murine RAW264.7 macrophages confirmed that ataxin-3 is phosphorylated in mice following NOD2/TLR2 stimulation (Figure 1, Appendix).

The phosphorylation site also resides in a cluster of other residues known to be phosphorylated, which again is frequently observed with functionally important residues[413]. Further, the sequence sits just outside the 2nd UIM, suggesting that phosphorylation could affect specificity of DUB target, as has been described for s256/260/261[304] (Figure 4.7 B). A 3-dimensional model of the structure of ataxin-3 containing the location of the phosphorylation site is displayed in Figure 4.7 C.

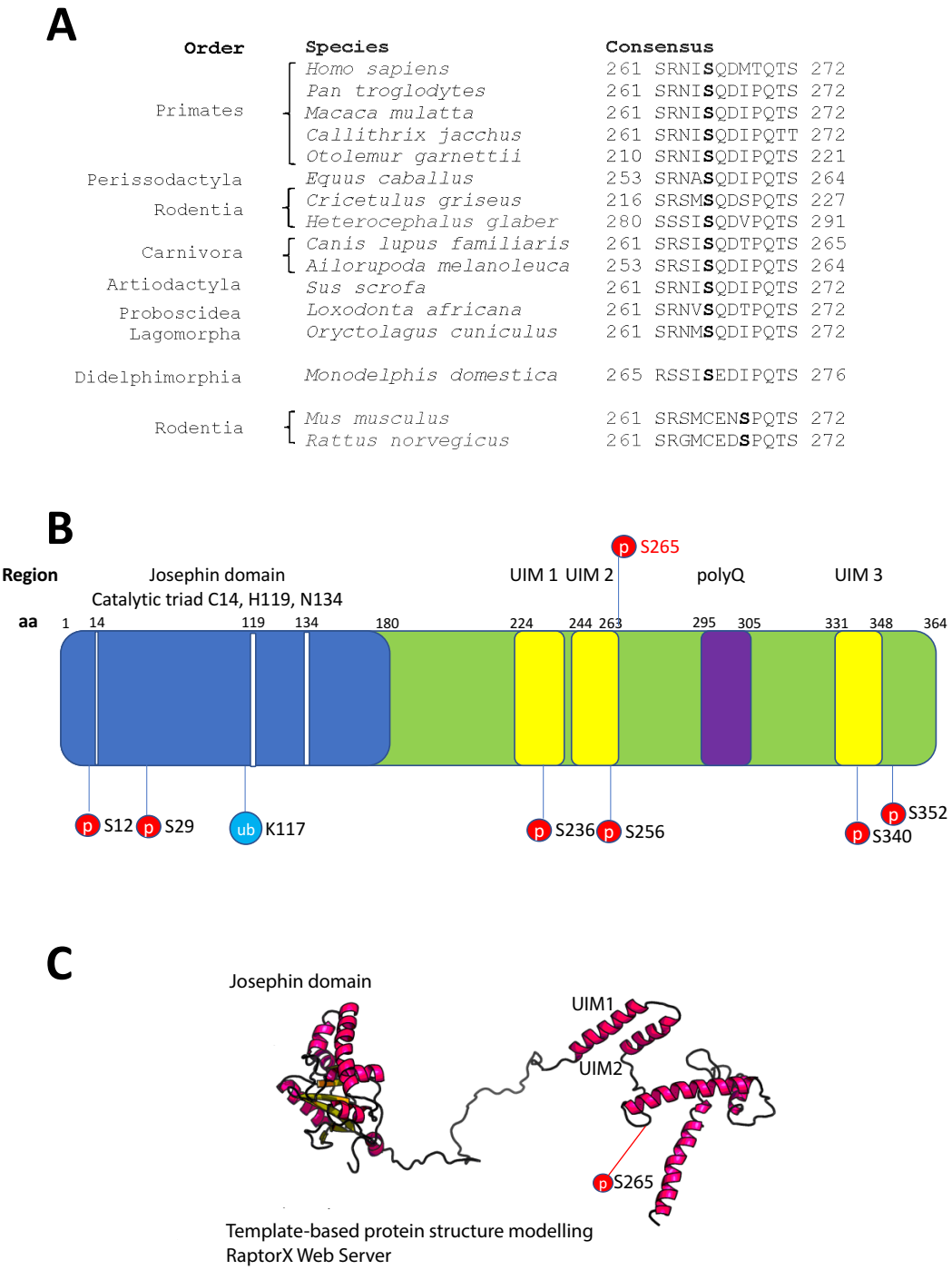


Figure 4.7 S265 in ataxin-3 is conserved in placental mammals and is located close to the 2nd UIM. **(A)** Sequence conservation in a range of placental mammals. **(B)** The location of S265 in relation to the functional domains of ataxin-3. **(C)** A 3-dimensional computer model of the structure of ataxin-3, with the S265 phosphorylation site indicated[415].

4.3.5 Identification of novel ataxin-3 binding partners

The discovery that endogenous ataxin-3 can be efficiently immunoprecipitated in primary moDCs also provided a method of identifying novel interacting proteins. Silver staining of IP samples detected the presence of multiple bands that were not found in the isotype control, suggestive of binding partners, in addition to a band for ataxin-3 at the expected height (Figure 4.8 A). An unbiased analysis of ataxin-3 interacting proteins was therefore conducted by MS. moDCs from 3 independent healthy donors were harvested on day 5 post isolation, and either left unstimulated or stimulated with MDP+PAM_3CSK_4 for 30 or 90 minutes. These time points were chosen on the basis that ataxin-3 phosphorylation is maximal in moDCs after 30 minutes, and thus any resultant change in protein interaction may be easiest to detect at, or shortly after, this time. IP with an isotype control antibody for each donor was also performed alongside. This allows subsequent filtering of any background proteins that have non-specifically bound to the antibody or support resin of the beads. The antibody-protein complex was eluted from the beads by boiling in LDS sample buffer containing DTT, as in this experiment there was no concern about protecting sensitive phosphorylation residues. Further, although harsher elution techniques may increase the detection of background proteins that have bound non-specifically, some proteomics facilities believe that this can be helpful in subsequent normalisation of the data (personal communication with Roman Fischer, Target Discovery Institute, University of Oxford). Following completion of the IP, quality control checks were performed. An aliquot of IP lysate was separated by SDS-Page and silver stain performed to verify the successful IP of ataxin-3 (4.8 B). Response of the cells to stimulation was confirmed by immunoblot of the whole cell lysate for p-p38 (4.8 C). Unique bands were excised. Both gel bands and in solution IP lysates were digested and subjected to LC-MS/MS analysis.

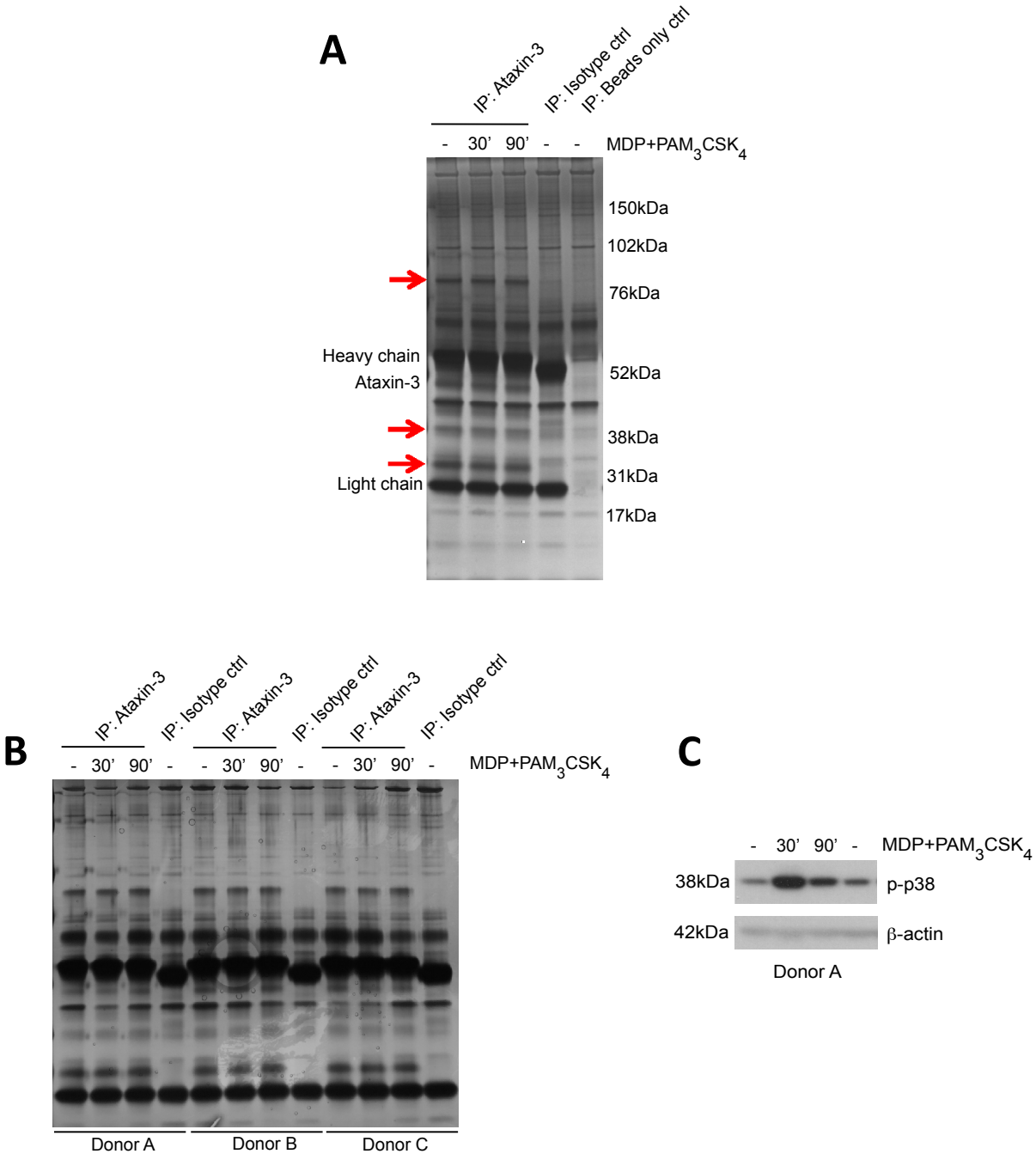


Figure 4.8 Immunoprecipitation of ataxin-3. **(A)** Silver stain of immunoprecipitation of ataxin-3 in moDCs either left unstimulated or stimulated with MDP+PAM$_3$CSK$_4$ for 30 or 90 minutes. Both an isotype control and beads only control are also shown. The red arrows indicate bands of unknown interacting proteins. **(B)** Silver stain of immunoprecipitation of ataxin-3 in moDCS in the 3 donors submitted for LC-MS/MS analysis. Samples were either left unstimulated or stimulated with MDP+PAM$_3$CSK$_4$ for 30 or 90 minutes. **(C)** Immunoblot using antibodies against p-p38 and β-actin of input lysate to confirm response of donors to stimulation in this experiment. Representative of the 3 donors.

The LC-MS/MS experiment and analysis was performed in collaboration with the Kessler Laboratory, Target Discovery Institute, University of Oxford. Applying a FDR of 1% and an Ions score of 20, with subsequent manual curation of the hits for background noise[416], 45 proteins were identified from the gel bands, and 82 from the in solution lysates, resulting in 117 unique proteins. Ataxin-3 was the most abundant protein detected, confirming the technical success of the IP. Just 4 proteins were found to change significantly on stimulation between the conditions (ANOVA $p<0.05$), but label-free quantitation in this setting is known to be an insensitive means of analysing changes in abundance. One protein, the mitochondrial membrane protein MIC19 (also known as CHCHD3), showed a significant increase in abundance on stimulation with MDP+PAM_3CSK_4, while the other three decreased in abundance (Table 1).

Protein	MASCOT Score	Fold change on MDP+PAM_3CSK_4 stimulation
MIC19	295.76	6.69
Paragranulin	123.17	0.67
Alpha-enolase	103.59	0.39
Creatine kinase M-type	82.11	0.09

Table 1 Proteins identified in the immunoprecipitation of ataxin-3 as changing significantly in abundance on stimulation with MDP+PAM_3CSK_4 ANOVA $p<0.05$.

The list of remaining proteins was further refined. Firstly, only proteins with a MASCOT score greater than 30 were considered. Secondly, the molecular weights of proteins identified in the gel bands were compared to the molecular weight of the gel band, as a match increases the likelihood of a genuine identification. Intriguingly, a further two mitochondrial proteins were identified. The mitochondrial transcription factor TFAM was identified with high confidence in the lysates. MIC60, which forms part of the mitochondrial contact site and crista organising system (MICOS) with MIC19, was identified in both the

lysates and in the gel band corresponding to its known molecular weight of 84kDa. Fragments of HIF1α were present in all the gel bands examined; this finding is particularly interesting given that ataxin-3 appears to be differentially regulated in hypoxia. Of relevance to ataxin-3's role in DNA repair was the identification of a DNA repair protein, PAXX, in all the gel bands examined. Finally a role for the DUB function of ataxin-3 was suggested by the identification of polyubiquitin-C in the lowest molecular weight gel band, corresponding to its known molecular weight of 34kDa.

Protein	MASCOT Score
TFAM	131.37
MIC60	101.84
HIF1α	75.16
PAXX	72.4
Polyubiquitin-C	36.69

Table 2 Selected proteins identified with high confidence in the immunoprecipitation of ataxin-3.

Next, validation of selected identified proteins (MIC19, MIC60, TFAM, HIF1α and PAXX) was undertaken, by immunoblot of IP samples with antibodies against the proteins of interest. MIC19 could not be identified following IP of ataxin-3, even following stimulation with MDP+PAM_3CSK_4 extended out to four hours (data not shown). However, MIC60 was identified in both unstimulated and stimulated samples, although there was no change in abundance (Figure 4.9 A). To further confirm that this was a genuine interaction, the reverse IP was performed, whereby endogenous MIC60 was pulled down, and the lysates blotted for ataxin-3. Ataxin-3 was significantly enriched in the MIC60 IP samples, and interestingly appeared at two molecular weights, suggesting that either two separate isoforms bind to MIC60, or it is post-translationally modified (Figure 4.9 B). Finally, immunofluorescence microscopy was undertaken to further investigate the interaction

between ataxin-3 and MIC60. In moDCs, ataxin-3 was found to form discrete punctae in the nucleus and cytoplasm, as expected. However, punctae were also found in close proximity to MIC60 (Figure 4.9 C). Super-resolution assessment using stimulated emission depletion (STED) microscopy confirmed that ataxin-3 punctae were indeed situated very closely to MIC60.

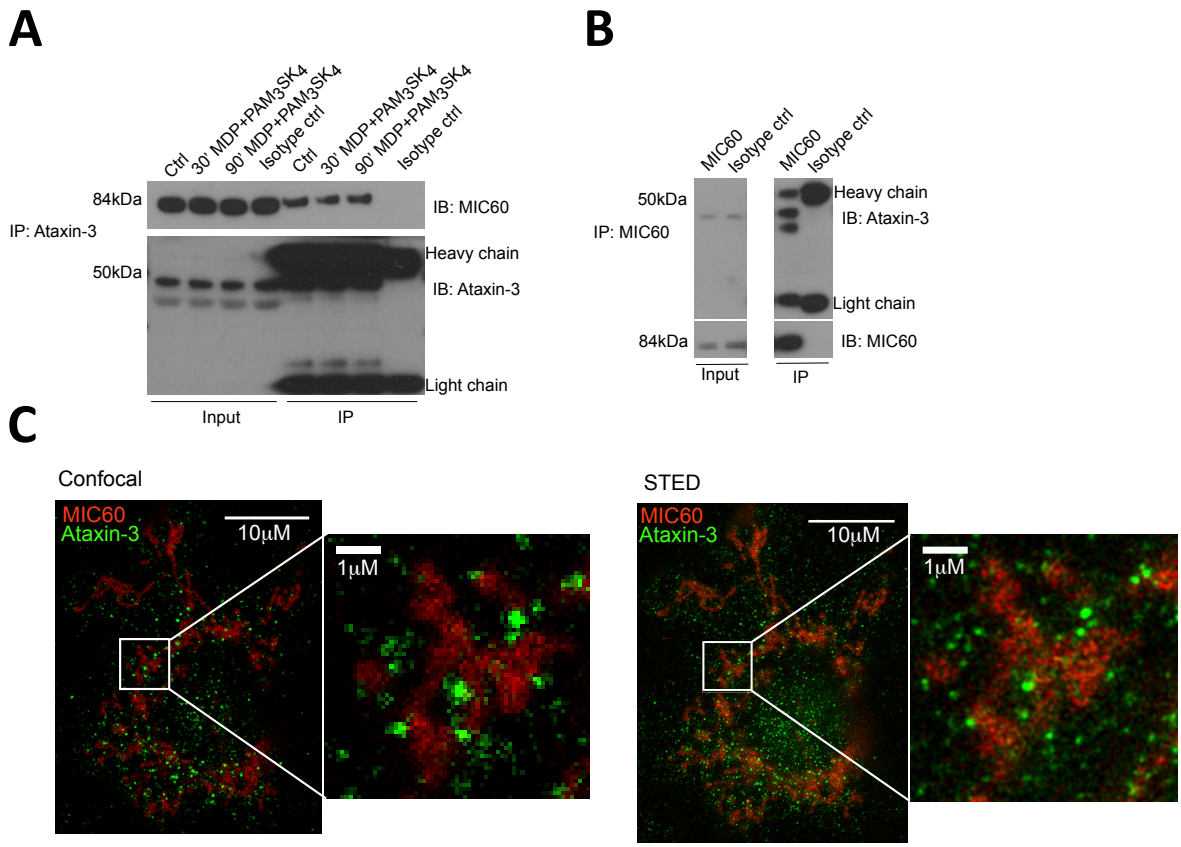


Figure 4.9 Ataxin-3 associates with the mitochondrial protein MIC60. **(A)** Immunoblot using antibodies against MIC60 and ataxin-3 of lysates where ataxin-3 has been immunoprecipitated from moDCs either left unstimulated or stimulated for 30 or 60 minutes with MDP+PAM_3CSK_4.
(B) Confocal and **(C)** STED microscopy using antibodies against ataxin-3 and MIC60 in moDCs.

Attempts to validate TFAM and PAXX were hindered by light chains from the antibodies obscuring visualisation. HIF1α could not be validated, even in samples cultured in hypoxia.

4.4 Discussion

The first part of this chapter dissected the innate signalling cascade to ataxin-3, and demonstrated that NOD2 is one of the key PRRs that triggers phosphorylation. The requirement of NOD2 for RIPK2 in this pathway was both expected and demonstrated. However, the identification of TBK1 as a phosphorylating kinase of ataxin-3 merits further discussion.

TBK1 is an IKK related kinase that consists of an N-terminal serine/threonine kinase domain, a ubiquitin-like domain (ULD), and two coiled-coil domains (CCD1 + 2) in the C terminus. The ULD regulates TBK1 by controlling kinase activation, substrate presentation and downstream signalling while the CCD mediates dimerisation which is important for activation[417]. TBK1 activity is strictly regulated by a series of post-translational modifications. Both ubiquitination of TBK1 at K30 and K401, and autophosphorylation at S172 is required for activation, and results in a conformational change that allows substrate binding[418,419, 420]. Historically TBK1 was primarily considered as a master regulator of the type 1 antiviral IFN response that is triggered by a broad range of PRRs including TLRs and RLRs[421]. Activated TBK1 consequently phosphorylates the transcription factor IRF3, leading to nuclear translocation and expression of both type 1 IFN and other antiviral genes[422]. TBK1 also regulates NF-κB signalling, but is not essential for this pathway[417].

More recently additional antimicrobial roles have been described for TBK1, most notably through regulation of autophagy. TBK1 has been found to phosphorylate functionally important sites in the autophagy receptors optineurin and p62, enhancing their binding to LC3 and ubiquitin respectively, and facilitating autophagic clearance of ubiquitin coated

bacteria through autophagy[13423]. TBK1 appears particularly important for the maturation of the autophagosome into the autophagolysosome, the key degradative step of autophagy[423]. A complementary pathway also exists whereby autophagy receptors can themselves recruit TBK1. Here, NDP52 recruits TBK1 to ubiquitin coated bacteria to facilitate autophagy[26,] acting at least in part through the autophagy protein WIPI2[424]. TBK1 also functions in another selective form of autophagy, mitophagy, to phosphorylate optineurin and p62 and regulate autophagy of ubiquitinated, damaged mitochondria[411, 425]. Importantly, despite the evidence outlined here, the functional role of TBK1in autophagy not yet been established using *in vivo* murine models. Intriguingly, it is thought that TBK1's proposed role in autophagy may explain the association with the inflammatory neurodegenerative diseases amyotrophic lateral sclerosis (ALS) and frontotemporal dementia (FTD)[426, 427]. This is supported by the observation that mutations in the TBK1 substrates p62 and optineurin are also found in ALS families[428, 429]. It has been suggested that mutations leading to partial loss of TBK1 function could result in defective removal of protein aggregates that may underlie both disease processes, but this remains to be clarified[430].

Work in this chapter has also identified the NOD2/TLR2 induced site of ataxin-3 phosphorylation as S265. While the location of this residue just outside the 2nd UIM suggests a possible functional role in determining DUB function, this must be further explored using site directed mutagenesis, which is described in the following chapter. Importantly, given that phosphorylation at four other serine residues leads to nuclear localisation of ataxin-3, NOD2/TLR2 stimulation did not change nuclear abundance.

Finally, an unbiased proteomics search for interaction partners of ataxin-3 in primary human moDCs provided a novel link to the mitochondria, and in particular the MICOS complex. To date, 8 proteins have been described as part of the MICOS complex, MIC10, 13, 14, 19, 23, 25, 27 and 60[431]. Interactions between ataxin-3 and two of these proteins, MIC19 and MIC60, have been suggested by work in this chapter. The association of ataxin-3 with MIC60 was convincingly demonstrated. While MIC19 could not be validated by the single technique attempted, it was identified with high confidence by the more sensitive technique of mass spectrometry, and its presence in the same complex of MIC60 further reinforces the likelihood it is a genuine interactor with ataxin-3. This association could be confirmed by performing an IP using an overexpression system, or attempting the reverse IP of MIC19 and immunoblotting for ataxin-3.

The highly conserved MICOS complex, first described in yeast, is embedded in the mitochondrial inner membrane. It acts as a key regulator of mitochondrial inner membrane shape and organisation. This is essential for cristae junction formation and assembly of respiratory chain complexes which are required for oxidative phosphorylation[432]. It is also involved in the formation of contact sites with the outer mitochondrial membrane, and associates directly with the sorting and assembly machinery (SAM) complex and translocase of the outer mitochondrial membrane (TOM) complex, which underlies an additional role in protein import[431, 433]. As the majority of mitochondrial proteins are encoded by nuclear DNA and synthesised in the cytosol as precursor proteins, their import into the mitochondria is fundamental to proper cellular function. It has been suggested that the MICOS subunits share non-redundant but common functions, as deletion of single subunits results in characteristic mitochondrial architectural defects and impairment of oxphos[434].

However, MIC10 and MIC60 are considered “core components” that direct MICOS assembly. The presence of two independent MICOS subcomplexes has been described in yeast, with MIC60 and MIC19 proposed to form one of these[434]. Indeed deletion of MIC60 leads to MIC19 instability, further supporting their apparent close interaction[432].

MIC60 is the largest protein in the MICOS complex and consists of an N-terminal domain that is anchored in the inner mitochondrial membrane, and a large hydrophilic section, which contains coiled-coil regions and a conserved mitofilin domain, and resides in the intermembrane space[435]. The regulation of MIC60 is uncertain, although the inner membrane mitochondrial protease YME1L may directly degrade MIC60 and control its stability[436]. Of relevance to ataxin-3, a number of highly conserved sites of ubiquitination have been described for MIC60 in large scale MS screens, but the importance of this post-translational modification has not been further explored[344]. MIC60 can also undergo protein kinase A (PKA) dependent phosphorylation at S528[437]. Phosphorylation negatively regulates parkin recruitment to damaged mitochondria, potentially by interrupting assembly of the PINK1 complex, as MIC60 was found to transiently interact with PINK1. This important role in mitophagy was also observed for MIC19, but not for any of the other MICOS subunits[437].

Additional specific roles for MIC60 include the import of proteins, as cells lacking MIC60 are less efficient in importing both cysteine-rich intermembrane space proteins and □-barrel proteins of the outer membrane[438, 439]. A potential role for ataxin-3 in this MIC60 mediated process is suggested by an additional tentative association of ataxin-3 with the TOM complex, which is itself crucial for mitochondrial protein import. A high throughput affinity purification MS screen in HEK293T cells suggested that ataxin-3 may interact with a

component of the TOM complex, TOMM20L[440], but this could not be validated in this work (data not shown). MIC60 also appears to act independently of the MICOS complex, and has recently been implicated in regulation of mtDNA transcription. The mitochondrial genome encodes just 13 proteins, all essential components of oxphos complexes I, III and IV. Transcription is controlled by the basal mitochondrial transcription machinery, which comprises TFAM, TFB2M and mitochondrial RNA polymerase (POLRMT). MIC60 was found to bind to both TFAM and TFB2M[441]. Depletion of MIC60 suppressed binding of TFAM to mtDNA promoters and reduced expression of mtDNA transcripts. The observed impairment of oxphos was linked to a specific reduction in the activity of oxphos complexes containing mtDNA encoded subunits. Activity of complex II, which is encoded exclusively by nuclear DNA, was unaffected[441]. It has also been suggested that mtDNA transcription in MIC60 depleted cells may be compromised by disorganisation of mtDNA nucleoids[436]. This role may not be independent of MICOS, as depletion of other MICOS subunits has also been implicated in impairment of mitochondrial genome maintenance[442]. To date, no known immune role for MIC60 or the MICOS complex has been described, but their importance in oxphos, mitophagy and maintenance of mtDNA make such a link highly plausible. It is noteworthy that in humans, mutations in MIC10 are associated with the neuroinflammatory diseases ALS and FTD-ALS across a range of patient cohorts[442, 443, 444, 445]. Once again, this recurring association with neurodegeneration is highly intriguing.

Chapter 5: Exploration of the roles of ataxin-3 in NOD2/TLR2 mediated immunity

5.1 Introduction

The focus of this work now turns to the functional importance of ataxin-3 in immunity. The discovery that ataxin-3 binds to a critical component of the MICOS complex, MIC60, suggests a role at the mitochondrion, an organelle integral to the cellular immune response. The first part of this chapter therefore centres around the importance of ataxin-3 to mitochondrial function. Next, the role of ataxin-3 in NOD2 mediated innate immune responses, converging upon the known associations of both NOD2 and TBK1 with autophagy and bacterial killing, will be explored. Finally, the deubiquitinating activity of ataxin-3, which appears to underlie the majority of this protein's defined roles to date, merits further exploration in an immune specific context in this chapter. The potential relevance of the DUB function is supported by the finding that the site of phosphorylation induced by NOD2/TLR2 stimulation resides just outside the 2nd UIM.

5.1.1 Ubiquitin signalling is critical to the immune response

Ubiquitin signalling represents an indispensable mechanism of regulating both the innate and adaptive immune response, and as outlined earlier is central to the NOD2 cascade[398]. Much like phosphorylation, it appears that the majority of proteins possess ubiquitination sites[446, 447]. Invading bacteria may also be ubiquitinated by the host cellular machinery to aid recognition and killing, and conversely may themselves seek to subvert the host Ub system to ensure survival and proliferation[448].

Ubiquitin is a 76-amino acid protein that is typically attached to a target protein by the consecutive actions of an activating E1 enzyme, a conjugating E2 enzyme and a ligase E3 enzyme. An important property of Ub is that it can be conjugated to substrates as a polymer. Additional Ub molecules can be ligated to one of seven lysine sites (K6, 11, 27, 29, 33, 48 and 63), resulting in a variety of specific linkages which may be either homogenous or mixed, while branched chains may also be formed[449]. The creation of such diverse Ub chains greatly expands the functional repertoire of Ub signalling. Homotypic K48 linked Ub chains account for over half of all linkages and classically target substrates to the proteasome for degradation[447], while the next most abundant K63 Ub chains target proteasome independent functions including DNA repair and delivery to endosomal-lysosomal pathways[450]. A further layer of control is provided by post-translational modification of Ub itself, a process important in mitophagy[451,452]. As with phosphorylation, Ub signalling is dynamic and reversible. Five specialised families of proteases, collectively termed DUBs, act to break ubiquitin chains through hydrolysis of the isopeptide bond between the Ub C-terminus and K amino ε-group[447]. Broadly, they can be divided into metalloproteases and cysteine proteases, with the cysteine proteases further subdivided into ubiquitin-specific proteases (USP), ubiquitin C-terminal hydrolases (UCH), ovarian tumour proteases (OTU) and Machado-Josephin domain proteases (MJD), of which ataxin-3 is a member[453]. Fewer than 100 DUBs have been described, which must function in a sophisticated and tightly regulated manner to modify the ubiquitin linkages of tens of thousands of proteins. DUB activity can be controlled through regulation of abundance, cellular localisation and post-translational modification[452]. Precise substrate binding sites and linkage specificity are also critical in ensuring accurate targeting of DUBs to their

substrates[452]. Here the apparent preference of ataxin-3 for cleaving K63 chains, and in particular K63 linkages in K63/K48 mixed chains with four or more ubiquitins is notable[300].

Mass spectrometry has become the method of choice for unbiased proteomic analysis of ubiquitination. Classically the ubiquitinated proteome, also termed the ubiquitome, was first enriched using His_6-tagged ubiquitinated conjugates under denaturing conditions. However, concerns exist over the impact of overexpressed modified His_6, which competes with endogenous ubiquitin, on the ubiquitome[454]. An alternative method of enrichment, using high affinity ubiquitin traps has therefore been developed. These tandem ubiquitin binding entities (TUBEs) specifically recognise, bind to, and stabilise polyubiquitinated proteins, protecting them from degradation by DUBs or the proteasome. The enriched ubiquitinated proteins can then be analysed by MS[454, 455, 456]. The ability of TUBEs to preferentially recognise either K48 or K63 linked polyubiquitin provides a further advantage. Consequently the use of a K63-TUBEs1 system which shows a 10 fold higher affinity for K63 linked chains, allows the selective enrichment of the K63 linked ubiquitome. This provides a specific means of purifying the K63 chains favoured by ataxin-3, and thus is employed in this chapter as a strategy for defining novel DUB targets of ataxin-3 in immune cells.

5.1.2 The ataxin-3 knockout mouse

Silencing gene expression represents perhaps the single most useful method of assessing the functional importance of a protein, and is utilised throughout this chapter in both primary cells and cell lines to interrogate the immune role of ataxin-3 in humans. This approach is complemented by the study of an ataxin-3 knockout mouse. In the last decade, several ataxin-3 knockout mice strains have been generated[287, 457, 458]. While these models

confirmed the *in vivo* DUB activity of ataxin-3, the inability to reproduce the neurological phenotype of SCA3, or indeed any significant neurological phenotype, led some researchers to question the importance of the wild type protein. However, more recent work has demonstrated the *in vivo* relevance of ataxin-3 in starvation induced autophagy, using an shRNA model[330]. A further intriguing finding was provided by the Infection and Immunity Immunophenotyping (3i) consortium, which has conducted a high throughput immunological phenotyping of hundreds of knockout mouse lines, including ataxin-3. A hit was scored in the ataxin-3 knockout mouse for the presence of autoantibodies, suggesting a role in immune regulation[459]. However, no statistically significant differences were seen between ataxin-3 knockout and WT mice in any other assay, including a DSS colitis screen. Notably, they utilised a targeted mutation 1a (tm1a) construct for one quarter of their original knockout lines, including ataxin-3. This gene trap mutation can potentially be skipped over, resulting in residual gene expression. Indeed, an internal unpublished study subsequently approximated that while 60% of the tm1a lines were complete knockouts, 16% were hypomorphic and 24% had residual gene expression (personal communication, 3i Project). As ataxin-3 expression was not checked, the degree of knockdown achieved is unknown and consequently it is difficult to interpret the results of the immunophenotyping screen. Further as it is a screen, small numbers of mice were used for each experiment and very stringent statistical criteria applied, and thus false negative results are likely. In light of the concerns over the tm1a construct, an alternative ataxin-3 knockout mouse model was utilised for this work, in collaboration with the Paulson laboratory, Department of Neurology, University of Michigan Health System. This mouse was originally generated at Lexicon Genetics from Omnibank embryonic stem cells containing a gene trap insertion in

the ATXN3 gene[457]. The gene trap vector, VICTR48, was inserted in the first intron downstream of the ATG. The intron sequence flanking the insertion site (*) is:

5' TCAAGTCATTTGGGTGTTTCTCGGACAA*CCATGTTTCATAATCATTTTAGGTTTGG 3'

The mice were bred into a C57Bl/6 background, with no detectable ataxin-3 at mRNA or protein level. As expected, there is an *in vivo* impairment of DUB activity, further confirming the knockdown[309].

5.2 Aims

This chapter aims to:

1. Interrogate the role of ataxin-3 in mitochondrial function

2. Investigate the importance of ataxin-3 in the innate immune response in both human and murine cell systems

3. Define the DUB targets of ataxin-3 in human immune cells

5.3 Results

5.3.1 Ataxin-3 is required for mitochondrial respiration and mROS production

In light of the finding from other laboratories that MIC60 depletion affects transcription of the mitochondrial genome[436, 441], the effect of ataxin-3 knockdown on mRNA expression of the mtDNA genes that encode components of the oxphos machinery was examined. Ataxin-3 was depleted using siRNA in primary human moDCs, with efficient knockdown confirmed by immunblot. Consistently, healthy donors were found to express either a single or double isoform of ataxin-3. The significance of this is unknown, but they both occurred with approximately equal frequency. Importantly, both isoforms could be efficiently depleted (Figure 5.1 A). 48 hours after transfection, RT-qPCR was performed to quantify mRNA

expression of the mtDNA genes of interest. mRNA abundance of these genes is sufficient to allow accurate assessment in whole cell lysates without the need for mitochondrial enrichment[436, 441], with the cDNA subsequently quantified with commercially available primers. 7 mtDNA genes were selected to ensure that all 4 of the oxphos complexes encoded by the mitochondrial genome were assessed. Ataxin-3 depletion led to a consistent two-fold upregulation of NADH-ubiquinone oxidoreductase 1 (MT-ND1), with a statistically significant upregulation observed for mRNA expression of two other genes from Complex I, MT-ND3 and MT-ND4L (Figure 5.1 B). In comparison, genes encoding components of Complex II, III and IV were broadly unaffected. It is noteworthy that mtDNA transcription is tightly regulated due to its close links to oxphos, and thus 1.5 to 2 fold changes in mRNA expression level represent a potentially functionally significant alteration[460]. Interestingly, the observed upregulation of mtDNA transcription following ataxin-3 depletion contrasts with the downregulation observed by others following MIC60 depletion, although the overall change in abundance is on a comparable scale[436, 441]. Next, the effect of NOD/TLR2 stimulation was examined on MT-ND1, the most significantly affected gene. Stimulation led to a significant upregulation in mRNA expression in both the control and ataxin-3 depleted cells, but there was significantly greater ND1 in the ataxin-3 depleted cells following stimulation (Figure 5.1 C). Finally, the effect of hypoxia on the observed upregulation was studied. Following 16 hours of hypoxia, the effect of ataxin-3 depletion on mtDNA transcription of Complex I was largely abrogated (Figure 5.1 D).

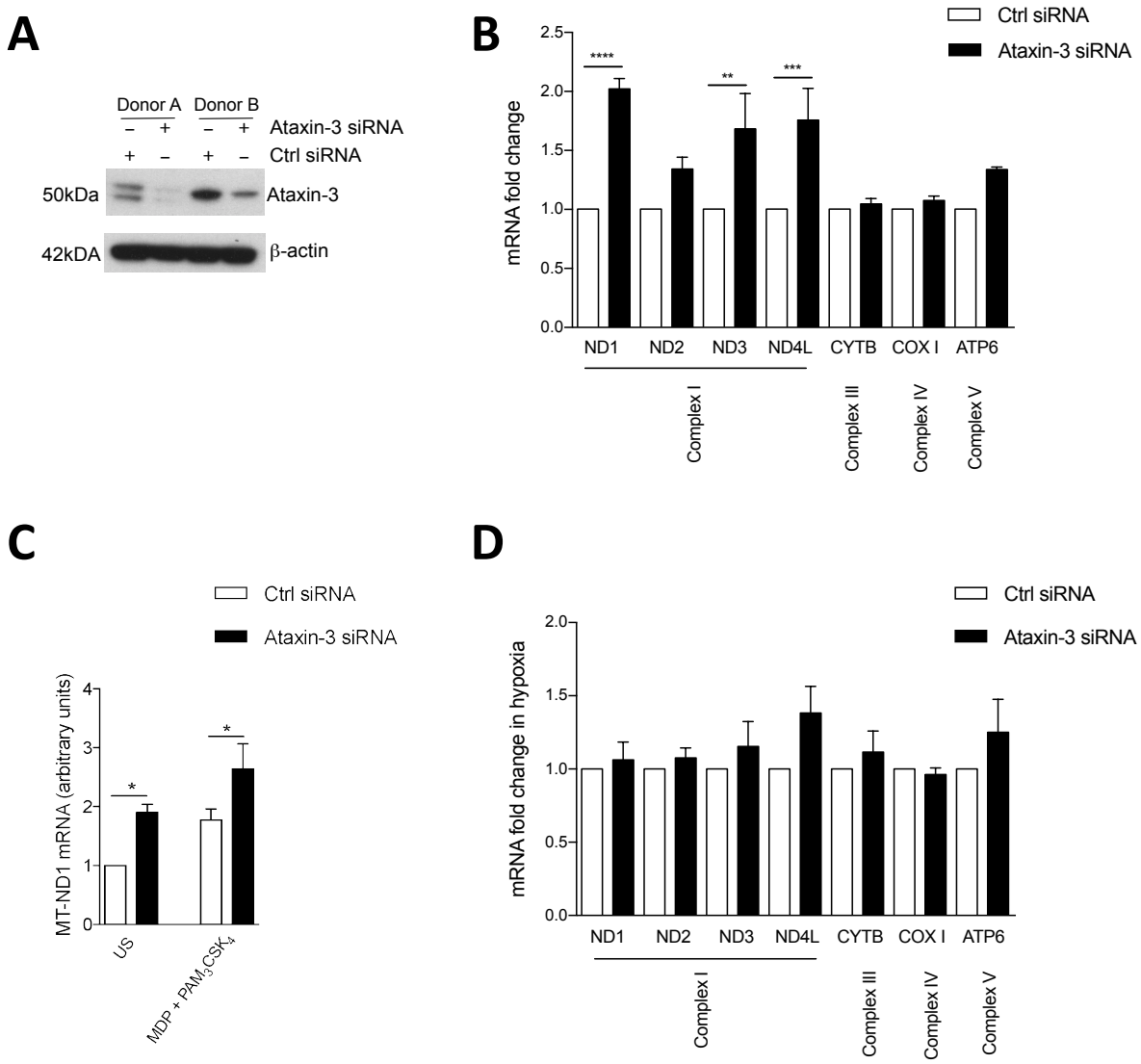


Figure 5.1 Ataxin-3 depletion in moDCs leads to dysregulation of mtDNA transcription.
(A) Immunoblot using antibodies against ataxin-3 and β-actin in moDCs following transfection with control or ataxin-3 siRNA. **(B)** RT-qPCR analysis of selected mitochondrial genome encoded transcripts following ataxin-3 depletion by siRNA in moDCs. **(C)** RT-qPCR analysis of MT-ND1 mRNA expression following ataxin-3 depletion by siRNA in moDCs subsequently left unstimulated or stimulated for 6 hours with MDP+PAM_3CSK_4 stimulation. **(D)** RT-qPCR analysis of selected mitochondrial genome encoded transcripts following ataxin-3 depletion by siRNA in moDCs and subsequent incubation in hypoxia (1% O_2) for 16 hrs. (B)+(D) n=3, (C) n=4. One way ANOVA, *p<0.05 **p<0.01 ***p<0.001 ****p<0.0001

To further investigate the functional relevance of these observed changes in mRNA expression of Complex I, an alternative method of ataxin-3 depletion was undertaken. Use of an immortalised cell line stably expressing a short hairpin RNA (shRNA) construct eliminates the need for multiple rounds of transfection, saving both time and expensive consumables, and also increases reproducibility of results[461]. Having already confirmed the NOD2 dependent phosphorylation of ataxin-3 in the THP-1 cell line, this represented an ideal cell line for transfection. 5 separate shRNA sequences to deplete ataxin-3 was purchased from Sigma, and transfected into THP-1 cells using lentivirus. As a control, a scrambled sequence purchased from Sigma was also transfected into THP-1 cells. The presence of a puromycin resistance gene in all constructs allowed puromycin selection of cells expressing the different shRNA constructs. Protein knockdown was then assessed by immunoblot (Figure 5.2 A). As expected, there was no difference in ataxin-3 protein expression between cells transfected with the control shRNA, and wild type, untransfected cells. Three ataxin-3 shRNA constructs showed significant protein knockdown. mRNA expression of ATXN3 in these three constructs was next assessed by RT-qPCR (Figure 5.2 B). Construct 5, which showed the best protein knockdown, also showed the most significant reduction in mRNA expression. Interestingly, construct 3 showed no significant reduction in ATXN3 mRNA expression despite a marked knockdown at protein level. This may be due to the shRNA sequence repressing translation only[461]. Alternatively, this may represent differences in detection of the various splice isoforms of ataxin-3 by the primer and antibody. mRNA expression of the three other members of the Josephin family, JOSD1, JOSD2 and ATXN3L, which share significant sequence homology, were also assessed. No significant differences in JOSD1 or JOSD2 was seen with constructs 1 and 5, but expression of JOSD1 appeared upregulated in construct 3 (5.2 C + D). The reason for this is unclear. No

antibodies reliably detect protein expression of these two members of the Josephin family, and thus protein expression could not be assessed. There was no detectable expression of ATXN3L at mRNA level, consistent with the body of evidence that suggests it is a pseudogene.

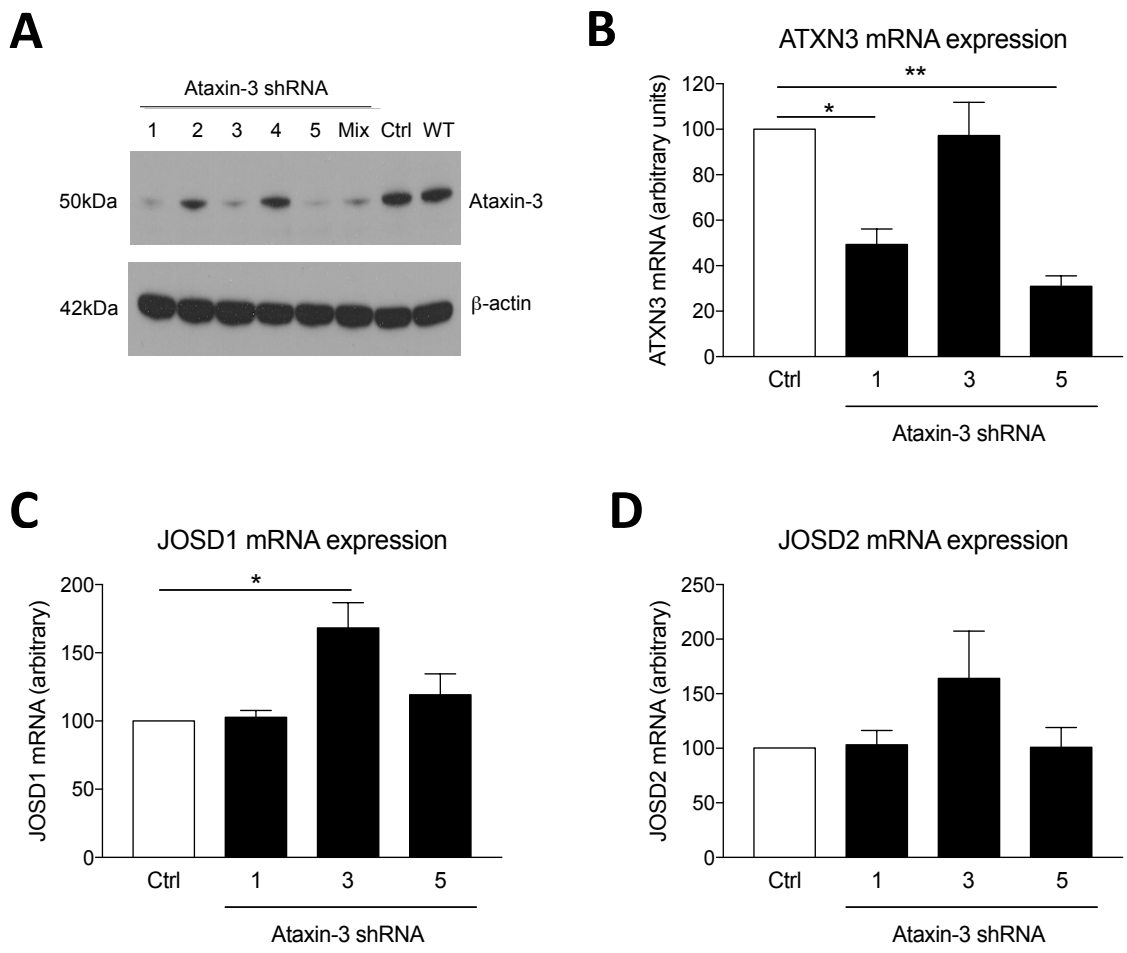


Figure 5.2 Ataxin-3 can be efficiently knocked down at both a protein and mRNA level using shRNA in the THP-1 cell line. **(A)** Immunblot using ataxin-3 and β-actin antibodies following lentiviral transfection of ataxin-3 or control shRNA constructs. The wild type (WT) protein expression is also shown. **(B), (C), (D)** RT-qPCR analysis of ATXN3, JOSD1 and JOSD2 mRNA expression in selected ataxin-3 or control shRNA constructs. n=3, one way ANOVA *p<0.05, **p<0.01.

Next, the effect of ataxin-3 depletion on mitochondrial DNA copy number was assessed, as an increase in copy number with a resultant increase in transcription could explain the upregulation of mtDNA encoded mRNA. Notably, TFAM is known to regulate mtDNA copy number[462], which is of direct relevance as MIC60 has previously been shown to interact with TFAM[441], while TFAM was also detected by MS in the IP of ataxin-3 in chapter 4 of this thesis. However, no significant difference in mtDNA copy number was found between the control and ataxin-3 depleted THP-1 cell line (Figure 5.3). This also suggests that there is no overall change in mitochondrial mass or turnover, even in dividing cells subject to prolonged ataxin-3 depletion.

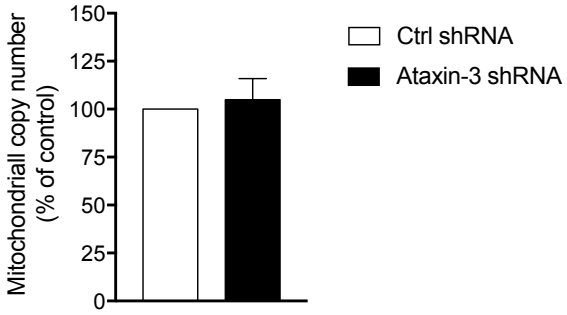


Figure 5.3 Ataxin-3 depletion does not affect mitochondrial copy number. SYBR Green based qPCR of a mitochondrial DNA fragment (mitochondrially encoded tRNA leucine 1) was performed, and the relative mtDNA copy number calculated by normalising to simultaneous qPCR of a nuclear DNA fragment (β2 microglobulin). n=2.

The functional effect of ataxin-3 depletion on mitochondrial respiration was then assessed, utilising the Seahorse platform. This allows the real time interrogation of oxidative phosphorylation in live cells by calculating the oxygen consumption rate using a highly reproducible microplate system[463]. Sequential addition of compounds that interfere with oxidative phosphorylation allow assessment of key parameters of mitochondrial respiration, namely basal respiration, ATP production, maximal respiration and spare capacity. First, oligomycin is added which blocks ATP synthase to inhibit ATP synthesis. Then FCCP

(carbonyl-cyanide *p*-tri-fluoro-methoxy-phenyl-hydrazone), is added which uncouples the electron transport chain from oxidative phosphorylation. Finally, mitochondrial respiration is entirely inhibited by the addition of antimycin-A and rotenone (Figure 5.4).

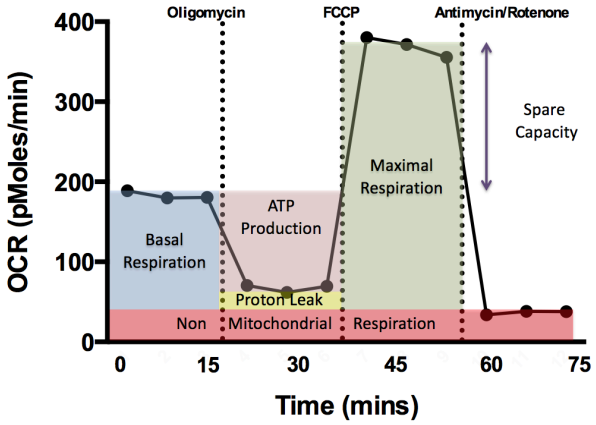


Figure 5.4 Representative graph of the OCR in cells following sequential addition of oligomycin, FCCP and antimycin A/rotenone, analysed by the Seahorse platform.

The experimental set-up for THP-1 cells was first optimised by determining the cell seeding density and working concentration of the compounds (data not shown). The undifferentiated monocyte phenotype was chosen for investigation as it provided a broader immune cell relevance. As undifferentiated THP-1 cells are non-adherent, the microplate was first coated with an inert adhesive, Cell-Tak (Corning), prior to cell seeding OCR measurements were also normalised following the end of the Seahorse readings using CyQUANT dye (Invitrogen), to ensure that cell detachment did not result in artefactual differences. Ataxin-3 depletion led to a significant reduction in all the key parameters of mitochondrial respiration assessed (Figure 5.5). This was confirmed with the use of two independent shRNA clones that had demonstrated the best knockdown of ataxin-3 (clones 1 + 5). The relationship between ataxin-3 depletion and impairment of OCR was further confirmed with the observation of a "dose response"; the clone in which ataxin-3 was most depleted (clone 5) showed the most marked impairment in OCR.

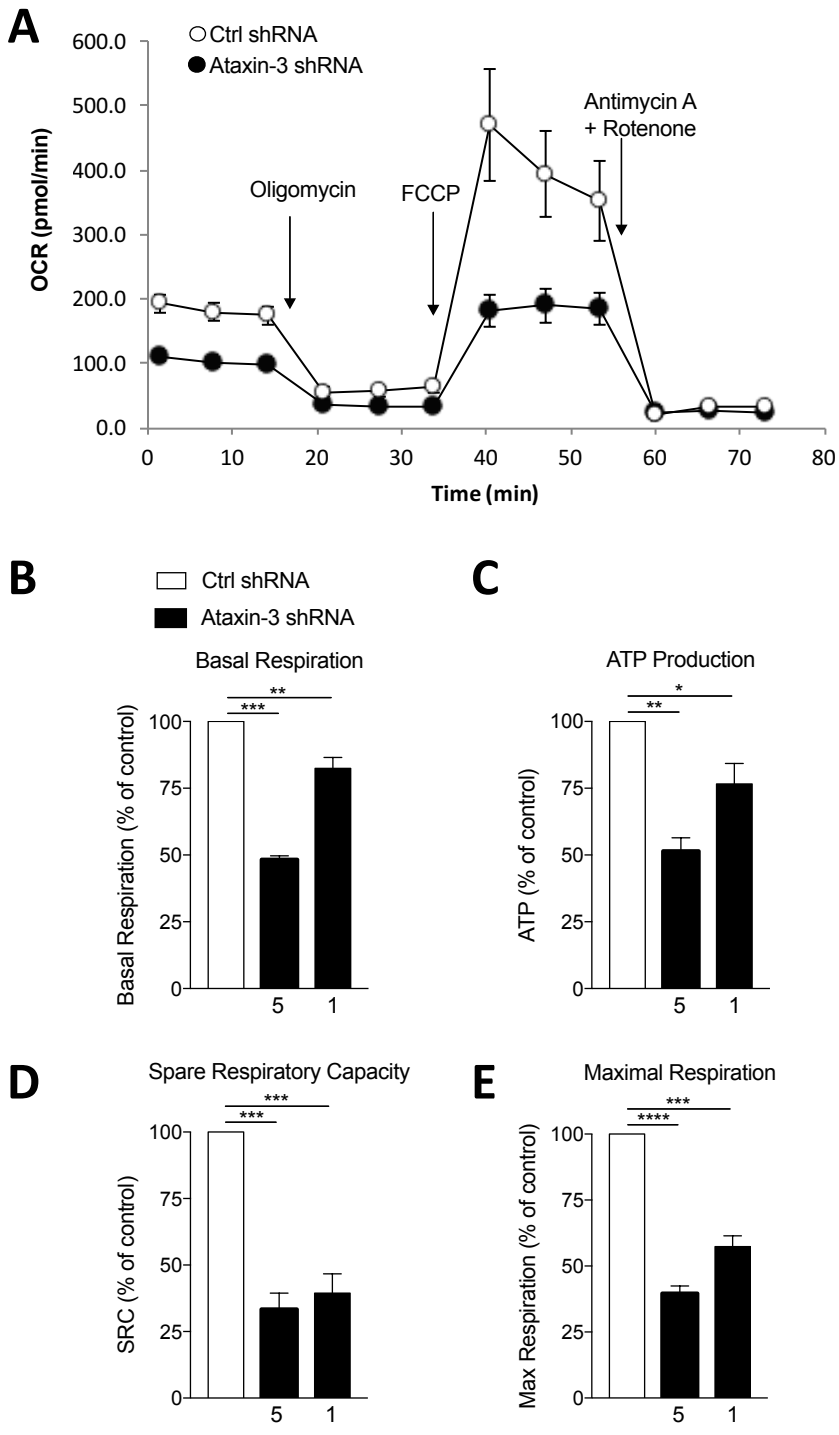


Figure 5.5 Mitochondrial respiration is impaired in ataxin-3 depleted THP-1 cells. Seahorse analysis of OCR in control and ataxin-3 shRNA cells. **(A)** Representative sequential OCR measurements of control and ataxin-3 shRNA cells. **(B-E)** Analysis of key mitochondrial respiration parameters in control shRNA cells and two independent ataxin-3 shRNA clones (1 + 5). **(A)** representative of 3 independent experiments. **(B)-(E)** n=3, one way ANOVA *p<0.05, **p<0.01, ***p<0.001, ****p<0.0001. OCR measurements normalised to cell number.

Next, the effect of NOD2/TLR2 stimulation in this experimental set-up was assessed. Prolonged triggering of these PRRs led to an expected metabolic shift, with downregulation of oxidative phosphorylation. In the ataxin-3 depleted cells the level of oxphos remained significantly lower than in the control cells following stimulation (Figure 5.6). The Seahorse experiments in THP-1 cells were performed in collaboration with Simon Wigfield, Harris Laboratory, Weatherall Institute of Molecular Medicine, University of Oxford.

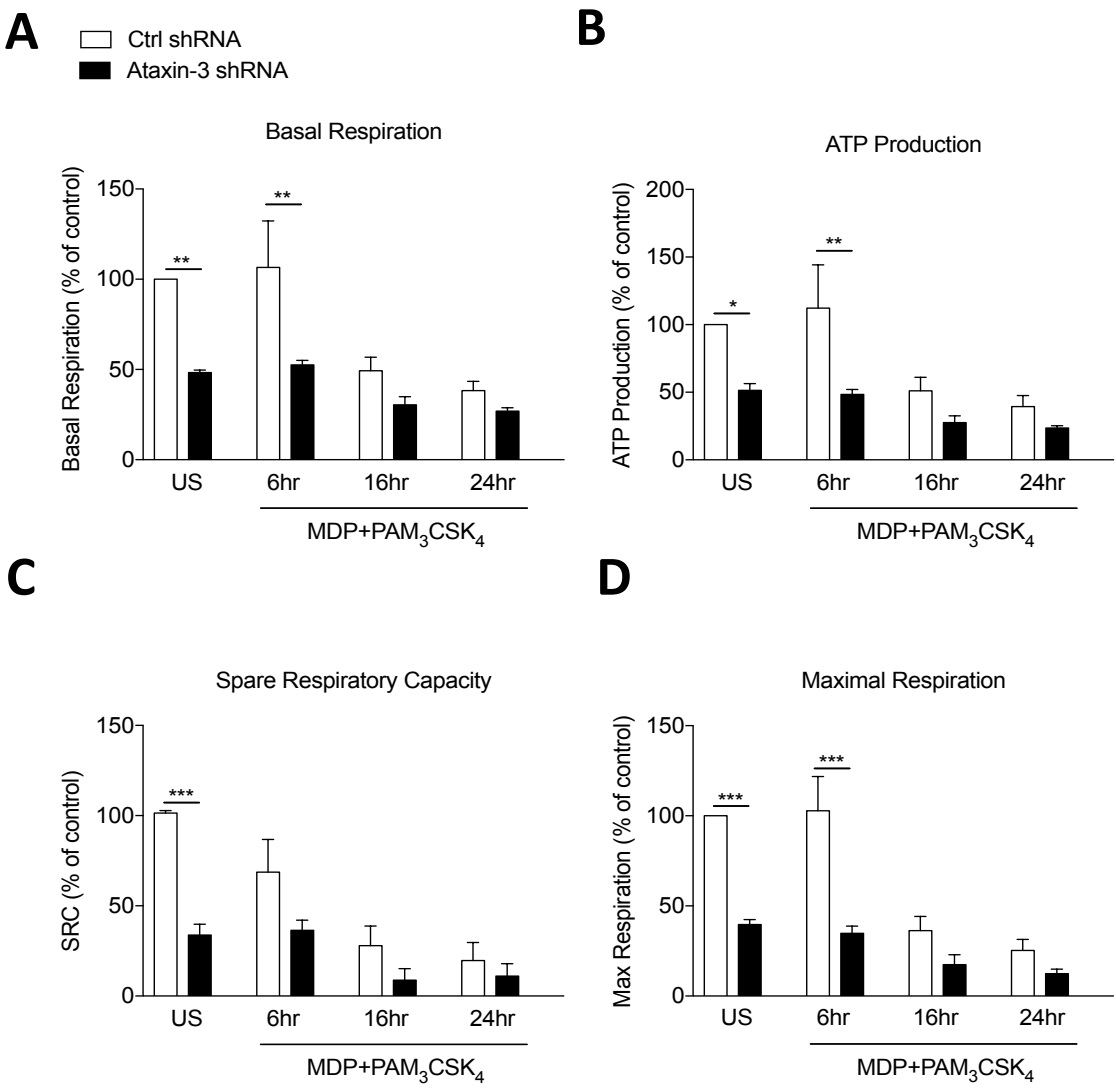


Figure 5.6 Mitochondrial respiration is more significantly impaired in the ataxin-3 depleted THP-1 cells following NOD2/TLR2 stimulation. (A)-(D) Seahorse analysis of OCR in control and ataxin-3 shRNA THP-1 cells that were either left unstimulated or stimulated for 6, 16 or 24hr with MDP+PAM$_3$CSK$_4$. n=3, one way ANOVA *p<0.05, **p<0.01, ***p<0.001. OCR measurements were normalised to cell number.

A key function of mitochondrial respiration in immune cells is the generation of mROS. This results from leakage of electrons, predominantly from Complex I and to a lesser extent from Complex III, which partially reduce oxygen to form superoxide[464]. The effect of ataxin-3 depletion on mROS and total cellular ROS was therefore examined. Ataxin-3 depletion led to a significant reduction in mROS (Figure 5.7 A). As expected, there was a corresponding decrease in total cellular ROS, to which mROS makes a significant contribution (Figure 5.7 B). The ability of immune cells to upregulate mROS production on pathogen challenge is crucial to the immune response; importantly, ataxin-3 depleted THP-1 cells also produced less mROS on NOD2/TLR2 stimulation (Figure 5.7 C). The FACS experiments in Figure 5.7 were performed in collaboration with Sumeet Pandey, Uhlig Laboratory, Translational Gastroenterology Unit, University of Oxford.

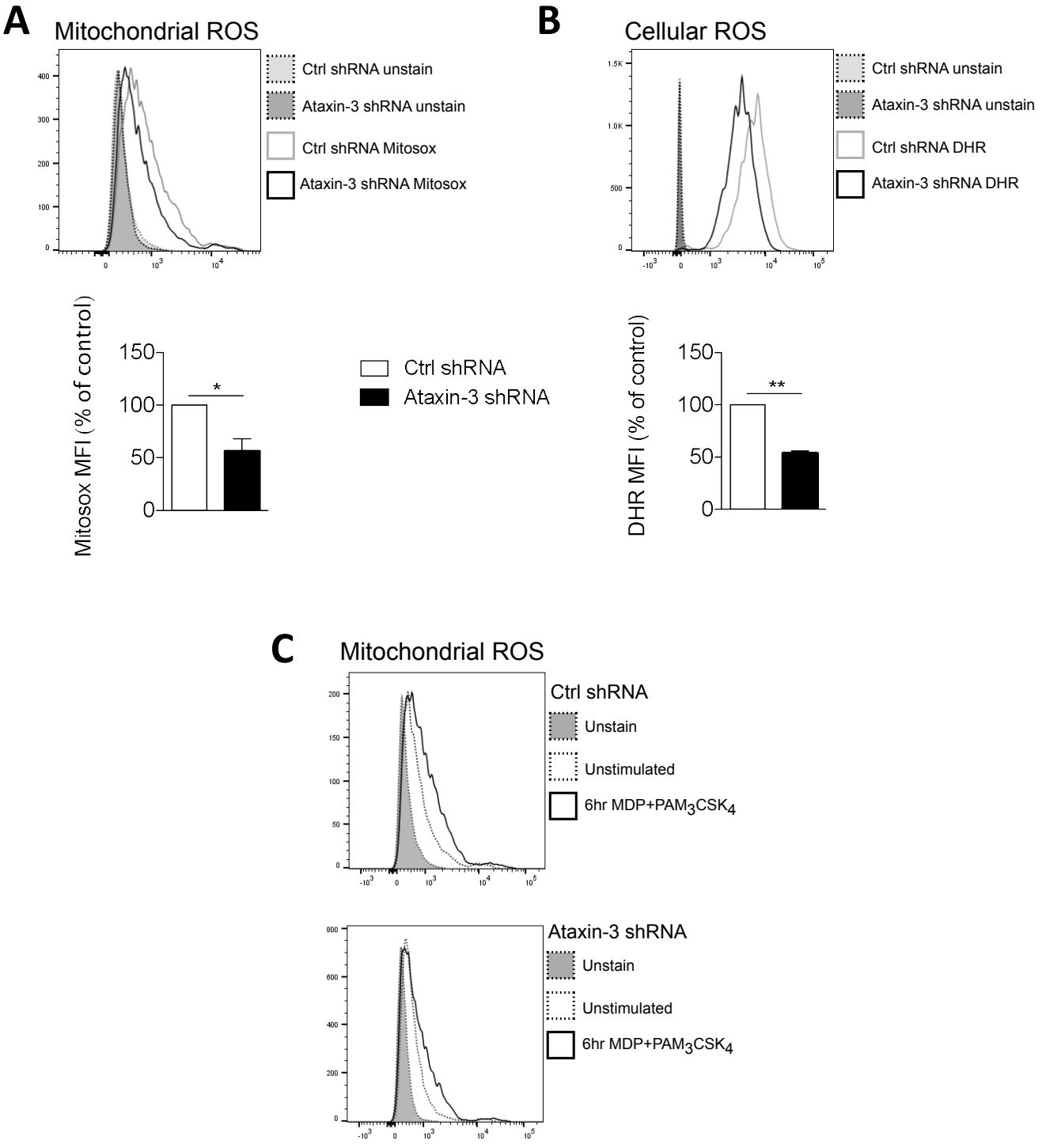


Figure 5.7 mROS is reduced in ataxin-3 depleted THP-1 cells. FACS analysis of **(A)** Mitosox to quantify mROS and **(B)** DHR to quantify total cellular ROS in control and ataxin-3 shRNA THP-1 cells. **(C)** FACS analysis of Mitosox to quantify mROS in control and ataxin-3 shRNA THP-1 cells either unstimulated or stimulated for 6hr with MDP+PAM_3CSK_4. **(A)**+**(B)** are FACS results from a single experiment, representative of 3 independent experiments, or 3 experiments combined for Student's paired t test, *$p<0.05$. **(C)** is a FACS result from a single experiment, representative of 3 independent experiments. Performed in collaboration with Sumeet Pandey.

5.3.2 Ataxin-3 may be important in NOD2 driven autophagy

A role for ataxin-3 in NOD2 stimulated autophagy was next investigated. A link seemed plausible for two reasons. Firstly, the association between the phosphorylating kinase of ataxin-3, TBK1, and xenophagy is well established[95, 97, 423, 424]. Secondly, there is increasing evidence that mitochondrial respiratory function is important for autophagy. Impairment of mitochondrial respiration was found to compromise amino acid starvation induced autophagy gene induction and autophagic flux in yeast[465]. Subsequent work has demonstrated the importance of mitochondrial respiration for lysosomal biogenesis, structure and function, including maintenance of autophagic flux[466, 467]. The immune relevance was shown in murine CD4+ T lymphocytes, where inhibition of mitochondrial respiration led to impaired lysosomal function and autophagy, subverting T cell differentiation towards pro-inflammatory Th1 subsets[468]. This exacerbated the *in vivo* inflammatory response in both a DSS colitis challenge, and a model of contact hypersensitivity. This pro-inflammatory phenotype could be rescued *in vitro* by increasing NAD+ levels to restore mitochondrial function.

Steady state autophagic flux was blocked in ataxin-3 depleted THP-1 cells, as indicated by increased LC3 levels and decreased clearance of the autophagy substrate p62, which persisted even after stimulation with MDP + PAM_3CSK_4 for 6 hours (Figure 5.8 A). Next, the effect of disrupting autophagic flux with bafilomycin A1 was examined. Bafilomycin A1 inhibits both vacuolar-type H+-ATPase (V-ATPase) dependent lysosomal acidification and Sarco/endoplasmic reticulum Ca(2+)-ATPase (SERCA-ATPase) dependent autophagosome-lysosome fusion[469]. To further interrogate the disruption of autophagic flux in ataxin-3 depleted cells, two important autophagy pathways were also assessed. The inhibitory effect

of mTORC1 (mammalian target of rapamycin complex 1) on autophagy is well established, with activity regulated by cellular nutritional status[470]. The effect of ataxin-3 depletion on the mTORC pathway was therefore assessed through immunoblot for phosphorylation of ribosomal protein S6, a downstream effector of mTORC1. Protein levels of beclin 1 were also assessed, given the finding published during towards the end of this research that ataxin-3 regulates the stability of this autophagy protein in starvation induced autophagy[330]. Pre-treatment of the ataxin-3 depleted and control cells with bafilomycin abrogated the differences in LC3 and p62 levels, confirming the defect in autophagic flux (Figure 5.8 B). Levels of both pS6 and beclin 1 were unchanged on ataxin-3 depletion. Finally, the lysosomal machinery was assessed. Proteins levels of lysosomal-associated membrane protein 1 (LAMP1) assessed by FACS, which indicate cellular lysosomal mass[468, 471], were significantly lower in the ataxin-3 depleted cells. Taken together, this data suggests that ataxin-3 depletion in immune cells results in an impairment of autophagic flux that may be mediated by impaired lysosomal degradation.

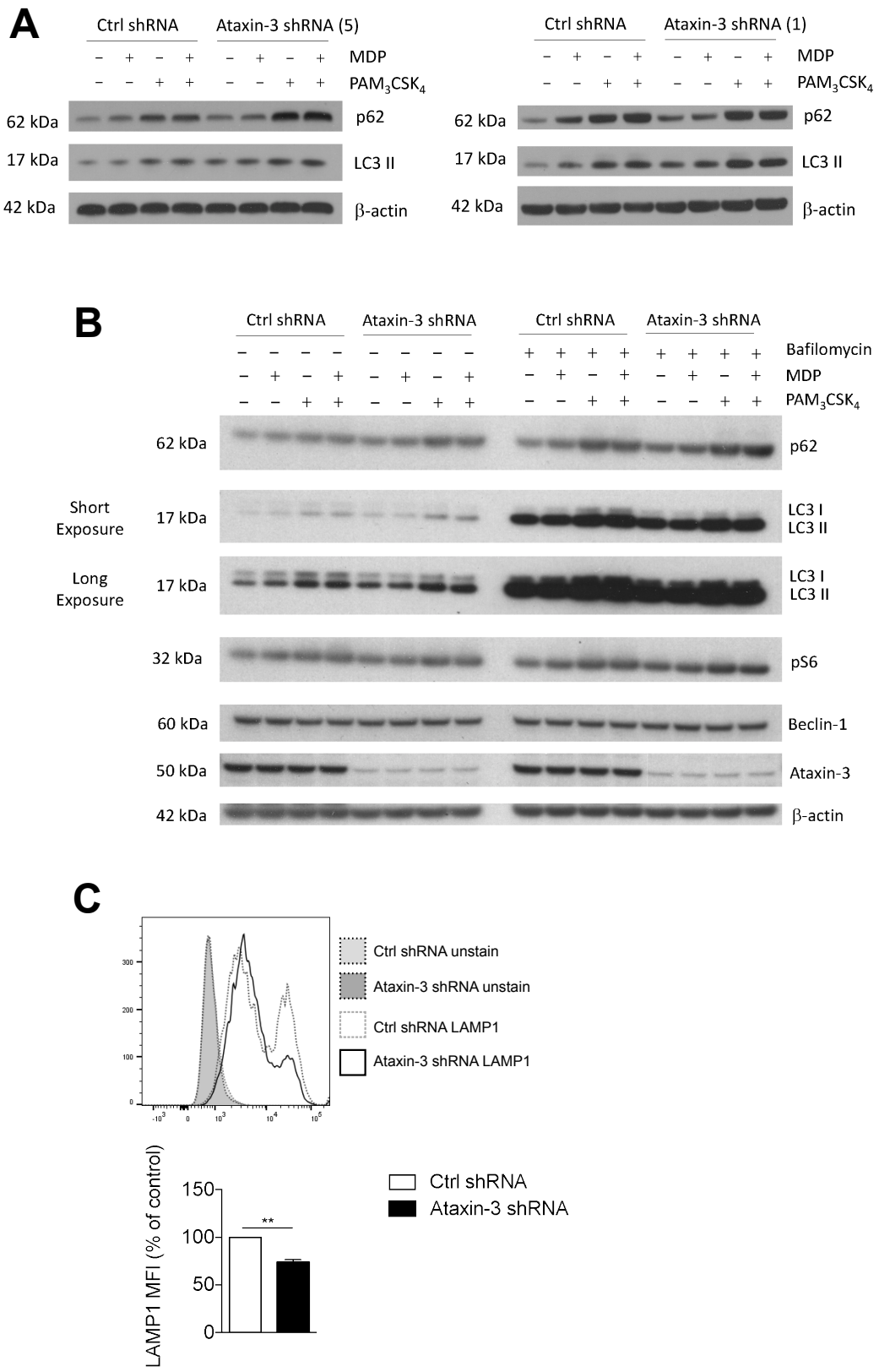


Figure 5.8 Ataxin-3 depletion affects autophagic flux in THP-1 cells. (A) Immunoblot using antibodies against ataxin-3, p62, LC3 and β-actin of control and two independent ataxin-3 shRNA clones at baseline and following 6hr of MDP or PAM_3CSK_4 or MDP+PAM_3CSK_4 stimulation. **(B)** Immunoblot using antibodies against ataxin-3, p62, LC3, pS6, beclin 1 and β-actin of control and ataxin-3 shRNA cells treated as in **(A)** with or without Bafilomycin A (Baf) 2hr prior to stimulation. **(C)** FACS plots of LAMP1 in control and ataxin-3 shRNA cells at baseline, representative of 3 independent experiments. Bar charts are n=3. Student's paired t-test, *p<0.05, **p<0.01.

Next, the importance of ataxin-3 for autophagy of bacteria, and bacterial killing was examined. Ataxin-3 depleted and control THP-1 cells were differentiated into a macrophage-like phenotype using phorbol 12-myristate 13-acetate (PMA) and infected with *Salmonella enterica* serovar Typhimurium. On confocal microcopy, LC3 was seen to successfully co-localise with bacteria in the ataxin-3 depleted cells, but there was a markedly greater accumulation of LC3 when compared to the control cells (Figure 5.9 A). Taken together with the previous immunoblots, this supports the hypothesis that ataxin-3 depletion leads to a blockage in autophagic flux. A gentamicin survival assay was then undertaken using the same model system to assess the requirement for ataxin-3 for bacterial killing. While bacterial invasion was unchanged, as evidenced by similar bacterial counts 1 hour post infection, there was subsequently significantly greater bacterial survival in the ataxin-3 depleted cells that was maximal at 6 - 8 hours (Figure 5.9 B). Interestingly by 24 hours, bacterial survival had reduced in the ataxin-3 depleted cells to the level seen in control cells. This suggests that other pathways required for bacterial killing are subsequently able to compensate for the earlier deficit. There were no significant differences in cell viability between the two groups at any of the infection time points, excluding differences in cell survival as a contributing factor in the bacterial killing deficit (Figure 5.9 C). All bacterial killing experiments were performed in collaboration with Anna Aulicino, Simmons Laboratory, Weatherall Institute of Molecular Medicine University of Oxford.

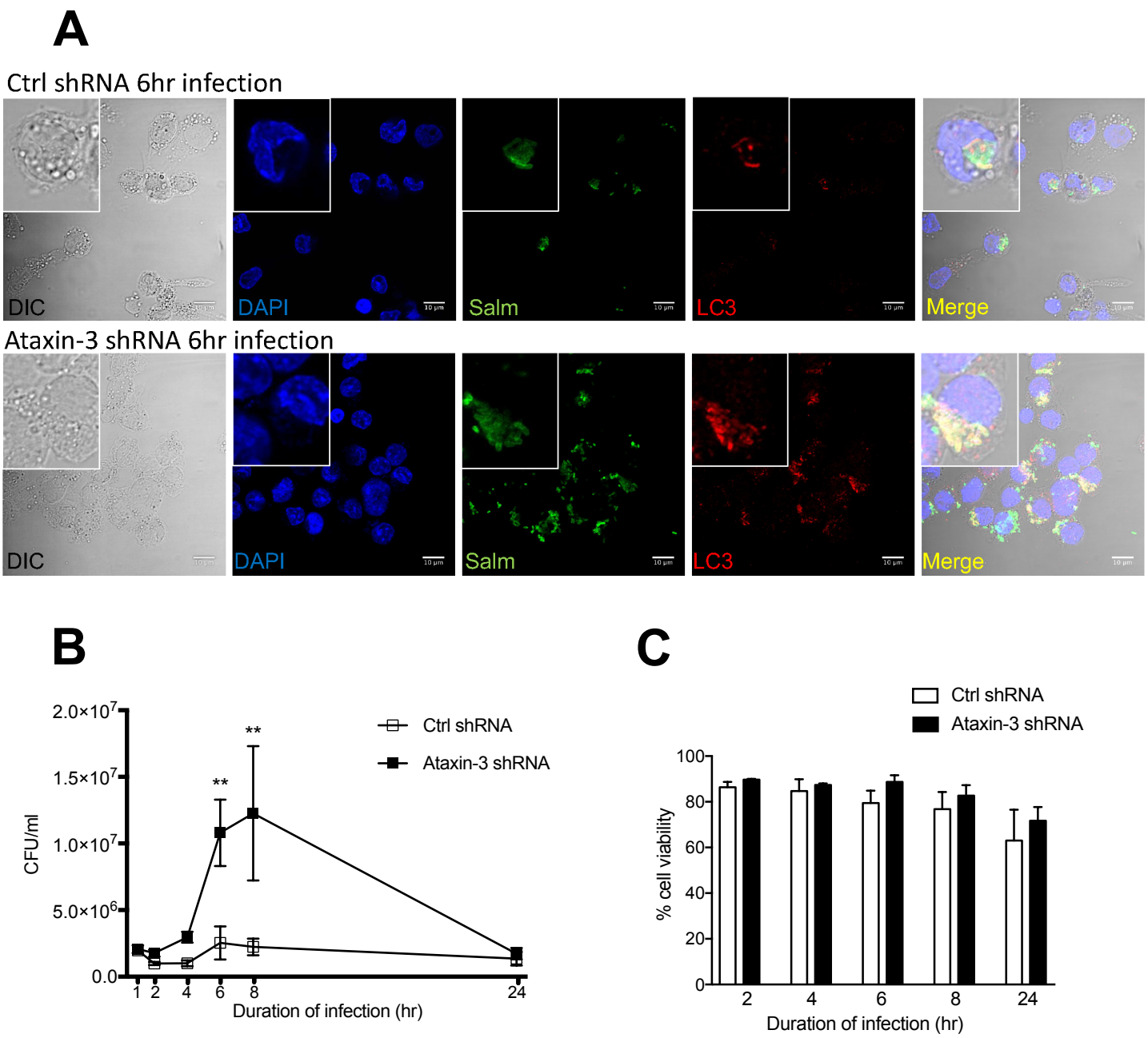


Figure 5.9 Ataxin-3 depleted THP-1 cells show defects in bacterial autophagy and killing.
(A) Confocal microscopy using antibodies against *Salmonella enterica* serovar Typhimurium and LC3 in ataxin-3 and control shRNA THP-1 cells infected for 6hr with *Salmonella* (scale bar 10μM). **(B)** Gentamicin survival assay and **(C)** THP-1 cell viability in ataxin-3 and control shRNA THP-1 cells infected for 1-24hr with *Salmonella enterica* serovar Typhimurium (MOI 20). **(B)** + **(C)** n=3, one way ANOVA **p<0.01. Performed in collaboration with Anna Aulicino.

5.3.3 The deubiquitinating function of ataxin-3 is important in monocytes following NOD2/TLR2 stimulation

To explore the importance of the deubiquitinating function of ataxin-3 in myeloid cells, the TUBEs system was used to enrich ubiquitinated proteins in ataxin-3 depleted and control THP-1 cells. In light of the known preference of ataxin-3 to cleave K63 chains, TUBEs1 beads which display a 10 fold higher affinity for K63 chains over K48 chains were selected. Further, an early experiment suggested TUBEs1 beads provided a cleaner enrichment than TUBEs2 beads in THP-1 cells when enriched fractions were subject to silver staining (data not shown). When whole cell lysates and TUBEs1 fractions were immunoblotted with an antibody against K63-linkage specific polyubiquitin, the efficacy of ubiquitin enrichment was confirmed. Strikingly, there was a marked increase in the levels of K63 ubiquitinated proteins in the ataxin-3 depleted cells, most notably at higher molecular weights (Figure 5.9). This is in agreement with previous published results in the ataxin-3 knockout mouse and in a human siRNA HeLa cell line model[287, 300]. The effect of stimulation with MDP + PAM_3CSK_4 for one hour was assessed concurrently. This time point was selected as NOD2/TLR2 induced phosphorylation of ataxin-3 in THP-1 cells is maximal at this time. A subtle shift in K63 ubiquitinated proteins was seen in both the ataxin-3 depleted and control cells following stimulation (Figure 5.10). Further, preliminary work has suggested that mutating the S265 residue may impair the deubiquitinating activity of ataxin-3 when either the S265 WT or A265 mutant were overexpressed with ubiquitin in a HEK293 model system (Figure 2, Appendix).

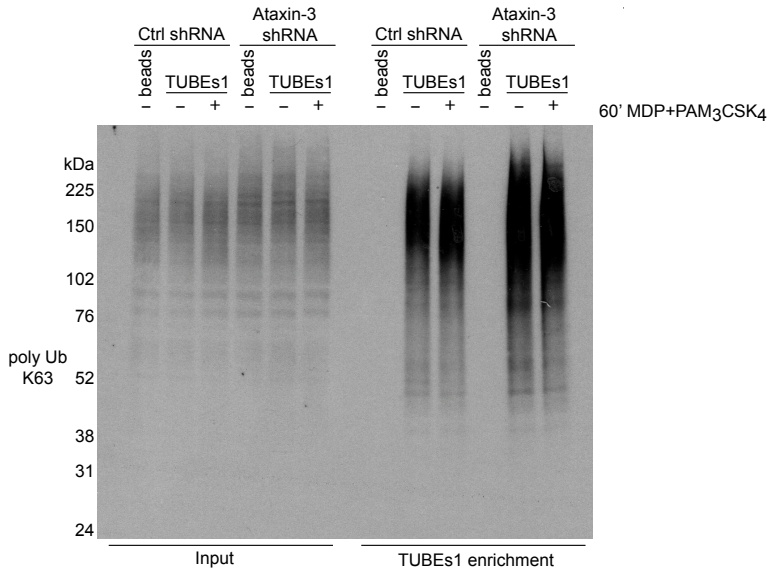


Figure 5.10 Ataxin-3 depletion in THP-1 cells leads to an accumulation of K63 polyubiquitinated proteins. Immunoblot using antibody against polyubiquitinated K63 in whole cell lysates (input) and TUBE1s enriched fractions of ataxin-3 depleted and control THP-1 cells. Cells were either left unstimulated or stimulated for 1 hour with MDP+PAM_3CSK_4 prior to lysis and ubiquitin enrichment. Performed in collaboration with Seiji Shiraishi.

Given this promising result, an unbiased screen of the ubiquitome in ataxin-3 depleted and control THP-1 cells was undertaken in collaboration with Seiji Shiraishi, Simmons Laboratory, Weatherall Institute of Molecular Medicine, University of Oxford. Cells were either left unstimulated or stimulated for one hour with MDP + PAM_3CSK_4, prior to lysis and enrichment of polyubiquitinated proteins using TUBEs1 beads. Three quality control checks were performed. Firstly, the response of the cells to stimulation was checked by immunoblotting the whole cell lysates for phosphorylation of p38. Secondly, the whole cell lysate and TUBEs1 fractions were immunoblotted for K63 ubiquitination. Finally, a silver stain of the TUBEs1 fractions was performed. Three biological replicates were submitted for LC-MS/MS analysis. A simplified experimental flow chart is shown in Figure 5.11 A, and the quality control checks for one of the replicates is shown in Figure 5.11 B - D.

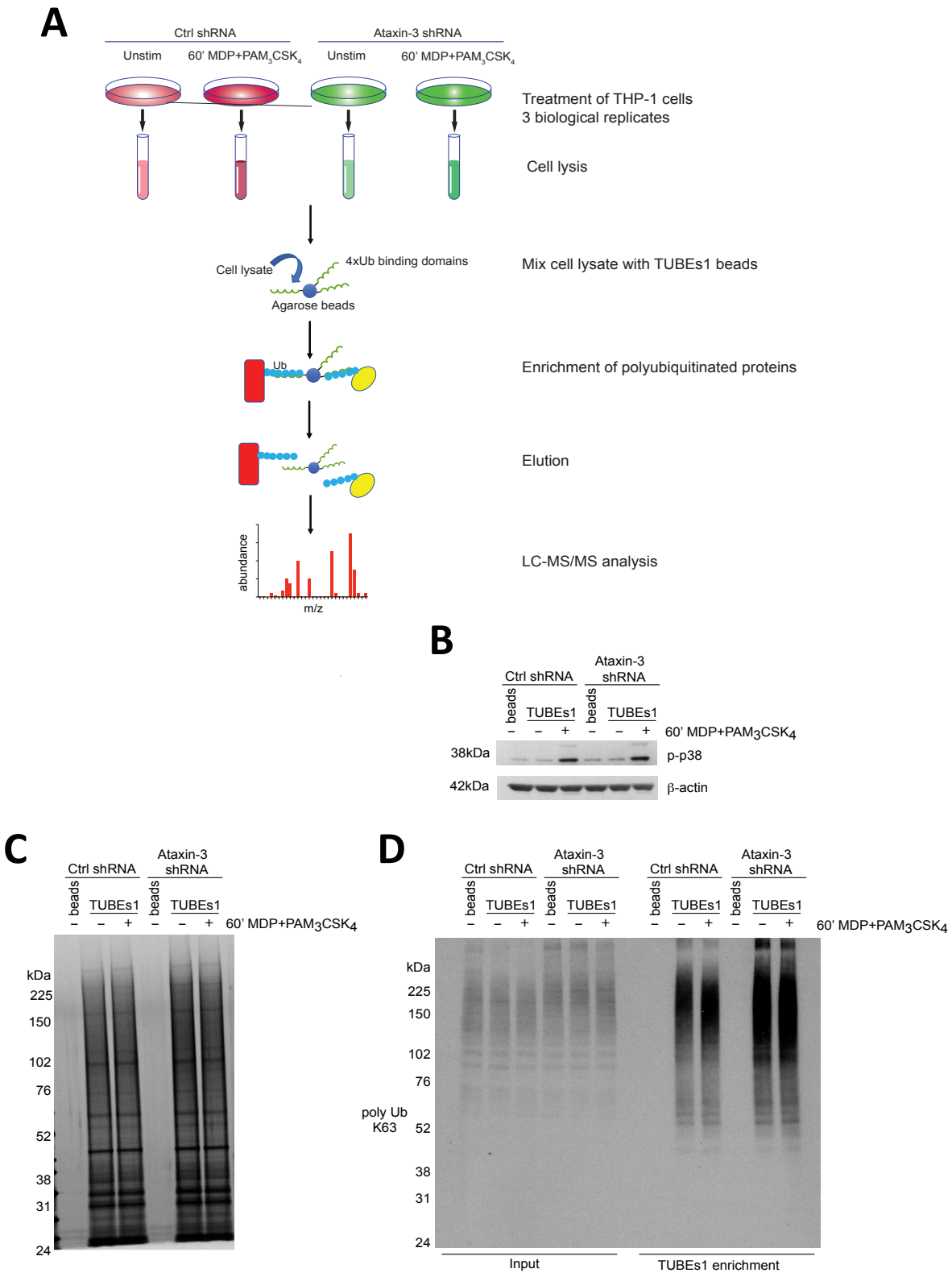


Figure 5.11 Defining the ubiquitome in ataxin-3 depleted THP-1 cells. **(A)** Flow chart showing experimental protocol. Control and ataxin-3 shRNA THP-1 cells were left unstimulated or stimulated for 60 minutes with MDP+PAM_3CSK_4 prior to ubiquitin enrichment using TUBEs1 beads. **(B)** Immunoblot of the whole cell lysates using antibodies against p-p38 and β-actin. **(C)** Silver stain of TUBEs1 enriched fractions or beads only control samples. **(D)** Immunoblot using antibody against K63 linked polyubiquitinated proteins of whole cell lysates (input) and TUBEs1 enriched fractions or beads only control samples. Representative of all 3 biological replicates. Performed in collaboration with Seiji Shiraishi.

The LC-MS/MS experiment and analysis was performed in collaboration with the Kessler Laboratory, Target Discovery Institute, University of Oxford. With an Ions score cut off of 20 and FDR of 1%, 1646 proteins were identified in all 4 conditions by LC-MS/MS. The data was normalised to all proteins identified in the samples. For each protein in each biological replicate, the relative change in protein abundance induced by any of the four conditions (unstimulated control shRNA, unstimulated ataxin-3 shRNA, MDP+PAM_3CSK_4 stimulated control shRNA, MDP+PAM_3CSK_4 stimulated ataxin-3 shRNA, corresponding to a change in ubiquitination, was determined as a change over its counterpart in a separate condition. 291 proteins were thus identified as changing significantly (ANOVA $p<0.05$) between any condition when averaged across the three biological replicates. Next, PCA was performed for these 291 proteins, confirming tight clustering of the biological replicates, and demonstrating the relative effects of ataxin-3 depletion and NOD2/TLR2 stimulation (Figure 5.12).

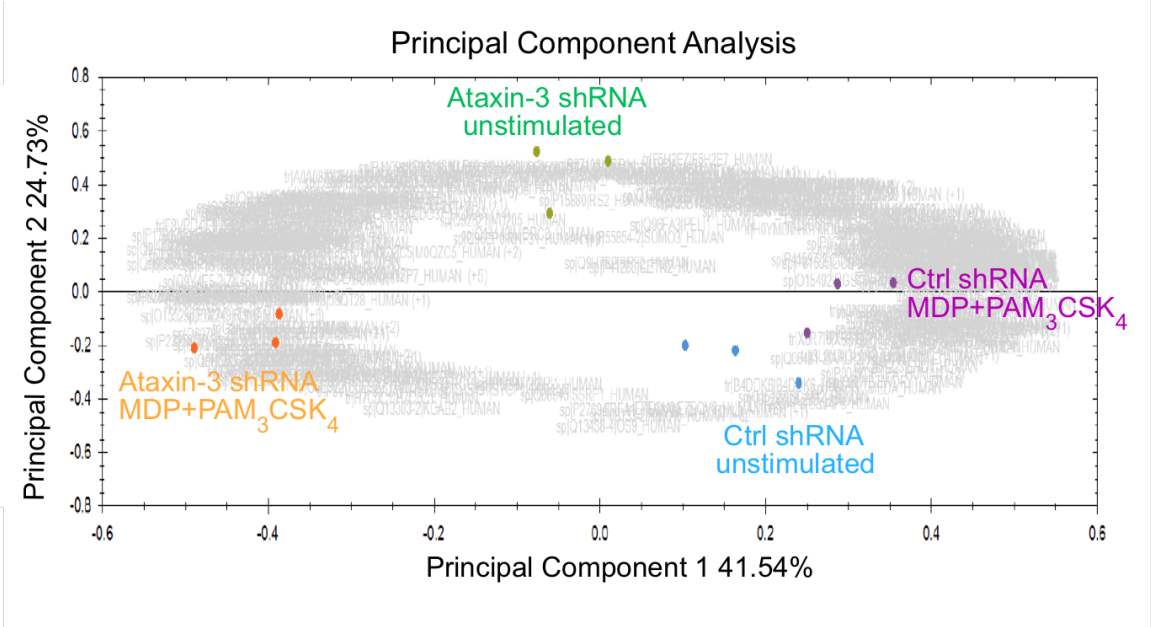


Figure 5.12 Principal Component Analysis of the 291 proteins identified as significant by ANOVA. Each dot represents a biological replicate, with the four separate colours representing the different experimental conditions.

To further refine the data, volcano plots were produced, plotting fold change in abundance on the x axis against statistical significance on the y axis. The technical success of the screen was confirmed by the volcano plot showing the effect of NOD/TLR2 stimulation in the control shRNA cells; key proteins known to be ubiquitinated upon NOD2 stimulation were found to be enriched in the TUBEs1 fraction following MDP+PAM_3CSK_4 treatment including RIPK2 (Figure 5.13 A). Next, the effect of ataxin-3 depletion alone on the ubiquitome was considered (Figure 5.13 B). As ataxin-3 acts as a DUB, ataxin-3 depletion would classically lead to an accumulation of ubiquitinated targets and thus particular attention was paid to those proteins that showed an increase in abundance in the ataxin-3 shRNA samples. However, as deubiquitination can also regulate protein stability, it is likely that a number of the proteins found to decrease in abundance on ataxin-3 depletion are also direct DUB targets of ataxin-3. Most notably, HIF1α was found to be more abundant in the ataxin-3 depleted cells, suggesting that ataxin-3 may deubiquitinate HIF1α. Table 1 in the appendix lists all proteins that showed a 2 fold or greater increase in abundance with $p<0.05$ (ataxin-3 shRNA unstimulated/control unstimulated). Finally, to specifically interrogate the importance of NOD2/TLR2 phosphorylation of ataxin-3 on DUB activity, the abundance of proteins in the ataxin-3 depleted cells was compared to the control cells following stimulation with MDP+PAM_3CSK_4. Strikingly, a cluster of proteins related to metabolism were noted in the ataxin-3 depleted cells (marked in red on Figure 5.13 C). Table 2 in the appendix lists all proteins that showed a 2 fold or greater increase in abundance with $p<0.05$ (ataxin-3 shRNA stimulated/control stimulated).

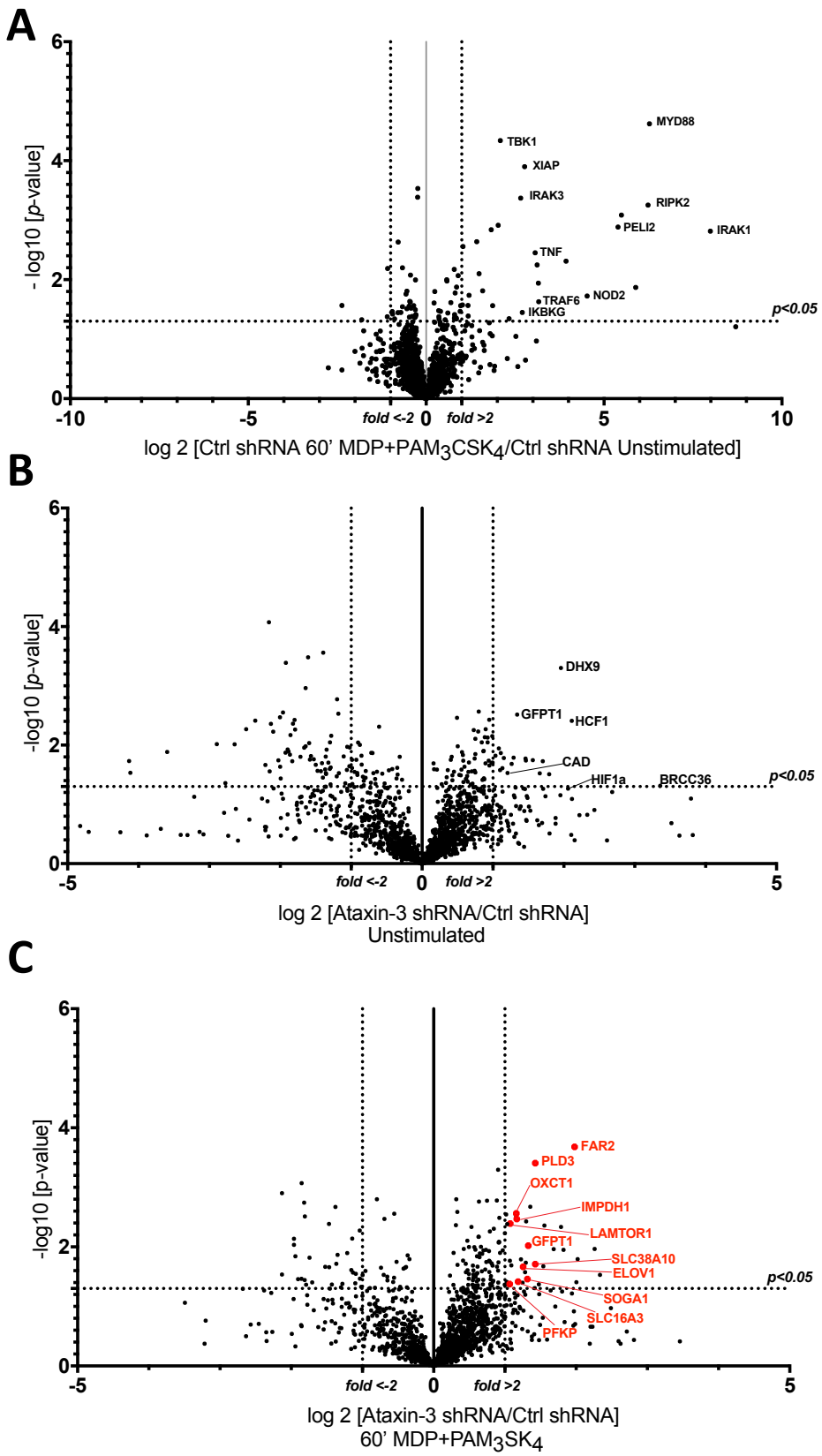


Figure 5.13 Analysis of the ubiquitome in ataxin-3 depleted THP-1 cells. Volcano plots in **(A)** Control cells following MDP+PAM_3CSK_4 stimulation, **(B)** ataxin-3 depleted cells at baseline and **(C)** ataxin-3 depleted cells following MDP+PAM_3CSK_4 stimulation with proteins related to metabolism highlighted in red. The dotted lines on the y-axes represents a p value of 0.05 (t-test), and on the x-axes represents fold change >2 or <-2.

The finding that HIF1α may be deubiquitinated by ataxin-3 was plausible, given the earlier findings in this work that ataxin-3 may behave differently in hypoxia and the apparent association between these two proteins in the MS analysis of the IP. A guided literature review, together with consideration of the abundance of the proteins which aids interrogation by methods less sensitive than MS, led to the selection of a further 4 candidates from the cluster of metabolism related proteins for validation by immunoblot. The first, phospholipase D3 (PLD3), was intriguing because it has been linked to lysosomal function[472], and mutations confer increased risk for the neurodegenerative disease Alzheimer's[473]. Ragulator complex protein LAMTOR1 forms part of the Ragulator complex essential for amino acid sensing and activation of mTORC1[474], but has also been linked to independent roles in lysosomal maturation[475] and M2 macrophage differentiation[476]. Two proteins related to fatty acid metabolism were also investigated, given the importance of this process to the immune response and mitochondrial function. One, fatty acyl-CoA reductase 2 (FAR2) is a peroxisomal protein that catalyses the reduction of fatty acyl-CoA to fatty alcohols and is required for synthesis of many phospholipids[477]. The other, elongation of very long chain fatty acids protein 1 (ELOV1/ELOVL1), catalyses the first and rate-limiting reaction of the fatty acid elongation cycle, and again is important in lipid synthesis[478].

HIF1α was validated as a DUB target of ataxin-3 in normoxia, with a significant increase in ubiquitinated HIF1α in the ataxin-3 depleted cells (Figure 5.14). HIF1a was detected in the whole cell lysates of both control and ataxin-3 depleted cells in normoxia, as the proteasome inhibitor MG132 which reduces the degradation of all ubiquitinated proteins was added to the cell suspension 30 minutes before the end of all TUBEs experiments.

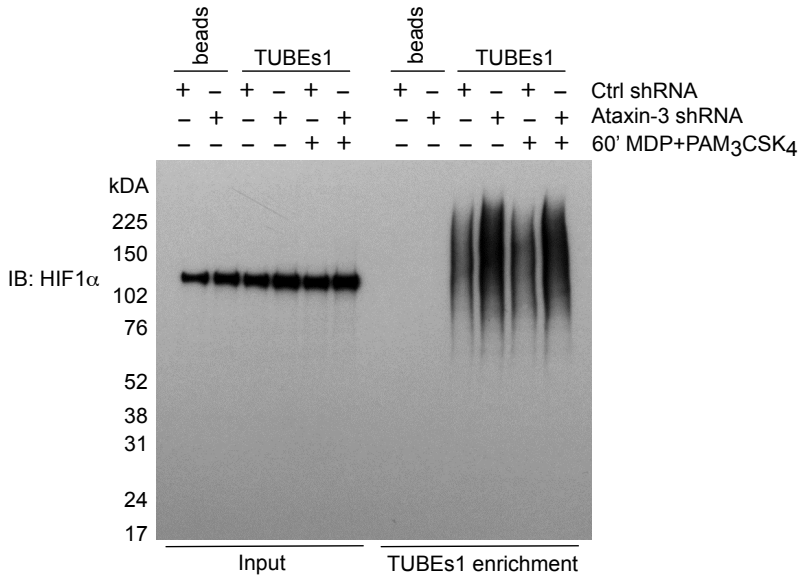


Figure 5.14 Ataxin-3 deubiquitinates HIF1α. Immunoblot using antibody against HIF1α in whole cell lysate (input) and TUBEs1 enriched fractions from control and ataxin-3 shRNA THP-1 cells left unstimulated or stimulated with 60' MDP+PAM_3CSK_4. Performed in collaboration with Seiji Shiraishi.

Next, PLD3 and LAMTOR1 were validated by immunoblot (Figure 5.15 A and B). Ataxin-3 depletion led to accumulation of ubiquitinated forms of both PLD3 and LAMTOR1, suggesting that ataxin-3 deubiquitinates these proteins. Strikingly, NOD2/TLR2 stimulation increased LAMTOR1 ubiquitination in the control cells, but there was markedly more LAMTOR1 ubiquitination in the stimulated ataxin-3 depleted cells (Figure 5.15 B). This suggests that ataxin-3 modulates the ubiquitination of LAMTOR1 induced by NOD2/TLR2 stimulation. Next, the effect of ubiquitination on total protein abundance was assessed. Ataxin-3 depleted cells were found to have more total PLD3, suggesting that ubiquitination of PLD3 increases stability (Figure 5.15 C). In keeping with the finding that NOD2/TLR2 stimulation did not affect PLD3 ubiquitination, it also had no effect on PLD3 abundance. No effect on LAMTOR1 abundance was found in response to NOD2/TLR2 stimulation and/or ataxin-3 depletion (Figure 5.15 D)

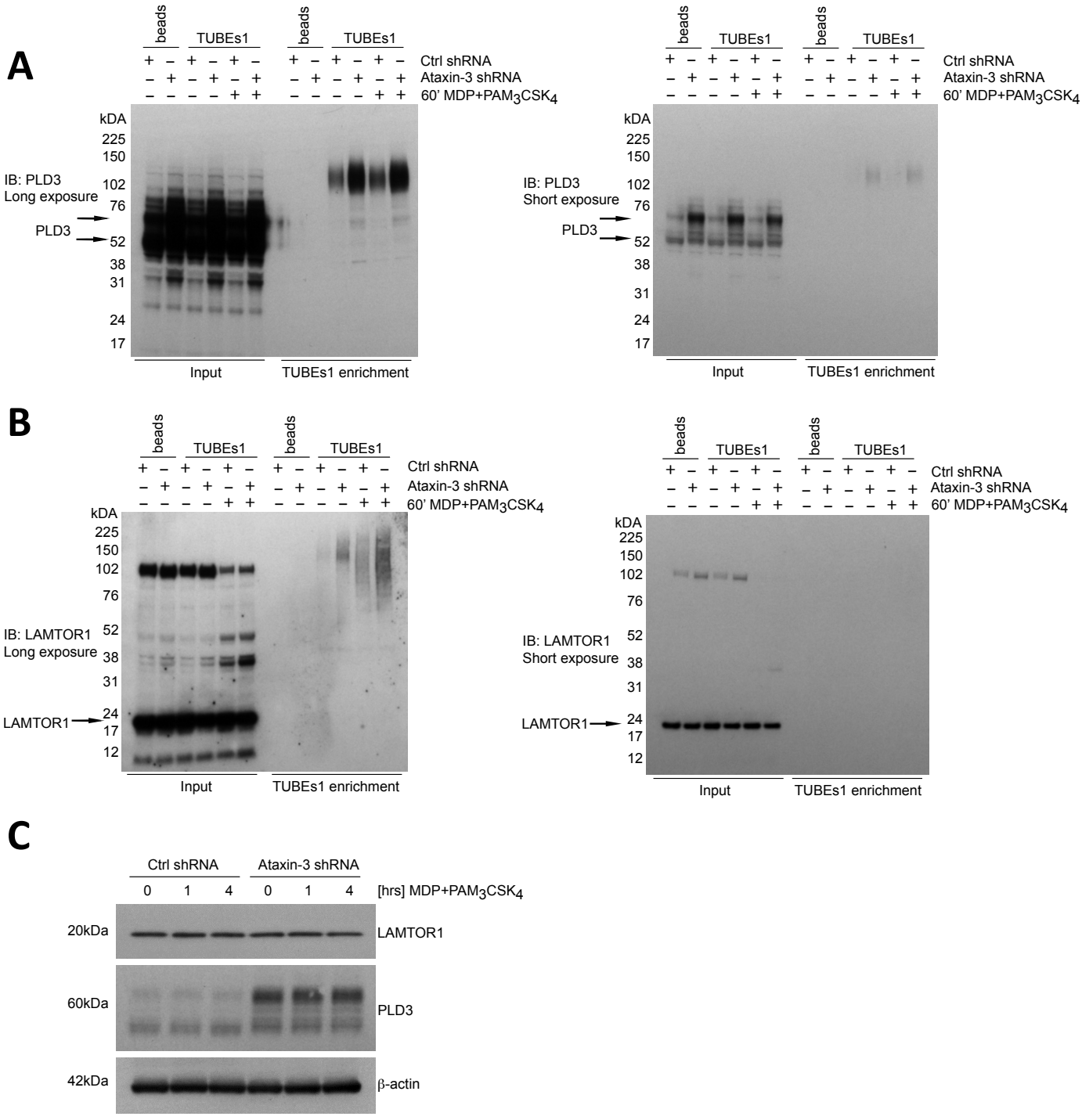


Figure 5.15 Ataxin-3 deubiquitinates PLD3 and LAMTOR1. Immunoblot using antibodies against **(A)** PLD3 and **(B)** LAMTOR1 in whole cell lysates (input) and TUBEs1 enriched fractions from control shRNA and ataxin-3 shRNA THP-1 cells left unstimulated or stimulated for 60 minutes with MDP+PAM_3CSK_4. **(C)** Immunoblot using antibodies against LAMTOR1, PLD3 and β-actin in whole cell lysates from control shRNA and ataxin-3 shRNA THP-1 cells left unstimulated or stimulated for 1 or 4 hours with MDP+PAM_3CSK_4. Performed in collaboration with Seiji Shiraishi.

Commercial antibodies against FAR2 and ELOV1 were found to detect numerous non-specific bands, and thus these two proteins could not be validated by immunoblot.

Further evidence of the direct interaction between ataxin-3 and the Ragulator complex was provided by the earlier MS data where ataxin-3 was immunoprecipitated to identify the phosphorylation site. Both LAMTOR1 and LAMTOR5 were identified in the NOD2/TLR2 stimulated sample but not in the unstimulated sample. No proteins from the Ragulator complex were identified in the original ataxin-3 IP – this may be due to differences in IP technique or digestion method. The direct interaction with LAMTOR1 could not be validated by immunoblot for endogenous LAMTOR1 following ataxin-3 IP, and therefore an overexpression system was employed in the human cell line HEK293. HA-ataxin-3 and GFP-LAMTOR1 was overexpressed, together with a GFP-control and then IP of HA-ataxin-3 performed using an antibody against the HA tag. Ataxin-3 was found to bind directly to LAMTOR1 (Figure 5.16 A). Next, the finding that LAMTOR1 is a direct DUB target of ataxin-3 was confirmed. Ubiquitin, GFP-LAMTOR1 and HA-ataxin-3 were overexpressed in HEK293 cells and IP of GFP-LAMTOR1 performed using an antibody against the GFP tag. The level of ubiquitinated GFP-LAMTOR1 was found to be significantly less in cells where HA-ataxin-3 was co-expressed (Figure 5.16 B).

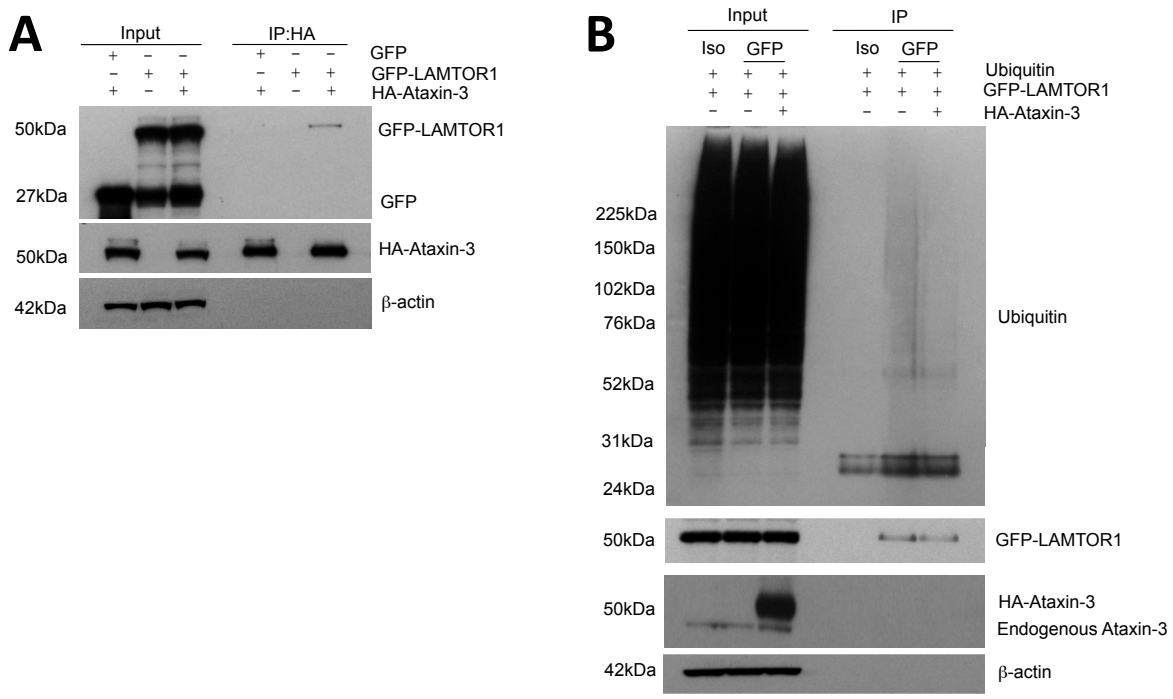


Figure 5.16 Ataxin-3 binds to and directly deubiquitinates LAMTOR-1. (A) Immunoblot using antibodies against GFP, HA and β-actin in input and HA-immunoprecipitated lysates, in HEK293 cells where GFP and/or GFP-LAMTOR1 and/or HA-ataxin-3 were overexpressed. **(B)** Immunoblot using antibodies against ubiquitin, GFP, ataxin-3 and b-actin in input and isotype control (iso) or GFP-immunoprecipitated lysates where Ubiquitin and GFP-LAMTOR1 were overexpressed with or without HA-ataxin-3. Performed in collaboration with Seiji Shiraishi.

Attention was next turned to the functional relevance of the finding that ataxin-3 may regulate protein levels of PLD3 through deubiquitination. PLD3 is a poorly characterised member of the PLD superfamily. The best described function of this family, through investigation of the isoforms PLD1 and PLD2, is the hydrolysis of phosphatidylcholine to produce choline and the second messenger signalling lipid phosphatidic acid (PA)[479]. While PLD3 also contains two phosphodiesterase domains which include the catalytically essential HKD motif[480], the enzymatic activity of PLD3 has not been definitively established. Given the importance of PLD generated PA in autophagosome formation and autophagolysosome fusion[481, 482], and described roles in the regulation of macrophage inflammatory response[483],

the effect of ataxin-3 depletion on cellular PA levels was explored. Total phosphatidic acid was purified from THP-1 cell lysates using chloroform-methanol extraction, and quantified by a coupled enzymatic reaction system. Notably the assay measures both phosphatidic acid and lysophosphatidic acid, the latter is produced by hydrolysis of phosphatidic acid, or by separate pathways involving autotaxin or lypophospholipase D[484]. Ataxin-3 depletion led to significantly less total phosphatidic acid (Figure 5.17).

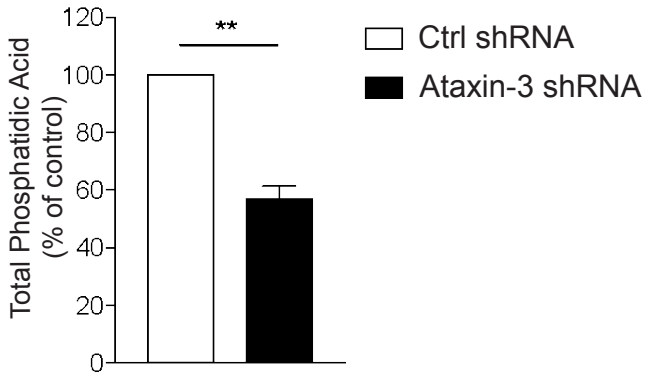


Figure 5.17 Ataxin-3 depletion is associated with reduced total phosphatidic acid levels. Quantification of total phosphatidic acid levels in ataxin-3 and control shRNA THP-1 cells. n=3, student's paired t test **p<0.01

It might be expected that the elevated levels of PLD3 seen in ataxin-3 depleted cells would enhance the production of phosphatidic acid, but it is possible that the ubiquitination of PLD3 also inhibits its enzymatic activity and hence reduced production of phosphatidic acid is seen. The role of PLD3 in phosphatidic acid production remains to be clarified, but this finding suggests it may be important.

5.3.4 Investigation of the functional importance of ataxin-3 in a knockout mouse model

Finally, the role of ataxin-3 was examined in a knockout mouse model. As the predominant functional findings in human cells were seen with a macrophage phenotype, M1 and M2 macrophages were assessed. M1 and M2 macrophages were generated from frozen bone marrow cells from ataxin-3 knockout mice provided by the Paulson laboratory. Macrophages generated from frozen bone marrow cells from age and sex matched controls from the same C57Bl/6 genetic background served as a control.

First, the importance of ataxin-3 for mitochondrial respiration was investigated using the Seahorse platform in collaboration with Sumeet Pandey, Uhlig Laboratory, Translational Gastroenterology Unit, University of Oxford. Cell density and drug dosage for murine macrophages was based on published work[240]. As expected, M2 macrophages exhibited markedly higher oxidative phosphorylation than M1 macrophages (Figure 5.18 A - D). There was a trend to reduced basal respiration in the M1 macrophages, that just failed to reach statistical significance following 1 hour of MDP+PAM_3CSK_4 stimulation (Figure 5.16 E). Mitochondrial spare respiratory capacity and maximal respiration was significantly impaired in the ataxin-3 knockout M2 macrophages at baseline, with all markers of mitochondrial respiration impaired following 1 hour of MDP+PAM_3CSK_4 stimulation (Figure 5.18 F-I). Thus the findings in human cells were recapitulated in the knockout mice.

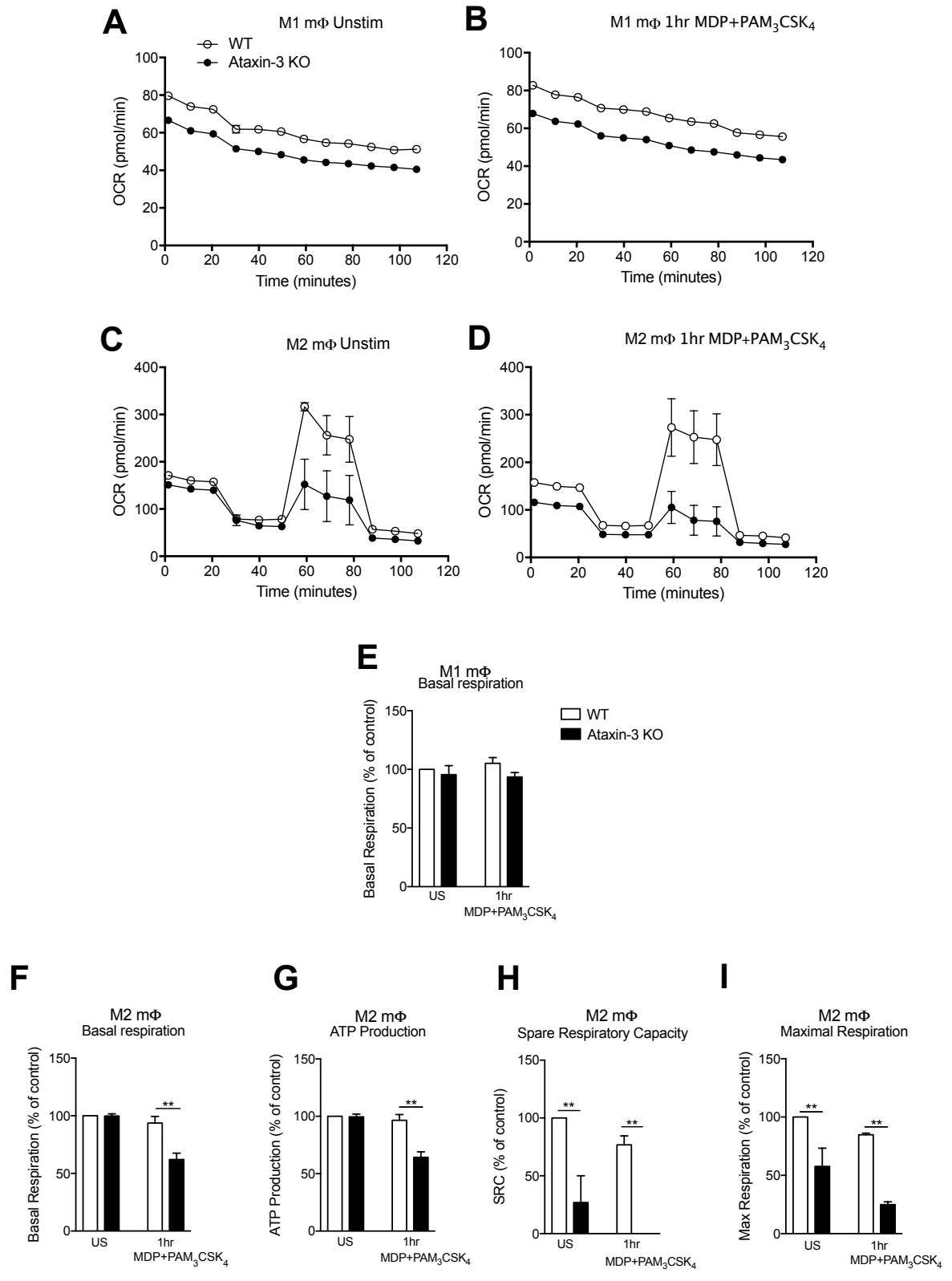


Figure 5.18 Loss of ataxin-3 impairs mitochondrial respiration in M2 macrophages. Seahorse analysis of OCR in control and ataxin-3 knockout murine macrophages. **(A-D)** Representative sequential OCR measurements of M1 and M2 macrophages at baseline and following 1hr MDP+PAM$_3$CSK$_4$. **(E-I)** Analysis of key mitochondrial respiration parameters at baseline and following 1hr MDP+PAM$_3$CSK$_4$ **(A-D)** representative of 3 independent experiments. **(E-I)** n=3, one way ANOVA **p<0.01. Performed in collaboration with Sumeet Pandey.

Next, the gentamicin survival assay was performed in collaboration with Anna Aulicino, Simmons Laboratory, Weatherall Institute of Molecular Medicine, University of Oxford. Surprisingly, no significant differences in bacterial killing of *Salmonella enterica* serovar Typhimurium were seen, despite assessing MO, M1 and M2 macrophages and also investigating the effect of serum starvation prior to infection. Attempts were made to study the protective effect of pre-stimulation with MDP or MDP+PAM_3CSK_4, which should result in enhanced bacterial killing[485]. However, this protective effect could not be reliably reproduced in the WT cells, and hence differences between the WT and KO cells could not be investigated (data not shown). Finally, given the importance of mitochondrial ROS and autophagy for inflammasome activation[261, 486], IL1β production following *S. Typhimurium* infection was studied. Preliminary data in the THP-1 model suggested that IL1β production may be impaired (data not shown). However, no consistent differences were seen in the murine model (Figure 5.19 A + B).

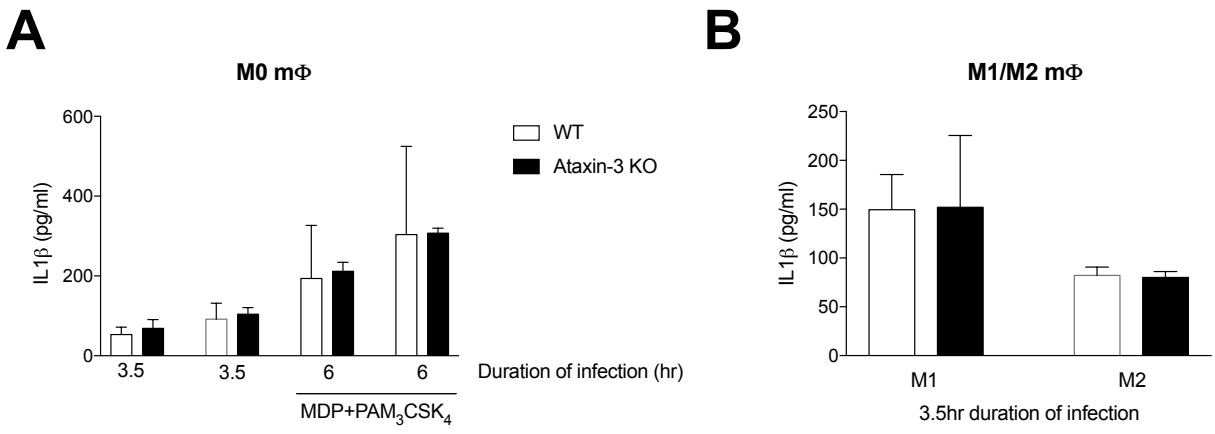


Figure 5.19 Ataxin-3 may not regulate IL1β release in murine macrophages following Salmonella infection. (A) ELISA of IL1β in the supernatants collected from M0 WT and ataxin-3 KO macrophages which were either pre-treated with 2hr MDP+PAM_3CSK_4 or left untreated prior to 3.5 or 6hr infection with *Salmonella enterica* serovar Typhimurium. **(B)** ELISA of IL1β in the supernatants collected from M1 and M2 WT and ataxin-3 KO macrophages following 3.5hr infection with *Salmonella enterica* serovar Typhimurium. n=2. Performed in collaboration with Anna Aulicino.

5.4 Discussion

Work in this chapter has begun to unravel the functional importance of ataxin-3 in immune cells. The link between ataxin-3 and the mitochondria first described in chapter 4 was shown to be functionally relevant, with ataxin-3 depleted cells showing dysregulation of mRNA transcripts of Complex I, impaired oxphos and reduced mROS generation. Given the previously discussed requirement for MIC60 for both transcription of the mitochondrial genome and oxphos, it is likely that ataxin-3's role at the mitochondria is linked to MIC60. However, it does not appear that MIC60 is a direct DUB target of ataxin-3, as the abundance of ubiquitinated MIC60 was unchanged in the ataxin-3 depleted cells in the MS screen of the ubiquitome. It is however important to formally confirm this. It seems plausible that ataxin-3 may instead form a complex with MIC60, which anchors ataxin-3 to bring it in close proximity with a separate substrate. Indeed, this mechanism of DUB anchoring to non-substrate proteins has been proposed as a general mechanism whereby DUBs can function at the mitochondria[487].

An unbiased screen of the ubiquitome in ataxin-3 depleted THP-1 cells has shed new light on the multiple DUB targets of ataxin-3. Remarkably, a preponderance of metabolism related proteins was found, further reinforcing the potential importance of ataxin-3 in cellular metabolism. Intriguingly, Ataxin-3 was shown to deubiquitinate HIF1α. It is known that K63 linked ubiquitin chain formation, mediated by the ubiquitin ligase CHIP/STUB1, results in chaperone-mediated autophagy of HIF1α [203], and ataxin-3 may regulate or counter this process. Indeed, ataxin-3 is already known to be a functional partner of CHIP, acting both to limit the length of chains attached to CHIP substrates and eventually terminate the ligase activity by deubiquitinating CHIP itself[309]. This link to HIF1α helps to

explain why ataxin-3 phosphorylation may be differentially regulated in hypoxia. A further noteworthy finding was the discovery that ataxin-3 may deubiquitinate CAD protein (carbamoyl-phosphate synthetase 2, aspartase transcarbamylase and dihydroorotase), which was identified with high confidence (MASCOT score 419.47). This protein, involved in the first three steps of pyrimidine biosynthesis[488], is known to be a negative regulator of NOD2[489], although the functional importance of deubiquitination is unknown.

LAMTOR1 was found to be a further novel DUB target of ataxin-3. Further, ataxin-3 appears to regulate the NOD2/TLR2 mediated ubiquitination of LAMTOR1. LAMTOR1, also known as p18, is a late endosome/lysosome membrane adapter protein that localises to the lipid rafts of these organelles[490, 491]. LAMTOR1 plays an essential role in the activation of the mTORC kinase complex in response to amino acid levels[474]. Through a mechanism involving the lysosomal v-ATPase in the presence of amino acid sufficiency, LAMTOR1 forms a scaffold at the lysosomal membrane with LAMTOR2,3,4 and 5 (the pentameric Ragulator complex) for the Rag GTPase complex (RagAB/CD)[474, 492, 493]. This leads to the recruitment and activation of mTORC1 which inhibits autophagy. The lysosomal v-ATPase-Ragulator complex also activates another critical metabolic sensor, AMP-activated protein kinase (AMPK), which responds to falling energy levels by driving cellular catabolism programmes and downregulating anabolic pathways[494]. Thus this complex is able to respond to both energy/nutrient sufficiency and deficiency. A further intriguing link between NOD2/TLR2, ataxin-3 and the Ragulator complex was provided by further analysis of MS data from the IP of ataxin-3, which suggested that ataxin-3 may also associate with LAMTOR5 on NOD2/TLR2 triggering, but this must be validated.

Strikingly, of all cells, macrophages express the highest levels of the five Ragulator components, suggesting their importance in the immune response[400]. Indeed, LAMTOR1 was recently found to be essential for the polarisation of M2 macrophages both *in vitro* and *in vivo* in a knockout mouse model, by coupling metabolism to immunity[476]. LAMTOR1, the lysosomal v-ATPase and mTORC1 respond to both extrinsic IL-4 and intracellular amino acid levels to regulate the production of 25-hydroxycholesterol and downstream activation of the transcription factor liver X receptor to drive M2 polarisation[476]. Finally, the Ragulator complex can also function independently of mTORC1 to regulate lysosomal function and phagocytic flux[495]. This separate role was demonstrated in microglia, with deficiency of LAMTOR4 and RagA leading to an accumulation of neuronal debris and aggregates, suggesting a potential importance in neurodegenerative diseases[495]. Although LAMTOR1 has been reported in multiple screens of ubiquitinated proteins, the functional relevance of ubiquitination has never been described[344]. Four sites of Ub have been described, but by far the most common is K20[344]. Little however is known about the structure of LAMTOR1, making further analysis of the relevance of the sites challenging. The precise downstream consequences of the NOD2/ataxin-3/LAMTOR1 signalling axis remain to be determined, but it is plausible that it mediates lysosomal degradation of autophagosomes, given the autophagy block seen in ataxin-3 depleted cells. It will also be important to explore the differentiation of ataxin-3 knockout M2 macrophages. Indeed, impaired differentiation could partly explain the observed oxphos impairment, although mitochondrial dysregulation in ataxin-3 depleted cells was also observed in dendritic cells and monocytes.

PLD3 was found to be another metabolism related DUB target of ataxin-3, and intriguingly has also been linked to lysosomal function. PLD3 is a type 2 transmembrane protein

predominantly located in the ER, where it is anchored by an N-terminus sequence that spans the ER membrane[496]. While PLD3 possesses a short cytoplasmic sequence, the important HKD catalytic domain is localised within the ER. Despite containing the two HKD catalytic motifs that are essential for the enzymatic activity of the superfamily, it lacks the PX and PH domains found in PLD1 and PLD2 that are thought to regulate subcellular location and binding to phosphatidylinositol phosphates[496]. Importantly, PLD3 has been reported to co-localise with endosomes and lysosomes[472, 497]. While loss of PLD3 was recently shown to alter lysosomal morphology both *in vitro* and *in vivo* in a knockout mouse model, its precise role at this organelle remains unclear[472].

PLD3 has been identified in a number of screens of the ubiquitome, with four putative ubiquitination sites proposed[344]. One, K11, resides in the short cytoplasmic sequence and it has been hypothesised that ubiquitination may allow sorting of PLD3 to endosomes[496]. The functional importance of this site is suggested by the finding that a PLD3 SNP that may increase risk for late onset AD is located in close proximity (M6R), which could affect ubiquitination[473, 496]. PLD3 was also identified as a potential target of the FBXO6 ubiquitin ligase complex which triggers ER associated degradation[498], with K309 suggested as the possible site of ubiquitination, as it resides in the ER lumen[496]. Given the known association of ataxin-3 with ERAD[308], it is therefore possible that ataxin-3 counteracts ERAD of PLD3 by deubiquitinating it. This would not however be consistent with the finding in this work that ataxin-3 depletion increases PLD3 protein levels. The discovery of reduced phosphatidic acid levels in the ataxin-3 depleted cells was also puzzling given an increase in PLD3 protein. Although the enzymatic target of PLD3 is still unknown, if it functions similarly to PLD1 and 2 then one might expect increased production of phosphatidic acid. However, it is possible

that ubiquitination of PLD3 also directly affects enzymatic activity, explaining this apparent contradiction. Alterations in phosphatidic acid levels would certainly provide a further explanation for the defective autophagic flux seen in ataxin-3 depleted cells, in addition to the direct and as yet unexplained lysosomal role of PLD3.

Work using macrophages from the ataxin-3 KO mouse confirmed the mitochondrial phenotype, but surprisingly failed to recapitulate the defect in bacterial killing. This could be for a variety of reasons. Firstly, the immune response of the mouse differs in important ways from the human[499, 500]. One important example in xenophagy is the TBK1 adapter NDP52, which has a quite different structure in mice and lacks the domain required for binding to ubiquitinated bacteria[95], suggesting a divergent role in this species. It is noteworthy that mice lack the S265 residue of ataxin-3 conserved in many other mammals, although it appears other neighbouring serine residues may perform a similar role. Secondly although the LT2 strain of *S. Typhimurium* tested in both the human and mouse work is widely used in mouse models, there are important differences in virulence between mice and humans. Thus it would be important to test bacterial killing of both other Salmonella strains and other species. Ongoing work is exploring the *in vivo* relevance of ataxin-3 through a peptidoglycan challenge in ataxin-3 KO mouse. Mice will be assessed for severity of sepsis, and then cytokine responses analysed in the serum.

6 Concluding Discussion

6.1 Introduction

The physiological importance of NOD2 in both the innate and adaptive immune response is well established, and mutations confer the greatest single genetic risk factor for Crohn's disease[30, 31], yet significant gaps remain in our knowledge of how this receptor exerts its effects. Notably although NOD2 typically functions in a hypoxic inflammatory milieu, almost nothing is known about how this might alter downstream signalling pathways and mechanism of action. Work in this study first sought to map signalling of NOD2, and its synergistic PRR partner TLR2, in hypoxia through quantitative phosphoproteomics. A cluster of proteins with no previous links to immunity, but associated with a spectrum of neurodegenerative diseases, were found to be differentially phosphorylated on NOD2/TLR2 stimulation in hypoxia. One of these proteins, the deubiquitinase ataxin-3, was selected for further study. It was found to be phosphorylated on S265 upon activation of NOD2, through a signalling cascade involving RIPK2 and TBK1. Immunoprecipitation and MS analysis of interacting partners established a novel link to the mitochondria, and a core component of the MICOS complex MIC60. Ataxin-3 was subsequently found to be important for mitochondrial respiration and mitochondrial ROS generation. The role of ataxin-3 in xenophagy was also explored, with a role for autophagic flux determined. Ataxin-3 depleted human cells, but not knockout mouse macrophages, were found to have defects in bacterial killing of *S. Typhimurium*. Finally, to dissect the DUB role of ataxin-3 in an immune context, an unbiased analysis of the ubiquitome was performed in ataxin-3 depleted monocytes at both baseline, and following NOD2/TLR2 stimulation. A preponderance of metabolism related proteins were discovered including HIF1α, phospholipase D3 and

LAMTOR1, underlining the role of ataxin-3 in immunometabolism, and helping to decipher the diverse mechanisms of action of this enigmatic protein in innate immunity.

6.2 Dissection of NOD2 signalling in hypoxia

With NOD2 previously little studied in hypoxia, the first part of this thesis described a preliminary investigation of NOD2 signalling in this physiologically relevant condition. It was found that NOD2 mediated mRNA expression of the cytokines IL8 and IL1β, and the downstream target of HIF1α, VEGF, are enhanced in hypoxia. This supported the initial hypothesis that hypoxia may lead to functionally relevant changes in NOD2 signalling, almost certainly driven by the master hypoxia regulator HIF1α. The finding that NOD2 signals to the key regulator of angiogenesis VEGF is particularly intriguing, given the potential importance of VEGF mediated microvascular dysfunction in Crohn's disease[501, 502]. Changes in microvascular density and leucocyte adhesion, correlating with VEGF expression, have been demonstrated in the intestinal tissue of patients with CD[502, 503], and it is plausible that this process may be dysregulated in the presence of NOD2 mutations. Next, quantitative phosphoproteomics were used to map the downstream signalling cascade from NOD2 in human moDCs in both normoxia and hypoxia. As only 10% of a cell's protein mass is phosphorylated at any time, phosphoprotein purification columns were used to enrich the phosphoproteome, reducing the complexity and increasing the sensitivity of downstream analysis. Shotgun proteomics was then undertaken, whereby digested phosphoenriched peptide mixtures were analysed by LC-MS/MS. The significant recent advances in instrument sensitivity and computational analysis allowed accurate quantification of phosphorylation changes in individual proteins to be performed without the need for labelling[343]. This high-throughput approach was technically successful, and led to the

identification of hundreds of proteins differentially phosphorylated by NOD2/TLR2 stimulation in normoxia and hypoxia. Importantly, hypoxia alone exerted a significant effect on the phosphorylation status of 98 proteins, with approximately two thirds not previously known to be hypoxia-regulated. This provides a potentially useful resource for further study. As expected, the phosphorylation status of many proteins (126/259) significantly regulated by NOD2/TLR2 was similar in both normoxia and hypoxia, but over one third (96/259) were altered in hypoxia alone, supporting the rationale for this experimental approach. Secondary validation revealed a caveat of the highly sensitive MS analysis of the phosphoproteome, namely that validation of identified proteins by methods such as immunoblot may struggle to demonstrate changes in low abundance proteins, and is highly dependent on the quality of available antibodies or other reagents. Further, this specific method of quantitative phosphoproteomic analysis does not map phosphorylation sites; however validation using phosphoprotein enriched fractions circumvented this issue by allowing the use of antibodies directed against the whole protein. A number of proteins not previously linked to NOD2 signalling, or in many cases to the immune response, were successfully validated. The majority of these apparently diverse proteins are associated with neurodegenerative diseases, the first of many such links in this work. A targeted secondary screen was undertaken, assessing the effect of individual knockdown of the proteins ataxin-3, aprataxin, DYNLT3 and BTAF1 on NOD2 mediated cytokine mRNA expression, with no significant differences found. However, a more extensive functional screen, which could not be undertaken in this work due to time constraints, may well reveal the importance of aprataxin, DYNLT3 and BTAF1 in innate immunity. While these proteins, together with LRBA and HDAC6 which could not be included in the targeted secondary

screen due to technical restrictions, represent enticing opportunities for further study, ataxin-3 was selected for further investigation.

6.3 Defining the signalling cascade and phosphorylation site of ataxin-3

Stimulation of a range of PRRs in addition to NOD2 (TLR2, TLR4 and TLR7/8) induced the phosphorylation of ataxin-3, suggesting that it is a broadly conserved signalling pathway in response to both viral and bacterial pathogens. However, the synergistic action of NOD2/TLR2 produced the most striking phosphorylation in both primary human moDCs and the human THP-1 cell line, suggesting ataxin-3 may be particularly relevant to this signalling cascade. While the requirement for RIPK2 and TBK1 was demonstrated for both NOD2 and synergistic NOD2/TLR2 mediated phosphorylation of ataxin-3, the upstream signalling cascade for TLR2 appeared separate and presumably involves a MyD88 dependent pathway. Mapping the precise phosphorylation site to S265 provided insight into its potential functional relevance. This residue lies just outside the second UIM, suggesting that modification may alter binding to ubiquitinated substrates, and thus regulate substrate specificity. Indeed, phosphorylation is known to regulate the deubiquitinating activity of a range of DUBs, including A20, USP7, USP8, USP10, USP16, USP25, USP28, USP44, and CYLD[504]. Ongoing work is examining the importance of S265 for the DUB function of ataxin-3, using a phosphomutant construct transfected into cell lines. While phosphorylation at separate residues is known to regulate nuclear translocation of ataxin-3[292], no evidence was found in this work for S265 performing this role. Confocal microscopy using overexpression of both the wild type S265 and A265 phosphomutant in HEK293 cells has also been undertaken, but both GFP and HA constructs led to diffuse non-specific staining and thus meaningful conclusions could not be drawn.

6.4 The interacting partners of ataxin-3

Two separate MS proteomic screens were undertaken to determine novel interacting partners of ataxin-3. The first, following an immunoprecipitation of ataxin-3, provided initial evidence of the potential importance of ataxin-3 in immunometabolism, through a link to the mitochondria. It remains to be clarified whether MIC60 simply provides a scaffold for ataxin-3 to act as the mitochondria, or whether the functions of MIC60 and perhaps the MICOS complex are regulated by ataxin-3. It is certainly plausible that some of the previously described mitochondrial functions of MIC60[436, 441], that show remarkable similarity with those of ataxin-3, could result from the loss of an ataxin-3 complex. However, the upregulation of specific mtDNA transcripts in ataxin-3 depleted cells contrasts with the more general downregulation of mtDNA transcripts described in MIC60 depleted cells, suggesting they may have separate roles[441]. Importantly, no change in mitochondrial copy number was found in ataxin-3 depleted cells, suggesting that biogenesis is unaffected. It is possible that the upregulation of mtDNA transcripts represents an attempt to compensate for impaired mitochondrial respiration, although the apparent specificity for transcripts of only certain mtDNA encoded oxphos complexes might argue against this.

The second screen addressed the specific DUB targets of ataxin-3, having established that ataxin-3 depletion in a THP-1 model system led to a remarkable increase in ubiquitinated substrates in pilot experiments. As with the phosphoproteomic approach, an unlabelled method was undertaken, avoiding any potential interference with cellular processes that might lead to artefact[505]. The master hypoxia regulator, HIF1α was found to be a novel DUB target of ataxin-3. The discovery in this work that NOD2/TLR2 mediated phosphorylation of ataxin-3 is reduced in hypoxia, taken together with the independent screen that suggests

downregulation of ataxin-3 mRNA expression in hypoxic lung tissue[397], imply that ataxin-3 activity is inhibited in hypoxia. This hypothesis is further supported by the finding that the dysregulation of Complex I mtDNA transcripts in ataxin-3 depleted moDCS is abrogated in hypoxia. More work is needed to compare the effect of ataxin-3 DUB activity on HIF1α in both normoxia and hypoxia, but it may be that ataxin-3 acts in normoxia to modulate HIF1α levels, with this regulatory effect inhibited in hypoxia. Overall, it is likely that ataxin-3 harnesses the known roles of HIF1α in metabolic reprogramming as part of an apparent broad regulation of metabolism. Indeed, it appears this wide-ranging metabolic role is central to ataxin-3's innate immune function, with a striking preponderance of metabolism related DUB targets found on NOD2/TLR2 stimulation.

6.5 The immune function of ataxin-3

Work in this thesis has demonstrated the importance of ataxin-3 in mitochondrial oxidative phosphorylation in both the human THP-1 cell line and murine bone marrow derived macrophages. A particularly striking impairment was found in maximal respiration and spare respiratory capacity (SRC). SRC represents the extra mitochondrial capacity available within a cell to produce energy under conditions of increased work or stress and is important for cellular function and survival[238, 506, 507]. Macrophages increase their SRC in response to bacterial infection to drive anti-microbial responses, and this is coordinated in part by modulation of the ETC Complexes I and II[253]. In M2 macrophages, SRC is critical for their activation and prolonged survival, and clearance of the parasitic helminth[235]. It was found in the present work that ataxin-3 depletion impaired mROS production at both baseline and in response to NOD2/TLR2 stimulation, demonstrating the functional relevance of the observed mitochondrial respiratory impairment. Given the emerging associations

between autophagic flux, lysosomal function and mitochondrial respiration[465, 466, 467, 468], it seems plausible that this mitochondrial phenotype may also contribute to the described defects in autophagic flux.

The newly described role for ataxin-3 in beclin1 mediated starvation induced autophagy has intriguing implications for the autophagy defect found in this thesis[330]. In contrast to this recent research paper which was performed in non-immune cells, beclin1 levels did not appear reduced in ataxin-3 depleted THP-1 cells, despite the known importance of beclin1 in TLR driven autophagy[508, 509]. Further, enhanced accumulation of LC3 was seen on NOD2/TLR2 stimulation, together with reduced LAMP1 levels, suggesting a defect in autophagic flux rather than initiation of autophagy. More work is needed to unravel the precise cause of the observed defect in autophagic flux, but further data from the ubiquitome screen supports a lysosomal cause. Specifically, two proteins that localise to the lysosome, PLD3 and LAMTOR1, were found to be novel DUB targets of ataxin-3. The recent discovery that PLD3 affects the morphology of the lysosomal system underlines its potential importance in regulating this organelle although its specific role remains unclear[472]. While LAMTOR1 plays important roles in regulating mTORC1, no clear differences in phosphorylation of S6 or ULK1, two important marker of mTOR activity were found in this thesis or in further work by Seiji Shiraishi (personal communication). It is therefore plausible that it acts here in an mTOR independent pathway to regulate lysosomal function, as has been described for other components of the ragulator complex in microglia[495]. Ongoing work will confirm or refute these hypotheses.

Finally, the direct consequences of the ataxin-3 mediated deubiquitination of diverse metabolism related proteins found through the ubiquitome screen remain to be explored. Metabolomics, which can be used to quantitatively profile the metabolic pathways of cells, provides a powerful method to further define the role of ataxin-3 in shaping cellular metabolism[510], and could be undertaken in ataxin-3 depleted human or mouse monocytes/macrophages.

6.6 Wider implications – the links to neurodegeneration

The recurring association with neurodegenerative diseases arising within this work merits further discussion. The first evidence for an innate inflammatory response in neurodegeneration was described over 20 years ago in Alzheimer's disease, and now extends to a diverse range of diseases including Parkinson's disease, amyotrophic lateral sclerosis, multiple sclerosis and frontotemporal dementia[511]. Interest in the burgeoning field of neuroinflammation is pertinent, given the huge socioeconomic costs of neurodegenerative diseases, with the annual cost of dementia care alone expected to reach $1 trillion over the next 15 years[512].

Microglia represent the key innate immune cell of the central nervous system, and are distributed in varying densities throughout the brain. Importantly, their basal activity is critical for normal brain functioning as they maintain tissue homeostasis through the removal of debris, and act to continually remodel neurones and synapses to ensure optimal neuronal network function[513]. They possess a range of TLRs including NOD2, and thus are equipped to respond to varied immune activators, including both DAMPs and PAMPs. Recent evidence suggests that as macrophages, microglia can assume both an M1 and M2-

like phenotype[514]. Activation of M1-like microglia leads to the production of ROS and pro-inflammatory cytokines such as IL1β, whereas M2-like microglia secrete neurotrophic factors and proteases and IL-4, and show enhanced phagocytic activity to clear cellular debris[513, 514]. It is proposed that skewing of this phenotype can either promote clearance of toxic cellular debris and resolution of inflammation, or lead to chronic neuroinflammation[513]. Indeed, exposure of microglia to LPS inhibits phagocytosis of amyloid, with amyloid accumulation a hallmark of many neurodegenerative conditions[515, 516]. Importantly, a range of other cells in the brain including astrocytes and neurones also express PRRs, while yet more express receptors for cytokines and other inflammatory mediators, suggesting a broad immune activation can occur[513]. It has been proposed that sustained inflammatory responses may result from positive feedback loops between these cells, potentially leading to ongoing immune activation that becomes independent of the original trigger[511]. Dysregulation of autophagy, which may be modulated by PRRs, also appears central to many neurodegenerative conditions, through the accumulation of both neurotoxic protein aggregates and dysfunctional mitochondria[517].

While direct CNS infections with a variety of pathogens have been proposed as a potential precipitant of neurodegeneration[513, 518, 519, 520], it is much more likely that CNS immune activation is triggered by local DAMPs, or from PAMPs that may both impair and cross the blood-brain barrier from the periphery. Indeed, a striking deterioration in cognitive function in patients with Alzheimer's is frequently observed during peripheral infections[512], and the neuroinflammatory properties of peripherally administered LPS are well described in murine models[521]. Further, peripheral infections have also been suggested as a precipitant for the relapses seen in multiple sclerosis[522]. DAMPs including misfolded and aggregated proteins

are also found in the brains of patients with neurodegeneration[513], while mitochondrial dysfunction, which is a common finding in neurodegeneration, may lead to the release of mitochondrial DAMPs[523].

In the case of spinocerebellar ataxia type 3, the neurodegenerative disease that results from mutations in ataxin-3, increased expression of pro-inflammatory cytokines together with reactive astrocytes and activated microglia have been described in brain sections from patients[402, 403,524]. It is plausible that as in bone marrow derived macrophages, dysregulation of ataxin-3 in microglia results in both mitochondrial dysfunction and a broader skewed immunometabolic phenotype that contributes to the neuroinflammation seen in the disease. Further, the potential importance of impaired PRR triggered autophagy in the disease process is supported by the recent discovery that the wild type polyglutamine tract is required for beclin1 mediated starvation induced autophagy, suggesting a broad role for ataxin-3 in autophagy that may be lost with the polyglutamine expansion[330]. Clearly it would be important to determine what effect the polyglutamine expansion has on microglial function to further explore this hypothesis.

A final intriguing observation is the association between metabolic dysregulation and numerous, apparently functionally diverse proteins that all result in the phenotypically similar family of spinocerebellar ataxias, including aprataxin, ataxin-2, ataxin-10 and now ataxin-3[371, 525, 526, 527]. Aprataxin, ataxin-2 and ataxin-3 mutations or depletion all result in mitochondrial dysfunction, while global proteomic and metabolomic profiling of ataxin-2 knockout mice suggested broader metabolic effects on both amino acid and fatty acid metabolism, and the TCA cycle[527]. It was recently shown that mitochondrial disease

frequently results in cerebellar ataxia, although the reason for the apparent predilection for this area of the brain remains unclear[528].

6.8 Closing remarks and future experiments

This work provides the first evidence of a new role for the deubiquitinase ataxin-3 in innate immunity. Unbiased proteomic approaches have proven central both to the initial identification of this protein, and to the subsequent interrogation of interacting partners and function. Present at the interface of immune and metabolic responses, ataxin-3 both modulates global adapters such as HIF1α, and regulates more specific metabolic pathways. Returning to an original question of this thesis, how might this be relevant for loss of function Crohn's disease associated NOD2 mutations? It is highly likely that the inability of these NOD2 SNPs to respond to MDP results in a loss of ataxin-3 phosphorylation, leading to dysregulation of a variety of processes implicated in Crohn's, including autophagy and mitochondrial function[79, 281]. The association with HIF1α is also pertinent, given the current interest in this protein as a therapeutic target in inflammatory bowel disease[215].

To take this work forward there are a number of important avenues that should be pursued. Firstly, the precise mechanism by which ataxin-3 modulates mitochondrial respiration remains to be elucidated. Although it is evident that ataxin-3 localises with the mitochondrial protein MIC60, the importance of this protein for the role of ataxin-3 in oxphos should be established. This could be addressed through knockdown and overexpression experiments assessing the relative contributions of both MIC60 and ataxin-3. It must also be clarified whether MIC60 is a direct DUB target, or whether it forms part of a scaffold allowing ataxin-3 to perform functions required for mitochondrial respiration.

Secondly, does the NOD2 mediated phosphorylation of ataxin-3 at S265 serve to regulate its deubiquitinating activity? Use of wildtype and phosphomutant constructs introduced into ataxin-3 knockout cell systems could be utilised to answer this question. Specifically, the importance of this serine residue for the deubiquitination of LAMTOR1, which appears driven by NOD2/TLR2 stimulation, should be assessed.

Thirdly, what is the functional consequence of NOD2/TLR2 triggered LAMTOR1 deubiquitination by ataxin-3? Preliminary work has suggested that in this context LAMTOR1 is acting in an mTOR independent pathway, but this must be confirmed by assessing markers of mTOR activation in ataxin-3 depleted cells. It is plausible that LAMTOR1 is regulating lysosomal function, which may be impaired in ataxin-3 depleted cells, with further experiments required to confirm or refute this hypothesis.

Fourthly, the functional relevance of the deubiquitination of other novel targets by ataxin-3, including HIF1α and PLD3 must be established. While it appears that deubiquitination of PLD3 regulates stability, and that this may affect phosphatidic acid levels, it remains to be seen whether this might also link back to lysosomal function. The discovery that many DUB targets of ataxin-3 may have links to cellular metabolic processes could be further explored by undertaking metabolomics in ataxin-3 KO or depleted cells.

Fifthly, the *in vivo* relevance of ataxin-3 to the immune response must be demonstrated. Work in collaboration with the Paulson lab, utilising the ataxin-3 KO mouse, will establish the importance of ataxin-3 in mediating an immune response to peptidoglycan. Wild type

and ataxin-3 knockout mice will be challenged with peptidoglycan, and scored for sepsis response, before cytokine responses including IL1β are studied.

Finally, the direct relevance of ataxin-3 to the pathogenesis of Crohn's disease remains to be elucidated. It must first be confirmed that monocytes from patients with Crohn's disease associated NOD2 mutations fail to phosphorylate ataxin-3 on NOD2 stimulation by MDP. Next, these cells should be assessed for impairment of mitochondrial oxphos and mROS production. Ongoing work to establish the functional relevance of the deubiquitination of LAMTOR1, PLD3 and HIF1α by ataxin-3 will also guide future experiments in patient cells.

Bibliography

1. Janeway CA, Jr., Medzhitov R. Innate immune recognition. *Annu Rev Immunol* 2002, **20:** 197-216.

2. Kimbrell DA, Beutler B. The evolution and genetics of innate immunity. *Nat Rev Genet* 2001, **2**(4)**:** 256-267.

3. Janeway CA, Jr. Approaching the asymptote? Evolution and revolution in immunology. *Cold Spring Harb Symp Quant Biol* 1989, **54 Pt 1:** 1-13.

4. Medzhitov R, Janeway CA, Jr. Innate immunity: impact on the adaptive immune response. *Curr Opin Immunol* 1997, **9**(1)**:** 4-9.

5. Kawai T, Akira S. Toll-like receptors and their crosstalk with other innate receptors in infection and immunity. *Immunity* 2011, **34**(5)**:** 637-650.

6. Lemaitre B, Nicolas E, Michaut L, Reichhart JM, Hoffmann JA. The dorsoventral regulatory gene cassette spatzle/Toll/cactus controls the potent antifungal response in Drosophila adults. *Cell* 1996, **86**(6)**:** 973-983.

7. Ishii KJ, Koyama S, Nakagawa A, Coban C, Akira S. Host innate immune receptors and beyond: making sense of microbial infections. *Cell Host Microbe* 2008, **3**(6)**:** 352-363.

8. Broz P, Monack DM. Newly described pattern recognition receptors team up against intracellular pathogens. *Nat Rev Immunol* 2013, **13**(8)**:** 551-565.

9. Shi Y, Evans JE, Rock KL. Molecular identification of a danger signal that alerts the immune system to dying cells. *Nature* 2003, **425**(6957)**:** 516-521.

10. Wang H, Bloom O, Zhang M, Vishnubhakat JM, Ombrellino M, Che J*, et al.* HMG-1 as a late mediator of endotoxin lethality in mice. *Science* 1999, **285**(5425)**:** 248-251.

11. Kawasaki T, Kawai T. Toll-like receptor signaling pathways. *Front Immunol* 2014, **5:** 461.

12. Ozinsky A, Underhill DM, Fontenot JD, Hajjar AM, Smith KD, Wilson CB*, et al.* The repertoire for pattern recognition of pathogens by the innate immune system is defined by cooperation between toll-like receptors. *Proc Natl Acad Sci U S A* 2000, **97**(25)**:** 13766-13771.

13. Jin MS, Kim SE, Heo JY, Lee ME, Kim HM, Paik SG*, et al.* Crystal structure of the TLR1-TLR2 heterodimer induced by binding of a tri-acylated lipopeptide. *Cell* 2007, **130**(6)**:** 1071-1082.

14. Takeuchi O, Kawai T, Muhlradt PF, Morr M, Radolf JD, Zychlinsky A*, et al.* Discrimination of bacterial lipoproteins by Toll-like receptor 6. *Int Immunol* 2001, **13**(7)**:** 933-940.

15. Deng L, Wang C, Spencer E, Yang L, Braun A, You J*, et al.* Activation of the IkappaB kinase complex by TRAF6 requires a dimeric ubiquitin-conjugating enzyme complex and a unique polyubiquitin chain. *Cell* 2000, **103**(2)**:** 351-361.

16. Kobayashi K, Inohara N, Hernandez LD, Galan JE, Nunez G, Janeway CA*, et al.* RICK/Rip2/CARDIAK mediates signalling for receptors of the innate and adaptive immune systems. *Nature* 2002, **416**(6877)**:** 194-199.

17. Moreira LO, El Kasmi KC, Smith AM, Finkelstein D, Fillon S, Kim YG*, et al.* The TLR2-MyD88-NOD2-RIPK2 signalling axis regulates a balanced pro-inflammatory and IL-10-mediated anti-inflammatory cytokine response to Gram-positive cell walls. *Cell Microbiol* 2008, **10**(10)**:** 2067-2077.

18. Magalhaes JG, Sorbara MT, Girardin SE, Philpott DJ. What is new with Nods? *Current Opinion in Immunology* 2011, **23**(1)**:** 29-34.

19. Inohara, Chamaillard, McDonald C, Nunez G. NOD-LRR proteins: role in host-microbial interactions and inflammatory disease. *Annu Rev Biochem* 2005, **74:** 355-383.

20. Jones JD, Dangl JL. The plant immune system. *Nature* 2006, **444**(7117)**:** 323-329.

21. Ting JP, Lovering RC, Alnemri ES, Bertin J, Boss JM, Davis BK*, et al.* The NLR gene family: a standard nomenclature. *Immunity* 2008, **28**(3)**:** 285-287.

22. Fritz JH, Kufer TA. Editorial: NLR-Protein Functions in Immunity. *Front Immunol* 2015, **6:** 306.

23. Maekawa T, Kufer TA, Schulze-Lefert P. NLR functions in plant and animal immune systems: so far and yet so close. *Nat Immunol* 2011, **12**(9)**:** 817-826.

24. Kufer TA, Sansonetti PJ. NLR functions beyond pathogen recognition. *Nat Immunol* 2011, **12**(2)**:** 121-128.

25. Strober W, Murray PJ, Kitani A, Watanabe T. Signalling pathways and molecular interactions of NOD1 and NOD2. *Nat Rev Immunol* 2006, **6**(1)**:** 9-20.

26. Zhong Y, Kinio A, Saleh M. Functions of NOD-Like Receptors in Human Diseases. *Front Immunol* 2013, **4:** 333.

27. Girardin SE, Boneca IG, Carneiro LA, Antignac A, Jehanno M, Viala J*, et al.* Nod1 detects a unique muropeptide from gram-negative bacterial peptidoglycan. *Science* 2003, **300**(5625)**:** 1584-1587.

28. Chamaillard M, Hashimoto M, Horie Y, Masumoto J, Qiu S, Saab L*, et al.* An essential role for NOD1 in host recognition of bacterial peptidoglycan containing diaminopimelic acid. *Nat Immunol* 2003, **4**(7)**:** 702-707.

29. Girardin SE, Boneca IG, Viala J, Chamaillard M, Labigne A, Thomas G*, et al.* Nod2 is a general sensor of peptidoglycan through muramyl dipeptide (MDP) detection. *J Biol Chem* 2003, **278**(11)**:** 8869-8872.

30. Ogura Y, Bonen DK, Inohara N, Nicolae DL, Chen FF, Ramos R*, et al.* A frameshift mutation in NOD2 associated with susceptibility to Crohn's disease. *Nature* 2001, **411**(6837)**:** 603-606.

31. Hugot JP, Chamaillard M, Zouali H, Lesage S, Cezard JP, Belaiche J*, et al.* Association of NOD2 leucine-rich repeat variants with susceptibility to Crohn's disease. *Nature* 2001, **411**(6837)**:** 599-603.

32. Ogura Y, Lala S, Xin W, Smith E, Dowds TA, Chen FF*, et al.* Expression of NOD2 in Paneth cells: a possible link to Crohn's ileitis. *Gut* 2003, **52**(11)**:** 1591-1597.

33. Barnich N, Hisamatsu T, Aguirre JE, Xavier R, Reinecker HC, Podolsky DK. GRIM-19 interacts with nucleotide oligomerization domain 2 and serves as downstream effector of anti-bacterial function in intestinal epithelial cells. *J Biol Chem* 2005, **280**(19)**:** 19021-19026.

34. Nigro G, Rossi R, Commere PH, Jay P, Sansonetti PJ. The cytosolic bacterial peptidoglycan sensor Nod2 affords stem cell protection and links microbes to gut epithelial regeneration. *Cell Host Microbe* 2014, **15**(6)**:** 792-798.

35. Owens BM, Steevels TA, Dudek M, Walcott D, Sun MY, Mayer A*, et al.* CD90(+) Stromal Cells are Non-Professional Innate Immune Effectors of the Human Colonic Mucosa. *Front Immunol* 2013, **4:** 307.

36. Gutierrez O, Pipaon C, Inohara N, Fontalba A, Ogura Y, Prosper F*, et al.* Induction of Nod2 in myelomonocytic and intestinal epithelial cells via nuclear factor-kappa B activation. *J Biol Chem* 2002, **277**(44)**:** 41701-41705.

37. Rahman MK, Midtling EH, Svingen PA, Xiong Y, Bell MP, Tung J*, et al.* The pathogen recognition receptor NOD2 regulates human FOXP3+ T cell survival. *J Immunol* 2010, **184**(12)**:** 7247-7256.

38. Sterka D, Jr., Marriott I. Characterization of nucleotide-binding oligomerization domain (NOD) protein expression in primary murine microglia. *J Neuroimmunol* 2006, **179**(1-2)**:** 65-75.

39. Sterka D, Jr., Rati DM, Marriott I. Functional expression of NOD2, a novel pattern recognition receptor for bacterial motifs, in primary murine astrocytes. *Glia* 2006, **53**(3)**:** 322-330.

40. Barnich N, Aguirre JE, Reinecker HC, Xavier R, Podolsky DK. Membrane recruitment of NOD2 in intestinal epithelial cells is essential for nuclear factor-{kappa}B activation in muramyl dipeptide recognition. *J Cell Biol* 2005, **170**(1)**:** 21-26.

41. Philpott DJ, Girardin SE. Nod-like receptors: sentinels at host membranes. *Curr Opin Immunol* 2010, **22**(4)**:** 428-434.

42. Travassos LH, Carneiro LA, Ramjeet M, Hussey S, Kim YG, Magalhaes JG*, et al.* Nod1 and Nod2 direct autophagy by recruiting ATG16L1 to the plasma membrane at the site of bacterial entry. *Nat Immunol* 2010, **11**(1)**:** 55-62.

43. Philpott DJ, Sorbara MT, Robertson SJ, Croitoru K, Girardin SE. NOD proteins: regulators of inflammation in health and disease. *Nat Rev Immunol* 2014, **14**(1)**:** 9-23.

44. Hu Z, Yan C, Liu P, Huang Z, Ma R, Zhang C*, et al.* Crystal structure of NLRC4 reveals its autoinhibition mechanism. *Science* 2013, **341**(6142)**:** 172-175.

45. Caruso R, Warner N, Inohara N, Nunez G. NOD1 and NOD2: signaling, host defense, and inflammatory disease. *Immunity* 2014, **41**(6)**:** 898-908.

46. Nigro G, Fazio LL, Martino MC, Rossi G, Tattoli I, Liparoti V*, et al.* Muramylpeptide shedding modulates cell sensing of Shigella flexneri. *Cell Microbiol* 2008, **10**(3)**:** 682-695.

47. Bielig H, Rompikuntal PK, Dongre M, Zurek B, Lindmark B, Ramstedt M*, et al.* NOD-like receptor activation by outer membrane vesicles from Vibrio cholerae non-O1 non-O139 strains is modulated by the quorum-sensing regulator HapR. *Infect Immun* 2011, **79**(4)**:** 1418-1427.

48. Nakamura N, Lill JR, Phung Q, Jiang Z, Bakalarski C, de Maziere A*, et al.* Endosomes are specialized platforms for bacterial sensing and NOD2 signalling. *Nature* 2014.

49. Boyle JP, Parkhouse R, Monie TP. Insights into the molecular basis of the NOD2 signalling pathway. *Open Biology* 2014, **4**(12).

50. Grimes CL, Ariyananda Lde Z, Melnyk JE, O'Shea EK. The innate immune protein Nod2 binds directly to MDP, a bacterial cell wall fragment. *J Am Chem Soc* 2012, **134**(33)**:** 13535-13537.

51. Mo J, Boyle JP, Howard CB, Monie TP, Davis BK, Duncan JA. Pathogen sensing by nucleotide-binding oligomerization domain-containing protein 2 (NOD2) is mediated by direct binding to muramyl dipeptide and ATP. *J Biol Chem* 2012, **287**(27)**:** 23057-23067.

52. Park JH, Kim YG, McDonald C, Kanneganti TD, Hasegawa M, Body-Malapel M*, et al.* RICK/RIP2 mediates innate immune responses induced through Nod1 and Nod2 but not TLRs. *J Immunol* 2007, **178**(4)**:** 2380-2386.

53. Bertrand MJ, Doiron K, Labbe K, Korneluk RG, Barker PA, Saleh M. Cellular inhibitors of apoptosis cIAP1 and cIAP2 are required for innate immunity signaling by the pattern recognition receptors NOD1 and NOD2. *Immunity* 2009, **30**(6)**:** 789-801.

54. Yang Y, Yin C, Pandey A, Abbott D, Sassetti C, Kelliher MA. NOD2 pathway activation by MDP or Mycobacterium tuberculosis infection involves the stable polyubiquitination of Rip2. *J Biol Chem* 2007, **282**(50)**:** 36223-36229.

55. Krieg A, Correa RG, Garrison JB, Le Negrate G, Welsh K, Huang Z*, et al.* XIAP mediates NOD signaling via interaction with RIP2. *Proc Natl Acad Sci U S A* 2009, **106**(34)**:** 14524-14529.

56. Damgaard RB, Nachbur U, Yabal M, Wong WW, Fiil BK, Kastirr M*, et al.* The ubiquitin ligase XIAP recruits LUBAC for NOD2 signaling in inflammation and innate immunity. *Mol Cell* 2012, **46**(6)**:** 746-758.

57. Damgaard RB, Fiil BK, Speckmann C, Yabal M, zur Stadt U, Bekker-Jensen S*, et al.* Disease-causing mutations in the XIAP BIR2 domain impair NOD2-dependent immune signalling. *EMBO Mol Med* 2013, **5**(8)**:** 1278-1295.

58. Zeissig Y, Petersen BS, Milutinovic S, Bosse E, Mayr G, Peuker K*, et al.* XIAP variants in male Crohn's disease. *Gut* 2015, **64**(1)**:** 66-76.

59. Tigno-Aranjuez JT, Asara JM, Abbott DW. Inhibition of RIP2's tyrosine kinase activity limits NOD2-driven cytokine responses. *Genes Dev* 2010, **24**(23)**:** 2666-2677.

60. Hasegawa M, Fujimoto Y, Lucas PC, Nakano H, Fukase K, Nunez G*, et al.* A critical role of RICK/RIP2 polyubiquitination in Nod-induced NF-kappaB activation. *EMBO J* 2008, **27**(2)**:** 373-383.

61. Hsu YM, Zhang Y, You Y, Wang D, Li H, Duramad O*, et al.* The adaptor protein CARD9 is required for innate immune responses to intracellular pathogens. *Nat Immunol* 2007, **8**(2)**:** 198-205.

62. Sabbah A, Chang TH, Harnack R, Frohlich V, Tominaga K, Dube PH*, et al.* Activation of innate immune antiviral responses by Nod2. *Nat Immunol* 2009, **10**(10)**:** 1073-1080.

63. Marinis JM, Homer CR, McDonald C, Abbott DW. A novel motif in the Crohn's disease susceptibility protein, NOD2, allows TRAF4 to down-regulate innate immune responses. *J Biol Chem* 2011, **286**(3)**:** 1938-1950.

64. Hitotsumatsu O, Ahmad RC, Tavares R, Wang M, Philpott D, Turer EE*, et al.* The ubiquitin-editing enzyme A20 restricts nucleotide-binding oligomerization domain containing 2-triggered signals. *Immunity* 2008, **28**(3)**:** 381-390.

65. McDonald C, Chen FF, Ollendorff V, Ogura Y, Marchetto S, Lecine P*, et al.* A role for Erbin in the regulation of Nod2-dependent NF-kappaB signaling. *J Biol Chem* 2005, **280**(48)**:** 40301-40309.

66. Eitel J, Krull M, Hocke AC, N'Guessan PD, Zahlten J, Schmeck B*, et al.* Beta-PIX and Rac1 GTPase mediate trafficking and negative regulation of NOD2. *J Immunol* 2008, **181**(4)**:** 2664-2671.

67. Morosky SA, Zhu J, Mukherjee A, Sarkar SN, Coyne CB. Retinoic acid-induced gene-I (RIG-I) associates with nucleotide-binding oligomerization domain-2 (NOD2) to negatively regulate inflammatory signaling. *J Biol Chem* 2011, **286**(32)**:** 28574-28583.

68. Stevens C, Henderson P, Nimmo ER, Soares DC, Dogan B, Simpson KW*, et al.* The intermediate filament protein, vimentin, is a regulator of NOD2 activity. *Gut* 2013, **62**(5)**:** 695-707.

69. Zhao Y, Alonso C, Ballester I, Song JH, Chang SY, Guleng B*, et al.* Control of NOD2 and Rip2-dependent innate immune activation by GEF-H1. *Inflamm Bowel Dis* 2012, **18**(4)**:** 603-612.

70. Kobayashi KS, Chamaillard M, Ogura Y, Henegariu O, Inohara N, Nunez G*, et al.* Nod2-dependent regulation of innate and adaptive immunity in the intestinal tract. *Science* 2005, **307**(5710)**:** 731-734.

71. Hsu LC, Ali SR, McGillivray S, Tseng PH, Mariathasan S, Humke EW*, et al.* A NOD2-NALP1 complex mediates caspase-1-dependent IL-1beta secretion in response to Bacillus anthracis infection and muramyl dipeptide. *Proc Natl Acad Sci U S A* 2008, **105**(22)**:** 7803-7808.

72. Bevins CL, Salzman NH. Paneth cells, antimicrobial peptides and maintenance of intestinal homeostasis. *Nat Rev Microbiol* 2011, **9**(5)**:** 356-368.

73. Magalhaes JG, Fritz JH, Le Bourhis L, Sellge G, Travassos LH, Selvanantham T*, et al.* Nod2-dependent Th2 polarization of antigen-specific immunity. *J Immunol* 2008, **181**(11)**:** 7925-7935.

74. Brain O, Owens BM, Pichulik T, Allan P, Khatamzas E, Leslie A*, et al.* The intracellular sensor NOD2 induces microRNA-29 expression in human dendritic cells to limit IL-23 release. *Immunity* 2013, **39**(3)**:** 521-536.

75. van Beelen AJ, Zelinkova Z, Taanman-Kueter EW, Muller FJ, Hommes DW, Zaat SA*, et al.* Stimulation of the intracellular bacterial sensor NOD2 programs dendritic cells to

promote interleukin-17 production in human memory T cells. *Immunity* 2007, **27**(4)**:** 660-669.

76. Divangahi M, Mostowy S, Coulombe F, Kozak R, Guillot L, Veyrier F*, et al.* NOD2-deficient mice have impaired resistance to Mycobacterium tuberculosis infection through defective innate and adaptive immunity. *J Immunol* 2008, **181**(10)**:** 7157-7165.

77. Shaw MH, Reimer T, Sanchez-Valdepenas C, Warner N, Kim YG, Fresno M*, et al.* T cell-intrinsic role of Nod2 in promoting type 1 immunity to Toxoplasma gondii. *Nat Immunol* 2009, **10**(12)**:** 1267-1274.

78. Geddes K, Rubino SJ, Magalhaes JG, Streutker C, Le Bourhis L, Cho JH*, et al.* Identification of an innate T helper type 17 response to intestinal bacterial pathogens. *Nat Med* 2011, **17**(7)**:** 837-844.

79. Cooney R, Baker J, Brain O, Danis B, Pichulik T, Allan P*, et al.* NOD2 stimulation induces autophagy in dendritic cells influencing bacterial handling and antigen presentation. *Nat Med* 2010, **16**(1)**:** 90-97.

80. Feng Y, He D, Yao Z, Klionsky DJ. The machinery of macroautophagy. *Cell Res* 2014, **24**(1)**:** 24-41.

81. Mizushima N, Levine B, Cuervo AM, Klionsky DJ. Autophagy fights disease through cellular self-digestion. *Nature* 2008, **451**(7182)**:** 1069-1075.

82. Lassen KG, Xavier RJ. Genetic control of autophagy underlies pathogenesis of inflammatory bowel disease. *Mucosal Immunol* 2017, **10**(3)**:** 589-597.

83. Deretic V, Levine B. Autophagy, immunity, and microbial adaptations. *Cell Host Microbe* 2009, **5**(6)**:** 527-549.

84. Shibutani ST, Saitoh T, Nowag H, Munz C, Yoshimori T. Autophagy and autophagy-related proteins in the immune system. *Nat Immunol* 2015, **16**(10)**:** 1014-1024.

85. Manzanillo PS, Ayres JS, Watson RO, Collins AC, Souza G, Rae CS*, et al.* The ubiquitin ligase parkin mediates resistance to intracellular pathogens. *Nature* 2013, **501**(7468)**:** 512-516.

86. Huett A, Heath RJ, Begun J, Sassi SO, Baxt LA, Vyas JM*, et al.* The LRR and RING domain protein LRSAM1 is an E3 ligase crucial for ubiquitin-dependent autophagy of intracellular Salmonella Typhimurium. *Cell Host Microbe* 2012, **12**(6)**:** 778-790.

87. Thurston TL, Wandel MP, von Muhlinen N, Foeglein A, Randow F. Galectin 8 targets damaged vesicles for autophagy to defend cells against bacterial invasion. *Nature* 2012, **482**(7385)**:** 414-418.

88. Hailey DW, Rambold AS, Satpute-Krishnan P, Mitra K, Sougrat R, Kim PK*, et al.* Mitochondria supply membranes for autophagosome biogenesis during starvation. *Cell* 2010, **141**(4)**:** 656-667.

89. Tooze SA, Yoshimori T. The origin of the autophagosomal membrane. *Nat Cell Biol* 2010, **12**(9)**:** 831-835.

90. Klionsky DJ, Schulman BA. Dynamic regulation of macroautophagy by distinctive ubiquitin-like proteins. *Nat Struct Mol Biol* 2014, **21**(4)**:** 336-345.

91. Klionsky DJ, Cregg JM, Dunn WA, Jr., Emr SD, Sakai Y, Sandoval IV*, et al.* A unified nomenclature for yeast autophagy-related genes. *Dev Cell* 2003, **5**(4)**:** 539-545.

92. Kraft C, Kijanska M, Kalie E, Siergiejuk E, Lee SS, Semplicio G*, et al.* Binding of the Atg1/ULK1 kinase to the ubiquitin-like protein Atg8 regulates autophagy. *EMBO J* 2012, **31**(18)**:** 3691-3703.

93. Noda NN, Kumeta H, Nakatogawa H, Satoo K, Adachi W, Ishii J*, et al.* Structural basis of target recognition by Atg8/LC3 during selective autophagy. *Genes Cells* 2008, **13**(12)**:** 1211-1218.

94. Ponpuak M, Davis AS, Roberts EA, Delgado MA, Dinkins C, Zhao Z*, et al.* Delivery of cytosolic components by autophagic adaptor protein p62 endows autophagosomes with unique antimicrobial properties. *Immunity* 2010, **32**(3)**:** 329-341.

95. Thurston TL, Ryzhakov G, Bloor S, von Muhlinen N, Randow F. The TBK1 adaptor and autophagy receptor NDP52 restricts the proliferation of ubiquitin-coated bacteria. *Nat Immunol* 2009, **10**(11)**:** 1215-1221.

96. Mostowy S, Sancho-Shimizu V, Hamon MA, Simeone R, Brosch R, Johansen T*, et al.* p62 and NDP52 proteins target intracytosolic Shigella and Listeria to different autophagy pathways. *J Biol Chem* 2011, **286**(30)**:** 26987-26995.

97. Wild P, Farhan H, McEwan DG, Wagner S, Rogov VV, Brady NR*, et al.* Phosphorylation of the autophagy receptor optineurin restricts Salmonella growth. *Science* 2011, **333**(6039)**:** 228-233.

98. Amer AO, Swanson MS. Autophagy is an immediate macrophage response to Legionella pneumophila. *Cell Microbiol* 2005, **7**(6)**:** 765-778.

99. Weidberg H, Shvets E, Shpilka T, Shimron F, Shinder V, Elazar Z. LC3 and GATE-16/GABARAP subfamilies are both essential yet act differently in autophagosome biogenesis. *EMBO J* 2010, **29**(11)**:** 1792-1802.

100. Berg TO, Fengsrud M, Stromhaug PE, Berg T, Seglen PO. Isolation and characterization of rat liver amphisomes. Evidence for fusion of autophagosomes with both early and late endosomes. *J Biol Chem* 1998, **273**(34)**:** 21883-21892.

101. Klionsky DJ, Eskelinen EL, Deretic V. Autophagosomes, phagosomes, autolysosomes, phagolysosomes, autophagolysosomes... wait, I'm confused. *Autophagy* 2014, **10**(4)**:** 549-551.

102. Martinez J, Almendinger J, Oberst A, Ness R, Dillon CP, Fitzgerald P*, et al.* Microtubule-associated protein 1 light chain 3 alpha (LC3)-associated phagocytosis is required for the efficient clearance of dead cells. *Proc Natl Acad Sci U S A* 2011, **108**(42)**:** 17396-17401.

103. Nakamura S, Yoshimori T. New insights into autophagosome-lysosome fusion. *J Cell Sci* 2017, **130**(7)**:** 1209-1216.

104. Wang H, Sun HQ, Zhu X, Zhang L, Albanesi J, Levine B*, et al.* GABARAPs regulate PI4P-dependent autophagosome:lysosome fusion. *Proc Natl Acad Sci U S A* 2015, **112**(22)**:** 7015-7020.

105. Lupfer C, Thomas PG, Anand PK, Vogel P, Milasta S, Martinez J*, et al.* Receptor interacting protein kinase 2-mediated mitophagy regulates inflammasome activation during virus infection. *Nat Immunol* 2013, **14**(5)**:** 480-488.

106. Schmid D, Pypaert M, Munz C. Antigen-loading compartments for major histocompatibility complex class II molecules continuously receive input from autophagosomes. *Immunity* 2007, **26**(1)**:** 79-92.

107. Sorbara MT, Ellison LK, Ramjeet M, Travassos LH, Jones NL, Girardin SE*, et al.* The protein ATG16L1 suppresses inflammatory cytokines induced by the intracellular sensors Nod1 and Nod2 in an autophagy-independent manner. *Immunity* 2013, **39**(5)**:** 858-873.

108. Cao X. Self-regulation and cross-regulation of pattern-recognition receptor signalling in health and disease. *Nat Rev Immunol* 2016, **16**(1)**:** 35-50.

109. Tada H, Aiba S, Shibata K, Ohteki T, Takada H. Synergistic effect of Nod1 and Nod2 agonists with toll-like receptor agonists on human dendritic cells to generate interleukin-12 and T helper type 1 cells. *Infect Immun* 2005, **73**(12)**:** 7967-7976.

110. Netea MG, Ferwerda G, de Jong DJ, Jansen T, Jacobs L, Kramer M*, et al.* Nucleotide-binding oligomerization domain-2 modulates specific TLR pathways for the induction of cytokine release. *J Immunol* 2005, **174**(10)**:** 6518-6523.

111. Ferwerda G, Girardin SE, Kullberg BJ, Le Bourhis L, de Jong DJ, Langenberg DM*, et al.* NOD2 and toll-like receptors are nonredundant recognition systems of Mycobacterium tuberculosis. *PLoS Pathog* 2005, **1**(3)**:** 279-285.

112. Ghorpade DS, Kaveri SV, Bayry J, Balaji KN. Cooperative regulation of NOTCH1 protein-phosphatidylinositol 3-kinase (PI3K) signaling by NOD1, NOD2, and TLR2

receptors renders enhanced refractoriness to transforming growth factor-beta (TGF-beta)- or cytotoxic T-lymphocyte antigen 4 (CTLA-4)-mediated impairment of human dendritic cell maturation. *J Biol Chem* 2011, **286**(36)**:** 31347-31360.

113. Watanabe T, Kitani A, Murray PJ, Strober W. NOD2 is a negative regulator of Toll-like receptor 2-mediated T helper type 1 responses. *Nat Immunol* 2004, **5**(8)**:** 800-808.

114. Watanabe T, Kitani A, Murray PJ, Wakatsuki Y, Fuss IJ, Strober W. Nucleotide binding oligomerization domain 2 deficiency leads to dysregulated TLR2 signaling and induction of antigen-specific colitis. *Immunity* 2006, **25**(3)**:** 473-485.

115. Borm ME, van Bodegraven AA, Mulder CJ, Kraal G, Bouma G. The effect of NOD2 activation on TLR2-mediated cytokine responses is dependent on activation dose and NOD2 genotype. *Genes Immun* 2008, **9**(3)**:** 274-278.

116. Adler J, Rangwalla SC, Dwamena BA, Higgins PD. The prognostic power of the NOD2 genotype for complicated Crohn's disease: a meta-analysis. *Am J Gastroenterol* 2011, **106**(4)**:** 699-712.

117. Jostins L, Ripke S, Weersma RK, Duerr RH, McGovern DP, Hui KY*, et al.* Host-microbe interactions have shaped the genetic architecture of inflammatory bowel disease. *Nature* 2012, **491**(7422)**:** 119-124.

118. Rubin GP, Hungin AP, Kelly PJ, Ling J. Inflammatory bowel disease: epidemiology and management in an English general practice population. *Aliment Pharmacol Ther* 2000, **14**(12)**:** 1553-1559.

119. Feuerstein JD, Cheifetz AS. Crohn Disease: Epidemiology, Diagnosis, and Management. *Mayo Clin Proc* 2017.

120. Wolters FL, Russel MG, Stockbrugger RW. Systematic review: has disease outcome in Crohn's disease changed during the last four decades? *Aliment Pharmacol Ther* 2004, **20**(5)**:** 483-496.

121. Lesage S, Zouali H, Cezard JP, Colombel JF, Belaiche J, Almer S*, et al.* CARD15/NOD2 mutational analysis and genotype-phenotype correlation in 612 patients with inflammatory bowel disease. *Am J Hum Genet* 2002, **70**(4)**:** 845-857.

122. Van Limbergen J, Radford-Smith G, Satsangi J. Advances in IBD genetics. *Nat Rev Gastroenterol Hepatol* 2014, **11**(6)**:** 372-385.

123. Rivas MA, Beaudoin M, Gardet A, Stevens C, Sharma Y, Zhang CK*, et al.* Deep resequencing of GWAS loci identifies independent rare variants associated with inflammatory bowel disease. *Nat Genet* 2011, **43**(11)**:** 1066-1073.

124. Hugot JP, Zaccaria I, Cavanaugh J, Yang H, Vermeire S, Lappalainen M*, et al.* Prevalence of CARD15/NOD2 mutations in Caucasian healthy people. *Am J Gastroenterol* 2007, **102**(6)**:** 1259-1267.

125. Sugimura K, Taylor KD, Lin YC, Hang T, Wang D, Tang YM*, et al.* A novel NOD2/CARD15 haplotype conferring risk for Crohn disease in Ashkenazi Jews. *Am J Hum Genet* 2003, **72**(3)**:** 509-518.

126. Maeda S, Hsu LC, Liu HJ, Bankston LA, Iimura M, Kagnoff MF*, et al.* Nod2 mutation in Crohn's disease potentiates NF-kappa B activity and IL-10 processing. *Science* 2005, **307**(5710)**:** 734-738.

127. Maeda S. Nod2 mutation in Crohn's disease potentiates NF-kappa B activity and IL-1 beta processing (February, pg 734, 2005). *Science* 2011, **333**(6040)**:** 288-288.

128. Kim YG, Shaw MH, Warner N, Park JH, Chen F, Ogura Y*, et al.* Cutting Edge: Crohn's Disease-Associated Nod2 Mutation Limits Production of Proinflammatory Cytokines To Protect the Host from Enterococcus faecalis-Induced Lethality. *Journal of Immunology* 2011, **187**(6)**:** 2849-2852.

129. van Heel DA, Ghosh S, Butler M, Hunt KA, Lundberg AM, Ahmad T*, et al.* Muramyl dipeptide and toll-like receptor sensitivity in NOD2-associated Crohn's disease. *Lancet* 2005, **365**(9473)**:** 1794-1796.

130. Inohara N, Ogura Y, Fontalba A, Gutierrez O, Pons F, Crespo J*, et al.* Host recognition of bacterial muramyl dipeptide mediated through NOD2. *Journal of Biological Chemistry* 2003, **278**(8)**:** 5509-5512.

131. Abbasi AZ, Gordijo CR, Amini MA, Maeda A, Rauth AM, DaCosta RS*, et al.* Hybrid Manganese Dioxide Nanoparticles Potentiate Radiation Therapy by Modulating Tumor Hypoxia. *Cancer Research* 2016, **76**(22)**:** 6643-6656.

132. Li J, Moran T, Swanson E, Julian C, Harris J, Bonen DK*, et al.* Regulation of IL-8 and IL-1 beta expression in Crohn's disease associated NOD2/CARD15 mutations. *Human Molecular Genetics* 2004, **13**(16)**:** 1715-1725.

133. Noguchi E, Homma Y, Kang X, Netea MG, Ma X. A Crohn's disease-associated NOD2 mutation suppresses transcription of human IL10 by inhibiting activity of the nuclear ribonucleoprotein hnRNP-A1. *Nat Immunol* 2009, **10**(5)**:** 471-479.

134. Wehkamp J, Salzman NH, Porter E, Nuding S, Weichenthal M, Petras RE*, et al.* Reduced Paneth cell alpha-defensins in ileal Crohn's disease. *Proceedings of the National Academy of Sciences of the United States of America* 2005, **102**(50)**:** 18129-18134.

135. Simms LA, Doecke JD, Walsh MD, Huang N, Fowler EV, Radford-Smith GL. Reduced alpha-defensin expression is associated with inflammation and not NOD2 mutation status in ileal Crohn's disease. *Gut* 2008, **57**(7)**:** 903-910.

136. Ramanan D, Tang MS, Bowcutt R, Loke P, Cadwell K. Bacterial Sensor Nod2 Prevents Inflammation of the Small Intestine by Restricting the Expansion of the Commensal Bacteroides vulgatus. *Immunity* 2014, **41**(2)**:** 311-324.

137. Shanahan MT, Carroll IM, Grossniklaus E, White A, von Furstenberg RJ, Barner R*, et al.* Mouse Paneth cell antimicrobial function is independent of Nod2. *Gut* 2014, **63**(6)**:** 903-910.

138. Robertson SJ, Zhou JY, Geddes K, Rubino SJ, Cho JH, Girardin SE*, et al.* Nod1 and Nod2 signaling does not alter the composition of intestinal bacterial communities at homeostasis. *Gut Microbes* 2013, **4**(3)**:** 222-231.

139. Strober W, Fuss IJ. Proinflammatory cytokines in the pathogenesis of inflammatory bowel diseases. *Gastroenterology* 2011, **140**(6)**:** 1756-1767.

140. Cheng Y, Zhu Y, Huang X, Zhang W, Han Z, Liu S. Association between TLR2 and TLR4 Gene Polymorphisms and the Susceptibility to Inflammatory Bowel Disease: A Meta-Analysis. *PLoS One* 2015, **10**(5)**:** e0126803.

141. Kim YG, Park JH, Shaw MH, Franchi L, Inohara N, Nunez G. The cytosolic sensors Nod1 and Nod2 are critical for bacterial recognition and host defense after exposure to toll-like receptor ligands. *Immunity* 2008, **28**(2)**:** 246-257.

142. Kramer M, Netea MG, de Jong DJ, Kullberg BJ, Adema GJ. Impaired dendritic cell function in Crohn's disease patients with NOD2 3020insC mutation. *J Leukoc Biol* 2006, **79**(4)**:** 860-866.

143. Parkes M, Barrett JC, Prescott NJ, Tremelling M, Anderson CA, Fisher SA*, et al.* Sequence variants in the autophagy gene IRGM and multiple other replicating loci contribute to Crohn's disease susceptibility. *Nat Genet* 2007, **39**(7)**:** 830-832.

144. Walter P, Ron D. The unfolded protein response: from stress pathway to homeostatic regulation. *Science* 2011, **334**(6059)**:** 1081-1086.

145. Kaser A, Lee AH, Franke A, Glickman JN, Zeissig S, Tilg H*, et al.* XBP1 links ER stress to intestinal inflammation and confers genetic risk for human inflammatory bowel disease. *Cell* 2008, **134**(5)**:** 743-756.

146. Barrett JC, Hansoul S, Nicolae DL, Cho JH, Duerr RH, Rioux JD*, et al.* Genome-wide association defines more than 30 distinct susceptibility loci for Crohn's disease. *Nat Genet* 2008, **40**(8)**:** 955-962.

147. Adolph TE, Tomczak MF, Niederreiter L, Ko HJ, Bock J, Martinez-Naves E*, et al.* Paneth cells as a site of origin for intestinal inflammation. *Nature* 2013, **503**(7475)**:** 272-276.

148. Tschurtschenthaler M, Adolph TE, Ashcroft JW, Niederreiter L, Bharti R, Saveljeva S*, et al.* Defective ATG16L1-mediated removal of IRE1alpha drives Crohn's disease-like ileitis. *J Exp Med* 2017, **214**(2)**:** 401-422.

149. Keestra-Gounder AM, Byndloss MX, Seyffert N, Young BM, Chavez-Arroyo A, Tsai AY*, et al.* NOD1 and NOD2 signalling links ER stress with inflammation. *Nature* 2016, **532**(7599)**:** 394-397.

150. Penn BH, Cox JS. Immunology: Organelle stress triggers inflammation. *Nature* 2016, **532**(7599)**:** 321-322.

151. Nabatov AA, Hatzis P, Rouschop KM, van Diest P, Vooijs M. Hypoxia inducible NOD2 interacts with 3-O-sulfogalactoceramide and regulates vesicular homeostasis. *Biochim Biophys Acta* 2013, **1830**(11)**:** 5277-5286.

152. Xiao S, Finkielstein CV, Capelluto DG. The enigmatic role of sulfatides: new insights into cellular functions and mechanisms of protein recognition. *Adv Exp Med Biol* 2013, **991:** 27-40.

153. Jeon SB, Yoon HJ, Park SH, Kim IH, Park EJ. Sulfatide, a major lipid component of myelin sheath, activates inflammatory responses as an endogenous stimulator in brain-resident immune cells. *J Immunol* 2008, **181**(11)**:** 8077-8087.

154. Appenrodt B, Grunhage F, Gentemann MG, Thyssen L, Sauerbruch T, Lammert F. Nucleotide-Binding Oligomerization Domain Containing 2 (NOD2) Variants Are Genetic Risk Factors for Death and Spontaneous Bacterial Peritonitis in Liver Cirrhosis. *Hepatology* 2010, **51**(4)**:** 1327-1333.

155. Berrington WR, Macdonald M, Khadge S, Sapkota BR, Janer M, Hagge DA*, et al.* Common Polymorphisms in the NOD2 Gene Region Are Associated with Leprosy and Its Reactive States. *Journal of Infectious Diseases* 2010, **201**(9)**:** 1422-1435.

156. Liu XJ, Chauhan VS, Young AB, Marriott I. NOD2 Mediates Inflammatory Responses of Primary Murine Glia to Streptococcus pneumoniae. *Glia* 2010, **58**(7)**:** 839-847.

157. Liu XJ, Han QZ, Leng JH. Analysis of nucleotide-binding oligomerization domain proteins in a murine model of pneumococcal meningitis. *Bmc Infectious Diseases* 2014, **14**.

158. Wouters CH, Maes A, Foley KP, Bertin J, Rose CD. Blau syndrome, the prototypic auto-inflammatory granulomatous disease. *Pediatr Rheumatol Online J* 2014, **12:** 33.

159. Caso F, Galozzi P, Costa L, Sfriso P, Cantarini L, Punzi L. Autoinflammatory granulomatous diseases: from Blau syndrome and early-onset sarcoidosis to NOD2-mediated disease and Crohn's disease. *RMD Open* 2015, **1**(1)**:** e000097.

160. Penack O, Smith OM, Cunningham-Bussel A, Liu X, Rao U, Yim N*, et al.* NOD2 regulates hematopoietic cell function during graft-versus-host disease. *J Exp Med* 2009, **206**(10)**:** 2101-2110.

161. Shaw PJ, Barr MJ, Lukens JR, McGargill MA, Chi H, Mak TW*, et al.* Signaling via the RIP2 adaptor protein in central nervous system-infiltrating dendritic cells promotes inflammation and autoimmunity. *Immunity* 2011, **34**(1)**:** 75-84.

162. Duan W, Mehta AK, Magalhaes JG, Ziegler SF, Dong C, Philpott DJ*, et al.* Innate signals from Nod2 block respiratory tolerance and program T(H)2-driven allergic inflammation. *J Allergy Clin Immunol* 2010, **126**(6)**:** 1284-1293 e1210.

163. Kabesch M, Peters W, Carr D, Leupold W, Weiland SK, von Mutius E. Association between polymorphisms in caspase recruitment domain containing protein 15 and allergy in two German populations. *J Allergy Clin Immunol* 2003, **111**(4)**:** 813-817.

164. Vieira SM, Cunha TM, Franca RF, Pinto LG, Talbot J, Turato WM*, et al.* Joint NOD2/RIPK2 signaling regulates IL-17 axis and contributes to the development of experimental arthritis. *J Immunol* 2012, **188**(10)**:** 5116-5122.

165. Saha S, Qi J, Wang S, Wang M, Li X, Kim YG*, et al.* PGLYRP-2 and Nod2 are both required for peptidoglycan-induced arthritis and local inflammation. *Cell Host Microbe* 2009, **5**(2)**:** 137-150.

166. Couturier-Maillard A, Secher T, Rehman A, Normand S, De Arcangelis A, Haesler R*, et al.* NOD2-mediated dysbiosis predisposes mice to transmissible colitis and colorectal cancer. *J Clin Invest* 2013, **123**(2)**:** 700-711.

167. Companioni O, Bonet C, Munoz X, Weiderpass E, Panico S, Tumino R*, et al.* Polymorphisms of Helicobacter pylori signaling pathway genes and gastric cancer risk in the European Prospective Investigation into Cancer-Eurgast cohort. *Int J Cancer* 2014, **134**(1)**:** 92-101.

168. Rosenstiel P, Hellmig S, Hampe J, Ott S, Till A, Fischbach W*, et al.* Influence of polymorphisms in the NOD1/CARD4 and NOD2/CARD15 genes on the clinical outcome of Helicobacter pylori infection. *Cell Microbiol* 2006, **8**(7)**:** 1188-1198.

169. O'Neill LA, Kishton RJ, Rathmell J. A guide to immunometabolism for immunologists. *Nat Rev Immunol* 2016, **16**(9)**:** 553-565.

170. Loftus RM, Finlay DK. Immunometabolism: Cellular Metabolism Turns Immune Regulator. *J Biol Chem* 2016, **291**(1)**:** 1-10.

171. Glover LE, Colgan SP. Hypoxia and metabolic factors that influence inflammatory bowel disease pathogenesis. *Gastroenterology* 2011, **140**(6)**:** 1748-1755.

172. Colgan SP, Taylor CT. Hypoxia: an alarm signal during intestinal inflammation. *Nat Rev Gastroenterol Hepatol* 2010, **7**(5)**:** 281-287.

173. Payne JG, Bowen JC. Hypoxia of canine gastric mucosa caused by Escherichia coli sepsis and prevented with methylprednisolone therapy. *Gastroenterology* 1981, **80**(1)**:** 84-93.

174. Arnold F, West D, Kumar S. Wound healing: the effect of macrophage and tumour derived angiogenesis factors on skin graft vascularization. *Br J Exp Pathol* 1987, **68**(4)**:** 569-574.

175. Campbell EL, Bruyninckx WJ, Kelly CJ, Glover LE, McNamee EN, Bowers BE*, et al.* Transmigrating neutrophils shape the mucosal microenvironment through localized oxygen depletion to influence resolution of inflammation. *Immunity* 2014, **40**(1)**:** 66-77.

176. Karhausen J, Furuta GT, Tomaszewski JE, Johnson RS, Colgan SP, Haase VH. Epithelial hypoxia-inducible factor-1 is protective in murine experimental colitis. *J Clin Invest* 2004, **114**(8)**:** 1098-1106.

177. Hauser CJ, Locke RR, Kao HW, Patterson J, Zipser RD. Visceral surface oxygen tension in experimental colitis in the rabbit. *J Lab Clin Med* 1988, **112**(1)**:** 68-71.

178. Wakefield AJ, Sawyerr AM, Dhillon AP, Pittilo RM, Rowles PM, Lewis AA*, et al.* Pathogenesis of Crohn's disease: multifocal gastrointestinal infarction. *Lancet* 1989, **2**(8671)**:** 1057-1062.

179. Kominsky DJ, Campbell EL, Colgan SP. Metabolic shifts in immunity and inflammation. *J Immunol* 2010, **184**(8)**:** 4062-4068.

180. Pollard TD, Borisy GG. Cellular motility driven by assembly and disassembly of actin filaments. *Cell* 2003, **112**(4)**:** 453-465.

181. Borregaard N, Herlin T. Energy metabolism of human neutrophils during phagocytosis. *J Clin Invest* 1982, **70**(3)**:** 550-557.

182. Colgan SP, Curtis VF, Campbell EL. The inflammatory tissue microenvironment in IBD. *Inflamm Bowel Dis* 2013, **19**(10)**:** 2238-2244.

183. Olive AJ, Sassetti CM. Metabolic crosstalk between host and pathogen: sensing, adapting and competing. *Nat Rev Microbiol* 2016, **14**(4)**:** 221-234.

184. Torres A, Luke JD, Kullas AL, Kapilashrami K, Botbol Y, Koller A*, et al.* Asparagine deprivation mediated by Salmonella asparaginase causes suppression of activation-induced T cell metabolic reprogramming. *J Leukoc Biol* 2016, **99**(2)**:** 387-398.

185. Palazon A, Goldrath AW, Nizet V, Johnson RS. HIF Transcription Factors, Inflammation, and Immunity. *Immunity* 2014, **41**(4)**:** 518-528.

186. Jantsch J, Chakravortty D, Turza N, Prechtel AT, Buchholz B, Gerlach RG*, et al.* Hypoxia and hypoxia-inducible factor-1 alpha modulate lipopolysaccharide-induced dendritic cell activation and function. *J Immunol* 2008, **180**(7)**:** 4697-4705.

187. Cramer T, Yamanishi Y, Clausen BE, Forster I, Pawlinski R, Mackman N*, et al.* HIF-1alpha is essential for myeloid cell-mediated inflammation. *Cell* 2003, **112**(5)**:** 645-657.

188. Wang GL, Jiang BH, Rue EA, Semenza GL. Hypoxia-inducible factor 1 is a basic-helix-loop-helix-PAS heterodimer regulated by cellular O2 tension. *Proc Natl Acad Sci U S A* 1995, **92**(12)**:** 5510-5514.

189. Semenza GL. Oxygen sensing, hypoxia-inducible factors, and disease pathophysiology. *Annu Rev Pathol* 2014, **9:** 47-71.

190. Ivan M, Kondo K, Yang H, Kim W, Valiando J, Ohh M*, et al.* HIFalpha targeted for VHL-mediated destruction by proline hydroxylation: implications for O2 sensing. *Science* 2001, **292**(5516)**:** 464-468.

191. D'Ignazio L, Bandarra D, Rocha S. NF-kappaB and HIF crosstalk in immune responses. *FEBS J* 2016, **283**(3)**:** 413-424.

192. Hu CJ, Wang LY, Chodosh LA, Keith B, Simon MC. Differential roles of hypoxia-inducible factor 1alpha (HIF-1alpha) and HIF-2alpha in hypoxic gene regulation. *Mol Cell Biol* 2003, **23**(24)**:** 9361-9374.

193. Blouin CC, Page EL, Soucy GM, Richard DE. Hypoxic gene activation by lipopolysaccharide in macrophages: implication of hypoxia-inducible factor 1alpha. *Blood* 2004, **103**(3)**:** 1124-1130.

194. Peyssonnaux C, Datta V, Cramer T, Doedens A, Theodorakis EA, Gallo RL*, et al.* HIF-1alpha expression regulates the bactericidal capacity of phagocytes. *J Clin Invest* 2005, **115**(7)**:** 1806-1815.

195. Rius J, Guma M, Schachtrup C, Akassoglou K, Zinkernagel AS, Nizet V*, et al.* NF-kappaB links innate immunity to the hypoxic response through transcriptional regulation of HIF-1alpha. *Nature* 2008, **453**(7196)**:** 807-811.

196. Walmsley SR, Print C, Farahi N, Peyssonnaux C, Johnson RS, Cramer T*, et al.* Hypoxia-induced neutrophil survival is mediated by HIF-1alpha-dependent NF-kappaB activity. *J Exp Med* 2005, **201**(1)**:** 105-115.

197. Culver C, Sundqvist A, Mudie S, Melvin A, Xirodimas D, Rocha S. Mechanism of hypoxia-induced NF-kappaB. *Mol Cell Biol* 2010, **30**(20)**:** 4901-4921.

198. Albina JE, Mastrofrancesco B, Vessella JA, Louis CA, Henry WL, Jr., Reichner JS. HIF-1 expression in healing wounds: HIF-1alpha induction in primary inflammatory cells by TNF-alpha. *Am J Physiol Cell Physiol* 2001, **281**(6)**:** C1971-1977.

199. Dang EV, Barbi J, Yang HY, Jinasena D, Yu H, Zheng Y*, et al.* Control of T(H)17/T(reg) balance by hypoxia-inducible factor 1. *Cell* 2011, **146**(5)**:** 772-784.

200. Hubbi ME, Hu H, Kshitiz, Ahmed I, Levchenko A, Semenza GL. Chaperone-mediated autophagy targets hypoxia-inducible factor-1alpha (HIF-1alpha) for lysosomal degradation. *J Biol Chem* 2013, **288**(15)**:** 10703-10714.

201. Ferreira JV, Fofo H, Bejarano E, Bento CF, Ramalho JS, Girao H*, et al.* STUB1/CHIP is required for HIF1A degradation by chaperone-mediated autophagy. *Autophagy* 2013, **9**(9)**:** 1349-1366.

202. Kaushik S, Cuervo AM. Chaperone-mediated autophagy: a unique way to enter the lysosome world. *Trends Cell Biol* 2012, **22**(8)**:** 407-417.

203. Ferreira JV, Soares AR, Ramalho JS, Pereira P, Girao H. K63 linked ubiquitin chain formation is a signal for HIF1A degradation by Chaperone-Mediated Autophagy. *Sci Rep* 2015, **5:** 10210.

204. Cramer T, Johnson RS. A novel role for the hypoxia inducible transcription factor HIF-1alpha: critical regulation of inflammatory cell function. *Cell Cycle* 2003, **2**(3)**:** 192-193.

205. Peyssonnaux C, Cejudo-Martin P, Doedens A, Zinkernagel AS, Johnson RS, Nizet V. Cutting edge: Essential role of hypoxia inducible factor-1alpha in development of lipopolysaccharide-induced sepsis. *J Immunol* 2007, **178**(12)**:** 7516-7519.

206. Elks PM, van Eeden FJ, Dixon G, Wang X, Reyes-Aldasoro CC, Ingham PW*, et al.* Activation of hypoxia-inducible factor-1alpha (Hif-1alpha) delays inflammation resolution by reducing neutrophil apoptosis and reverse migration in a zebrafish inflammation model. *Blood* 2011, **118**(3)**:** 712-722.

207. Kohler T, Reizis B, Johnson RS, Weighardt H, Forster I. Influence of hypoxia-inducible factor 1alpha on dendritic cell differentiation and migration. *Eur J Immunol* 2012, **42**(5)**:** 1226-1236.

208. Fluck K, Breves G, Fandrey J, Winning S. Hypoxia-inducible factor 1 in dendritic cells is crucial for the activation of protective regulatory T cells in murine colitis. *Mucosal Immunol* 2015.

209. Mimouna S, Bazin M, Mograbi B, Darfeuille-Michaud A, Brest P, Hofman P*, et al.* HIF1A regulates xenophagic degradation of adherent and invasive Escherichia coli (AIEC). *Autophagy* 2014, **10**(12)**:** 2333-2345.

210. Doedens AL, Phan AT, Stradner MH, Fujimoto JK, Nguyen JV, Yang E*, et al.* Hypoxia-inducible factors enhance the effector responses of CD8(+) T cells to persistent antigen. *Nat Immunol* 2013, **14**(11)**:** 1173-1182.

211. Finlay DK, Rosenzweig E, Sinclair LV, Feijoo-Carnero C, Hukelmann JL, Rolf J*, et al.* PDK1 regulation of mTOR and hypoxia-inducible factor 1 integrate metabolism and migration of CD8+ T cells. *J Exp Med* 2012, **209**(13)**:** 2441-2453.

212. Kojima H, Gu H, Nomura S, Caldwell CC, Kobata T, Carmeliet P*, et al.* Abnormal B lymphocyte development and autoimmunity in hypoxia-inducible factor 1alpha -deficient chimeric mice. *Proc Natl Acad Sci U S A* 2002, **99**(4)**:** 2170-2174.

213. Robinson A, Keely S, Karhausen J, Gerich ME, Furuta GT, Colgan SP. Mucosal protection by hypoxia-inducible factor prolyl hydroxylase inhibition. *Gastroenterology* 2008, **134**(1)**:** 145-155.

214. Keely S, Campbell EL, Baird AW, Hansbro PM, Shalwitz RA, Kotsakis A*, et al.* Contribution of epithelial innate immunity to systemic protection afforded by prolyl hydroxylase inhibition in murine colitis. *Mucosal Immunol* 2014, **7**(1)**:** 114-123.

215. Cummins EP, Doherty GA, Taylor CT. Hydroxylases as therapeutic targets in inflammatory bowel disease. *Lab Invest* 2013, **93**(4)**:** 378-383.

216. Xue X, Ramakrishnan S, Anderson E, Taylor M, Zimmermann EM, Spence JR*, et al.* Endothelial PAS domain protein 1 activates the inflammatory response in the intestinal epithelium to promote colitis in mice. *Gastroenterology* 2013, **145**(4)**:** 831-841.

217. O'Neill LA, Pearce EJ. Immunometabolism governs dendritic cell and macrophage function. *J Exp Med* 2016, **213**(1)**:** 15-23.

218. Warburg O, Wind F, Negelein E. The Metabolism of Tumors in the Body. *J Gen Physiol* 1927, **8**(6)**:** 519-530.

219. Krawczyk CM, Holowka T, Sun J, Blagih J, Amiel E, DeBerardinis RJ*, et al.* Toll-like receptor-induced changes in glycolytic metabolism regulate dendritic cell activation. *Blood* 2010, **115**(23)**:** 4742-4749.

220. Pearce EL, Pearce EJ. Metabolic pathways in immune cell activation and quiescence. *Immunity* 2013, **38**(4)**:** 633-643.

221. Martinez FO, Gordon S. The M1 and M2 paradigm of macrophage activation: time for reassessment. *F1000Prime Rep* 2014, **6:** 13.

222. Anthony RM, Rutitzky LI, Urban JF, Jr., Stadecker MJ, Gause WC. Protective immune mechanisms in helminth infection. *Nat Rev Immunol* 2007, **7**(12)**:** 975-987.

223. Nagy C, Haschemi A. Time and Demand are Two Critical Dimensions of Immunometabolism: The Process of Macrophage Activation and the Pentose Phosphate Pathway. *Front Immunol* 2015, **6:** 164.

224. Haschemi A, Kosma P, Gille L, Evans CR, Burant CF, Starkl P*, et al.* The sedoheptulose kinase CARKL directs macrophage polarization through control of glucose metabolism. *Cell Metab* 2012, **15**(6)**:** 813-826.

225. Tannahill GM, Curtis AM, Adamik J, Palsson-McDermott EM, McGettrick AF, Goel G*, et al.* Succinate is an inflammatory signal that induces IL-1beta through HIF-1alpha. *Nature* 2013, **496**(7444)**:** 238-242.

226. Jha AK, Huang SC, Sergushichev A, Lampropoulou V, Ivanova Y, Loginicheva E*, et al.* Network integration of parallel metabolic and transcriptional data reveals metabolic modules that regulate macrophage polarization. *Immunity* 2015, **42**(3)**:** 419-430.

227. Kelly B, O'Neill LA. Metabolic reprogramming in macrophages and dendritic cells in innate immunity. *Cell Res* 2015, **25**(7)**:** 771-784.

228. Rath M, Muller I, Kropf P, Closs EI, Munder M. Metabolism via Arginase or Nitric Oxide Synthase: Two Competing Arginine Pathways in Macrophages. *Front Immunol* 2014, **5:** 532.

229. Everts B, Amiel E, van der Windt GJ, Freitas TC, Chott R, Yarasheski KE*, et al.* Commitment to glycolysis sustains survival of NO-producing inflammatory dendritic cells. *Blood* 2012, **120**(7)**:** 1422-1431.

230. Cleeter MW, Cooper JM, Darley-Usmar VM, Moncada S, Schapira AH. Reversible inhibition of cytochrome c oxidase, the terminal enzyme of the mitochondrial respiratory chain, by nitric oxide. Implications for neurodegenerative diseases. *FEBS Lett* 1994, **345**(1)**:** 50-54.

231. Infantino V, Convertini P, Cucci L, Panaro MA, Di Noia MA, Calvello R*, et al.* The mitochondrial citrate carrier: a new player in inflammation. *Biochem J* 2011, **438**(3)**:** 433-436.

232. Michelucci A, Cordes T, Ghelfi J, Pailot A, Reiling N, Goldmann O*, et al.* Immune-responsive gene 1 protein links metabolism to immunity by catalyzing itaconic acid production. *Proc Natl Acad Sci U S A* 2013, **110**(19)**:** 7820-7825.

233. Mills EL, Kelly B, Logan A, Costa AS, Varma M, Bryant CE*, et al.* Succinate Dehydrogenase Supports Metabolic Repurposing of Mitochondria to Drive Inflammatory Macrophages. *Cell* 2016, **167**(2)**:** 457-470 e413.

234. Vats D, Mukundan L, Odegaard JI, Zhang L, Smith KL, Morel CR*, et al.* Oxidative metabolism and PGC-1beta attenuate macrophage-mediated inflammation. *Cell Metab* 2006, **4**(1)**:** 13-24.

235. Huang SC, Everts B, Ivanova Y, O'Sullivan D, Nascimento M, Smith AM*, et al.* Cell-intrinsic lysosomal lipolysis is essential for alternative activation of macrophages. *Nat Immunol* 2014, **15**(9)**:** 846-855.

236. Albina JE, Mills CD, Henry WL, Jr., Caldwell MD. Temporal expression of different pathways of 1-arginine metabolism in healing wounds. *J Immunol* 1990, **144**(10)**:** 3877-3880.

237. Drummond RA, Collar AL, Swamydas M, Rodriguez CA, Lim JK, Mendez LM*, et al.* CARD9-Dependent Neutrophil Recruitment Protects against Fungal Invasion of the Central Nervous System. *PLoS Pathog* 2015, **11**(12)**:** e1005293.

238. van der Windt GJW, Everts B, Chang CH, Curtis JD, Freitas TC, Amiel E*, et al.* Mitochondrial Respiratory Capacity Is a Critical Regulator of CD8(+) T Cell Memory Development. *Immunity* 2012, **36**(1)**:** 68-78.

239. Ecker J, Liebisch G, Englmaier M, Grandl M, Robenek H, Schmitz G. Induction of fatty acid synthesis is a key requirement for phagocytic differentiation of human monocytes. *Proc Natl Acad Sci U S A* 2010, **107**(17)**:** 7817-7822.

240. Cader MZ, Boroviak K, Zhang Q, Assadi G, Kempster SL, Sewell GW*, et al.* C13orf31 (FAMIN) is a central regulator of immunometabolic function. *Nat Immunol* 2016, **17**(9)**:** 1046-1056.

241. Wakil SM, Monies DM, Abouelhoda M, Al-Tassan N, Al-Dusery H, Naim EA*, et al.* Association of a mutation in LACC1 with a monogenic form of systemic juvenile idiopathic arthritis. *Arthritis Rheumatol* 2015, **67**(1)**:** 288-295.

242. Liu H, Irwanto A, Fu X, Yu G, Yu Y, Sun Y*, et al.* Discovery of six new susceptibility loci and analysis of pleiotropic effects in leprosy. *Nat Genet* 2015, **47**(3)**:** 267-271.

243. Patel N, El Mouzan MI, Al-Mayouf SM, Adly N, Mohamed JY, Al Mofarreh MA*, et al.* Study of Mendelian forms of Crohn's disease in Saudi Arabia reveals novel risk loci and alleles. *Gut* 2014, **63**(11)**:** 1831-1832.

244. Satpathy AT, Wu X, Albring JC, Murphy KM. Re(de)fining the dendritic cell lineage. *Nat Immunol* 2012, **13**(12)**:** 1145-1154.

245. Mellman I, Steinman RM. Dendritic cells: specialized and regulated antigen processing machines. *Cell* 2001, **106**(3)**:** 255-258.

246. Everts B, Amiel E, Huang SC, Smith AM, Chang CH, Lam WY*, et al.* TLR-driven early glycolytic reprogramming via the kinases TBK1-IKKvarepsilon supports the anabolic demands of dendritic cell activation. *Nat Immunol* 2014, **15**(4)**:** 323-332.

247. Malinarich F, Duan K, Hamid RA, Bijin A, Lin WX, Poidinger M*, et al.* High mitochondrial respiration and glycolytic capacity represent a metabolic phenotype of human tolerogenic dendritic cells. *J Immunol* 2015, **194**(11)**:** 5174-5186.

248. Pearce EJ, Everts B. Dendritic cell metabolism. *Nat Rev Immunol* 2015, **15**(1)**:** 18-29.

249. Lane N, Martin W. The energetics of genome complexity. *Nature* 2010, **467**(7318)**:** 929-934.

250. West AP, Shadel GS, Ghosh S. Mitochondria in innate immune responses. *Nat Rev Immunol* 2011, **11**(6)**:** 389-402.

251. Schmidt O, Pfanner N, Meisinger C. Mitochondrial protein import: from proteomics to functional mechanisms. *Nat Rev Mol Cell Biol* 2010, **11**(9)**:** 655-667.

252. Mills EL, Kelly B, O'Neill LAJ. Mitochondria are the powerhouses of immunity. *Nat Immunol* 2017, **18**(5)**:** 488-498.

253. Garaude J, Acin-Perez R, Martinez-Cano S, Enamorado M, Ugolini M, Nistal-Villan E*, et al.* Mitochondrial respiratory-chain adaptations in macrophages contribute to antibacterial host defense. *Nat Immunol* 2016, **17**(9)**:** 1037-1045.

254. Buck MD, O'Sullivan D, Klein Geltink RI, Curtis JD, Chang CH, Sanin DE*, et al.* Mitochondrial Dynamics Controls T Cell Fate through Metabolic Programming. *Cell* 2016, **166**(1)**:** 63-76.

255. West AP, Brodsky IE, Rahner C, Woo DK, Erdjument-Bromage H, Tempst P*, et al.* TLR signalling augments macrophage bactericidal activity through mitochondrial ROS. *Nature* 2011, **472**(7344)**:** 476-480.

256. Vogel RO, Janssen RJ, van den Brand MA, Dieteren CE, Verkaart S, Koopman WJ*, et al.* Cytosolic signaling protein Ecsit also localizes to mitochondria where it interacts with chaperone NDUFAF1 and functions in complex I assembly. *Genes Dev* 2007, **21**(5)**:** 615-624.

257. Emre Y, Hurtaud C, Nubel T, Criscuolo F, Ricquier D, Cassard-Doulcier AM. Mitochondria contribute to LPS-induced MAPK activation via uncoupling protein UCP2 in macrophages. *Biochem J* 2007, **402**(2)**:** 271-278.

258. Arsenijevic D, Onuma H, Pecqueur C, Raimbault S, Manning BS, Miroux B*, et al.* Disruption of the uncoupling protein-2 gene in mice reveals a role in immunity and reactive oxygen species production. *Nat Genet* 2000, **26**(4)**:** 435-439.

259. Bai Y, Onuma H, Bai X, Medvedev AV, Misukonis M, Weinberg JB*, et al.* Persistent nuclear factor-kappa B activation in Ucp2-/- mice leads to enhanced nitric oxide and inflammatory cytokine production. *J Biol Chem* 2005, **280**(19)**:** 19062-19069.

260. Sonoda J, Laganiere J, Mehl IR, Barish GD, Chong LW, Li X*, et al.* Nuclear receptor ERR alpha and coactivator PGC-1 beta are effectors of IFN-gamma-induced host defense. *Genes Dev* 2007, **21**(15)**:** 1909-1920.

261. Schroder K, Tschopp J. The inflammasomes. *Cell* 2010, **140**(6)**:** 821-832.

262. Heid ME, Keyel PA, Kamga C, Shiva S, Watkins SC, Salter RD. Mitochondrial reactive oxygen species induces NLRP3-dependent lysosomal damage and inflammasome activation. *J Immunol* 2013, **191**(10)**:** 5230-5238.

263. Bulua AC, Simon A, Maddipati R, Pelletier M, Park H, Kim KY*, et al.* Mitochondrial reactive oxygen species promote production of proinflammatory cytokines and are elevated in TNFR1-associated periodic syndrome (TRAPS). *J Exp Med* 2011, **208**(3)**:** 519-533.

264. Weinberg SE, Sena LA, Chandel NS. Mitochondria in the regulation of innate and adaptive immunity. *Immunity* 2015, **42**(3)**:** 406-417.

265. Seth RB, Sun LJ, Ea CK, Chen ZJJ. Identification and characterization of MAVS, a mitochondrial antiviral signaling protein that activates NF-kappa B and IRF3. *Cell* 2005, **122**(5)**:** 669-682.

266. Castanier C, Garcin D, Vazquez A, Arnoult D. Mitochondrial dynamics regulate the RIG-I-like receptor antiviral pathway. *Embo Reports* 2010, **11**(2)**:** 133-138.

267. Tal MC, Sasai M, Lee HK, Yordy B, Shadel GS, Iwasaki A. Absence of autophagy results in reactive oxygen species-dependent amplification of RLR signaling. *Proc Natl Acad Sci U S A* 2009, **106**(8)**:** 2770-2775.

268. Park S, Juliana C, Hong S, Datta P, Hwang I, Fernandes-Alnemri T*, et al.* The mitochondrial antiviral protein MAVS associates with NLRP3 and regulates its inflammasome activity. *J Immunol* 2013, **191**(8)**:** 4358-4366.

269. Iyer SS, He Q, Janczy JR, Elliott EI, Zhong Z, Olivier AK*, et al.* Mitochondrial cardiolipin is required for Nlrp3 inflammasome activation. *Immunity* 2013, **39**(2)**:** 311-323.

270. Zhang Q, Raoof M, Chen Y, Sumi Y, Sursal T, Junger W*, et al.* Circulating mitochondrial DAMPs cause inflammatory responses to injury. *Nature* 2010, **464**(7285)**:** 104-107.

271. West AP, Shadel GS. Mitochondrial DNA in innate immune responses and inflammatory pathology. *Nat Rev Immunol* 2017, **17**(6)**:** 363-375.

272. Nakahira K, Haspel JA, Rathinam VA, Lee SJ, Dolinay T, Lam HC*, et al.* Autophagy proteins regulate innate immune responses by inhibiting the release of mitochondrial DNA mediated by the NALP3 inflammasome. *Nat Immunol* 2011, **12**(3)**:** 222-230.

273. Jabir MS, Hopkins L, Ritchie ND, Ullah I, Bayes HK, Li D*, et al.* Mitochondrial damage contributes to Pseudomonas aeruginosa activation of the inflammasome and is downregulated by autophagy. *Autophagy* 2015, **11**(1)**:** 166-182.

274. Lood C, Blanco LP, Purmalek MM, Carmona-Rivera C, De Ravin SS, Smith CK*, et al.* Neutrophil extracellular traps enriched in oxidized mitochondrial DNA are interferogenic and contribute to lupus-like disease. *Nat Med* 2016, **22**(2)**:** 146-153.

275. West AP, Khoury-Hanold W, Staron M, Tal MC, Pineda CM, Lang SM*, et al.* Mitochondrial DNA stress primes the antiviral innate immune response. *Nature* 2015, **520**(7548)**:** 553-557.

276. Zhou R, Yazdi AS, Menu P, Tschopp J. A role for mitochondria in NLRP3 inflammasome activation. *Nature* 2011, **469**(7329)**:** 221-225.

277. Delpre G, Avidor I, Steinherz R, Kadish U, Ben-Bassat M. Ultrastructural abnormalities in endoscopically and histologically normal and involved colon in ulcerative colitis. *Am J Gastroenterol* 1989, **84**(9)**:** 1038-1046.

278. Rodenburg W, Keijer J, Kramer E, Vink C, van der Meer R, Bovee-Oudenhoven IM. Impaired barrier function by dietary fructo-oligosaccharides (FOS) in rats is accompanied by increased colonic mitochondrial gene expression. *BMC Genomics* 2008, **9:** 144.

279. Beltran B, Nos P, Dasi F, Iborra M, Bastida G, Martinez M*, et al.* Mitochondrial Dysfunction, Persistent Oxidative Damage, and Catalase Inhibition in Immune Cells of Naive and Treated Crohn's Disease. *Inflammatory Bowel Diseases* 2010, **16**(1)**:** 76-86.

280. Mottawea W, Chiang CK, Muhlbauer M, Starr AE, Butcher J, Abujamel T*, et al.* Altered intestinal microbiota-host mitochondria crosstalk in new onset Crohn's disease. *Nat Commun* 2016, **7:** 13419.

281. Novak EA, Mollen KP. Mitochondrial dysfunction in inflammatory bowel disease. *Front Cell Dev Biol* 2015, **3:** 62.

282. Shekhawat PS, Srinivas SR, Matern D, Bennett MJ, Boriack R, George V*, et al.* Spontaneous development of intestinal and colonic atrophy and inflammation in the carnitine-deficient jvs (OCTN2(-/-)) mice. *Mol Genet Metab* 2007, **92**(4)**:** 315-324.

283. Bar F, Bochmann W, Widok A, Von Medem K, Pagel R, Hirose M*, et al.* Mitochondrial Gene Polymorphisms That Protect Mice From Colitis. *Gastroenterology* 2013, **145**(5)**:** 1055-+.

284. Uhlen M, Fagerberg L, Hallstrom BM, Lindskog C, Oksvold P, Mardinoglu A*, et al.* Proteomics. Tissue-based map of the human proteome. *Science* 2015, **347**(6220)**:** 1260419.

285. Kawaguchi Y, Okamoto T, Taniwaki M, Aizawa M, Inoue M, Katayama S*, et al.* Cag Expansions in a Novel Gene for Machado-Joseph Disease at Chromosome 14q32.1. *Nature Genetics* 1994, **8**(3)**:** 221-228.

286. Evers MM, Toonen LJ, van Roon-Mom WM. Ataxin-3 protein and RNA toxicity in spinocerebellar ataxia type 3: current insights and emerging therapeutic strategies. *Mol Neurobiol* 2014, **49**(3)**:** 1513-1531.

287. Schmitt I, Linden M, Khazneh H, Evert BO, Breuer P, Klockgether T*, et al.* Inactivation of the mouse Atxn3 (ataxin-3) gene increases protein ubiquitination. *Biochem Biophys Res Commun* 2007, **362**(3)**:** 734-739.

288. Switonski PM, Szlachcic WJ, Krzyzosiak WJ, Figiel M. A new humanized ataxin-3 knock-in mouse model combines the genetic features, pathogenesis of neurons and glia and late disease onset of SCA3/MJD. *Neurobiol Dis* 2015, **73:** 174-188.

289. Tait D, Riccio M, Sittler A, Scherzinger E, Santi S, Ognibene A*, et al.* Ataxin-3 is transported into the nucleus and associates with the nuclear matrix. *Human Molecular Genetics* 1998, **7**(6)**:** 991-997.

290. Pozzi C, Valtorta M, Tedeschi G, Galbusera E, Pastori V, Bigi A*, et al.* Study of subcellular localization and proteolysis of ataxin-3. *Neurobiol Dis* 2008, **30**(2)**:** 190-200.

291. Antony PMA, Mantele S, Mollenkopf P, Boy J, Kehlenbach RH, Riess O*, et al.* Identification and functional dissection of localization signals within ataxin-3. *Neurobiology of Disease* 2009, **36**(2)**:** 280-292.

292. Mueller T, Breuer P, Schmitt I, Walter J, Evert BO, Wullner U. CK2-dependent phosphorylation determines cellular localization and stability of ataxin-3. *Hum Mol Genet* 2009, **18**(17)**:** 3334-3343.

293. Pastori V, Sangalli E, Coccetti P, Pozzi C, Nonnis S, Tedeschi G*, et al.* CK2 and GSK3 phosphorylation on S29 controls wild-type ATXN3 nuclear uptake. *Biochim Biophys Acta* 2010, **1802**(7-8)**:** 583-592

294. Trottier Y, Cancel G, An-Gourfinkel I, Lutz Y, Weber C, Brice A*, et al.* Heterogeneous intracellular localization and expression of ataxin-3. *Neurobiol Dis* 1998, **5**(5)**:** 335-347.

295. Wang Q, Li L, Ye Y. Regulation of retrotranslocation by p97-associated deubiquitinating enzyme ataxin-3. *J Cell Biol* 2006, **174**(7)**:** 963-971.

296. Nicastro G, Menon RP, Masino L, Knowles PP, McDonald NQ, Pastore A. The solution structure of the Josephin domain of ataxin-3: structural determinants for molecular recognition. *Proc Natl Acad Sci U S A* 2005, **102**(30)**:** 10493-10498.

297. Berke SJ, Chai Y, Marrs GL, Wen H, Paulson HL. Defining the role of ubiquitin-interacting motifs in the polyglutamine disease protein, ataxin-3. *J Biol Chem* 2005, **280**(36)**:** 32026-32034.

298. Nicastro G, Masino L, Esposito V, Menon RP, De Simone A, Fraternali F*, et al.* Josephin domain of ataxin-3 contains two distinct ubiquitin-binding sites. *Biopolymers* 2009, **91**(12)**:** 1203-1214.

299. Burnett B, Li FS, Pittman RN. The polyglutamine neurodegenerative protein ataxin-3 binds polyubiquitylated proteins and has ubiquitin protease activity. *Human Molecular Genetics* 2003, **12**(23)**:** 3195-3205.

300. Winborn BJ, Travis SM, Todi SV, Scaglione KM, Xu P, Williams AJ*, et al.* The deubiquitinating enzyme ataxin-3, a polyglutamine disease protein, edits Lys63 linkages in mixed linkage ubiquitin chains. *J Biol Chem* 2008, **283**(39)**:** 26436-26443.

301. Todi SV, Winborn BJ, Scaglione KM, Blount JR, Travis SM, Paulson HL. Ubiquitination directly enhances activity of the deubiquitinating enzyme ataxin-3. *Embo Journal* 2009, **28**(4)**:** 372-382.

302. Todi SV, Scaglione KM, Blount JR, Basrur V, Conlon KP, Pastore A*, et al.* Activity and cellular functions of the deubiquitinating enzyme and polyglutamine disease protein ataxin-3 are regulated by ubiquitination at lysine 117. *J Biol Chem* 2010, **285**(50)**:** 39303-39313.

303. Fei E, Jia N, Zhang T, Ma X, Wang H, Liu C*, et al.* Phosphorylation of ataxin-3 by glycogen synthase kinase 3beta at serine 256 regulates the aggregation of ataxin-3. *Biochem Biophys Res Commun* 2007, **357**(2)**:** 487-492.

304. Mao Y, Senic-Matuglia F, Di Fiore PP, Polo S, Hodsdon ME, De Camilli P. Deubiquitinating function of ataxin-3: insights from the solution structure of the Josephin domain. *Proc Natl Acad Sci U S A* 2005, **102**(36)**:** 12700-12705.

305. Matos CA, Nobrega C, Louros SR, Almeida B, Ferreiro E, Valero J*, et al.* Ataxin-3 phosphorylation decreases neuronal defects in spinocerebellar ataxia type 3 models. *J Cell Biol* 2016, **212**(4)**:** 465-480.

306. Doss-Pepe EW, Stenroos ES, Johnson WG, Madura K. Ataxin-3 interactions with rad23 and valosin-containing protein and its associations with ubiquitin chains and the proteasome are consistent with a role in ubiquitin-mediated proteolysis. *Mol Cell Biol* 2003, **23**(18)**:** 6469-6483.

307. Paulson H. Machado-Joseph disease/spinocerebellar ataxia type 3. *Handb Clin Neurol* 2012, **103:** 437-449.

308. Zhong X, Pittman RN. Ataxin-3 binds VCP/p97 and regulates retrotranslocation of ERAD substrates. *Hum Mol Genet* 2006, **15**(16)**:** 2409-2420.

309. Scaglione KM, Zavodszky E, Todi SV, Patury S, Xu P, Rodriguez-Lebron E*, et al.* Ube2w and ataxin-3 coordinately regulate the ubiquitin ligase CHIP. *Mol Cell* 2011, **43**(4)**:** 599-612.

310. Zhu X, Zhang J, Sun H, Jiang C, Dong Y, Shan Q*, et al.* Ubiquitination of inositol-requiring enzyme 1 (IRE1) by the E3 ligase CHIP mediates the IRE1/TRAF2/JNK pathway. *J Biol Chem* 2014, **289**(44)**:** 30567-30577.

311. Laco MN, Cortes L, Travis SM, Paulson HL, Rego AC. Valosin-containing protein (VCP/p97) is an activator of wild-type ataxin-3. *PLoS One* 2012, **7**(9)**:** e43563.

312. Yang M, Wang C, Zhu X, Tang S, Shi L, Cao X*, et al.* E3 ubiquitin ligase CHIP facilitates Toll-like receptor signaling by recruiting and polyubiquitinating Src and atypical PKC{zeta}. *J Exp Med* 2011, **208**(10)**:** 2099-2112.

313. Shang Y, He J, Wang Y, Feng Q, Zhang Y, Guo J*, et al.* CHIP/Stub1 regulates the Warburg effect by promoting degradation of PKM2 in ovarian carcinoma. *Oncogene* 2017.

314. Kitada T, Asakawa S, Hattori N, Matsumine H, Yamamura Y, Minoshima S*, et al.* Mutations in the parkin gene cause autosomal recessive juvenile parkinsonism. *Nature* 1998, **392**(6676)**:** 605-608.

315. Ali S, Vollaard AM, Widjaja S, Surjadi C, van de Vosse E, van Dissel JT. PARK2/PACRG polymorphisms and susceptibility to typhoid and paratyphoid fever. *Clin Exp Immunol* 2006, **144**(3)**:** 425-431.

316. Mira MT, Alcais A, Nguyen VT, Moraes MO, Di Flumeri C, Vu HT*, et al.* Susceptibility to leprosy is associated with PARK2 and PACRG. *Nature* 2004, **427**(6975)**:** 636-640.

317. Durcan TM, Kontogiannea M, Thorarinsdottir T, Fallon L, Williams AJ, Djarmati A*, et al.* The Machado-Joseph disease-associated mutant form of ataxin-3 regulates parkin ubiquitination and stability. *Hum Mol Genet* 2011, **20**(1)**:** 141-154.

318. Tanaka A, Cleland MM, Xu S, Narendra DP, Suen DF, Karbowski M*, et al.* Proteasome and p97 mediate mitophagy and degradation of mitofusins induced by Parkin. *J Cell Biol* 2010, **191**(7)**:** 1367-1380.

319. Geisler S, Holmstrom KM, Skujat D, Fiesel FC, Rothfuss OC, Kahle PJ*, et al.* PINK1/Parkin-mediated mitophagy is dependent on VDAC1 and p62/SQSTM1. *Nature Cell Biology* 2010, **12**(2)**:** 119-U170.

320. Durcan TM, Tang MY, Perusse JR, Dashti EA, Aguileta MA, McLelland GL*, et al.* USP8 regulates mitophagy by removing K6-linked ubiquitin conjugates from parkin. *EMBO J* 2014, **33**(21)**:** 2473-2491.

321. Burnett BG, Pittman RN. The polyglutamine neurodegenerative protein ataxin 3 regulates aggresome formation. *Proc Natl Acad Sci U S A* 2005, **102**(12)**:** 4330-4335.

322. Tyedmers J, Mogk A, Bukau B. Cellular strategies for controlling protein aggregation. *Nat Rev Mol Cell Biol* 2010, **11**(11)**:** 777-788.

323. Wang H, Ying Z, Wang G. Ataxin-3 regulates aggresome formation of copper-zinc superoxide dismutase (SOD1) by editing K63-linked polyubiquitin chains. *J Biol Chem* 2012, **287**(34)**:** 28576-28585.

324. Chatterjee A, Saha S, Chakraborty A, Silva-Fernandes A, Mandal SM, Neves-Carvalho A*, et al.* The role of the mammalian DNA end-processing enzyme polynucleotide kinase 3'-phosphatase in spinocerebellar ataxia type 3 pathogenesis. *PLoS Genet* 2015, **11**(1)**:** e1004749.

325. Gao R, Liu Y, Silva-Fernandes A, Fang X, Paulucci-Holthauzen A, Chatterjee A*, et al.* Inactivation of PNKP by mutant ATXN3 triggers apoptosis by activating the DNA damage-response pathway in SCA3. *PLoS Genet* 2015, **11**(1)**:** e1004834.

326. Tu Y, Liu H, Zhu X, Shen H, Ma X, Wang F*, et al.* Ataxin-3 promotes genome integrity by stabilizing Chk1. *Nucleic Acids Res* 2017.

327. Liu H, Li X, Ning G, Zhu S, Ma X, Liu X*, et al.* The Machado-Joseph Disease Deubiquitinase Ataxin-3 Regulates the Stability and Apoptotic Function of p53. *PLoS Biol* 2016, **14**(11)**:** e2000733.

328. Li F, Macfarlan T, Pittman RN, Chakravarti D. Ataxin-3 is a histone-binding protein with two independent transcriptional corepressor activities. *J Biol Chem* 2002, **277**(47)**:** 45004-45012.

329. Evert BO, Araujo J, Vieira-Saecker AM, de Vos RA, Harendza S, Klockgether T*, et al.* Ataxin-3 represses transcription via chromatin binding, interaction with histone deacetylase 3, and histone deacetylation. *J Neurosci* 2006, **26**(44)**:** 11474-11486.

330. Ashkenazi A, Bento CF, Ricketts T, Vicinanza M, Siddiqi F, Pavel M*, et al.* Polyglutamine tracts regulate beclin 1-dependent autophagy. *Nature* 2017, **545**(7652)**:** 108-111.

331. Wirawan E, Lippens S, Vanden Berghe T, Romagnoli A, Fimia GM, Piacentini M*, et al.* Beclin1: a role in membrane dynamics and beyond. *Autophagy* 2012, **8**(1)**:** 6-17.

332. Venegas V, Halberg MC. Measurement of mitochondrial DNA copy number. *Methods Mol Biol* 2012, **837:** 327-335.

333. Naldini L, Blomer U, Gallay P, Ory D, Mulligan R, Gage FH*, et al.* In vivo gene delivery and stable transduction of nondividing cells by a lentiviral vector. *Science* 1996, **272**(5259)**:** 263-267.

334. Pfisterer U, Kirkeby A, Torper O, Wood J, Nelander J, Dufour A*, et al.* Direct conversion of human fibroblasts to dopaminergic neurons. *Proc Natl Acad Sci U S A* 2011, **108**(25)**:** 10343-10348.

335. Cohen P. The origins of protein phosphorylation. *Nat Cell Biol* 2002, **4**(5)**:** E127-130.

336. Hunter T. Signaling--2000 and beyond. *Cell* 2000, **100**(1)**:** 113-127.

337. Venerando A, Cesaro L, Pinna LA. From phosphoproteins to phosphoproteomes: a historical account. *FEBS J* 2017.

338. Mann M, Ong SE, Gronborg M, Steen H, Jensen ON, Pandey A. Analysis of protein phosphorylation using mass spectrometry: deciphering the phosphoproteome. *Trends in Biotechnology* 2002, **20**(6)**:** 261-268.

339. Matthews HR. Protein-Kinases and Phosphatases That Act on Histidine, Lysine, or Arginine Residues in Eukaryotic Proteins - a Possible Regulator of the Mitogen-Activated Protein-Kinase Cascade. *Pharmacology & Therapeutics* 1995, **67**(3)**:** 323-350.

340. Serber Z, Ferrell JE, Jr. Tuning bulk electrostatics to regulate protein function. *Cell* 2007, **128**(3)**:** 441-444.

341. Oeckinghaus A, Ghosh S. The NF-kappaB family of transcription factors and its regulation. *Cold Spring Harb Perspect Biol* 2009, **1**(4)**:** a000034.

342. Christian F, Smith EL, Carmody RJ. The Regulation of NF-kappaB Subunits by Phosphorylation. *Cells* 2016, **5**(1).

343. Kosako H, Nagano K. Quantitative phosphoproteomics strategies for understanding protein kinase-mediated signal transduction pathways. *Expert Rev Proteomics* 2011, **8**(1)**:** 81-94.

344. Hornbeck PV, Zhang B, Murray B, Kornhauser JM, Latham V, Skrzypek E. PhosphoSitePlus, 2014: mutations, PTMs and recalibrations. *Nucleic Acids Res* 2015, **43**(Database issue)**:** D512-520.

345. Sjoelund V, Smelkinson M, Nita-Lazar A. Phosphoproteome profiling of the macrophage response to different toll-like receptor ligands identifies differences in global phosphorylation dynamics. *J Proteome Res* 2014, **13**(11)**:** 5185-5197.

346. Weintz G, Olsen JV, Fruhauf K, Niedzielska M, Amit I, Jantsch J*, et al.* The phosphoproteome of toll-like receptor-activated macrophages. *Mol Syst Biol* 2010, **6:** 371.

347. Uchida T, Rossignol F, Matthay MA, Mounier R, Couette S, Clottes E*, et al.* Prolonged hypoxia differentially regulates hypoxia-inducible factor (HIF)-1alpha and HIF-2alpha expression in lung epithelial cells: implication of natural antisense HIF-1alpha. *J Biol Chem* 2004, **279**(15)**:** 14871-14878.

348. Mancino A, Schioppa T, Larghi P, Pasqualini F, Nebuloni M, Chen IH*, et al.* Divergent effects of hypoxia on dendritic cell functions. *Blood* 2008, **112**(9)**:** 3723-3734.

349. Caradec J, Sirab N, Keumeugni C, Moutereau S, Chimingqi M, Matar C*, et al.* 'Desperate house genes': the dramatic example of hypoxia. *Br J Cancer* 2010, **102**(6)**:** 1037-1043.

350. Krock BL, Skuli N, Simon MC. Hypoxia-induced angiogenesis: good and evil. *Genes Cancer* 2011, **2**(12)**:** 1117-1133.

351. Blagoev B, Ong SE, Kratchmarova I, Mann M. Temporal analysis of phosphotyrosine-dependent signaling networks by quantitative proteomics. *Nat Biotechnol* 2004, **22**(9)**:** 1139-1145.

352. Khurana P, Sugadev R, Jain J, Singh SB. HypoxiaDB: a database of hypoxia-regulated proteins. *Database (Oxford)* 2013, **2013:** bat074.

353. Alangari A, Alsultan A, Adly N, Massaad MJ, Kiani IS, Aljebreen A*, et al.* LPS-responsive beige-like anchor (LRBA) gene mutation in a family with inflammatory bowel disease and combined immunodeficiency. *J Allergy Clin Immunol* 2012, **130**(2)**:** 481-488 e482.

354. Lopez-Herrera G, Tampella G, Pan-Hammarstrom Q, Herholz P, Trujillo-Vargas CM, Phadwal K*, et al.* Deleterious mutations in LRBA are associated with a syndrome of immune deficiency and autoimmunity. *Am J Hum Genet* 2012, **90**(6)**:** 986-1001.

355. Lee K, Ban HS, Naik R, Hong YS, Son S, Kim BK*, et al.* Identification of Malate Dehydrogenase 2 as a Target Protein of the HIF-1 Inhibitor LW6 using Chemical Probes. *Angewandte Chemie-International Edition* 2013, **52**(39)**:** 10286-10289.

356. Date H, Onodera O, Tanaka H, Iwabuchi K, Uekawa K, Igarashi S*, et al.* Early-onset ataxia with ocular motor apraxia and hypoalbuminemia is caused by mutations in a new HIT superfamily gene. *Nature Genetics* 2001, **29**(2)**:** 184-188.

357. Chu Y, Morfini GA, Langhamer LB, He Y, Brady ST, Kordower JH. Alterations in axonal transport motor proteins in sporadic and experimental Parkinson's disease. *Brain* 2012, **135**(Pt 7)**:** 2058-2073.

358. d'Ydewalle C, Bogaert E, Van Den Bosch L. HDAC6 at the Intersection of Neuroprotection and Neurodegeneration. *Traffic* 2012, **13**(6)**:** 771-779.

359. Patel H, Cross H, Proukakis C, Hershberger R, Bork P, Ciccarelli FD*, et al.* SPG20 is mutated in Troyer syndrome, an hereditary spastic paraplegia. *Nature Genetics* 2002, **31**(4)**:** 347-348.

360. Friedman MJ, Shah AG, Fang ZH, Ward EG, Warren ST, Li SH*, et al.* Polyglutamine domain modulates the TBP-TFIIB interaction: implications for its normal function and neurodegeneration. *Nature Neuroscience* 2007, **10**(12)**:** 1519-1528.

361. Perkins DN, Pappin DJC, Creasy DM, Cottrell JS. Probability-based protein identification by searching sequence databases using mass spectrometry data. *Electrophoresis* 1999, **20**(18)**:** 3551-3567.

362. Jackson AL, Burchard J, Leake D, Reynolds A, Schelter J, Guo J*, et al.* Position-specific chemical modification of siRNAs reduces "off-target" transcript silencing. *RNA* 2006, **12**(7)**:** 1197-1205.

363. Parsons BD, Schindler A, Evans DH, Foley E. A direct phenotypic comparison of siRNA pools and multiple individual duplexes in a functional assay. *PLoS One* 2009, **4**(12)**:** e8471.

364. Hannus M, Beitzinger M, Engelmann JC, Weickert MT, Spang R, Hannus S*, et al.* siPools: highly complex but accurately defined siRNA pools eliminate off-target effects. *Nucleic Acids Res* 2014, **42**(12)**:** 8049-8061.

365. Marques JT, Williams BR. Activation of the mammalian immune system by siRNAs. *Nat Biotechnol* 2005, **23**(11)**:** 1399-1405.

366. Du HW, Chen GY, Yang CH, Li CB, Xun YP, Liu J*, et al.* Multiple correlations of mRNA expression and protein abundance in human cytokine profile. *Mol Biol Rep* 2014, **41**(10)**:** 6985-6993.

367. Kijas AW, Harris JL, Harris JM, Lavin MF. Aprataxin forms a discrete branch in the HIT (histidine triad) superfamily of proteins with both DNA/RNA binding and nucleotide hydrolase activities. *J Biol Chem* 2006, **281**(20)**:** 13939-13948.

368. Tumbale P, Williams JS, Schellenberg MJ, Kunkel TA, Williams RS. Aprataxin resolves adenylated RNA-DNA junctions to maintain genome integrity. *Nature* 2014, **506**(7486)**:** 111-115.

369. Sykora P, Croteau DL, Bohr VA, Wilson DM, 3rd. Aprataxin localizes to mitochondria and preserves mitochondrial function. *Proc Natl Acad Sci U S A* 2011, **108**(18)**:** 7437-7442.

370. Akbari M, Sykora P, Bohr VA. Slow mitochondrial repair of 5'-AMP renders mtDNA susceptible to damage in APTX deficient cells. *Sci Rep* 2015, **5:** 12876.

371. Garcia-Diaz B, Barca E, Balreira A, Lopez LC, Tadesse S, Krishna S*, et al.* Lack of aprataxin impairs mitochondrial functions via downregulation of the APE1/NRF1/NRF2 pathway. *Hum Mol Genet* 2015, **24**(16)**:** 4516-4529.

372. Sano Y, Date H, Igarashi S, Onodera O, Oyake M, Takahashi T*, et al.* Aprataxin, the causative protein for EAOH is a nuclear protein with a potential role as a DNA repair protein. *Ann Neurol* 2004, **55**(2)**:** 241-249.

373. Nakad R, Schumacher B. DNA Damage Response and Immune Defense: Links and Mechanisms. *Front Genet* 2016, **7:** 147.

374. Weirather JL, Duggal P, Nascimento EL, Monteiro GR, Martins DR, Lacerda HG*, et al.* Fine mapping under linkage peaks for symptomatic or asymptomatic outcomes of Leishmania infantum infection in Brazil. *Infect Genet Evol* 2016, **43:** 1-5.

375. Nascimento MSL, Ferreira MD, Quirino GFS, Maruyama SR, Krishnaswamy JK, Liu D*, et al.* NOD2-RIP2-Mediated Signaling Helps Shape Adaptive Immunity in Visceral Leishmaniasis. *Journal of Infectious Diseases* 2016, **214**(11)**:** 1647-1657.

376. Li Y, Shin D, Kwon SH. Histone deacetylase 6 plays a role as a distinct regulator of diverse cellular processes. *Febs Journal* 2013, **280**(3)**:** 775-793.

377. Yan B, Xie SB, Liu Z, Ran J, Li YY, Wang J*, et al.* HDAC6 Deacetylase Activity Is Critical for Lipopolysaccharide-Induced Activation of Macrophages. *Plos One* 2014, **9**(10).

378. Wang B, Rao YH, Inoue M, Hao R, Lai CH, Chen D*, et al.* Microtubule acetylation amplifies p38 kinase signalling and anti-inflammatory IL-10 production. *Nat Commun* 2014, **5:** 3479.

379. Kawaguchi Y, Kovacs JJ, McLaurin A, Vance JM, Ito A, Yao TP. The deacetylase HDAC6 regulates aggresome formation and cell viability in response to misfolded protein stress. *Cell* 2003, **115**(6)**:** 727-738.

380. Lee JY, Koga H, Kawaguchi Y, Tang W, Wong E, Gao YS*, et al.* HDAC6 controls autophagosome maturation essential for ubiquitin-selective quality-control autophagy. *EMBO J* 2010, **29**(5)**:** 969-980.

381. Deribe YL, Wild P, Chandrashaker A, Curak J, Schmidt MH, Kalaidzidis Y*, et al.* Regulation of epidermal growth factor receptor trafficking by lysine deacetylase HDAC6. *Sci Signal* 2009, **2**(102)**:** ra84.

382. Watabe M, Nakaki T. Protein kinase CK2 regulates the formation and clearance of aggresomes in response to stress. *J Cell Sci* 2011, **124**(Pt 9)**:** 1519-1532.

383. Roberts AJ, Kon T, Knight PJ, Sutoh K, Burgess SA. Functions and mechanics of dynein motor proteins. *Nat Rev Mol Cell Biol* 2013, **14**(11)**:** 713-726.

384. Tai AW, Chuang JZ, Bode C, Wolfrum U, Sung CH. Rhodopsin's carboxy-terminal cytoplasmic tail acts as a membrane receptor for cytoplasmic dynein by binding to the dynein light chain Tctex-1. *Cell* 1999, **97**(7)**:** 877-887.

385. Yeh TY, Chuang JZ, Sung CH. Dynein light chain rp3 acts as a nuclear matrix-associated transcriptional modulator in a dyneinin-dependent pathway. *Journal of Cell Science* 2005, **118**(15)**:** 3431-3443.

386. Vahedi S, Rajabian M, Misaghian A, Grbec D, Simon HH, Alavian KN. Parkinson's disease candidate gene prioritization based on expression profile of midbrain dopaminergic neurons. *J Biomed Sci* 2010, **17:** 66.

387. Arai T, Oh-ishi T, Yamamoto H, Nunoi H, Kamizono J, Uehara M*, et al.* Copy number variations due to large genomic deletion in X-linked chronic granulomatous disease. *PLoS One* 2012, **7**(2)**:** e27782.

388. Marks DJ, Miyagi K, Rahman FZ, Novelli M, Bloom SL, Segal AW. Inflammatory bowel disease in CGD reproduces the clinicopathological features of Crohn's disease. *Am J Gastroenterol* 2009, **104**(1)**:** 117-124.

389. Chicca JJ, 2nd, Auble DT, Pugh BF. Cloning and biochemical characterization of TAF-172, a human homolog of yeast Mot1. *Mol Cell Biol* 1998, **18**(3)**:** 1701-1710.

390. Stevanin G, Brice A. Spinocerebellar ataxia 17 (SCA17) and Huntington's disease-like 4 (HDL4). *Cerebellum* 2008, **7**(2)**:** 170-178.

391. Klejman MP, Zhao XM, van Schaik FMA, Herr W, Timmers HTM. Mutational analysis of BTAF1-TBP interaction: BTAF1 can rescue DNA-binding defective TBP mutants. *Nucleic Acids Research* 2005, **33**(17)**:** 5426-5436.

392. Yagi Y, Ip YT. Helicase89B is a Mot1p/BTAF1 homologue that mediates an antimicrobial response in Drosophila. *Embo Reports* 2005, **6**(11)**:** 1088-1094.

393. Wang JW, Howson J, Haller E, Kerr WG. Identification of a novel lipopolysaccharide-inducible gene with key features of both a kinase anchor proteins and chs1/beige proteins. *Journal of Immunology* 2001, **166**(7)**:** 4586-4595.

394. Alkhairy OK, Abolhassani H, Rezaei N, Fang M, Andersen KK, Chavoshzadeh Z*, et al.* Spectrum of Phenotypes Associated with Mutations in LRBA. *J Clin Immunol* 2016, **36**(1)**:** 33-45.

395. Lo B, Zhang KJ, Lu W, Zheng LX, Zhang Q, Kanellopoulou C*, et al.* Patients with LRBA deficiency show CTLA4 loss and immune dysregulation responsive to abatacept therapy. *Science* 2015, **349**(6246)**:** 436-440.

396. Gamez-Diaz L, Neumann J, Jager F, Proietti M, Felber F, Soulas-Sprauel P*, et al.* Immunological phenotype of the murine Lrba knockout. *Immunol Cell Biol* 2017.

397. Costello CM, Howell K, Cahill E, McBryan J, Konigshoff M, Eickelberg O*, et al.* Lung-selective gene responses to alveolar hypoxia: potential role for the bone morphogenetic antagonist gremlin in pulmonary hypertension. *Am J Physiol Lung Cell Mol Physiol* 2008, **295**(2)**:** L272-284.

398. Hu H, Sun SC. Ubiquitin signaling in immune responses. *Cell Res* 2016, **26**(4)**:** 457-483.

399. Heng TS, Painter MW, Immunological Genome Project C. The Immunological Genome Project: networks of gene expression in immune cells. *Nat Immunol* 2008, **9**(10)**:** 1091-1094.

400. Wu C, Orozco C, Boyer J, Leglise M, Goodale J, Batalov S*, et al.* BioGPS: an extensible and customizable portal for querying and organizing gene annotation resources. *Genome Biol* 2009, **10**(11)**:** R130.

401. Hruz T, Laule O, Szabo G, Wessendorp F, Bleuler S, Oertle L*, et al.* Genevestigator v3: a reference expression database for the meta-analysis of transcriptomes. *Adv Bioinformatics* 2008, **2008:** 420747.

402. Evert BO, Vogt IR, Kindermann C, Ozimek L, de Vos RA, Brunt ER*, et al.* Inflammatory genes are upregulated in expanded ataxin-3-expressing cell lines and spinocerebellar ataxia type 3 brains. *J Neurosci* 2001, **21**(15)**:** 5389-5396.

403. Evert BO, Schelhaas J, Fleischer H, de Vos RA, Brunt ER, Stenzel W*, et al.* Neuronal intranuclear inclusions, dysregulation of cytokine expression and cell death in spinocerebellar ataxia type 3. *Clin Neuropathol* 2006, **25**(6)**:** 272-281.

404. Olejniczak M, Urbanek MO, Krzyzosiak WJ. The role of the immune system in triplet repeat expansion diseases. *Mediators Inflamm* 2015, **2015:** 873860.

405. Jurk M, Heil F, Vollmer J, Schetter C, Krieg AM, Wagner H*, et al.* Human TLR7 or TLR8 independently confer responsiveness to the antiviral compound R-848. *Nat Immunol* 2002, **3**(6)**:** 499.

406. Canning P, Ruan Q, Schwerd T, Hrdinka M, Maki JL, Saleh D*, et al.* Inflammatory Signaling by NOD-RIPK2 Is Inhibited by Clinically Relevant Type II Kinase Inhibitors. *Chem Biol* 2015, **22**(9)**:** 1174-1184.

407. Kapoor A, Fan YH, Arav-Boger R. Bacterial Muramyl Dipeptide (MDP) Restricts Human Cytomegalovirus Replication via an IFN-beta-Dependent Pathway. *Sci Rep* 2016, **6:** 20295.

408. Xu J, Jiang C, Zhu W, Wang B, Yan J, Min Z*, et al.* NOD2 pathway via RIPK2 and TBK1 is involved in the aberrant catabolism induced by T-2 toxin in chondrocytes. *Osteoarthritis and Cartilage* 2015, **23**(9)**:** 1575-1585.

409. Watanabe T, Asano N, Fichtner-Feigl S, Gorelick PL, Tsuji Y, Matsumoto Y*, et al.* NOD1 contributes to mouse host defense against Helicobacter pylori via induction of type I IFN and activation of the ISGF3 signaling pathway. *J Clin Invest* 2010, **120**(5)**:** 1645-1662.

410. Clark K, Plater L, Peggie M, Cohen P. Use of the Pharmacological Inhibitor BX795 to Study the Regulation and Physiological Roles of TBK1 and I kappa B Kinase epsilon A DISTINCT UPSTREAM KINASE MEDIATES SER-172 PHOSPHORYLATION AND ACTIVATION. *Journal of Biological Chemistry* 2009, **284**(21)**:** 14136-14146.

411. Matsumoto G, Shimogori T, Hattori N, Nukina N. TBK1 controls autophagosomal engulfment of polyubiquitinated mitochondria through p62/SQSTM1 phosphorylation. *Human Molecular Genetics* 2015, **24**(15)**:** 4429-4442.

412. Reina CP, Zhong X, Pittman RN. Proteotoxic stress increases nuclear localization of ataxin-3. *Hum Mol Genet* 2010, **19**(2)**:** 235-249.

413. Dephoure N, Gould KL, Gygi SP, Kellogg DR. Mapping and analysis of phosphorylation sites: a quick guide for cell biologists. *Mol Biol Cell* 2013, **24**(5)**:** 535-542.

414. Niu S, Wang Z, Ge D, Zhang G, Li Y. Prediction of functional phosphorylation sites by incorporating evolutionary information. *Protein Cell* 2012, **3**(9)**:** 675-690.

415. Kallberg M, Wang HP, Wang S, Peng J, Wang ZY, Lu H*, et al.* Template-based protein structure modeling using the RaptorX web server. *Nature Protocols* 2012, **7**(8)**:** 1511-1522.

416. Mellacheruvu D, Wright Z, Couzens AL, Lambert JP, St-Denis NA, Li T*, et al.* The CRAPome: a contaminant repository for affinity purification-mass spectrometry data. *Nat Methods* 2013, **10**(8)**:** 730-736.

417. Yu T, Yi YS, Yang Y, Oh J, Jeong D, Cho JY. The pivotal role of TBK1 in inflammatory responses mediated by macrophages. *Mediators Inflamm* 2012, **2012:** 979105.

418. Shu C, Sankaran B, Chaton CT, Herr AB, Mishra A, Peng J*, et al.* Structural insights into the functions of TBK1 in innate antimicrobial immunity. *Structure* 2013, **21**(7)**:** 1137-1148.

419. Zhang M, Wu X, Lee AJ, Jin W, Chang M, Wright A*, et al.* Regulation of IkappaB kinase-related kinases and antiviral responses by tumor suppressor CYLD. *J Biol Chem* 2008, **283**(27)**:** 18621-18626.

420. Tu D, Zhu Z, Zhou AY, Yun CH, Lee KE, Toms AV*, et al.* Structure and ubiquitination-dependent activation of TANK-binding kinase 1. *Cell Rep* 2013, **3**(3)**:** 747-758.

421. Zhao W. Negative regulation of TBK1-mediated antiviral immunity. *FEBS Lett* 2013, **587**(6)**:** 542-548.

422. Fitzgerald KA, McWhirter SM, Faia KL, Rowe DC, Latz E, Golenbock DT*, et al.* IKK epsilon and TBK1 are essential components of the IRF3 signaling pathway. *Nature Immunology* 2003, **4**(5)**:** 491-496.

423. Pilli M, Arko-Mensah J, Ponpuak M, Roberts E, Master S, Mandell MA*, et al.* TBK-1 promotes autophagy-mediated antimicrobial defense by controlling autophagosome maturation. *Immunity* 2012, **37**(2)**:** 223-234.

424. Thurston TL, Boyle KB, Allen M, Ravenhill BJ, Karpiyevich M, Bloor S*, et al.* Recruitment of TBK1 to cytosol-invading Salmonella induces WIPI2-dependent antibacterial autophagy. *EMBO J* 2016, **35**(16)**:** 1779-1792.

425. Richter B, Sliter DA, Herhaus L, Stolz A, Wang C, Beli P*, et al.* Phosphorylation of OPTN by TBK1 enhances its binding to Ub chains and promotes selective autophagy of damaged mitochondria. *Proc Natl Acad Sci U S A* 2016, **113**(15)**:** 4039-4044.

426. Oakes JA, Davies MC, Collins MO. TBK1: a new player in ALS linking autophagy and neuroinflammation. *Mol Brain* 2017, **10**(1)**:** 5.

427. Freischmidt A, Wieland T, Richter B, Ruf W, Schaeffer V, Muller K*, et al.* Haploinsufficiency of TBK1 causes familial ALS and fronto-temporal dementia. *Nat Neurosci* 2015, **18**(5)**:** 631-636.

428. Maruyama H, Morino H, Ito H, Izumi Y, Kato H, Watanabe Y*, et al.* Mutations of optineurin in amyotrophic lateral sclerosis. *Nature* 2010, **465**(7295)**:** 223-226.

429. Fecto F, Yan J, Vemula SP, Liu E, Yang Y, Chen W*, et al.* SQSTM1 mutations in familial and sporadic amyotrophic lateral sclerosis. *Arch Neurol* 2011, **68**(11)**:** 1440-1446.

430. Ahmad L, Zhang SY, Casanova JL, Sancho-Shimizu V. Human TBK1: A Gatekeeper of Neuroinflammation. *Trends Mol Med* 2016, **22**(6)**:** 511-527.

431. Kozjak-Pavlovic V. The MICOS complex of human mitochondria. *Cell Tissue Res* 2017, **367**(1)**:** 83-93.

432. Harner M, Korner C, Walther D, Mokranjac D, Kaesmacher J, Welsch U*, et al.* The mitochondrial contact site complex, a determinant of mitochondrial architecture. *EMBO J* 2011, **30**(21)**:** 4356-4370.

433. Xie J, Marusich MF, Souda P, Whitelegge J, Capaldi RA. The mitochondrial inner membrane protein mitofilin exists as a complex with SAM50, metaxins 1 and 2, coiled-coil-helix coiled-coil-helix domain-containing protein 3 and 6 and DnaJC11. *Febs Letters* 2007, **581**(18)**:** 3545-3549.

434. Friedman JR, Mourier A, Yamada J, McCaffery JM, Nunnari J. MICOS coordinates with respiratory complexes and lipids to establish mitochondrial inner membrane architecture. *Elife* 2015, **4**.

435. John GB, Shang Y, Li L, Renken C, Mannella CA, Selker JM*, et al.* The mitochondrial inner membrane protein mitofilin controls cristae morphology. *Mol Biol Cell* 2005, **16**(3)**:** 1543-1554.

436. Li H, Ruan Y, Zhang K, Jian F, Hu C, Miao L*, et al.* Mic60/Mitofilin determines MICOS assembly essential for mitochondrial dynamics and mtDNA nucleoid organization. *Cell Death Differ* 2015.

437. Akabane S, Uno M, Tani N, Shimazaki S, Ebara N, Kato H*, et al.* PKA Regulates PINK1 Stability and Parkin Recruitment to Damaged Mitochondria through Phosphorylation of MIC60. *Mol Cell* 2016, **62**(3)**:** 371-384.

438. von der Malsburg K, Muller JM, Bohnert M, Oeljeklaus S, Kwiatkowska P, Becker T*, et al.* Dual role of mitofilin in mitochondrial membrane organization and protein biogenesis. *Dev Cell* 2011, **21**(4)**:** 694-707.

439. Bohnert M, Wenz LS, Zerbes RM, Horvath SE, Stroud DA, von der Malsburg K*, et al.* Role of mitochondrial inner membrane organizing system in protein biogenesis of the mitochondrial outer membrane. *Mol Biol Cell* 2012, **23**(20)**:** 3948-3956.

440. Huttlin EL, Ting L, Bruckner RJ, Gebreab F, Gygi MP, Szpyt J*, et al.* The BioPlex Network: A Systematic Exploration of the Human Interactome. *Cell* 2015, **162**(2)**:** 425-440.

441. Yang RF, Sun LH, Zhang R, Zhang Y, Luo YX, Zheng W*, et al.* Suppression of Mic60 compromises mitochondrial transcription and oxidative phosphorylation. *Sci Rep* 2015, **5:** 7990.

442. Genin EC, Plutino M, Bannwarth S, Villa E, Cisneros-Barroso E, Roy M*, et al.* CHCHD10 mutations promote loss of mitochondrial cristae junctions with impaired

mitochondrial genome maintenance and inhibition of apoptosis. *EMBO Mol Med* 2016, **8**(1)**:** 58-72.

443. Johnson JO, Glynn SM, Gibbs R, Nalls MA, Sabatelli M, Restagno G*, et al.* Mutations in the CHCHD10 gene are a common cause of familial amyotrophic lateral sclerosis. *Brain* 2014, **137**.

444. Bannwarth S, Ait-El-Mkadem S, Chaussenot A, Genin EC, Lacas-Gervais S, Fragaki K*, et al.* A mitochondrial origin for frontotemporal dementia and amyotrophic lateral sclerosis through CHCHD10 involvement. *Brain* 2014, **137:** 2329-2345.

445. Chio A, Mora G, Sabatelli M, Caponnetto C, Traynor BJ, Johnson JO*, et al.* CHCH10 mutations in an Italian cohort of familial and sporadic amyotrophic lateral sclerosis patients. *Neurobiol Aging* 2015, **36**(4)**:** 1767 e1763-1766.

446. Kim W, Bennett EJ, Huttlin EL, Guo A, Li J, Possemato A*, et al.* Systematic and quantitative assessment of the ubiquitin-modified proteome. *Mol Cell* 2011, **44**(2)**:** 325-340.

447. Swatek KN, Komander D. Ubiquitin modifications. *Cell Res* 2016, **26**(4)**:** 399-422.

448. Maculins T, Fiskin E, Bhogaraju S, Dikic I. Bacteria-host relationship: ubiquitin ligases as weapons of invasion. *Cell Research* 2016, **26**(4)**:** 499-510.

449. Weissman AM. Themes and variations on ubiquitylation. *Nat Rev Mol Cell Biol* 2001, **2**(3)**:** 169-178.

450. Chen ZJ, Sun LJ. Nonproteolytic functions of ubiquitin in cell signaling. *Mol Cell* 2009, **33**(3)**:** 275-286.

451. Huguenin-Dezot N, De Cesare V, Peltier J, Knebel A, Kristaryianto YA, Rogerson DT*, et al.* Synthesis of Isomeric Phosphoubiquitin Chains Reveals that Phosphorylation Controls Deubiquitinase Activity and Specificity. *Cell Reports* 2016, **16**(4)**:** 1180-1193.

452. Mevissen TET, Komander D. Mechanisms of Deubiquitinase Specificity and Regulation. *Annu Rev Biochem* 2017, **86:** 159-192.

453. Reyes-Turcu FE, Ventii KH, Wilkinson KD. Regulation and Cellular Roles of Ubiquitin-Specific Deubiquitinating Enzymes. *Annual Review of Biochemistry* 2009, **78:** 363-397.

454. Azkargorta M, Escobes I, Elortza F, Matthiesen R, Rodriguez MS. TUBEs-Mass Spectrometry for Identification and Analysis of the Ubiquitin-Proteome. *Methods Mol Biol* 2016, **1449:** 177-192.

455. Hjerpe R, Aillet F, Lopitz-Otsoa F, Lang V, England P, Rodriguez MS. Efficient protection and isolation of ubiquitylated proteins using tandem ubiquitin-binding entities. *Embo Reports* 2009, **10**(11)**:** 1250-1258.

456. Xolalpa W, Mata-Cantero L, Aillet F, Rodriguez MS. Isolation of the Ubiquitin-Proteome from Tumor Cell Lines and Primary Cells Using TUBEs. *Proteostasis: Methods and Protocols* 2016, **1449:** 161-175.

457. Reina CP, Nabet BY, Young PD, Pittman RN. Basal and stress-induced Hsp70 are modulated by ataxin-3. *Cell Stress Chaperones* 2012, **17**(6)**:** 729-742.

458. Skarnes WC, Rosen B, West AP, Koutsourakis M, Bushell W, Iyer V*, et al.* A conditional knockout resource for the genome-wide study of mouse gene function. *Nature* 2011, **474**(7351)**:** 337-342.

459. Consortium TIaIIi. The Infection and Immunity Immunophenotyping (3i) Consortium 2017 [cited 2017 17/7/2017]Available from:

460. Rebelo AP, Dillon LM, Moraes CT. Mitochondrial DNA transcription regulation and nucleoid organization. *J Inherit Metab Dis* 2011, **34**(4)**:** 941-951.

461. Moore CB, Guthrie EH, Huang MT, Taxman DJ. Short hairpin RNA (shRNA): design, delivery, and assessment of gene knockdown. *Methods Mol Biol* 2010, **629:** 141-158.

462. Ekstrand MI, Falkenberg M, Rantanen A, Park CB, Gaspari M, Hultenby K*, et al.* Mitochondrial transcription factor A regulates mtDNA copy number in mammals. *Hum Mol Genet* 2004, **13**(9)**:** 935-944.

463. Gerencser AA, Neilson A, Choi SW, Edman U, Yadava N, Oh RJ*, et al.* Quantitative microplate-based respirometry with correction for oxygen diffusion. *Anal Chem* 2009, **81**(16)**:** 6868-6878.

464. Murphy MP. How mitochondria produce reactive oxygen species. *Biochemical Journal* 2009, **417:** 1-13.

465. Graef M, Nunnari J. Mitochondria regulate autophagy by conserved signalling pathways. *EMBO J* 2011, **30**(11)**:** 2101-2114.

466. Demers-Lamarche J, Guillebaud G, Tlili M, Todkar K, Belanger N, Grondin M*, et al.* Loss of Mitochondrial Function Impairs Lysosomes. *J Biol Chem* 2016, **291**(19)**:** 10263-10276.

467. Fernandez-Mosquera L, Diogo CV, Yambire KF, Santos GL, Luna Sanchez M, Benit P*, et al.* Acute and chronic mitochondrial respiratory chain deficiency differentially regulate lysosomal biogenesis. *Sci Rep* 2017, **7:** 45076.

468. Baixauli F, Acin-Perez R, Villarroya-Beltri C, Mazzeo C, Nunez-Andrade N, Gabande-Rodriguez E*, et al.* Mitochondrial Respiration Controls Lysosomal Function during Inflammatory T Cell Responses. *Cell Metab* 2015, **22**(3)**:** 485-498.

469. Mauvezin C, Neufeld TP. Bafilomycin A1 disrupts autophagic flux by inhibiting both V-ATPase-dependent acidification and Ca-P60A/SERCA-dependent autophagosome-lysosome fusion. *Autophagy* 2015, **11**(8)**:** 1437-1438.

470. Kim J, Kundu M, Viollet B, Guan KL. AMPK and mTOR regulate autophagy through direct phosphorylation of Ulk1. *Nature Cell Biology* 2011, **13**(2)**:** 132-U171.

471. Mrschtik M, Ryan KM. Lysosomal proteins in cell death and autophagy. *FEBS J* 2015, **282**(10)**:** 1858-1870.

472. Fazzari P, Horre K, Arranz AM, Frigerio CS, Saito T, Saido TC*, et al.* PLD3 gene and processing of APP. *Nature* 2017, **541**(7638)**:** E1-E2.

473. Cruchaga C, Karch CM, Jin SC, Benitez BA, Cai Y, Guerreiro R*, et al.* Rare coding variants in the phospholipase D3 gene confer risk for Alzheimer's disease. *Nature* 2014, **505**(7484)**:** 550-554.

474. Sancak Y, Bar-Peled L, Zoncu R, Markhard AL, Nada S, Sabatini DM. Ragulator-Rag complex targets mTORC1 to the lysosomal surface and is necessary for its activation by amino acids. *Cell* 2010, **141**(2)**:** 290-303.

475. Takahashi Y, Nada S, Mori S, Soma-Nagae T, Oneyama C, Okada M. The late endosome/lysosome-anchored p18-mTORC1 pathway controls terminal maturation of lysosomes. *Biochem Biophys Res Commun* 2012, **417**(4)**:** 1151-1157.

476. Kimura T, Nada S, Takegahara N, Okuno T, Nojima S, Kang S*, et al.* Polarization of M2 macrophages requires Lamtor1 that integrates cytokine and amino-acid signals. *Nat Commun* 2016, **7:** 13130.

477. Cheng JB, Russell DW. Mammalian wax biosynthesis. I. Identification of two fatty acyl-Coenzyme A reductases with different substrate specificities and tissue distributions. *J Biol Chem* 2004, **279**(36)**:** 37789-37797.

478. Ohno Y, Suto S, Yamanaka M, Mizutani Y, Mitsutake S, Igarashi Y*, et al.* ELOVL1 production of C24 acyl-CoAs is linked to C24 sphingolipid synthesis. *Proceedings of the National Academy of Sciences of the United States of America* 2010, **107**(43)**:** 18439-18444.

479. Peng X, Frohman MA. Mammalian phospholipase D physiological and pathological roles. *Acta Physiol (Oxf)* 2012, **204**(2)**:** 219-226.

480. Pedersen KM, Finsen B, Celis JE, Jensen NA. Expression of a novel murine phospholipase D homolog coincides with late neuronal development in the forebrain. *J Biol Chem* 1998, **273**(47)**:** 31494-31504.

481. Dall'Armi C, Hurtado-Lorenzo A, Tian H, Morel E, Nezu A, Chan RB*, et al.* The phospholipase D1 pathway modulates macroautophagy. *Nat Commun* 2010, **1:** 142.

482. Bae EJ, Lee HJ, Jang YH, Michael S, Masliah E, Min DS*, et al.* Phospholipase D1 regulates autophagic flux and clearance of alpha-synuclein aggregates. *Cell Death Differ* 2014, **21**(7)**:** 1132-1141.

483. Lim HK, Choi YA, Park W, Lee T, Ryu SH, Kim SY*, et al.* Phosphatidic acid regulates systemic inflammatory responses by modulating the Akt-mammalian target of rapamycin-p70 S6 kinase 1 pathway. *J Biol Chem* 2003, **278**(46)**:** 45117-45127.

484. Aoki J, Inoue A, Okudaira S. Two pathways for lysophosphatidic acid production. *Biochim Biophys Acta* 2008, **1781**(9)**:** 513-518.

485. Schwerd T, Pandey S, Yang HT, Bagola K, Jameson E, Jung J*, et al.* Impaired antibacterial autophagy links granulomatous intestinal inflammation in Niemann-Pick disease type C1 and XIAP deficiency with NOD2 variants in Crohn's disease. *Gut* 2016.

486. Shi CS, Shenderov K, Huang NN, Kabat J, Abu-Asab M, Fitzgerald KA*, et al.* Activation of autophagy by inflammatory signals limits IL-1beta production by targeting ubiquitinated inflammasomes for destruction. *Nat Immunol* 2012, **13**(3)**:** 255-263.

487. Shanbhag R, Shi G, Rujiviphat J, McQuibban GA. The emerging role of proteolysis in mitochondrial quality control and the etiology of Parkinson's disease. *Parkinsons Dis* 2012, **2012:** 382175.

488. Huang M, Graves LM. De novo synthesis of pyrimidine nucleotides; emerging interfaces with signal transduction pathways. *Cell Mol Life Sci* 2003, **60**(2)**:** 321-336.

489. Richmond AL, Kabi A, Homer CR, Marina-Garcia N, Nickerson KP, Nesvizhskii AI*, et al.* The nucleotide synthesis enzyme CAD inhibits NOD2 antibacterial function in human intestinal epithelial cells. *Gastroenterology* 2012, **142**(7)**:** 1483-1492 e1486.

490. Nada S, Hondo A, Kasai A, Koike M, Saito K, Uchiyama Y*, et al.* The novel lipid raft adaptor p18 controls endosome dynamics by anchoring the MEK-ERK pathway to late endosomes. *EMBO J* 2009, **28**(5)**:** 477-489.

491. Guillaumot P, Luquain C, Malek M, Huber AL, Brugiere S, Garin J*, et al.* Pdro, a protein associated with late endosomes and lysosomes and implicated in cellular cholesterol homeostasis. *PLoS One* 2010, **5**(6)**:** e10977.

492. Zoncu R, Bar-Peled L, Efeyan A, Wang S, Sancak Y, Sabatini DM. mTORC1 senses lysosomal amino acids through an inside-out mechanism that requires the vacuolar H(+)-ATPase. *Science* 2011, **334**(6056)**:** 678-683.

493. Bar-Peled L, Schweitzer LD, Zoncu R, Sabatini DM. Ragulator is a GEF for the rag GTPases that signal amino acid levels to mTORC1. *Cell* 2012, **150**(6)**:** 1196-1208.

494. Zhang CS, Jiang B, Li MQ, Zhu MJ, Peng YY, Zhang YL*, et al.* The Lysosomal v-ATPase-Ragulator Complex Is a Common Activator for AMPK and mTORC1, Acting as a Switch between Catabolism and Anabolism. *Cell Metabolism* 2014, **20**(3)**:** 526-540.

495. Shen K, Sidik H, Talbot WS. The Rag-Ragulator Complex Regulates Lysosome Function and Phagocytic Flux in Microglia. *Cell Rep* 2016, **14**(3)**:** 547-559.

496. Nelson RK, Frohman MA. Physiological and pathophysiological roles for phospholipase D. *J Lipid Res* 2015, **56**(12)**:** 2229-2237.

497. Brunner Y, Coute Y, Iezzi M, Foti M, Fukuda M, Hochstrasser DF*, et al.* Proteomics analysis of insulin secretory granules. *Mol Cell Proteomics* 2007, **6**(6)**:** 1007-1017.

498. Liu B, Zheng Y, Wang TD, Xu HZ, Xia L, Zhang J*, et al.* Proteomic identification of common SCF ubiquitin ligase FBXO6-interacting glycoproteins in three kinds of cells. *J Proteome Res* 2012, **11**(3)**:** 1773-1781.

499. Seok J, Warren HS, Cuenca AG, Mindrinos MN, Baker HV, Xu WH*, et al.* Genomic responses in mouse models poorly mimic human inflammatory diseases. *Proceedings of the National Academy of Sciences of the United States of America* 2013, **110**(9)**:** 3507-3512.

500. Tompkins RG. Genomic Responses in Mouse Models Poorly Mimic Human Inflammatory Diseases. *Annals of the Rheumatic Diseases* 2014, **73:** 37-37.

501. Binion DG, Rafiee P. Is inflammatory bowel disease a vascular disease? Targeting angiogenesis improves chronic inflammation in inflammatory bowel disease. *Gastroenterology* 2009, **136**(2)**:** 400-403.

502. Scaldaferri F, Vetrano S, Sans M, Arena V, Straface G, Stigliano E*, et al.* VEGF-A links angiogenesis and inflammation in inflammatory bowel disease pathogenesis. *Gastroenterology* 2009, **136**(2)**:** 585-595 e585.

503. Alkim C, Savas B, Ensari A, Alkim H, Dagli U, Parlak E*, et al.* Expression of p53, VEGF, microvessel density, and cyclin-D1 in noncancerous tissue of inflammatory bowel disease. *Dig Dis Sci* 2009, **54**(9)**:** 1979-1984.

504. Kessler BM, Edelmann MJ. PTMs in conversation: activity and function of deubiquitinating enzymes regulated via post-translational modifications. *Cell Biochem Biophys* 2011, **60**(1-2)**:** 21-38.

505. Mann M. Functional and quantitative proteomics using SILAC. *Nature Reviews Molecular Cell Biology* 2006, **7**(12)**:** 952-958.

506. Yadava N, Nicholls DG. Spare respiratory capacity rather than oxidative stress regulates glutamate excitotoxicity after partial respiratory inhibition of mitochondrial complex I with rotenone. *Journal of Neuroscience* 2007, **27**(27)**:** 7310-7317.

507. Ferrick DA, Neilson A, Beeson C. Advances in measuring cellular bioenergetics using extracellular flux. *Drug Discovery Today* 2008, **13**(5-6)**:** 268-274.

508. Shi CS, Kehrl JH. MyD88 and Trif target Beclin 1 to trigger autophagy in macrophages. *J Biol Chem* 2008, **283**(48)**:** 33175-33182.

509. Shi CS, Kehrl JH. TRAF6 and A20 regulate lysine 63-linked ubiquitination of Beclin-1 to control TLR4-induced autophagy. *Sci Signal* 2010, **3**(123)**:** ra42.

510. Johnson CH, Ivanisevic J, Siuzdak G. Metabolomics: beyond biomarkers and towards mechanisms. *Nat Rev Mol Cell Biol* 2016, **17**(7)**:** 451-459.

511. Glass CK, Saijo K, Winner B, Marchetto MC, Gage FH. Mechanisms underlying inflammation in neurodegeneration. *Cell* 2010, **140**(6)**:** 918-934.

512. McManus RM, Heneka MT. Role of neuroinflammation in neurodegeneration: new insights. *Alzheimers Res Ther* 2017, **9**(1)**:** 14.

513. Heneka MT, Kummer MP, Latz E. Innate immune activation in neurodegenerative disease. *Nat Rev Immunol* 2014, **14**(7)**:** 463-477.

514. Tang Y, Le W. Differential Roles of M1 and M2 Microglia in Neurodegenerative Diseases. *Mol Neurobiol* 2016, **53**(2)**:** 1181-1194.

515. Sheng JG, Bora SH, Xu G, Borchelt DR, Price DL, Koliatsos VE. Lipopolysaccharide-induced-neuroinflammation increases intracellular accumulation of amyloid precursor protein and amyloid beta peptide in APPswe transgenic mice. *Neurobiol Dis* 2003, **14**(1)**:** 133-145.

516. Qiao X, Cummins DJ, Paul SM. Neuroinflammation-induced acceleration of amyloid deposition in the APPV717F transgenic mouse. *Eur J Neurosci* 2001, **14**(3)**:** 474-482.

517. Menzies FM, Fleming A, Rubinsztein DC. Compromised autophagy and neurodegenerative diseases. *Nat Rev Neurosci* 2015, **16**(6)**:** 345-357.

518. Balin BJ, Gerard HC, Arking EJ, Appelt DM, Branigan PJ, Abrams JT*, et al.* Identification and localization of Chlamydia pneumoniae in the Alzheimer's brain. *Med Microbiol Immunol* 1998, **187**(1)**:** 23-42.

519. Alonso R, Pisa D, Marina AI, Morato E, Rabano A, Carrasco L. Fungal infection in patients with Alzheimer's disease. *J Alzheimers Dis* 2014, **41**(1)**:** 301-311.

520. Itzhaki RF, Lin WR, Shang D, Wilcock GK, Faragher B, Jamieson GA. Herpes simplex virus type 1 in brain and risk of Alzheimer's disease. *Lancet* 1997, **349**(9047)**:** 241-244.

521. Catorce MN, Gevorkian G. LPS-induced Murine Neuroinflammation Model: Main Features and Suitability for Pre-clinical Assessment of Nutraceuticals. *Curr Neuropharmacol* 2016, **14**(2)**:** 155-164.

522. Sospedra M, Martin R. Immunology of Multiple Sclerosis. *Semin Neurol* 2016, **36**(2)**:** 115-127.

523. Wilkins HM, Weidling IW, Ji Y, Swerdlow RH. Mitochondria-Derived Damage-Associated Molecular Patterns in Neurodegeneration. *Front Immunol* 2017, **8:** 508.

524. Rub U, Brunt ER, Gierga K, Schultz C, Paulson H, de Vos RA*, et al.* The nucleus raphe interpositus in spinocerebellar ataxia type 3 (Machado-Joseph disease). *J Chem Neuroanat* 2003, **25**(2)**:** 115-127.

525. Schafer M, Oeing CU, Rohm M, Baysal-Temel E, Lehmann LH, Bauer R*, et al.* Ataxin-10 is part of a cachexokine cocktail triggering cardiac metabolic dysfunction in cancer cachexia. *Molecular Metabolism* 2016, **5**(2)**:** 67-78.

526. Carmo-Silva S, Nobrega C, de Almeida LP, Cavadas C. Unraveling the Role of Ataxin-2 in Metabolism. *Trends in Endocrinology and Metabolism* 2017, **28**(4)**:** 309-318.

527. Meierhofer D, Halbach M, Sen NE, Gispert S, Auburger G. Ataxin-2 (Atxn2)-Knock-Out Mice Show Branched Chain Amino Acids and Fatty Acids Pathway Alterations. *Molecular & Cellular Proteomics* 2016, **15**(5)**:** 1728-1739.

528. Bargiela D, Shanmugarajah P, Lo C, Blakely EL, Taylor RW, Horvath R*, et al.* Mitochondrial pathology in progressive cerebellar ataxia. *Cerebellum Ataxias* 2015, **2:** 16.

Appendix

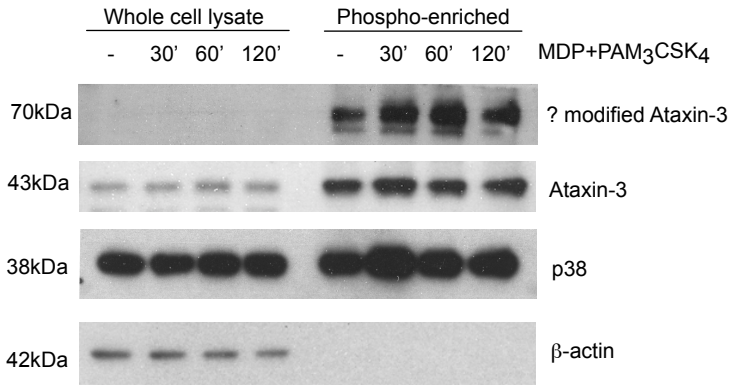


Figure 1 Ataxin-3 is phosphorylated in a murine macrophage cell line on NOD2/TLR2 stimulation. Immunoblot using antibodies against ataxin-3, p38 and β-actin in whole cell lysates and phosphoprotein enriched fractions from the murine RAW264.7 cell line that was either left unstimulated or stimulated with for 30-120min with MDP+PAM_3CSK_4. A higher band at around 70kDa was detected in the phosphoprotein enriched fraction only with two separate antibodies to ataxin-3, both raised against different epitopes, suggesting it is a specific ataxin-3 band. The signal abundance increased markedly on stimulation with MDP+PAM_3CSK_4. This band is likely to represent a modified form of phosphorylated ataxin-3.

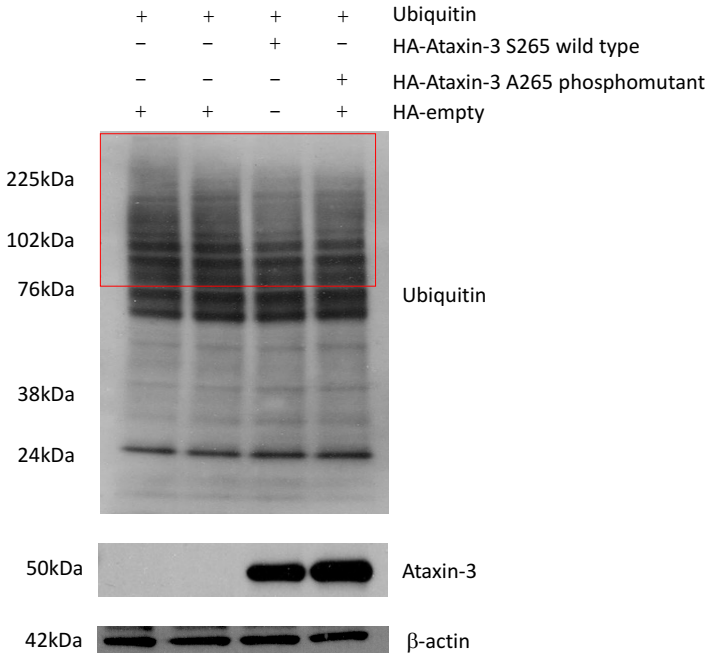


Figure 2 The S265 residue may be important for the DUB activity of ataxin-3. Immunoblot using antibodies against ubiquitin, ataxin-3 and β-actin in whole cell lysates of HEK293 cells transfected with ubiquitin alone or in combination with ataxin-3 S265 WT or ataxin-3 A265 mutant. The red box indicates the high molecular weight ubiquitinated proteins that appear less abundant in the ataxin-3 265 WT.

Protein	MASCOT Score	Fold change on ataxin-3 depletion
Lys063-specific deubiquitinase BRCC36 (BRCC36)	53.96	10.26
Host cell factor 1 (HCF1)	80.51	4.32
ATP dependent DNA helicase Q1 (DHX9)	1260.23	3.89
Cyclin-dependent kinase 2 (CDK2)	147.42	3.46
Xaa-Pro aminopeptidase 1 (XPNPEP1)	147.36	3.26
Syndecan 2 (SDC2)	54.96	3.16
Mitochondrial ES1 protein Homolog	37.67	2.96
RIPK2	655.66	2.76
Glutamine-fructose-6-phosphate aminotransferase 1 (GFPT1)	316.77	2.54
Phospholipid-transporting ATPase IK	39.59	2.45
Phospolipase D3 (PLD3)	303.09	2.40
CAD protein	419.47	2.31
Moloney leukaemia virus 10, homolog (MOV10)	127.93	2.22
Proteasome subunit alpha type (PSMA6)	2112.98	2.20
Glutathione S-transferase Mu 5 (GSTM5)	97.92	2.16
Integral membrane protein 2C (ITM2C)	263.12	2.15
Sideroreflexin 1 (SFXN1)	147.74	2.12
Carbonyl reductase (NADPH) 1	430.76	2.05

Table 1 List of proteins from TUBEs LC-MS/MS screen with ≥2 fold increase in abundance in ataxin-3 shRNA cells in comparison to control shRNA cells at baseline (Student's paired t-test p<0.05).

Protein	MASCOT Score	Fold change on ataxin-3 depletion
Serine/threonine-protein phosphatase 6 regulatory subunit 1 (PPP6R1)	98.03	5.05
Serine/threonine-protein phosphatase 1A 65kDa regulatory subunit A (PPP2R1A)	75.76	4.79
Caspase-7 (CASP7)	136.11	4.06
Ubiquitin conjugation factor E4 A (UBE4A)	83.08	4.01
Fatty acyl-CoA reductase 2 (FAR2)	195.52	3.94
TFIIH basal transcription factor complex helicase XPB subunit (ERCC3)	68.42	3.54
Cyclin-dependent kinase 2 (CDK2)	147.42	3.45
Cyclin-A2 (CCNA2)	44.70	3.22
RNA-binding protein PNO1 (PNO1)	66.63	2.94
Flotillin-1 (FLOT1)	380.25	2.91
Zinc finger CCCH-type antiviral protein 1 (ZC3)	176.16	2.78

Phospholipase D3 (PLD3)	303.09	2.69
Putative sodium-coupled neutral amino acid transporter 10 (SLC38A10)	760.47	2.69
E3 ubiquitin-protein ligase ARIH1 (ARIH1)	37.63	2.67
Myeloid cell nuclear differentiation antigen (MNDA)	306.83	2.56
Glutamine-fructose-6-phosphate aminotransferase 1 (GFPT1)	316.77	2.51
Plasminogen activator inhibitor 1 RNA-binding protein (SERBP1)	161.86	2.49
Oxysterol-binding protein-related protein 5 (OSBPL5)	34.86	2.46
Solute carrier family 12 member 2 (SLC12A2)	87.03	2.45
Suppressor of glucose, autophagy associated 1 (SOGA1)	743.76	2.44
Elongation of very long chain fatty acids protein 1 (ELOV1)	127.82	2.39
Chromodomain-helicase-DNA-binding protein 4 (CHD4)	150.32	2.38
Golgin-45 (BLZF1)	90.23	2.34
Monocarboxylate transporter 4 (SLC16A3)	220.81	2.28
Inosine-5'-monophosphate dehydrogenase (IMPDH1)	225.13	2.34
Mitochondrial succinyl-CoA:3-ketoacid coenzyme A transferase 1 (OXCT1)	120.68	2.22
Centrin-3 (CETN3)	44.14	2.13
Moloney leukaemia virus 10, homolog (MOV10)	127.93	2.11
Far upstream element-binding protein 3 (FUBP3)	86.96	2.10
40S ribosomal protein S18 (RPS18)	562.73	2.09
ATP-dependent 6-phosphofructokinase, platelet type (PFKP)	547.48	2.09
Ragulator complex protein LAMTOR1 (LAMTOR1)	166.27	2.05
Endoplasmic reticulum resident protein 44 (ERP44)	50.22	2.04
Ubiquitin carboxyl-terminal hydrolase isozyme L5 (UCHL5)	86.44	0.042
Torsin-1A-interacting protein 1 (TOR1AIP1)	99.61	2.02
Pericentriolar material protein (PCM1)	326.48	2.00

Table 2 List of proteins from TUBEs LC-MS/MS screen with $\geq$2 fold increase in abundance in ataxin-3 shRNA cells following MDP+PAM_3CSK_4 in comparison to control shRNA cells (Student's paired t test $p<0.05$).

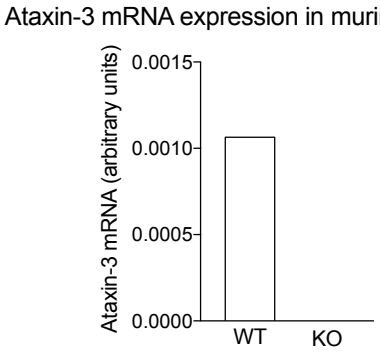


Figure 3 Confirmation of ataxin-3 knockout. RT-qPCR of WT and KO macrophages using primer against ataxin-3, normalised to β-actin.